Imperial College London
Department of the Life Sciences

Neurocranial anatomy of three unusual placoderms revealed by computed tomography scanning, and their implications for early gnathostomes evolution

Marco Castiello

January 2018

Supervised by Martin. D. Brazeau

Submitted in partial fulfillment of the requirements for the degree of
Doctor of Philosophy in the Life Sciences of Imperial College London
and the Diploma of Imperial College London

DECLARATION

The work contained in this thesis is my own. Collaborative parts of this work are acknowledged in the "contribution of authors" section in chapter 1.

Marco Castiello

Copyright Declaration

The copyright of this thesis rests with the author and is made available under a Creative Commons Attribution Non-Commercial No Derivatives licence. Researchers are free to copy, distribute or transmit the thesis on the condition that they attribute it, that they do not use it for commercial purposes and that they do not alter, transform or build upon it. For any reuse or redistribution, researchers must make clear to others the licence terms of this work

"Ignorance more frequently begets confidence than does knowledge: it is those who know little, and not those who know much, who so positively assert that this or that problem will never be solved by science."

Charles Darwin

Acknowledgements

When I started my PhD four years ago, I could not have imagined it was going to be such an incredible long adventure. I met many people, travelled to places I will likely not see again. I attended conferences, parties, events. I sang, danced, played theatre plays and discovered a whole new word of cultures, lifestyles and activities. I truly changed since I left home back then. And I think this experience made me a better person.

The list of people I would like to thank will probably be as long as this PhD thesis. Just imagined I thanked you all. However, still I want to personally thank some of you.

First, I would like to thank my supervisor Dr Martin D. Brazeau, who has always been very patient with me, supporting me during my time as a PhD student and gave me a lot of advice about how to be a good scientist. Also, he brought me to very exciting remote localities doing one of the things we like most, collecting fossils fishes, and introduced me to the palaeontology community.

My PhD would not have been as enjoyable if it wasn't for my lab friends. Richard, Anna and Thomas has been fundamental for the work presented in this thesis, not only giving me support and advises, but also for the social interaction and the family atmosphere they create in the lab. I will miss our board game lunch very very much! Also thank you Richard for your endless trial to embrace me with the British culture and be my paleo travel friend, to Anna for teaching me how to knit a hat and to help me with digital drawings and draft proofing, and to Thomas to teach me how to use latex and be a better drinker. Also, a big thank to all the students that have done their project in the lab during those years, in particular to Victoria Stanley and Vinni Jane. A special thank go to Charline Pinna and her work on *Kolymaspis*, as well

as been a very important person for me during her staying in our lab. Also, thank to my friend Maria Igorevna Balandina for her translation of the original *Kolymaspis* paper from Russian to English.

There are no words to explain what Silwood Park Campus and the Silwood community has been for me during my PhD time. I met incredible people and each of them has been important for me, in the good or in the bad. I learn how to do many activities that I have never done before, like climbing or singing in a choir, and I will always remember the contribution that this place has gave me. True silwoodians knows how hard will be for me to not be there anymore.

Among Silwood people, huge thanks goes to my PhD fellows and friends, Richard, Jack, Laura, Andrew, Adam, Matt, Edicson, Paula, Ana, Marie Claire, Sophie, Margaux, Marina, Camilla, Rishi. The moment we spent together have been priceless. A big thanks also to all the Italians that have been in Silwood park and made me feel like home, particularly to Bruno, my Silwood little brother (Grazie ragazzi!). I cannot thank Joanna to all she has done for me and how kindly she took care of my during my last year of my PhD, there will always be a special place for her in my heart.

Talking about fossil fishes with Emma Randle, Sam Giles and Ben King have been fun and inspiring, and I need to thank them for all the useful discussions and help they gave me during this PhD. Also, thanks for sharing with me the burden of working on unpopular, obscure group of fossil vertebrates. Also thank to Emma Dunne, Ryan Marek, Alessandro Chiarenza and Valentina Rossi for all the nice moments we had during palaeo conferences. They would not have been as enjoyable without you.

A big hug to my parents and my sister, who have always supported me and ask me about my work and providing me lots of affection from distance. The final thanks go to my old friends from Italy and my university friends, Elia, Matteo, Alex, Giorgio, Sonia, Ricco, Nabo, Galbu, Mora, Ste, Lampu, Giuliano, Federica, Silvia. And especially to Chiara Maffioletti, who I really need to say I am sorry, but also thank you because you have always been next to me, even when things went wrong.

Dear friends, I know those years have changed a bit our relationships, because living apart is hard, not sharing the same moments is hard, not being able to have a spontaneous meeting is hard, but whatever I have done, wherever I have been, I felt like you were with me and if I have done all this is also because I know some kind of knots never untie.

Abstract

Placoderms are the only known stem-group jawed vertebrates with jaws and their phylogenetic relationships have become central to the question of how gnathostomes evolved. Among placoderms, petalichthyids and "acanthothoracids" have taken a pivotal position in the debate on placoderm paraphyly, owing to their similarities with the jawless outgroups of jawed vertebrates. Nevertheless, their endocranial anatomy is still poorly known, preventing a thorough comparative analysis with the other early gnathostomes. In this thesis, I present the neurocranial anatomy of three exceptionally preserved placoderms, the petalichthyids *Shearsbyaspis* and *Ellopetalichthys*, and the "acanthothoracid" *Kolymaspis*. Using X-ray computed microtomography, I generated three-dimensional reconstructions of their endocranial surfaces, orbital walls, and cranial endocavity. The investigation of the endocranial anatomy of *Shearsbyaspis* revealed a combination of both derived and plesiomorphic characters never observed before in a placoderm, particularly in its orbital morphology and palatal architecture. *Ellopetalichthys* provided new evidence to help understanding the functional morphology and evolution of the inner ear and neck articulation in petalichthyids and early jawed vertebrates. *Kolymaspis* is revealed as an intermediate morphology between long- and short-nosed "acanthothoracids", suggesting that placoderms with similar orbitonasal anatomy might represent a highly specialized morphology rather than being plesiomorphic for jawed gnathostomes. With the aim of testing competing hypothesis on placoderm relationships, I performed different phylogenetic analyses on a new dataset comprising a wide range of early gnathostomes. Parsimony and Bayesian analyses resulted in competing hypotheses regarding placoderm monophyly and we compared the strengths and weaknesses of competing scenarios of placoderm relationships. Placoderms monophyly may

indicate new scenarios for the early evolution of jawed vertebrates, implying a primitive architecture similar to those of early arthrodires, maxillate "placoderms" and bony fishes. Similarities between jawless fishes and certain placoderms may instead represent convergent adaptations.

Table of Contents

Acknowledgements . . . 5

Abstract . . . 8

Table of Contents . . . 10

List of Figures . . . 12

1 Introduction . . . 1
- 1.1 An overview on the placoderm problem . . . 3
- 1.2 Investigating stem-gnathostomes neurocrania using CT techniques . . . 11
- 1.3 Phylogenetic analysis . . . 14
- 1.4 Data Archiving Statement . . . 15
- 1.5 Contribution of authors . . . 16

2 The braincase and brain cavity of the Petalichthyid *Shearbyaspis oepiki* Young 1985 (Placodermi, Early Devonian) . . . 18
- 2.1 Introduction . . . 18
- 2.2 Material and Methods . . . 21
- 2.3 Description . . . 21
- 2.4 Discussion . . . 40
- 2.5 Conclusion . . . 49
- 2.6 Acknowledgements . . . 50

3 New information on the endocranial morphology of *Ellopetalichthys scheii* Kjær 1915 (Placodermi, Middle Devonian), with remarks on the morphology and function of the inner ear and shoulder/neck region in placoderms . . . 51
- 3.1 Introduction . . . 51
- 3.2 Material and Methods . . . 53
- 3.3 Description . . . 54
- 3.4 Discussion . . . 65

3.5 Conclusion 79

4 Computed tomographic investigation of the endocranium of *Kolymaspis sibirica* Bystrow 1956 (Vertebrata: Placodermi) with remarks on the endocranial anatomy of "acanthothoracid" placoderms 81
4.1 Introduction 81
4.2 Methods 83
4.3 Description 85
4.4 Discussion 106
4.5 Conclusion 119

5 Phylogenetic analysis of placoderms with a particular attention of the relationships of petalichthyids and "acanthothoracids" . . 121
5.1 Introduction 121
5.2 Data and Methodology 124
5.3 Character list 129
5.4 Results 178
5.5 Discussion 184
5.6 Conclusion 193

6 Conclusion 195

Appendices 228

A Appendix. 228
A.1 List of taxa with references 228
A.2 Characters removed from King et al. 2016 236
A.3 Supplementary figures 240

List of Figures

Figure 1.1 Composite tree showing the relationships of modern gnathostome lineages and their jawless and jawed Palaeozoic representatives through time, with some taxa omitted for clarity and including the key petalichthyid taxa analysed in this study. Topology and time calibration from Zhu and Wang (1996) for Petalichthyida and Brazeau and Friedman (2015) for the rest of the taxa. . . . 3

Figure 1.2 Restoration of various placoderms (not in scale) to show placoderms diversity. (a) The antiarch *Bothriolepis*; (b) *Materpiscis*, a ptyctodontid; (c) *Gemuendina*, a rhenanid; (d) the petalichthyid *Lunaspis*; (e), *Wuttagoonaspis*, a wuttagoonaspids arthrodire; (f), *Entelognathus*, a maxillate placoderm ; (g) the arthrodire *Dunkleosteus*. Pictures from http://www.eartharchives.org, Kahless28 on DeviantArt, Young 2010, Zhu et al. 2013 and Dmitry Bogdanov on Wikipedia. 5

Figure 1.3 Restoration of the skull roof of the currently known petalichthyids (not in scale). Pictures redrawn from Denison 1978; Zhu 1991; Liu 1991; Zhu and Wang 1996; Ji 1996; Zhu 2000; Zhao and Zhu 2010; Pan et al. 2015 7

Figure 1.4 Restoration of the skull roof of the currently known "acanthothoracids" (not in scale). Pictures redrawn from Mark-Kurik 1973; Ørvig 1975; Denison 1978; Goujet 1984b; Young 2010; Dupret et al. 2011; Olive et al. 2011; Vaškaninová and Ahlberg 2017.. 10

Figure 1.5 Summary diagram of the x-ray computed tomography technique. An x-ray beam is directed through the specimen which sits on a rotating stage in front of a detector. An individual projection from the detector is taken at each stage of rotation. After 180- or 360-degrees rotation, the resulting images can be reconstructed into a computed tomogram. The complete virtual dataset will be composed by a series of tomograms. From Sutton 2008. 13

FIGURE 2.1 Skull roof and sensory lines of NHMUK P33580. A, photograph in dorsal view. B-C, 3D model in: B, dorsal; C, right lateral view. D, skull roof of *Shearsbyaspis*, redrawn after Young (1985), with the highlighted in blue. Abbreviations: ioc, infraorbital sensory canal; lc, main lateral line sensory canal; pmc, postmarginal sensory canal; ppl, posterior pit line canal; soc, supraorbital sensory canal. Scale bars represent 10 mm. 23

FIGURE 2.2 NHMUK P33580. A, left orbit redrawn after Young (1985). B, 3D model of the left orbit. Abbreviations: N.II, optic nerve foramen; N.III, oculomotor nerve foramen; N.IIIa, foramen for anterior branch of N.III; N.IIIp, foramen for posterior branch of N.III; N.Vpf, foramen for the profundus nerve; cav. pro, lateral preorbital space; eys, eyestalk attachment area; op.lat, canal for the ramus ophthalmicus superficialis lateralis; pr.ant, antorbital process; ri, ridge separating lateral preorbital space from orbital cavity; v.pit, foramen for pituitary vein. 24

FIGURE 2.3 3D rendering (top) and line drawing (bottom) of right lateral surface of the braincase and endocavity of NHMUK P33580. Abbreviations: my3, myodome associated with cranial nerve III; my6, myodome associated with cranial nerve VI; my.a, anterior myodome; my.v, ventral myodome. Scale bar represents 5 mm.. 25

FIGURE 2.4 3D model (top) and line drawing (bottom) of the endocavity and braincase of NHMUK P33580, dorsal view. Scale bar represents 5 mm. 27

FIGURE 2.5 3D rendering of NHMUK P33580, ventral view . Scale represents 5 mm . . . 28

FIGURE 2.6 Drawing of the braincase of NHMUK P33580 in ventral view as preserved (top) and partly restored (bottom). Scale bar represents 5 mm.. 29

FIGURE 2.7 Internal view of the right orbit of *Shearsbyaspis* with dorsal part of the orbital wall removed to reveal the interpreted position of the extrinsic eye-muscle myodomes and related innervations. Abbreviations: N.II, optic nerve canal; N.III oculomotor nerve canal; N.IV abducens nerve canal; N.V 2,3 trigeminal maxillary and mandibular canal; N.VII, main facial nerve canal; N.VII hm, canal for the hyomandibular branch of the facial; my.a, anterior myodome for an oculomotor-innervated eye-muscle; my.v, ventral myodome for an oculomotor-innervated eye-muscles; my3, myodome for an oculomotor-innervated eye-muscle; my6, myodome for abducens-innervated eye-muscles. Scale bar represents 2.5 mm. 30

FIGURE 2.8 The parasphenoid of *Shearsbyaspis oepiki*. A, tomogram of the parasphenoid in coronal section. B, 3D rendering of the parasphenoid in ventral view. C, tomogram of the parasphenoid in axial section. Scale bar represents 2 mm. . . 32
FIGURE 2.9 3D model (top) and line drawing (bottom) of the endocast of NHMUK P33580, ventral view. Scale bar represents 5 mm. 35
FIGURE 2.10 3D model of the endocast of NHMUK P33580 with the addition of the endocast of the orbital cavity, ventral view. Scale bar represents 5 mm. 37
FIGURE 2.11 The morphology of the skeletal labyrinth of *Shearsbyaspis* (left) and *Macropetalichthys* (right) compared. *Macropetalichthys* is redrawn from Stensiö (1969) with original labelling. The "anterior ampulla" is a doubtful interpretation (see text). . . . 40
FIGURE 2.12 The distribution of the parasphenoid, the optic fissure and of the transverse pituitary vein on different unrooted topologies showing the evolutionary cost for each topology. A, data matrix with the scoring of the characters for each examined taxa. B, topology 1 represents the most parsimonious output for the distribution of: 1a, parasphenoid; 1b, optic fissure; 1c, transverse pituitary vein. C, topology 2 represents the character distribution with a paraphyletic Placodermi as found in Giles et al., 2015. D, topology 3 tests the result with a monophyletic Placodermi as found by King et al. (2016). E, topology 4 presents a monophyletic Placodermi with *Shearsbyaspis* resolved as sister to arthrodires. F, topology 5 presents a monophyletic subset of placoderms with *Shearsbyaspis* resolved as sister to the rest of the placoderms. 42
FIGURE 2.13 Endocranial cavities of several gnathostomes, in ventral view, highlighting the morphology of the trigeminal, abducens and facial nerves and of the pituitary vein. A, *Shearsbyaspis*, a petalichthyid placoderm. B, *Norselaspis*, an osteostracan (after Janvier, 1981). C, *Shuyu*, a galeaspid (after Gai et al. 2011). D, *Cladodoides*, a chondrichthyan (after Maisey, 2005). E, *Lawrenciella*, an osteichthyans (after Hamel and Poplin 2008). F, *Kujdanowiaspis*, an arthrodire placoderm (after Goujet 1984a). G, *Brindabellaspis*, an "acanthothoracid" placoderm (after Young 1980). H, *Romundina*, an "acanthothoracid" placoderm (after Dupret et al. 2014). Not to scale. 47

FIGURE 3.1 Skull roof and sensory lines of A13047. A, original photograph in dorsal view (from Ørvig 1957). B, 3D model in dorsal view; C restoration of the dermal skull roof pattern and sensory line of *Ellopetalichthys*, based on this study and Ørvig (1957); D, 3D model in right lateral view. Scale bars represent 10 mm. . 55

FIGURE 3.2 3D model (top) and line drawing (bottom) of the endocavity and braincase of A13047, dorsal view. Abbreviation given in the text. Scale bar represents 0.5 cm. 57
FIGURE 3.3 3D model (top) and line drawing (bottom) of the endocavity and braincase of A13047, ventral view. Abbreviation given in the text. Scale bar represents 5 mm.. 58
FIGURE 3.4 3D model (top) and line drawing (bottom) of the occipital region of A13047, posterior view. Scale bar represents 5 mm. 61
FIGURE 3.5 Line drawing of the endocavity and braincase of A13047, ventral. Transparency has been applied to show the relationships between some nerve canals and endocranial fossae. Abbreviation for nerves given in the text.Scale bar represents 5 mm. 64
FIGURE 3.6 Line drawing reconstruction of the endocavity of A13047, dorsal view. Abbreviation for nerves given in the text. Scale bar represents 1 cm.. 65
FIGURE 3.7 The morphology of the skeletal labyrinth of *Shearsbyaspis* (left), *Macropetalichthys* (center) and *Ellopetalichthys* compared. *Macropetalichthys* is redrawn from Stensiö (1969) with label changed after chapter 2 and this chapter. Abbreviations: a.ampulla, anterior ampulla; a.semi.c, anterior semicircular canal; d.end, endolymphatic duct; e.ampulla, external ampulla;, e.semi.c, external semicircular canal; f.end, endolymphatic fossa; o.end, endolymphatic opening; p.ampulla, posterior ampulla; p.semi.c, posterior semicircular canal; sac.end, endolymphatic sac; N. VII, facial nerve; N.VIII, acoustic nerve; N. IX, glossopharyngeal nerve; N. X, vagus nerve. Not in scale. 69
FIGURE 3.8 Occipital region of the petalichthyids *Ellopetalichthys* ("spoon-like" neck joint) and *Wijdeaspis* ("spoon-like" neck joint) (after Young 1978), the quasipetalichthyids *Pauropetalichthys* (possibly "spoon-like" neck joint) (after Pan et al. 2015) and *Diandongpetalichthys* ("spoon-like" neck joint) (after Zhu 1991), the ”acanthothoracid” *Arabosteus* (sliding neck joint) (after Olive et al. 2011) and the phlyctaenioid arthrodire *Buchanosteus* (ginglymoid neck joint) (after Young 1979). Ventral view. Not to scale.. 72

FIGURE 3.9 Occipital region in posterior view of of the petalichthyids *Ellopetalichthys* (spoon-like neck joint) and *Wijdeaspis* (spoon-like neck joint) (after Young, 1978), the actinolepid arthrodire *Kujdanowiaspis* (sliding neck joint) (after Stensiö 1969), the "acanthothoracid" *Arabosteus* (sliding neck joint) (after Olive et al. 2011), the phlyctaenioid arthrodire *Buchanosteus* (ginglymoid neck joint) (after Young 1979) and the antiarch *Yunnanolepis* ("reverse-ginglymoid" neck joint) (after Zhang, 1980). Not to scale. 73

FIGURE 3.10 Braincase in ventral view of of the petalichthyids *Ellopetalichthys*, the "acanthothoraicic" *Brindabellaspis* (after Young, 1980) and the arthrodires *Dicksonousteus* (after Goujet 1984a) and *Buchanosteus* (after Young 1979). Not to scale. 77

FIGURE 4.1 Photographs of 7656. A, dorsal view; B, dorsal view; C close-up on the ornamentation of the premedian plate; D, close-up on the ornamentation of the central area of the skull roof. 86

FIGURE 4.2 3D model (top) and line drawing (bottom) of the skull roof and braincase of 7656, dorsal view. Scale bar represents 10 mm. 88

FIGURE 4.3 3D model (top) and line drawing (bottom) of the orbital region of 7656, anterolateral view. Abbreviations in abbreviation list. Scale bar represents 5 mm. 90

FIGURE 4.4 3D model (top) and line drawing (bottom) of the orbital region of 7656, posterolateral view. Abbreviations in abbreviation list. Scale bar represents 5 mm. 91

FIGURE 4.5 3D model (top) and line drawing (bottom) of the endocavity of 7656, dorsal view. Abbreviation in abbreviation list. Scale bar represents 10 mm. 95

FIGURE 4.6 3D models of the skull roof and endocast of 7656, right lateral view. A, complete view; B, right view with transparent skull roof; C, endocavities only. Scale bar 5mm 97

FIGURE 4.7 3D model (top) and line drawing (bottom) of the endocavity of 7656, ventral view. Abbreviation in abbreviation list. Scale bar represents 10 mm. 100

FIGURE 4.8 3D model (top) and line drawing (bottom) of the skull roof and braincase of 7656, ventral view. Scale bar represents 10 mm. 102

FIGURE 4.9 3D model (top) and line drawing (bottom) of the occipital area of 7656. A, posterior view; B, ventral view. Abbreviations in abbreviation list. Scale bar represents 10 mm.. 105

FIGURE 4.10 The morphology of the premedian plate and ethmoid commissure in the "acanthothoracid" *Kolymaspis*, the antiarch *Asterolepis* (after Lukševičs 2001), the "acanthothoracid" *Romundina* (after Ørvig 1975; Dupret et al. 2010) and the rhenanid *Gemuendina* (after Gross 1963; Denison 1978). All in dorsal view. Not in scale. 109

FIGURE 4.11 The morphology of the canals of the preorbital region in *Kolymaspis* (A,B,C) and *Brindabellaspis* (D, E, F) (after Young, 1980). Not in scale. A, ventral view; B, dorsal view; C, lateral view; D, ventral view with original labelling by Young (1980); E, dorsal view with original labelling from Young (1980); F, lateral view with the new labelling after this work. Abbreviations: c.pro, preorbital canals; c.prod, dorsal preorbital canal; c. prov, ventral preorbital canal; gr.max, groove for the maxillary branch of the trigeminal nerve; V maxillary, maxillary branch of the trigeminal nerve; V ophthalmicus superficialis, ramus ophthalmicus superficialis of the trigeminal nerve; V profundus, profundus branch of the trigeminal nerve; VII buccalis lateralis, ramus buccalis lateralis of the facial nerve. 112

FIGURE 4.12 The morphology of the skeletal labyrinth of several stem gnathostomes. From left to right, top to bottom: the "acanthothoracid" placoderm *Brindabellaspis* (after Young 1980), the "acanthothoracid" placoderm *Kolymaspis*, the "acanthothoracid" placoderm *Romundina* (after Dupret et al. 2017), the arthrodiran placoderm *Dicksonosteus* (after Goujet, 1984a), the petalichthyid placoderm *Ellopetalichthys* (from chapter 3), the rhenanid placoderm *Jagorina* (after Stensiö 1969), the galeaspid *Shuyu* (after Gai et al. 2011) and the osteostracan *Norselaspis* (after Janvier, 1981). Not to scale. 115

FIGURE 4.13 The position of the nasal capsules inside the orbit in the "acanthothoracid" *Kolymaspis*, the "acanthothoracid" *Brindabellaspis* (after Young 1980) and the arthrodire *Parabuchanosteus* (after Young 1979). Not to scale. 118

FIGURE 5.1 Strict consensus tree arising from the parsimony ratchet analysis (183 MPTs, tree lenght 1174) 179

FIGURE 5.2 Strict consensus trees from the Parsimony Ratchet (left) and the TNT analysis (right) for the placoderm clade. 181

FIGURE 5.3 Strict consensus trees from the Parsimony Ratchet (left) and the TNT analysis (right) for the jawed vertebrate clade with outgroups and "traditional" placoderms collapsed.. 183

FIGURE 5.4 Majority-rule consensus tree resulting from Bayesian inference analysis. Frequencies of bipartitions among sampled trees (Bayesian posterior probabilities) are indicated for each node. 184

FIGURE A.1 Strict consensus tree resulting from TNT analysis. 240

FIGURE A.2 Majority-rule consensus tree for "placoderms" resulting from Bayesian inference analysis. Frequencies of bipartitions among sampled trees (Bayesian posterior probabilities) are indicated for each node. 241

FIGURE A.3 Majority-rule consensus tree resulting from Bayesian inference analysis. Outgroups and "traditional" placoderms collapsed. Frequencies of bipartitions among sampled trees (Bayesian posterior probabilities) are indicated for each node. . 242

CHAPTER 1

INTRODUCTION

Living vertebrates comprise over 66,000 species, exhibiting an incredible array of ecological and morphological diversity, dominating many habitats and niches on our planet. Extant vertebrate diversity comprises two principal groups, the jawless Cyclostomata (hagfishes and lampreys) and the jawed Gnathostomata. Modern jawed gnathostomes include both chondrichthyans (sharks, skates and rays, and ratfishes) and osteichthyans (bony fishes and tetrapods). Modern gnathostomes represent the vast majority of living vertebrates and are unique in their possession of vertically biting jaws, paired fins, a horizontal semicircular canal in the inner ear and other soft anatomical and physiological features: they are thus the most studied group of animals.

In spite of a general scientific consensus on deep phylogenetic relationships of modern gnathostomes, our understanding of the early morphological history of the group is unclear. This is mainly related to the great morphological gap left by the extinctions of numerous lineages during the more than 420 million years of gnathostome evolution. The ancestral condition of modern gnathostomes and the evolutionary steps leading to their origin are thus incompletely understood from living groups alone. For this reason, we must turn to the fossil record in order to reconstruct the early morphological evolution and palaeobiological significance of the origin of jawed vertebrates.

The fossil record of vertebrates from the Palaeozoic Era (about 541-252 million years ago) comprises an array of forms of much-debated phylogenetic affinities, but generally agreed to represent the oldest vertebrates and gnathostomes (Janvier, 1996a). This fossil archive includes the earliest members of the two extant gnatho-

stome divisions, (chondrichthyans and osteichthyans) which together delimit the gnathostome crown group, as well as an array of enigmatic jawless and jawed forms (Fig. 1.1). A significant phylogenetic advance in the last three decades has been the recognition that the armoured jawless fishes of the Palaeozoic (traditionally called "ostracoderms") form a paraphyletic gnathostome stem group (Forey, 1984; Forey and Janvier, 1993; Donoghue et al., 2000; Janvier, 2008, 2015) (Fig. 1.1). These results have laid a foundation for subsequent studies of gnathostome origins by establishing approximate sequences of character evolution leading to modern gnathostomes. However, even though the fossil record of these early vertebrates has been known and studied for almost two centuries, the transition from jawless to jawed vertebrates and the phylogeny of the more crownward parts of the gnathostome stem lineage, the group called placoderms (Fig. 1.1), remain the principal problems in the study of the origin of modern jawed gnathostomes (Brazeau and Friedman, 2014, 2015).

The group collectively known as placoderms (early Silurian to Late Devonian) represents the only examples f stem-gnathostomes known to have jaws. Placoderms are characterized by a heavy dermal exoskeleton, covering the head and the shoulder girdle, and by bony jaw plates. Ranging from the early Silurian to the Late Devonian, they represent one of the most diverse groups of Palaeozoic fish (Fig. 1.2). Several different placoderm subgroups have been recognized (Stensiö, 1969; Denison, 1978; Janvier, 1996a), historically distinguished by the pattern of dermal plates and ornamentation (see Young 2010 for a brief review).

Placoderms possess pelvic fins and three pairs of semicircular canals and these characters, in addition to jaws, support their phylogenetic affinity to crown gnathostomes to the exclusion of all other stem-group gnathostomes (Young, 1986; Goujet, 2001; Goujet and Young, 2004). Hence, they occupy an important position in studies of character transformation near the origin of the last common ancestor of modern gnathostomes. However, even though placoderms have been known and studied for nearly two centuries, their systematic position and their relationship with extant and

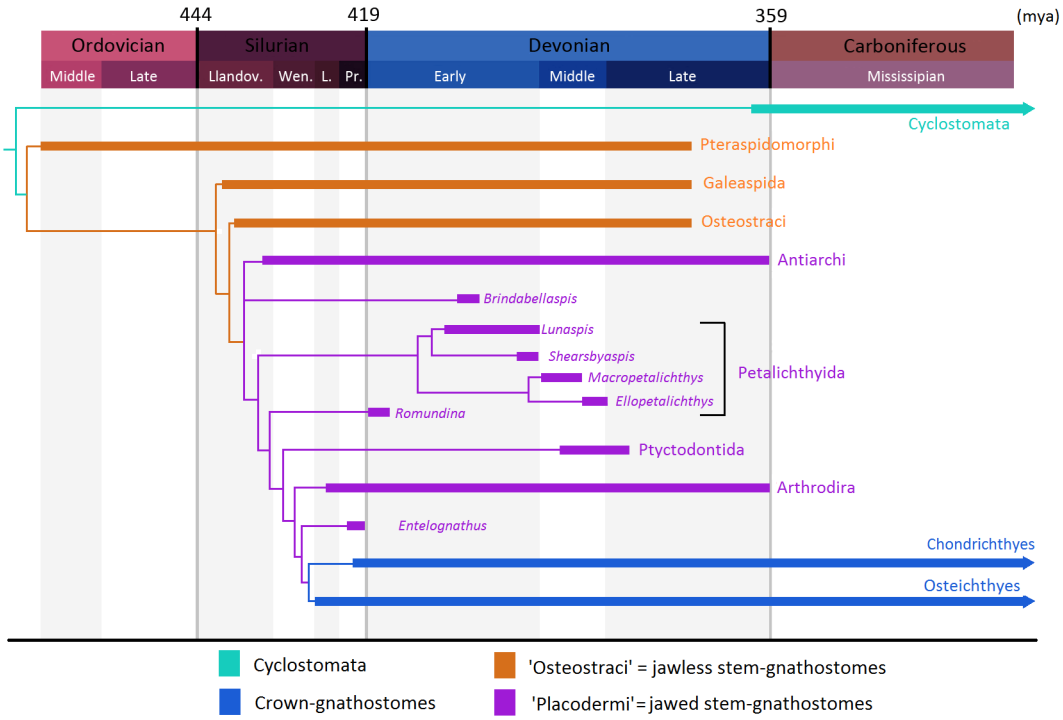

FIGURE 1.1: Composite tree showing the relationships of modern gnathostome lineages and their jawless and jawed Palaeozoic representatives through time, with some taxa omitted for clarity and including the key petalichthyid taxa analysed in this study. Topology and time calibration from Zhu and Wang (1996) for Petalichthyida and Brazeau and Friedman (2015) for the rest of the taxa.

extinct vertebrates remain highly debated (Brazeau, 2009; Brazeau and Friedman, 2014). This is in part related to how placoderm characters have been interpreted, often reflecting scientific fashions of particular eras. Indeed, new discoveries and reinvestigations of several stem gnathostomes have recently cast doubts on our current understanding of their relationships and have shifted our interpretations of the evolutionary meaning of the different lineages (Gai et al., 2011; Zhu et al., 2013; Giles et al., 2015b; Zhu et al., 2016).

1.1 AN OVERVIEW ON THE PLACODERM PROBLEM

Placodermi was initially erected by M'Coy (1848) as a group of both jawless and jawed fish, characterized by large, tuberculated plates protecting the head and the trunk, and aligned with the extant gnathostomes (Huxley, 1861; Newberry, 1875;

Crane, 1877; Cope, 1882, 1889; Regan, 1904). Nevertheless, even then there was disagreement on placoderm monophyly, with some authors considering them a polyphyletic assemblage of taxa (Woodward, 1891). In the beginning of the last century, the discovery of new specimens and more detailed re-examinations led to the reunion of the placoderms (Dean, 1899, 1901; Patten, 1904; Hussakof, 1905, 1906; Stensiö, 1925), even if their membership varied, for example with the inclusion of some "acanthodians" (Watson, 1937; Moy-Thomas, 1939; Romer, 1945, 1966). Placodermi as an early group of jawed fish phylogenetically close to modern gnathostomes became spread and accepted, setting the scene for the modern concept of placoderms (Gross, 1937; Ørvig, 1957; Stensiö, 1963b, 1969; Moy-Thomas and Miles, 1971; Jarvik, 1980).

The second half of the last century saw the emergence of placoderm systematics based on modern phylogenetic notions and character comparison. Pioneer authors were Denison (1975) and Miles and Young (1977), who reviewed the anatomy of placoderms and centred their systematic hypotheses on the distribution of these characters. Following these works came several investigations into placoderm interrelationship and affinity with modern gnathostomes (e.g. Young 1980; Gardiner 1984a; Goujet 1984a,b; Forey and Gardiner 1986; Young 1986). Some authors related them to osteichthyans (Forey, 1980; Gardiner, 1984b,a; Forey and Gardiner, 1986), based on the presence of dermal armour, to chondrichthyans using endocranial features and the presence of claspers (Miles and Young, 1977; Jarvik, 1980; Goujet, 1982), or resolving them as the sister-clade to all the other jawed vertebrates (Schaeffer, 1975; Denison, 1978; Young, 1986). However, the primary interest in these works was investigating the interrelationships within placoderms rather than evaluating the monophyly of the group and their unique synapomorphies. Indeed, their hypotheses implicitly assumed the validity of Placodermi as a group.

Placoderm monophyly was given its first explicit empirical justification by Goujet (1982, 1984a,b, 2001) and later Young (1986, 2008, 2009, 2010), who proposed a series of placoderm synapomorphies. However, these characters have been shown

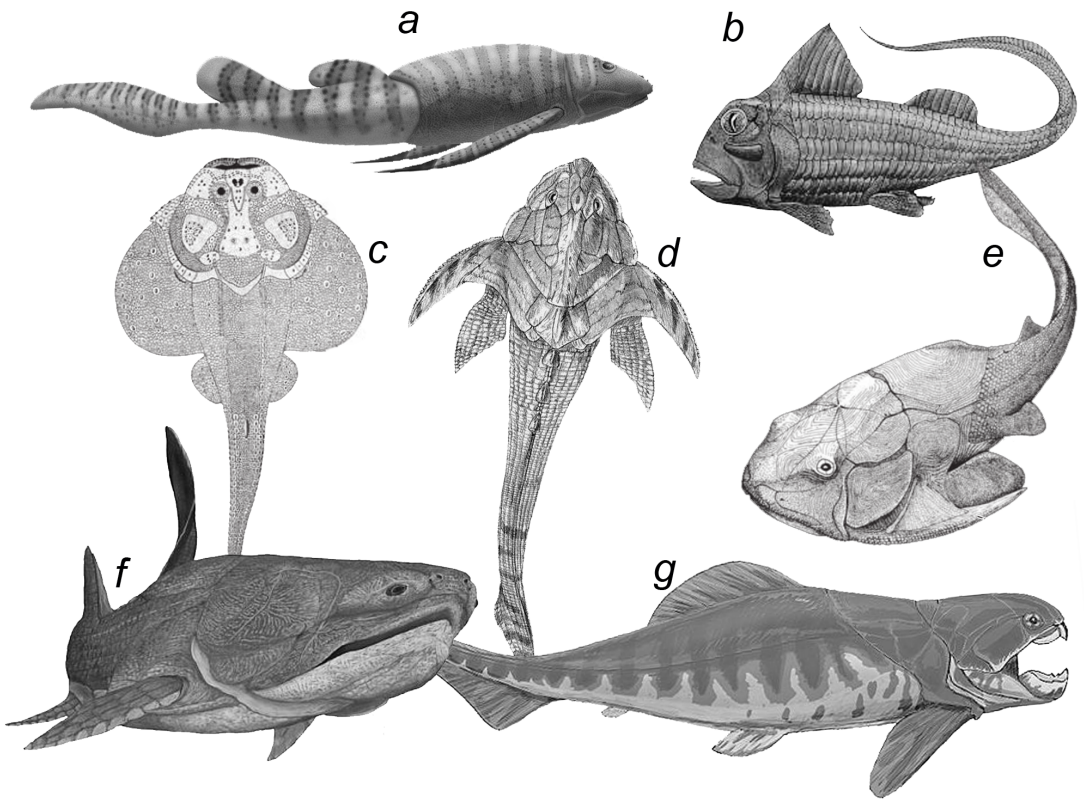

FIGURE 1.2: Restoration of various placoderms (not in scale) to show placoderms diversity. (a) The antiarch *Bothriolepis*; (b) *Materpiscis*, a ptyctodontid; (c) *Gemuendina*, a rhenanid; (d) the petalichthyid *Lunaspis*; (e), *Wuttagoonaspis*, a wuttagoonaspids arthrodire; (f), *Entelognathus*, a maxillate placoderm ; (g) the arthrodire *Dunkleosteus*. Pictures from http://www.eartharchives.org, Kahless28 on DeviantArt, Young 2010, Zhu et al. 2013 and Dmitry Bogdanov on Wikipedia.

to either be not unique of placoderms, possibly gnathostomes plesiomorphies, or not universally distributed in all placoderm groups, and therefore cannot be used to group all placoderms *a priori* (Brazeau and Friedman, 2014). Furthermore, these lists of synapomorphies were based on the prior assumption of placoderm monophyly.

Despite the great diversity of placoderm fossils, only a small proportion of them feature in these works. In fact, our understanding of this group is heavily influenced by its most diverse clade, Arthrodira. Arthrodiran placoderms have been studied in great details due to the good preservation of their head skeleton and therefore are often used as the interpretive model for placoderms (Coates and Sequeira, 2001;

Coates et al., 2017; Zhu et al., 2006, 2009). However, recent studies focussed on less known subgroups of placoderms have often found unexpected combinations of anatomical characters (Long et al., 2009; Rücklin et al., 2012; Dupret et al., 2014; Long et al., 2015; Brazeau et al., 2017). These have highlighted how the dominance of studies on arthrodiran placoderms is in fact biasing our perspective on an instead rather morphologically diverse group of animals (Fig. 1.2).

Among the more obscure subgroups of placoderms, Petalichthyida and "Acanthothoracida", for instance, have recently become central in the debate about placoderm relationships and primitive gnathostomes anatomical condition as they exhibit a combination of both jawless and jawed endocranial traits (Janvier, 1996b; Brazeau, 2009; Brazeau and Friedman, 2014; Dupret et al., 2014, 2017a). Consequently, these differences between those "jawless-looking" groups and the other placoderms have led some authors to question placoderm monophyly and to suggest that they instead represent a sub-grade of stem gnathostomes (Brazeau, 2009; Davis et al., 2012; Zhu et al., 2013; Dupret et al., 2014; Giles et al., 2015b).

Several recent phylogenetic studies (Brazeau, 2009; Davis et al., 2012; Zhu et al., 2013; Long et al., 2015; Giles et al., 2015b; Zhu et al., 2016) indeed failed to recover placoderm monophyly, resolving instead placoderms as a paraphyletic assemblage of jawed stem-gnathostomes, lying between the jawless forms and the crown-gnathostome node. However, these studies descend from the same dataset (Brazeau, 2009) and are, thus, not independent tests of placoderm paraphyly. Moreover, recent work by King et al. (2016) based on different phylogenetic techniques (i.e. Bayes analysis with tip-dating) have recovered a monophyletic Placodermi, highlighting how the controversy on placoderm monophyly and intrarelationship is still far from being resolved. This means that the role of placoderms in our understanding of gnathostomes evolution is still unclear.

1.1.1 **Petalichthyida**

Petalichthyida is a sub-group of flat-headed placoderms with dorsolaterally facing eyes, probably having had a demersal habit, characterized roughly by an elongated median skull-roofing bone (nuchal plate) and a unique pattern of the sensory line systems (Denison, 1978; Zhu, 1991) (Fig. 1.3). 19 genera of petalichthyids have been described so far, spanning from the late Silurian to the Late Devonian, with a global distribution (Zhu and Wang, 1996; Pan et al., 2015). However, despite the good number of taxa known, very few petalichthyid taxa have been investigated in detail, so that many aspects of their anatomy are still unclear. For this reason, the phylogenetic position of the Petalichthyida within the placoderms or the paraphyletic stem-gnathostomes is still disputed and the hierarchic character distribution of Petalichthyida remains obscure.

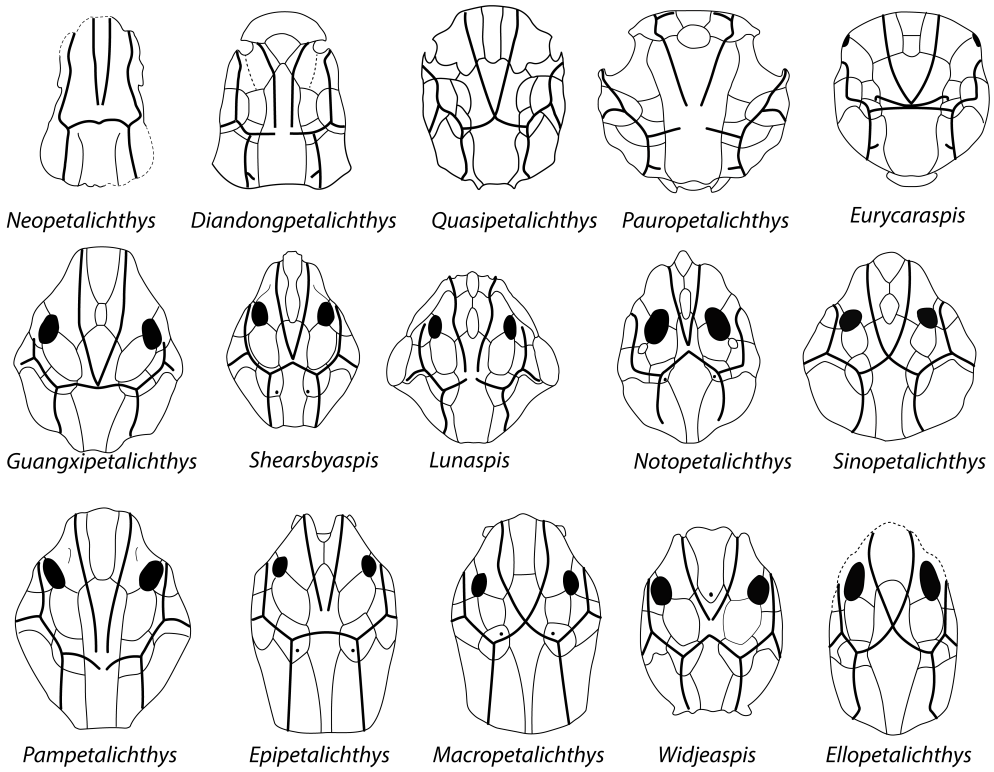

FIGURE 1.3: Restoration of the skull roof of the currently known petalichthyids (not in scale). Pictures redrawn from Denison 1978; Zhu 1991; Liu 1991; Zhu and Wang 1996; Ji 1996; Zhu 2000; Zhao and Zhu 2010; Pan et al. 2015

Due to a relative lack of knowledge on their endoskeleton, petalichthyids are represented by only a very small sample in contemporary gnathostome phylogenies (Brazeau, 2009; Davis et al., 2012; Zhu et al., 2013; Dupret et al., 2014; Giles et al., 2015b; Zhu et al., 2016; King et al., 2016), with *Macropetalichthys* being the only taxon which internal anatomy has been studied in detail (Stensiö, 1925, 1969). Moreover, little is known about the endocranial morphology of the earliest petalichthyids such as *Diandongpetalichthys*, *Eurycaraspis*, *Quasipetalichthys* and *Pauropetalichthys* (Fig. 1.3), making the relationship between them and the rest of the petalichthyids still unclear. In fact, these early Chinese forms, known as the quasipetalichthyids, have been suggested to be either sister group to the other petalichthyids (Zhu and Wang, 1996; Pan et al., 2015; Zhu et al., 2016) or to be in a more distant phylogenetic position, closer to phyllolepid arthrodires (Giles et al., 2015b). Since some quasipetalichthyids, such as *Eurycaraspis*, have been used as examples of petalichthyids in some recent analyses (Dupret, 2004; Dupret and Zhu, 2007; Dupret et al., 2009, 2017b), a deeper understanding of the systematics of the Petalichthyida is crucial as their unique combination of features constitute one of the main issues regarding placoderm monophyly and early gnathostomes evolution.

In chapter 2 and 3 of this thesis, I present the result from my investigation on the neurocranial anatomy of two petalichthyid placoderms, *Shearsbyaspis oepiki* Young 1985 and *Ellopetalichthys scheii* Kjaer 1915 (Fig. 1.3). They are the first petalichthyid endocavities to be investigated with CT scanning. They provide a great wealth of data improving our knowledge of petalichthyids as well as enabling a reappraisal of old material with new techniques.

The significance of petalichthyids to the issue of placoderm monophyly stems largely from the resemblance of their endocranial anatomy with the jawless osteostracans (Janvier, 1996b; Brazeau, 2009; Brazeau and Friedman, 2014). Osteostracans are considered the nearest jawless outgroup to the gnathostomes (Donoghue and Smith, 2001; Donoghue et al., 2006b) and are therefore pivotal in our understanding of early gnathostome character polarities. Petalichthyids and jawless osteostracans

differ from most other placoderms and crown-gnathostomes, for example, in the arrangement of the pituitary vein and trigeminal nerve, as well as in the morphology of some eye-muscles (Stensiö (1969); Janvier (1996b); Brazeau (2009); Brazeau and Friedman (2014) and chapter 2). Taken together, the general architecture of petalichthyid skulls is intermediate between conditions seen in the jawless osteostracans and the jaw-bearing placoderms. Thus it is fundamental to try to understand if these shared cranial conditions of petalichthyids and jawless outgroups are retained primitive gnathostome conditions or are independently derived. In chapter 5, we test the intra and interspecific relationships of petalichthyids by including 14 genera of petalichthyids in our large dataset of stem-gnathostomes, adding several characters related to our new findings. Results of this analysis are presented in chapter 5.

1.1.2 **"Acanthothoracida"**

The name "Acanthothoracida" has historically referred to a group comprising a series of taxa showing a peculiar mix of plesiomorphic features (e.g., dorsally placed eyes and nostrils) and apomorphic characters (e.g., distinct morphology of some skull roof plates) (Ørvig, 1975; Denison, 1978; Goujet and Young, 1995, 2004). Because of those similarities with jawless fishes, some authors have considered "acanthothoracids" to fall close to the root of jawed vertebrates and to represent the primitive condition for jawed vertebrate (Dupret et al., 2014, 2017a). Nevertheless, studies have failed to propose unambiguous synapomorphies for "Acanthothoracida", making the affinity and monophyly of the group contentious (Goujet, 1984b; Janvier, 1996a; Goujet and Young, 2004; Brazeau, 2009).

Out of the handful of known "acanthothoracids" (Gross, 1959; Ørvig, 1975; Mark-Kurik, 1973; Bystrow, 1956; Young, 1980; Olive et al., 2011; Vaškaninová and Ahlberg, 2017) (Fig. 1.4), only few "acanthothoracid" endocrania have been studied in detail (Young, 1980; Olive et al., 2011; Dupret et al., 2014, 2017a). Indeed, the most recent phylogenetic analyses on stem-gnathostomes usually include only *Brindabellaspis*

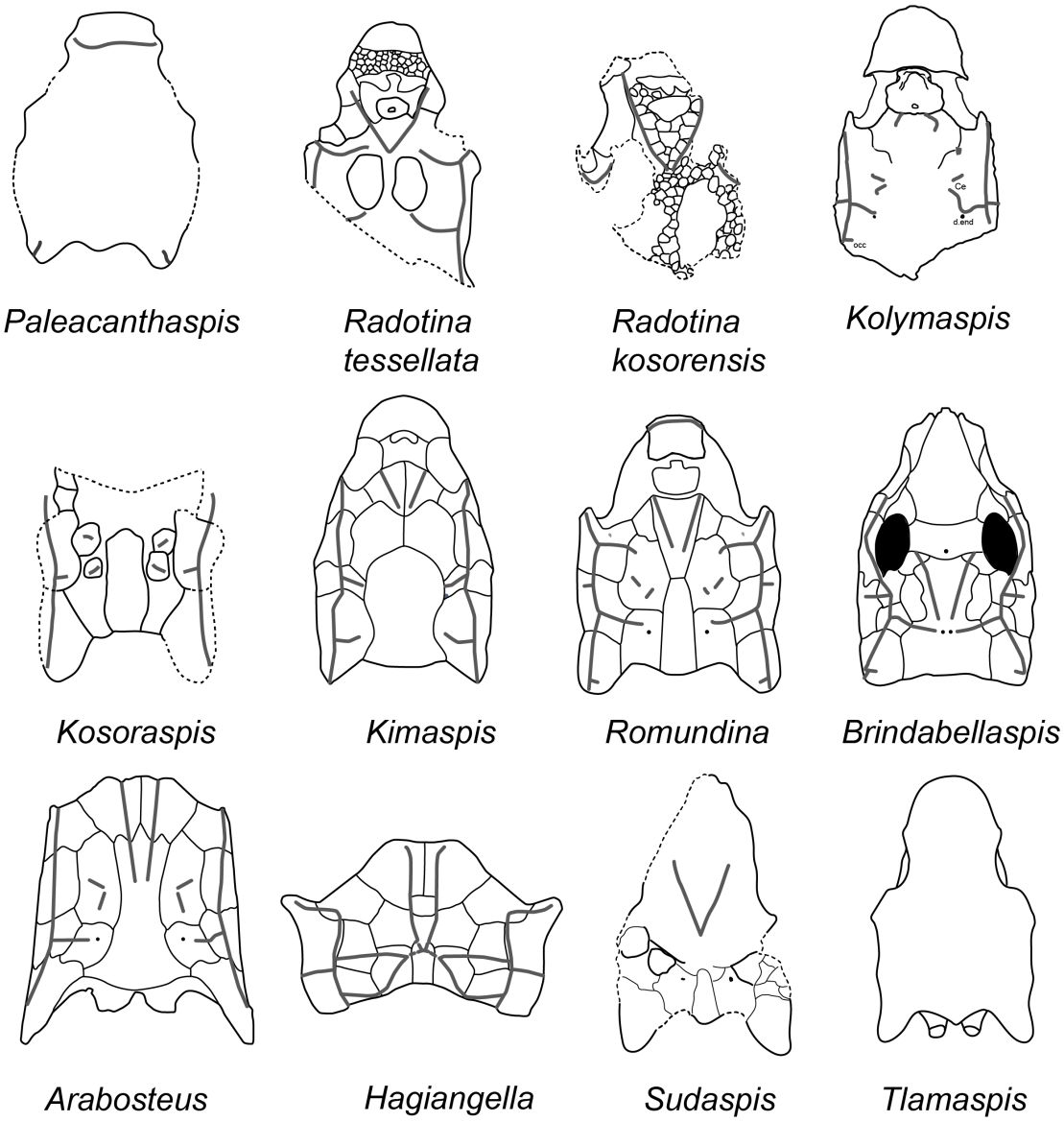

FIGURE 1.4: Restoration of the skull roof of the currently known "acanthothoracids" (not in scale). Pictures redrawn from Mark-Kurik 1973; Ørvig 1975; Denison 1978; Goujet 1984b; Young 2010; Dupret et al. 2011; Olive et al. 2011; Vaškaninová and Ahlberg 2017.

and/or *Romundina* among "acanthothoracids" (Brazeau, 2009; Davis et al., 2012; Zhu et al., 2013; Dupret et al., 2014; Giles et al., 2015b; Zhu et al., 2016; King et al., 2016) (Fig. 1.4). Some of these studies have resolved these taxa in distant positions, with *Brindabellaspis* being placed closer to the root of jawed vertebrates and with *Romundina* placed closer to crown-gnathostomes (Giles et al., 2015b; King et al., 2016). How-

ever, some studies have suggested that *Brindabellaspis* could represent a specialized form respect to a more "*Romundina*-like" generalized "acanthothoracid" morphology (King et al., 2016; Dupret et al., 2017a). This has cast doubts on the assumption that these placoderms exhibit the primitive condition for jawed vertebrates.

Obtaining a broader sample of neurocranial morphology from other "acanthothoracids" is thus vital in order to understand the anatomical diversity and phylogenetic significance of this group of animals. Moreover, including a broader sample of "acanthothoracids" in phylogenetic analyses is essential to try to polarize the morphology of these taxa and resolve the debate on the monophyly of the group. In chapter 4 of this thesis, we present new data on the neurocranial anatomy of the "acanthothoracid" *Kolymaspis sibirica* (Fig. 1.4), which shows a combination of anatomical features between *Romundina* and *Brindabellaspis* and thus offers a great contribution in illuminating the morphology of this group. Moreover, in chapter 5 we test the monophyly of "Acanthothoracida" including a large number of "acanthothoracids" taxa and characters to a broad dataset of stem-gnathostomes. The results and implications of this analysis are discussed in chapter 5.

1.2 INVESTIGATING STEM-GNATHOSTOMES NEUROCRANIA USING CT TECHNIQUES

Recent studies on early gnathostomes evolution have received great insight from the examination of braincase morphology. The braincase, or neurocranium, is a central structure of the vertebrate head, enclosing the brain cavity and the cranial nerve and blood vessels related to it. As such, the neurocranium constitutes a crucial source of information, as it holds many anatomical characters and features. Moreover, as a braincase is present in every vertebrate, the study of this structure is vital to be able to compare early vertebrates, a rather anatomically disparate group. Thus, comprehensive descriptions of braincase morphology constitute the base for our phylogenetic studies and interpretations of all placoderm diversity.

Successful examinations of the internal structures of stem-gnathostome braincases were carried out by Stensiö (1925, 1950, 1963b,a, 1969) initially using the Sollas' serial grinding technique (Sollas, 1904; Sollas and Sollas, 1914). This method involves grinding the specimen in multiple sections and photographing or drawing the exposed surface at each step. A three-dimensional wax model can be constructed from the resultant photographs and illustrations. However, the process completely destroys the original specimen and it is extremely time-consuming. Repeating the study and replicating any interpretations will depend on the quality of the records kept during these investigations and the resultant wax models.

The development of modern x-ray computed microtomogragphy (XR-μCT) now allows internal anatomical reconstructions of fossil vertebrates -even in microscopic detail- without destroying the specimen (Rogers, 1999; Sampson and Witmer, 2007; Pradel, 2010; Gai et al., 2011; Giles et al., 2015b) (Fig. 1.5). Furthermore, it is possible to use XR-μCT data to create virtual three-dimensional models of the scanned object. These can be viewed in any orientation, as well as virtually dissected or highlighted in chosen areas. In addition, the resultant dataset can be easily stored in portable device, are accessible in long term and are repeatable and revisable, allowing the verification of current interpretations (Sutton et al., 2001; Sutton, 2008; Sutton et al., 2014).

X-ray computed techniques have been recently used to investigate the neurocranial anatomy of several different group of both jawless and jawed vertebrates. These have uncovered previously unknown information that have improved our understanding of the evolution of early gnathostomes and revealed, for example, the presence of paired olfactory lobes in jawless fish associated with an unpaired nasal opening (Gai et al., 2011), in addition to helping to illuminate the early history of bony fishes (Lu et al., 2016). For this reason, in this thesis we used modern computed techniques to gather information on the neurocranial anatomy of the petalichthyids *Shearsbyaspis* and *Ellopetalichthys*, as well as of the "acanthothoracid" *Kolymaspis*.

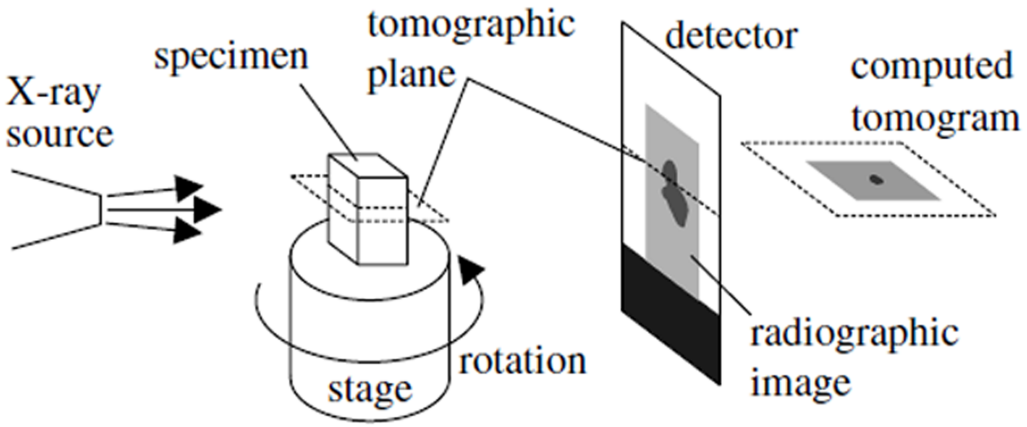

FIGURE 1.5: Summary diagram of the x-ray computed tomography technique. An x-ray beam is directed through the specimen which sits on a rotating stage in front of a detector. An individual projection from the detector is taken at each stage of rotation. After 180- or 360-degrees rotation, the resulting images can be reconstructed into a computed tomogram. The complete virtual dataset will be composed by a series of tomograms. From Sutton 2008.

The specimens examined in this thesis have been scanned at the Imaging and Analysis Centre at the Natural History Museum in London, using X-ray micro-CT scanner. The specimens were prepared for scanning by inserting them in a paper cylinder, filling the empty spaces with floral foam and securing them with a rubber band. Scanning were then accomplished by x-rays passing through a thick copper filter and taking around 6000 projections of the specimen while it was rotating. Segmentation of the resulting tomographic image sets have been completed using the software Mimics version from 15.01 to 19.01 (Materialise Technologielaan, Leuven, Belgium). Using defined grey value thresholds and the manual editing tools it is possible to segment the different anatomical parts of the dermal bones and braincase, as well as to create a space-fill model to represent the endocavity of the braincase. These are generated in separate masks to create independently manipulated virtual 3D objects. The 3D models can then be rotated, zoomed and combined each others, allowing a detailed investigation of the cranial cavity of the examined specimen. Also, 3D objects can be imported on appropriate program for digital visualization,

like the software Blender, which allows to produce high-quality render imagines with different degree of lighting and orientation. This permits elaborate and thorough anatomical descriptions and represents a great source of data for phylogenetic and comparative analysis.

1.3 PHYLOGENETIC ANALYSIS

To understand extant organismal diversity, a primary aim should be to reconstruct the historical events that led to this observed diversity. Phylogenetics forms the theoretical underpinning of all comparative investigations of deep evolutionary history, speciation and character evolution. This is particularly important when studying events in the geological past, such as the origin of jaws and the assemblage of modern vertebrates from their early ancestors.

In chapter 5, we provide a novel phylogenetic analysis based on a revised dataset from King et al. (2016), with addition on new characters and placoderm taxa, especially petalichthyids and "acanthothoracids". To date, this matrix represents the most comprehensive dataset for both petalichthyids and "acanthothoracids". Although being far from representing a definite and final solution to the debate of placoderm monophyly, this analysis has nonetheless reported some important results, for example the potential support for a monophyletic Placodermi, the non-support of a monophyletic "Acanthothoracida" and the position of petalichthyids (with the inclusion of ptyctodontids) as the sister group to all other non-maxillate placoderms within the placoderm clade. Implication for the primitive condition and the evolution of early jawed vertebrates are also discussed.

1.4 DATA ARCHIVING STATEMENT

Data underpinning this thesis are uploaded on figshare (links provided below). For any problem, the research team can be contacted at m.castiello13@imperial.ac.uk

Chapter 2:

The 3D models produced and analysed for *Shearsbyaspis oepiki*
https://figshare.com/s/7fc6522a7ca4e2930f39
Video of the tomographic section through the parasphenoid
https://figshare.com/s/06c097d925ab4d121f4e.

Chapter 3:

The 3D models produced and analysed for *Ellopetalichthys scheii*
https://figshare.com/s/8250d8abd8a86129ac3b

Chapter 4:

The 3D models produced and analysed for *Kolymaspis sibirica*
https://figshare.com/s/87c6b5c62465c00b11f7

Chapter 5:

Data matrix, parsimony ratchet and bayesian analysis scripts
https://figshare.com/s/6822a517712f68751f84

1.5 CONTRIBUTION OF AUTHORS

Chapter 2: The braincase and brain cavity of the Petalichthyid *Shearbyaspis oepiki* Young 1985 (Placodermi, Early Devonian)

This chapter has been written in the style of a manuscript for *Palaeontology*. The manuscript has already been accepted and it is currently under preparation for printing.

Dr. Martin D. Brazeau conceived this project and conducted the CT scanning. I generated the CT renderings and produced figures and tables. I wrote the description and interpretation of the specimen data. Dr. Martin D. Brazeau provided comments and edits on the drafts. Dr. Zhu Min and an anonymous reviewer provided useful comments, which were incorporated into the manuscript presented here. Anna Jarve contributed helping with the drawings.

Chapter 3: Re-examination of the endocranial morphology of *Ellopetalichthys scheii* Kjaer 1915 (Placodermi, Middle Devonian), with remarks on the inner ear and occipital joint in petalichthyids

Dr. Martin D. Brazeau and Dr. Matt Friedman conceived this project and conducted the CT scanning. I generated the CT renderings and produced figures and tables. I wrote the description and interpretation of the specimen data. Dr. Martin D. Brazeau provided comments and edits on the drafts. Dr. Anna Jarve contributed helping with the drawings.

Chapter 4: Redescription of the anatomy of *Kolymaspis sibirica* Bystrow 1956 (Vertebrata: Placodermi) using X-ray computed tomography

This work was conceived by Dr. Martin Brazeau and Dr. Matt Friedman. The basis of this chapter were firstly part of an MRes project by Charline Pinna and supervised by me and Dr. Martin Brazeau. Charline Pinna generated the initial CT renderings and the first interpretation for the orbital area of the specimen. I then completed the CT renderings and described, illustrated and interpreted the whole of the specimen data. Dr. Martin D. Brazeau conceived the project, conducted the CT scan and provided comments and edits on the drafts. Anna Jarve contributed helping with the drawings. We also thank Dr. Sasha Ivanov for contributing to this work and providing the specimen.

Chapter 5: Phylogenetic analysis of placoderms with a particular attention of the relationships of petalichthyids and "acanthothoracids"

I planned and implemented the experimental and procedural approaches. I compiled the data matrix, revised and build the characters set and scored the matrix. I performed the data analyses, created figures and wrote the manuscript. Dr. Martin D. Brazeau provided comments on the drafts of the manuscript, along as advising on all stages of the experimental process. I thank Sam Giles and Richard Dearden for useful comments during the experimental process.

CHAPTER 2

THE BRAINCASE AND BRAIN CAVITY OF THE PETALICHTHYID *Shearbyaspis oepiki* YOUNG 1985 (PLACODERMI, EARLY DEVONIAN)

2.1 INTRODUCTION

Placoderms are generally considered to be the outgroup of modern jawed vertebrates (Young, 1986; Janvier, 1996a,b; Goujet, 2001; Goujet and Young, 2004; Brazeau, 2009) and thus illuminate key phases in the stepwise evolution of jawed vertebrate anatomy. Placoderms have received renewed attention owing to recent investigations casting doubt on their monophyly (Friedman, 2007; Brazeau, 2009; Davis et al., 2012; Zhu et al., 2013; Long et al., 2015; Zhu et al., 2016). This debate impacts evolutionary questions ranging from the problem of morphological intermediates between jawless and jawed vertebrates to the evolution of vertebrate reproductive modes (Zhu et al., 2013, 2016; Brazeau and Friedman, 2014; Long et al., 2015). In this paper, we add new observational data on the anatomy and diversity of placoderm cranial conditions and critically evaluate competing hypotheses of placoderm relationships in light of these data.

Of particular importance in phylogenetic studies of early vertebrates is the anatomy of the braincase. Our knowledge of placoderm endocranial anatomy is derived largely from the most diverse subgroup: the Arthrodira. Until recently, arthrodires were the predominant representatives of the placoderms, functioning as outgroup taxa in analyses of chondrichthyan (Coates and Sequeira, 1998, 2001) and osteichthyan relationships (Zhu and Schultze, 1997; Zhu et al., 1999a, 2006, 2009). As arthrodire braincases are usually interpreted in light of crown gnathostome models,

this potentially biases phylogenetic investigations (Brazeau and Friedman, 2014). Since the works of Stensiö (1925, 1950, 1963b,a, 1969), only a few detailed descriptions of non-arthrodiran braincases have been published (Ørvig, 1975; Young, 1978, 1980; Trinajstic et al., 2012; Dupret et al., 2017a). Many of these non-arthrodiran taxa exhibit braincases departing significantly from an arthrodire "model" and represent significant source of data on placoderm relationships (Brazeau, 2009).

Petalichthyida are non-arthrodiran placoderms that have recently become central in the debate about placoderm relationships and primitive gnathostome anatomical conditions. This is due to perceived endocranial similarities with the jawless osteostracans and galeaspids (Janvier, 1996a,b; Brazeau, 2009; Brazeau and Friedman, 2014). This has led to rejections of placoderm monophyly in numerical phylogenetic analyses, resulting in their recovery as a sub-grade of stem-group gnathostomes (Brazeau, 2009; Davis et al., 2012; Zhu et al., 2013, 2016; Dupret et al., 2014; Giles et al., 2015b).

Petalichthyida is presumed to be a monophyletic group, characterized by an X-shaped sensory line pattern, two pairs of paranuchal plates and an elongated nuchal plate (Janvier, 1996a). Within Petalichthyida, two divisions have been recognized: Macropetalichthyidae (Eastman, 1898) and Quasipetalichthyidae (Liu, 1991). Along with these are forms like *Diandongpetalichthys* (P'an and Wang, 1978), often recovered as sister to all other petalichthyids (Zhu, 1991; Pan et al., 2015). Phylogenetic analyses suggest that quasipetalichthyids could either be sister group to the other petalichthyids (Zhu and Wang, 1996; Pan et al., 2015) or fall in a more distant phylogenetic position from *Macropetalichthys*, closer to phyllolepid arthrodires (Giles et al., 2015b). Therefore, some uncertainty about the monophyly of petalichthyids exists, though the latter analysis lacked many of the aforementioned petalichthyid apomorphies. Nevertheless, some of the characters used to define Petalichthyida, such as the X-shaped sensory line pattern, are also present in other non-petalichthyid placoderms (e.g. ptyctodonts) and might therefore be uninformative in characterizing petalichthyids. Furthermore, the phylogenetic position of the Petalichthyida within the stem-

gnathostomes is still disputed. Since some quasipetalichthyds, such as *Eurycaraspis*, have been used as examples of petalichthyids in recent analyses (Dupret et al., 2009, 2017b; Zhu et al., 2010a), a better understanding of the systematics of the Petalichthyida will be crucial. A more detailed analysis of petalichthyid relationships is currently being undertaken by the authors.

Very few neurocranial remains are known for petalichthyids. The braincase of *Macropetalichthys*, a macropetalichthyid, currently being the most studied taxon. The first endocranial description of this placoderm was carried out by Stensiö (1925) and was based on a specimen from the Middle Devonian Onondaga Formation, New York. In this original description, the endocranial surface was exposed by fracturing the specimen with a hammer. Stensiö (1963b,a, 1969) later revised this reconstruction based on a mechanically prepared specimen, offering a more complete description of the endocavity. However, no other comprehensive examinations of petalichthyid internal anatomy have been carried out since, meaning that our knowledge of the endocranial anatomy of this group relies almost solely on Stensiö's interpretations.

Here we present our investigation of the cranial anatomy of *Shearsbyaspis oepiki* Young 1985, a petalichthyid placoderm from the Early Devonian of New South Wales, Australia. It was first described by Young (1985) on the basis of two specimens: an incomplete skull roof with endocranial ossifications attached and an incomplete skull roof preserved in visceral view. The holotype of *Shearsbyaspis*, is notable for its three-dimensional preservation and perichondrally ossified neurocranium. The specimen was initially prepared using acetic acid, which allowed Young (1985) to describe important details of the orbit and the anterolateral margin of the braincase. However, this has also eliminated much of the matrix infill, allowing unimpeded X-ray computed tomography scanning. Our study reveals the external endocranial surface, the endocranial cavity, cranial nerve and blood vessel canals, as well as additional details of the dermal and oral skeleton. These results will help to inform current debates on early jawed vertebrate anatomical conditions.

2.2 MATERIAL AND METHODS

The following description of the neurocranium of *Shearsbyaspis oepiki* Young 1985 is based on the holotype specimen (NHMUK P33580), an incomplete skull roof with endocranial ossification. The specimen originates from the Shearsby's Wallpaper outcrop, in the *Spirifer yassensis* Limestone, the lowest unit of the Taemas Formation in the Murrumbidgee Group in New South Wales, Australia, dated to the Early Devonian (Emsian; Young 1978, 1980, 1985).

The specimen was scanned at the Imaging and Analysis Centre at the Natural History Museum in London, using a Nikon Metrology HMX ST 225 X-ray micro-CT scanner. Scanning parameters were: 180 kV; 180 A; 0.1 mm thick copper filter; 6284 projections and voxel size 15.3 μm. The resulting tomographic data was segmented and rendered in 3D using the software Mimics 15.01 (Materialise Technologielaan, Leuven, Belgium). The 3D models produced with Mimics were imported in Blender for scientific image preparation (following Garwood and Dunlop 2014).

Institutional abbreviations. CPC, Commonwealth Palaeontological Collection, Canberra, Australia; NHMUK, Natural History Museum, London, UK.

2.3 DESCRIPTION

2.3.1 **Skull roof**

PRESERVATION AND GENERAL FEATURES — NHMUK P33580 consists of an incomplete skull with most of the underlying neurocranial ossification preserved. The tip of the rostral plate and the remainder of the skull posterior to the otic region are missing. The dorsal side of the skull roof is exposed and well-preserved, showing clearly the pores of the lateral line system, the pineal foramen and the orbits (Fig. 2.1). The visceral surface of the skull roof is visible from the CT data, displaying the prominent ridges corresponding to the passages of the sensory canals.

The skull roof has a slight dorsally convex axial profile (Fig. 2.1). It reaches its maximum width at the level of the skeletal labyrinth, behind the posterior corner

of the orbit. The lateral margins of the skull narrow anterior to the orbits, forming a broad, snout-like projection. The orbits are dorsolaterally placed and display an anterodorsal torus, so that between the orbits the skull roof is slightly depressed (Figs 2.2-2.4). The individual dermal plates are rarely distinct but some margins can be inferred from ornamentation patterns and radiating ridges corresponding to ossification centres. The dermal ornamentation consists of low concentric or radiating ridges, with rounded tubercles irregularly located along them.

The skull roof pattern (Fig. 2.1D) has already been described and figured by Young (1985) and we agree with his interpretations. Initially, the complete separation of the preorbitals by rostrals and pineal elements present in *Shearsbyaspis* was assigned as a diagnostic feature of this taxon. However, the same feature has since been observed in *Pampetalichthys longhuansis* (Zhu and Wang, 1996; Zhu, 2000). Nevertheless, *Shearsbyaspis* differs from *Pampetalichthys* in having anastomotic posterior pit line and supraorbital canals and cannot be considered synonyms.

SENSORY LINE CANALS — The sensory lines canals of NHMUK P33580 are well-developed and clearly distinguishable on the dermal armour and illustrated in Figure 2.1D. They consist of enclosed tubes deeply situated in the bones, opening to the exterior through a single row of large pores, as in other petalichthyids and ptyctodontids (e.g. Stensiö 1925; Miles 1967; Denison 1978; Young 1978, 1985; Forey and Gardiner 1986; Zhu 1991; Trinajstic et al. 2012; Pan et al. 2015). Due to the incompleteness of the specimen, only the supraorbital sensory canals (soc) and part of the infraorbital sensory canals (ioc) are preserved in NHMUK P33580 (Fig. 2.1), but a complete restoration of the sensory line system of *Shearsbyaspis* can be made comparing both available specimens (NHMUK P33580 and CPC24622) as shown in Young (1985, text-fig. 5)

The supraorbital sensory canal opens as pores or grooves depending on the position in the skull (Fig. 2.1B). In the rostral part of the skull, anterior to the eyes, each canal opens in a broad, deeply sunken groove. Nearer and posterior to the eyes they

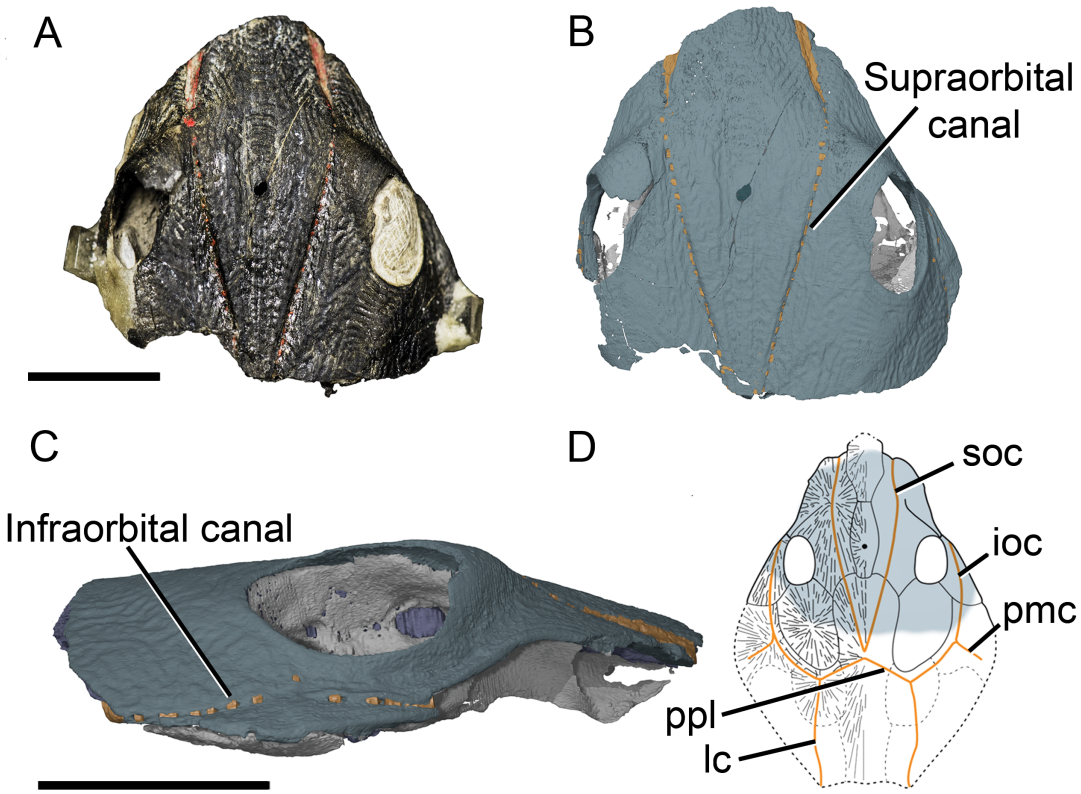

FIGURE 2.1: Skull roof and sensory lines of NHMUK P33580. A, photograph in dorsal view. B-C, 3D model in: B, dorsal; C, right lateral view. D, skull roof of *Shearsbyaspis*, redrawn after Young (1985), with the highlighted in blue. Abbreviations: ioc, infraorbital sensory canal; lc, main lateral line sensory canal; pmc, postmarginal sensory canal; ppl, posterior pit line canal; soc, supraorbital sensory canal. Scale bars represent 10 mm.

open as a row of distinct rounded and shallow pores. A similar condition is present in *Notopetalichthys* (Woodward, 1941) and *Ellopetalichthys* (Ørvig, 1957). There is a single enlarged pore opening marking the contact between the preorbital and nuchal plates as in the ptyctodontid *Materpiscis* (Trinajstic et al., 2012).

The infraorbital canal extends along the lateral margin of the postorbital plate and opens to the exterior as a single row of pores (Fig. 2.1C). The pores are more evenly spaced and sized in the posterior part of this sensory line, becoming a single narrow grove near the anterior part of the orbit. All the pore openings fall into a low, arcing line, except for a single pore situated as an outlier, nearer to the margin of the orbit (Fig. 2.1C). The tomographic image data show that this pore is associated with

a set of numerous short and narrow canals connecting the orbit to the infraorbital canal, possibly representing a special sensorial area.

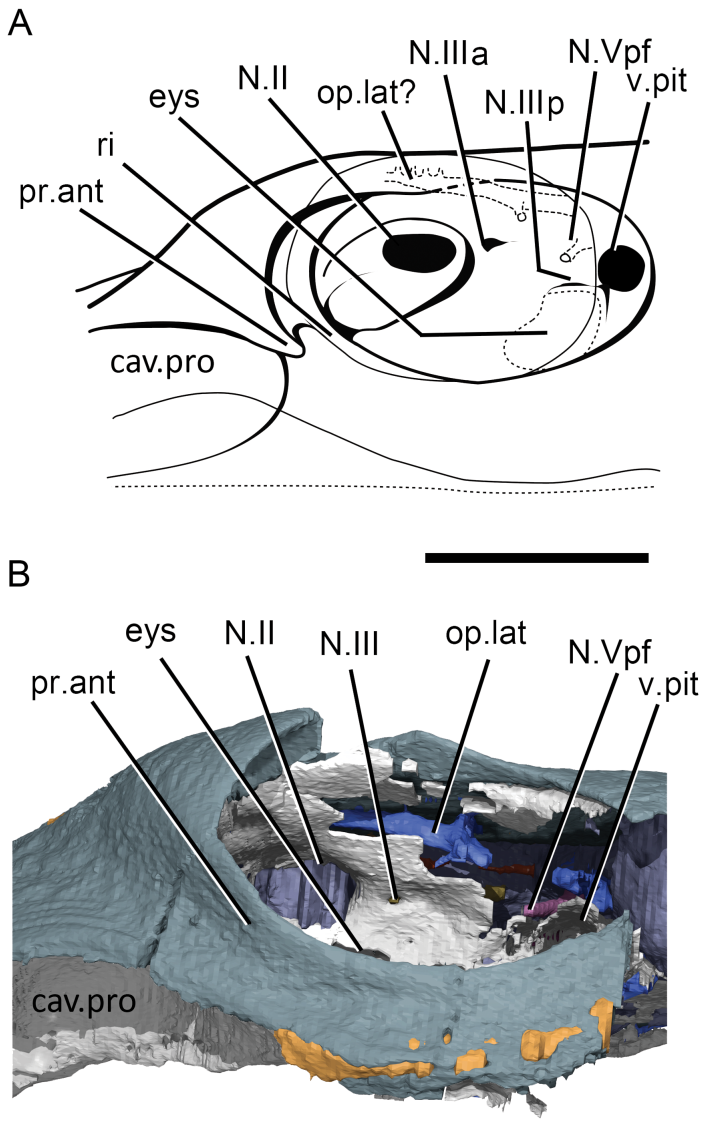

FIGURE 2.2: NHMUK P33580. A, left orbit redrawn after Young (1985). B, 3D model of the left orbit. Abbreviations: N.II, optic nerve foramen; N.III, oculomotor nerve foramen; N.IIIa, foramen for anterior branch of N.III; N.IIIp, foramen for posterior branch of N.III; N.Vpf, foramen for the profundus nerve; cav. pro, lateral preorbital space; eys, eyestalk attachment area; op.lat, canal for the ramus ophthalmicus superficialis lateralis; pr.ant, antorbital process; ri, ridge separating lateral preorbital space from orbital cavity; v.pit, foramen for pituitary vein.

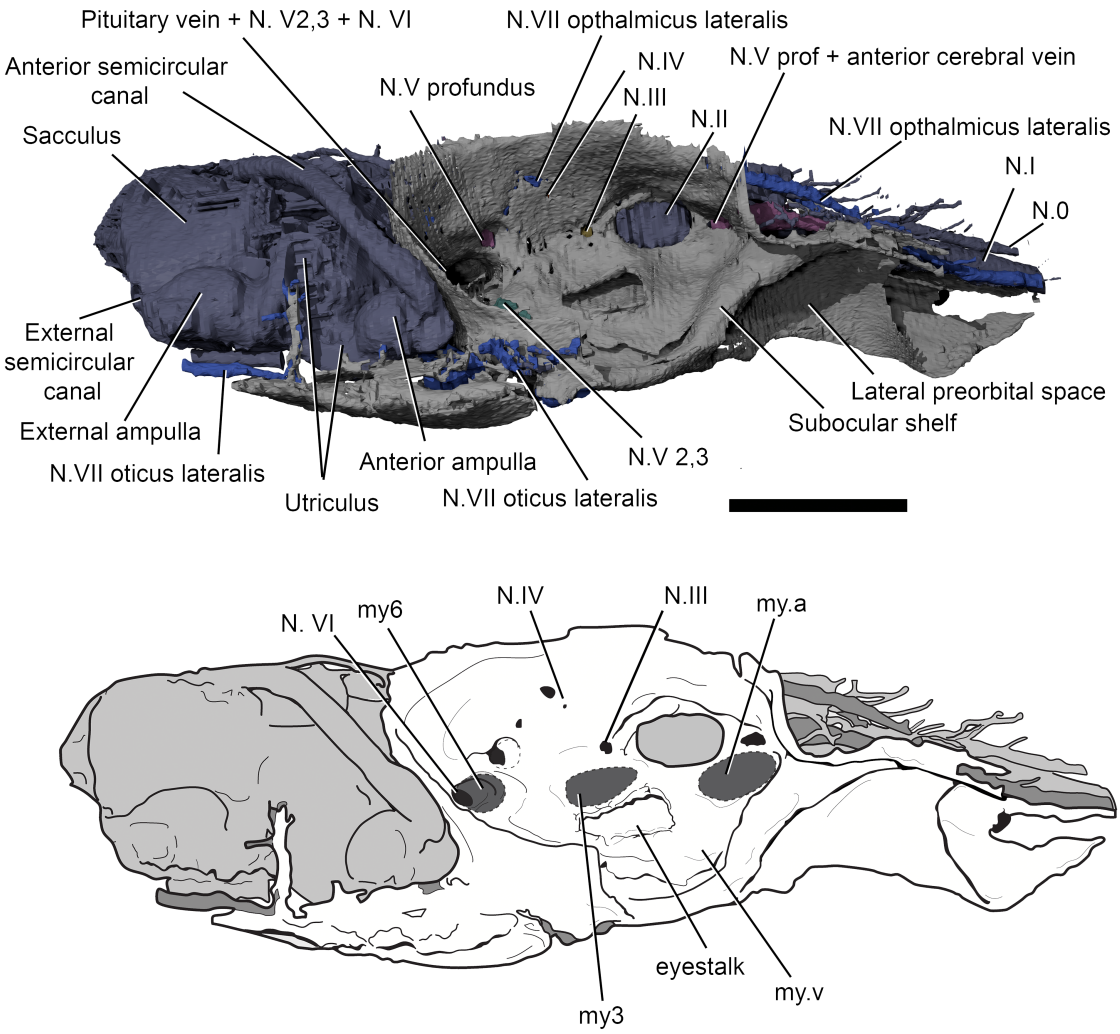

FIGURE 2.3: 3D rendering (top) and line drawing (bottom) of right lateral surface of the braincase and endocavity of NHMUK P33580. Abbreviations: my3, myodome associated with cranial nerve III; my6, myodome associated with cranial nerve VI; my.a, anterior myodome; my.v, ventral myodome. Scale bar represents 5 mm.

2.3.2 **Endocranium**

GENERAL FEATURES — In overall shape, the neurocranium is broad and flat, with a deeply concave ventral surface in transverse profile (Figs 2.3-2.6). The braincase is surrounded by a thin layer of perichondral bone on the ventral and lateral side, while on the dorsal, a dorsal perichondral surface (if present) cannot be distinguished from the overlaying dermal bone. No evidence of an optic fissure is detected. The

endocavity extends between the orbits, and an interorbital septum is not present, so that the braincase can be described as platybasic (Maisey, 2007). In ventral view, the neurocranium is narrowest anteriorly, and broadens mediolaterally up to the lateral edges of the orbits (Figs 2.5, 2.6).

On the ventral surface, grooves and foramina are observed indicating the passage of blood vessels and nerves (Figs 2.5, 2.6). On the ventral side of the subocular shelf, a series of grooves and foramina represent the course of the efferent pseudobranchial artery, the exit of the internal carotid, the palatine branch of the facial nerve (N.VII palatine) and other unidentified canals possibly representing blood vessels (Fig. 2.6). A parasphenoid is visible, surrounding the foramen for the hypophyseal duct. The parasphenoid is flanked by a pair of depressions (Figs 2.5, 2.6), similar to the hypophysial depressions in *Brindabellaspis* (Young 1980, text-fig. 7). However, the depression on the anatomical left side is slightly obscured by breakage (Fig. 2.5).

ORBITAL AND LATERAL ANTORBITAL AREA — The left orbit is exposed and described by Young (1985). However, much of it is incompletely preserved (Fig. 2.2). The right orbit is still filled by matrix and thus relatively untouched by chemical or mechanical preparation (Figs 2.1C, 3), permitting a more complete description.

The orbits resemble *Macropetalichthys* in being set as dorsolaterally opening cavities (Figs 2.1-2.4). The orbital cavity is bounded by anterior and posterior walls and a well-developed subocular shelf (Figs 2.3, 2.4, 2.7). Therefore, contrary to the description of Young (1985), the preorbital space is not in communication with the orbit. Unlike in *Macropetalichthys* (Stensiö, 1969), the lateral margin of the shelf is straight, rather than deeply embayed (Fig. 2.3). A large diameter opening for the optic tract (N.II) occurs in the anterior third of the medial wall of the orbit. The eyestalk attachment is present on the subocular shelf as an oval opening into the interperichondral space surrounded by an everted rim (Figs 2.3, 2.7). The position of the eyestalk attachment is here shown to be much more anterior and ventrolaterally

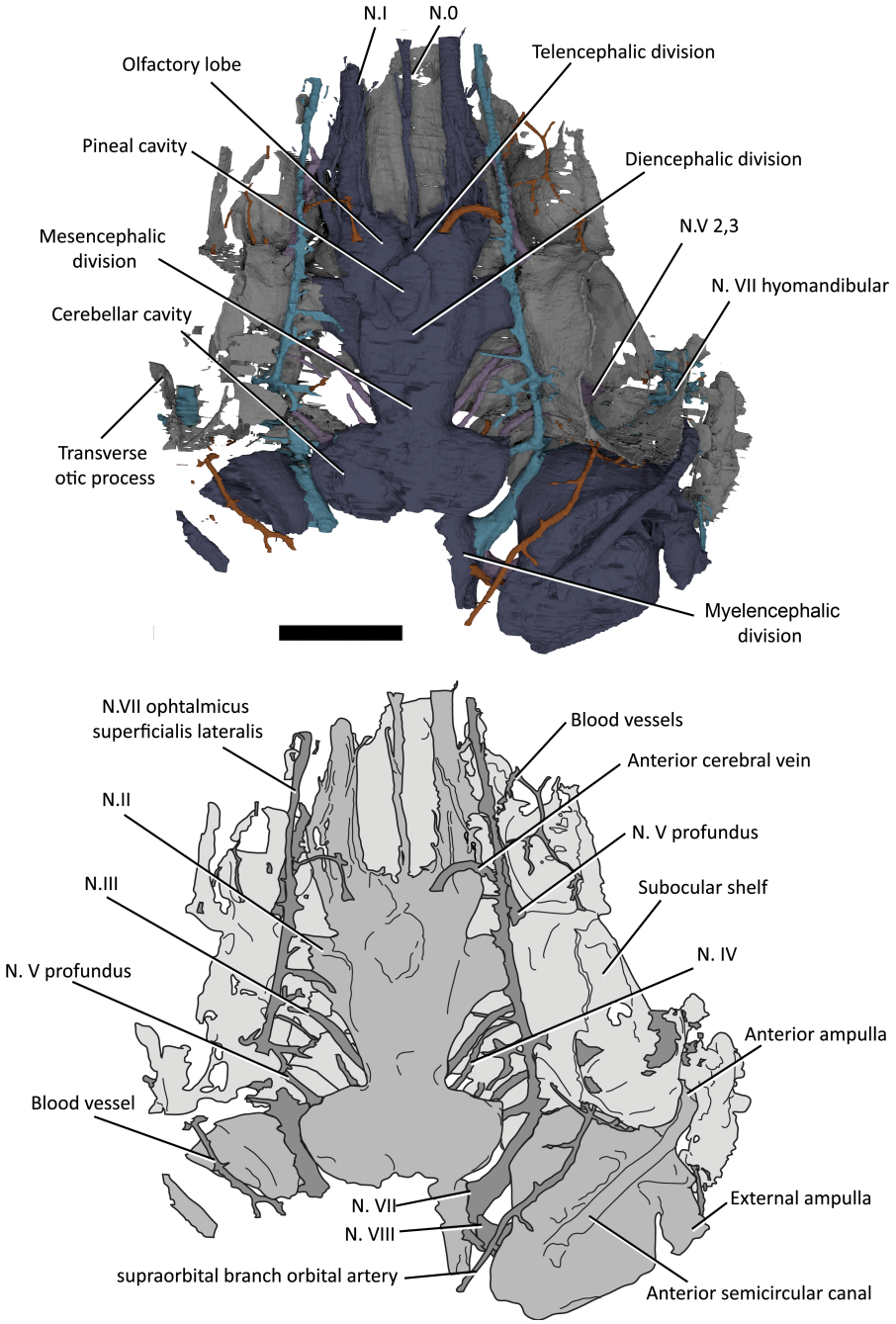

FIGURE 2.4: 3D model (top) and line drawing (bottom) of the endocavity and braincase of NHMUK P33580, dorsal view. Scale bar represents 5 mm.

placed relative to the optic nerve foramen than in Young's (1985) original interpretations (Figs 2.2, 2.3).

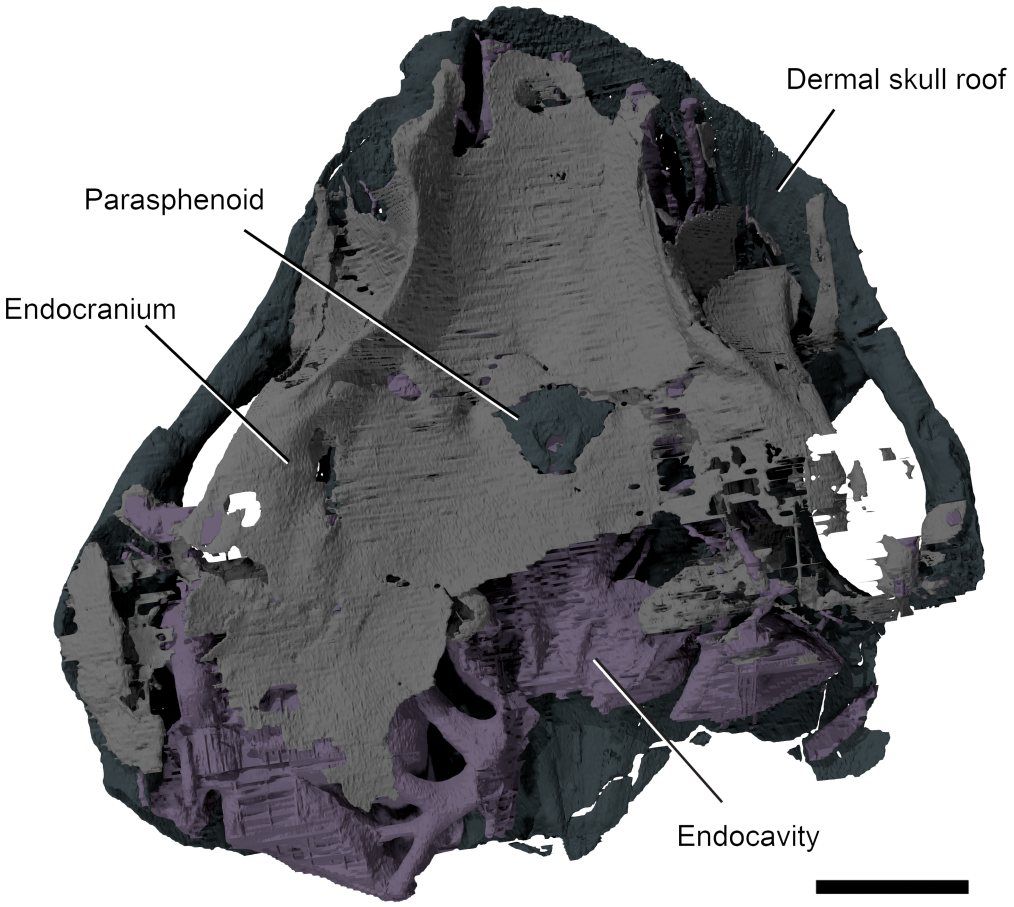

FIGURE 2.5: 3D rendering of NHMUK P33580, ventral view . Scale represents 5 mm

The arrangement of foramina and inferred myodomes are shown in Figures 2.3 and 2.7. Myodomes associated with cranial nerves III and VI (my3 and my6, respectively) are relatively unproblematic, resembling the disposition in other placoderms. Myodome 3 is situated immediately above the eyestalk attachment and immediately below the opening for the oculomotor nerve (N.III; Figs 2.3-2.7). The posteroventral myodome (my6) is developed as a deep, blind sac-like pocket that accommodates openings for the trigeminal (N.V 2,3) and abducens (N.VI) nerves, and the pituitary vein (see endocavity description). This myodome has been interpreted as accommodating two rectus muscles in placoderms (Young, 1980) and osteostracans (Janvier, 1975).

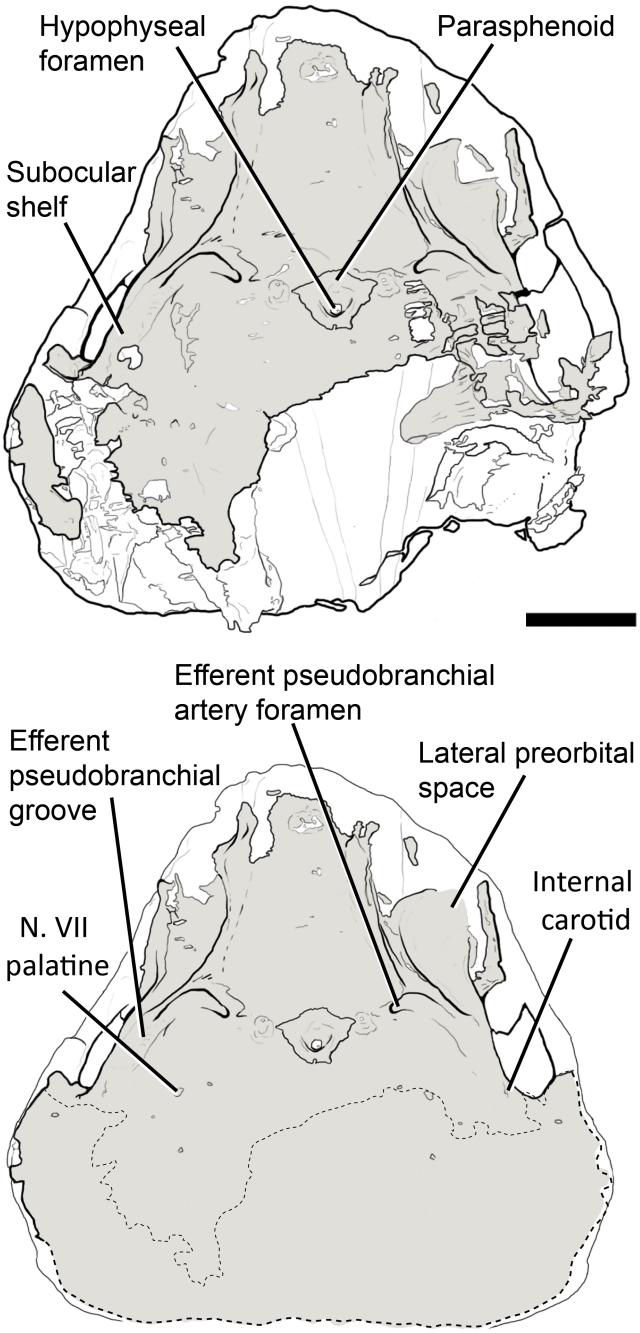

FIGURE 2.6: Drawing of the braincase of NHMUK P33580 in ventral view as preserved (top) and partly restored (bottom). Scale bar represents 5 mm.

Two additional putative myodomes are also observed on the orbital wall. There is a clear depression located immediately anterior to the optic tract (N.II) opening,

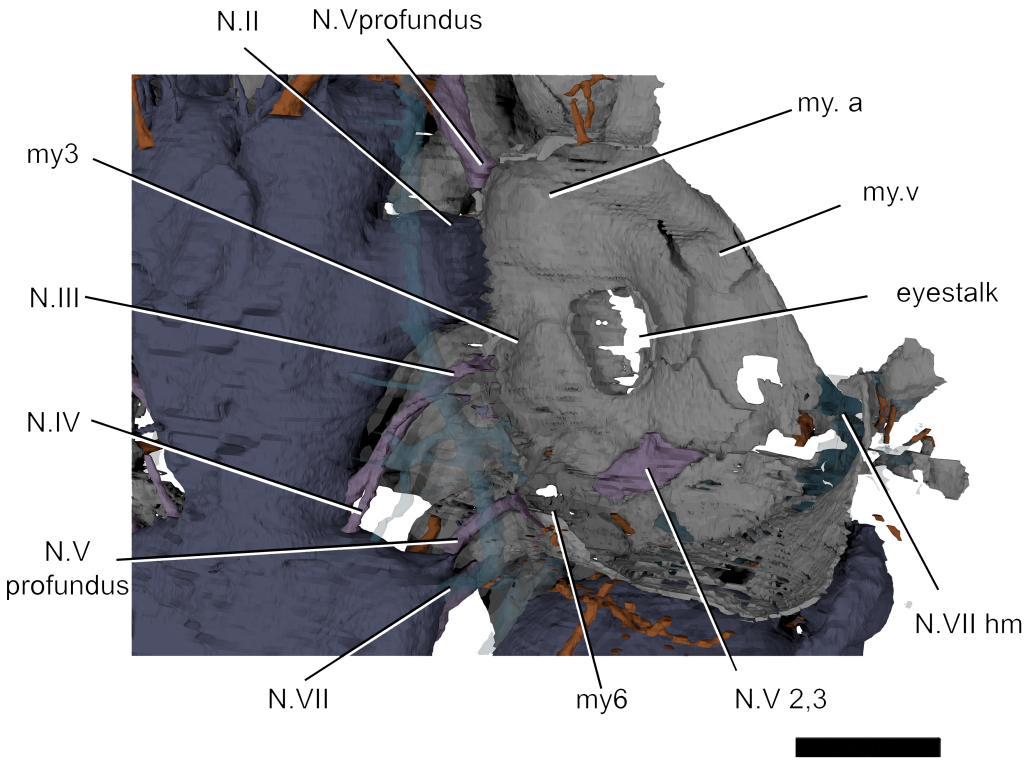

FIGURE 2.7: Internal view of the right orbit of *Shearsbyaspis* with dorsal part of the orbital wall removed to reveal the interpreted position of the extrinsic eye-muscle myodomes and related innervations. Abbreviations: N.II, optic nerve canal; N.III oculomotor nerve canal; N.IV abducens nerve canal; N.V 2,3 trigeminal maxillary and mandibular canal; N.VII, main facial nerve canal; N.VII hm, canal for the hyomandibular branch of the facial; my.a, anterior myodome for an oculomotor-innervated eye-muscle; my.v, ventral myodome for an oculomotor-innervated eye-muscles; my3, myodome for an oculomotor-innervated eye-muscle; my6, myodome for abducens-innervated eye-muscles. Scale bar represents 2.5 mm.

which we consider to be an anterior myodome (my.a; corresponding to my_i of Stensiö 1969) possibly accommodating an oblique eye muscle. We cannot observe a ventral myodome (my.v) with confidence, as seen in many other placoderm taxa. This structure is normally located immediately below the eyestalk base. The corresponding area in *Shearsbyaspis* is located on the subocular shelf, which is broken on both sides of the specimen. However, a distinct pocket (Figs 2.3, 2.7, my.v) is visible near the anterolateral margin of the shelf. This myodome is commonly associated with the opening for the ophthalmica magna 10 artery. Because the shelf is fragmented, we cannot verify this opening. However, a positionally correspondent opening is

identified by Stensiö (1969, text-fig. 69) in *Macropetalichthys*, which he interpreted as accommodating the palatine branch of the facial nerve. However, we note that this canal communicates with the arterial canals in Stensiö's reconstruction.

A myodome associated with the trochlear nerve (N.IV) is non visible in *Shearsbyaspis* (Fig. 2.3). This nerve canal opens in the posterodorsal corner of the orbit, as in other placoderms. However, the surrounding perichondral surface is unimpressed by a myodome, as in arthrodires (Young, 1978; Goujet, 1984a). Stensiö (1969, text-fig. 22B) reconstructed this nerve in *Macropetalichthys* in a more anterior position, confluent with the optic tract opening. This differs from the condition observed in *Shearsbyaspis* and all other placoderms. This therefore casts doubt on Stensiö's interpretation, and it is parsimonious to assume one of the more posterior openings documented in the orbit of *Macropetalichthys* corresponds to the trochlear nerve.

The profundus nerve opens posteroventrally to the trochlear nerve opening, at the same dorsoventral level as the optic tract opening (Fig. 3, N.V profundus). This opening occurs within a funnel-shaped depression. While it is tempting to interpret this cavity as a myodome, we note that a similar cavity is observed around the profundus opening in other placoderms, such as *Buchanosteus* (Young 1979, text-figs 4, 8) and *Romundina* (Dupret et al. 2017a). On the dorsal surface of the subocular shelf, a wide groove extends anterorlaterally from the posteroventral myodome. This probably accommodated the mandibular and maxillary branches of the trigeminal nerve (N.V 2,3 Fig. 2.7). The course of the facial nerve (N.VII) is described later.

2.3.3 **Parasphenoid**

At mid-length along the basicranial surface, surrounding the hypophyseal opening is a distinct, spongiose dermal ossification applied to the perichondral bone which we identify as the parasphenoid bone (Fig. 2.8). The sub-axial and sub-coronal tomography orientations reveal that the bone has a clear separation from the perichondral bone and is thus a separate ossification (Fig. 2.8). The bone is as wide as it

is long, flared anteriorly and tapering posteriorly (Fig. 2.8B), giving it a pentagonal shape. The buccohypophyseal foramen is a distinct, subcircular opening posterior to the centre of the parasphenoid. The opening is situated in a round depression surrounded by a raised ridge (Fig. 2.8B). The bone is thickest and spongiose near its geometrical centre, and thins out towards the margins (Fig. 2.8). The ventral (oral) surface of the bone bears irregularly sized protrusions which we interpret as denticles (Fig. 2.8B-C). They are unevenly distributed, and increasing in size near the buccohypophyseal foramen. The parasphenoid differs from arthrodires in lacking foramina or grooves for the paired hypophyseal vein (Stensiö, 1969; Goujet, 1984a; Dupret, 2010).

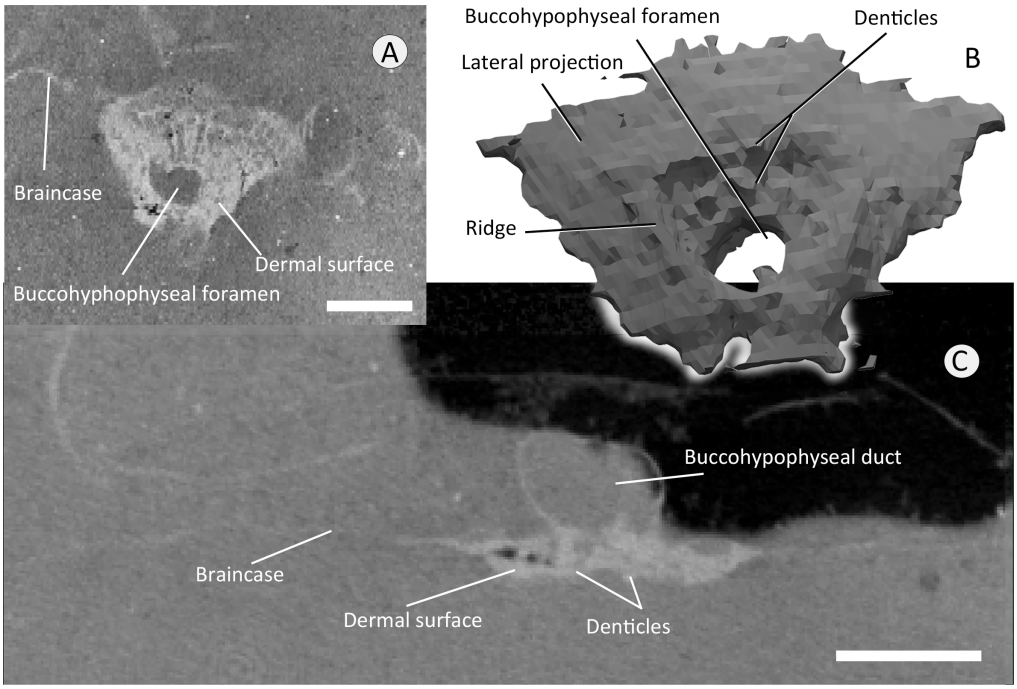

FIGURE 2.8: The parasphenoid of *Shearsbyaspis oepiki*. A, tomogram of the parasphenoid in coronal section. B, 3D rendering of the parasphenoid in ventral view. C, tomogram of the parasphenoid in axial section. Scale bar represents 2 mm.

2.3.4 **Endocranial cavity**

The cranial endocast is well preserved, but incomplete posterior to the otic capsules (Figs 2.4, 2.9). It is long and narrow, with anteriorly directed elongated olfactory ducts, similar to *Macropetalichthys* (Stensiö, 1925, 1963b, 1969). The endocavity of NHMUK P33580 resembles that of other placoderms, as well as many chondrichthyans in being situated directly between the orbits (platybasic) (Fig. 2.4).

The division between the telencephalon and diencephalon is most clearly visible on the ventral surface. There is a pair of well-developed cavities, anterior to the optic tract canals, representing the olfactory lobes. The ventral portion of the olfactory lobes appears longer, extending posteriorly to level the hypophysial canal opening (Fig. 2.4).

The diencephalon cavity issues the optic nerve (N.II) canal, as well as the pineal cavity and the hypophysial cavities. In ventral view (Fig. 2.9), the diencephalon cavity of *Shearsbyaspis* differs from *Macropetalichthys* in two aspects. *Shearsbyaspis* lacks two well differentiated lobes in the hypothalamus cavity. Furthermore, the pineal cavity is lozenge-shape and asymmetrical instead of tubular and wider at the base as described in *Macropetalichthys* (Stensiö, 1969). Two ridges associated with the central body of the pineal gland could be related with the parietal organ. The pineal organ opens on the dermal skull through a foramen between the anterior parts of the orbits. The hypophyseal duct is placed slightly posteriorly in respect of the pineal gland and projects anteroventrally, opening through the palate with a single foramen in the parasphenoid (Figs 2.5, 2.6, 2.8).

The anterior limit of the midbrain cavity is not clear, but must be placed behind the optic nerve and the hypophyseal duct. In dorsal view, its posterior boundary is clearly marked by the sharp lateral expansion of the cerebellar cavity (Fig. 2.4). No distinct optic lobe cavities are present.

The hindbrain cavity is partially preserved as a complete metencephalon cavity and the partial right side of the myelencephalon cavity. The division between the

metencephalic and the myelencephalic cavities is clearly marked by a constriction (visible in dorsal or ventral views) anterior to the trunk of the facial nerve canal (Figs 4, 9). The metencephalon is constituted by two symmetrical rounded lobes, probably representing the location of the cerebellum, while the myelencephalic portion is straight and narrow (Figs 2.4, 2.9).

CRANIAL NERVES —

Terminal, olfactory and optic nerve Two long, large diameter olfactory tract (N.I) canals extend from the olfactory lobes of the telencephalon to the anterior margin of the skull (Figs 2.4, 2.9, 2.10). The nasal capsules are not preserved, but considering the course of the olfactory nerve, they would have been situated at the anteriormost margin of the skull. An unpaired canal extending between the olfactory canals from the anterior ventral edge of the telencephalic, is interpreted as an unpaired terminal nerve (N.0) (Figs 2.4, 2.9, 2.10).

Optic, oculomotor, trochlear and abducens nerve canals. The optic nerve (N.II) tract (Figs 2.4, 2.9, 2.10) arises from the diencephalic portion of the endocranial cavity (Figs 4, 9, 10). The oculomotor (N.III) canal (Figs 2.4, 2.9, 2.10) exits from the mesencephalic cavity and extends anterolaterally, paralleling the optic tract, to connect to the orbital wall. It opens posterior to the optic nerve foramen, anteriorly to the myodome for the internal rectus muscle (my3; Figs 2.3, 2.7). The trochlear (N.IV) nerve canal (Figs 2.4, 2.9, 2.10) extends from the anterior boundary of the cerebellar cavity, at the narrow waist between the optic lobe and cerebellum and parallels the course of the oculomotor canal. It meets the orbital wall and opens as a foramen located directly dorsal to the oculomotor foramen. The abducens (N.VI) nerve canal (Figs 2.9, 2.10) is a narrow-diameter canal extending from the ventral surface of the cerebellar cavity to posteromedial corner of the posteroventral myodome (Fig. 2.10).

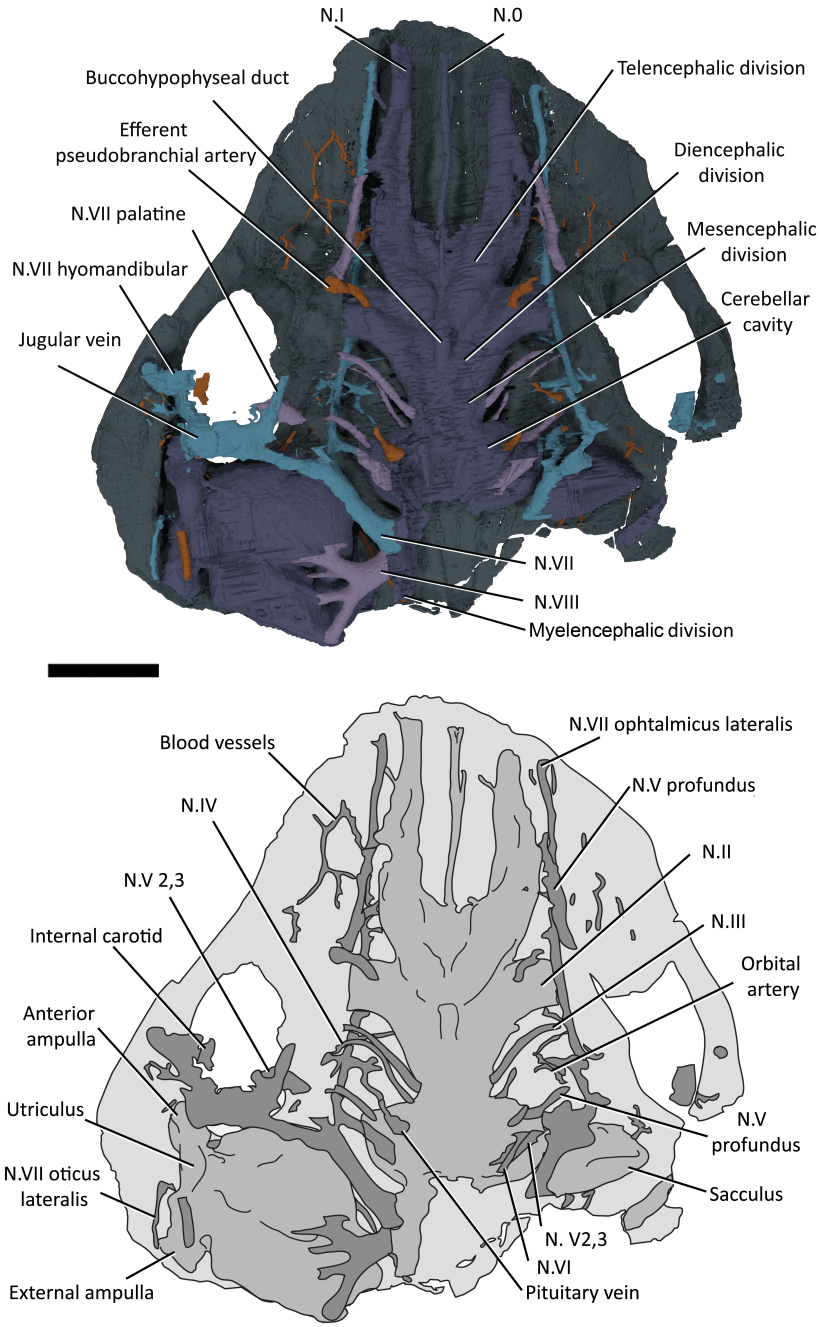

FIGURE 2.9: 3D model (top) and line drawing (bottom) of the endocast of NHMUK P33580, ventral view. Scale bar represents 5 mm.

Trigeminal nerve canals There are two distinct canals accommodating branches of the trigeminal (N.V) (Figs 2.4, 2.9, 2.10), as opposed to a single, laterally projecting

trigeminal trunk recess as in arthrodires (Stensiö, 1963b, 1969; Young, 1979; Goujet, 1984a). The profundus (V pf) canal originates separately from the common canal of the remaining branches. It extends from the dorsal anterior edge of the cerebellar cavity to a foramen situated above the posteroventral myodome (Figs 3, 4, 7). Unlike in other placoderms (e.g. in *Buchanosteus*, Young 1979, text- fig. 4) there is no groove on the orbital wall to distinguish its course. However, a canal exiting the anteromedial wall of the orbit and paralleling the course of the ophthalmic branch of the facial nerve (described below) can be interpreted as the continuation of the profundus nerve canal (Figs 2.3, 2.4, 2.7).

The remaining trigeminal nerves canals (N.V 2,3; Figs 2.9, 2.10) extend from the ventral side of the cerebellum to the posteroventral myodome, piercing its ventral wall. Here, it would have divided into the maxillary and mandibular branches. A broad groove exiting from the posteroventral myodome on the ventral side of the orbital wall (N.V 2,3; Figs 2.3, 2.4, 2.7) may have accommodated the course of these two branches (cf. *Romundina*, Dupret et al. 2014, 2017a).

Facial nerve canals The trunk of the facial (N.VII) canal exits immediately anterior to the trunk of the acoustic nerve canal (see below), with the two canals (VII and VIII) being nearly confluent at the endocavity wall (Figs 2.4, 2.9, 2.10). A very short common canal for the ophthalmicus superficial lateralis and the ramus buccalis lateralis divides from the main facial nerve canal just medial to the level of the orbital wall (Figs 2.4, 2.9). A short canal for the ramus buccalis lateralis enters the orbit via the posterior wall of the posteroventral myodome (Figs 2.4, 2.9). The ophthalmic superficialis lateralis canal (N.VII oph. lat) extends dorsally from the main canal at a high angle before bending sharply towards the snout. It runs anteriorly between the orbital and endocranial cavities following the course of the supraorbital sensory canal (Figs 2.4, 2.9). The ophthalmic superficialis lateralis canal merges with the profundus nerve canals and the olfactory tracts as it extends towards the snout (Figs 2.4, 2.9).

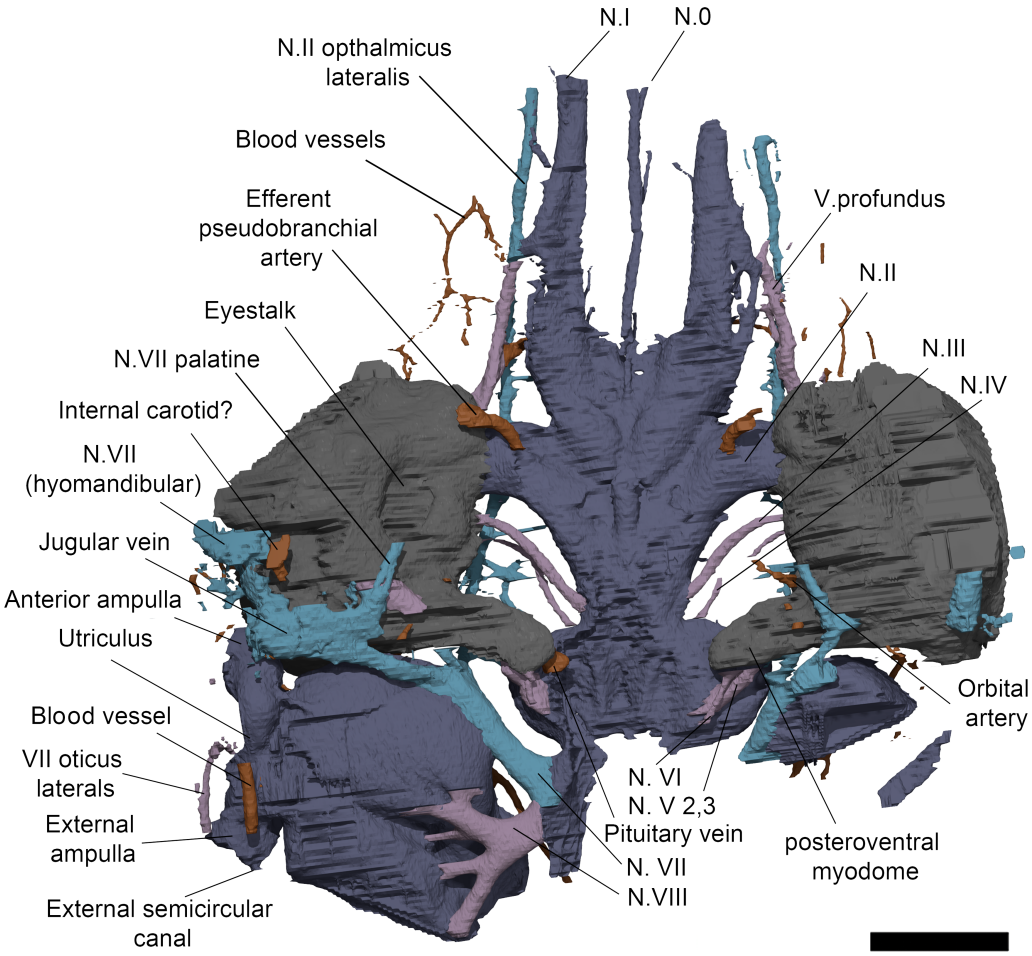

FIGURE 2.10: 3D model of the endocast of NHMUK P33580 with the addition of the endocast of the orbital cavity, ventral view. Scale bar represents 5 mm.

The main body of the facial nerve passes behind the orbit towards external (lateral) side of the braincase. It divides into the palatine branch (N.VII. palatine) and the hyomandibular branch (N.VII hyomandibular) (Figs 2.9, 2.10). The palatine branch passes beneath the orbit, remaining invested in the subocular shelf, and opens to the basicranium beneath the orbit. The hyomandibular branch enters the orbit, and continues as a sulcus in the posterior floor of the orbit before passing out the lateral side of the orbit as a short (partially preserved canal) in the transverse otic process (N.VII hm; Figs 2.3, 2.7). Several small canals, branching anterior to the anterior ampulla and ultimately connected with the infraorbital sensory canal.

These are interpreted as canals for the ramus oticus lateralis (N.VII ot.lat.) (Figs 2.9, 2.10).

Acoustic nerve The acoustic (N.VIII) nerve innervated the labyrinth through an anterior and a posterior branch. Each branch further divided into two small canals before entering the ventromesial wall of the saccular chamber (Figs 2.9, 2.10).

VASCULAR SYSTEM CANAL — Even if most of the anterior part of the braincase and the cerebral cavity is preserved, not many details could be obtain about the cranial circulation of *Shearsbyaspis*. Many small canals are visible in the CT data but most of them are difficult to follow due to the resolution of the scan, or only partially preserved, so that the identification is very unclear.

Arteries The course of the efferent pseudobranchial artery is indicated by a groove on the ventral side of the subocular shelf. It pierces the braincase next to the parasphenoid (Figs 2.5, 2.6, 2.9, 2.10) and enters the endocavity via the optic tract canal. A short canal pierces the base of the transverse otic process, and corresponds with the position of the orbital artery canal in *Buchanosteus* (Young, 1979). Another pair of canals, extending above the sacculus and entering in the posterodorsal wall of the orbit (Fig. 2.10), are tentatively assigned to the supraorbital branches of the orbital artery (cf. *Brindabellaspis*; Young 1980, text-fig. 10).

Veins The pituitary vein in *Shearsbyaspis* is hypothesized to have entered the orbit via the posteroventral myodome as two separate canals (Figs 2.9, 2.10). Unlike other placoderms, there is no sign of the hypophysial vein. Only a short anterior segment of the jugular vein canal is preserved (Figs 2.9, 2.10). It opens at the back of the orbit, confluent with the facial nerve canal.

A pair of canals originates from the dorsal portion of the telencephalon and loop back toward the orbit, opening on the anterodorsal wall of the orbital cavity (Fig. 2.4). In shape, they are very similar to that which been has identified in *Brindabellaspis* as

the terminal nerve (N.0) (Young, 1980). Here, however, the nasal capsules are located far anterior to the orbits so that these canals are more likely to have carried a blood vessel. A similar pair of canals, exiting from the telencephalic region and entering the anterior wall of the orbit, have instead been identified as the anterior cerebral vein in many placoderms (e.g. Young 1979; Dupret et al. 2014, 2017a,b) and osteostracans (e.g. Janvier 1985a). A partial corresponding canal was figured in *Macropetalichthys* by Stensiö (1969), but was left unidentified.

2.3.5 **Labyrinth cavity**

Parts of both the labyrinth cavity are preserved in NHMUK P33580 (Figs 2.3, 2.4, 2.9, 2.10). The right labyrinth preserves the position and morphology of the vestibule apparatus and related cranial nerves entering in it (Figs 2.3, 2.4, 2.9, 2.10). Only the anterior semicircular canal is completely preserved, and a short anterior segment of the horizontal canal is preserved. The saccular portion is deep and as large as, or larger, than the orbit (Fig. 2.4). The orbit and the labyrinth are almost in contact with one another (Figs 2.3, 2.4), so that the facial nerve passes so close to the labyrinth that it intersects the saccular wall (Figs 2.4, 2.9, 2.10).

The anterior ampulla is situated very close to the posterior margin of the orbit (Figs 2.3, 2.4). The anterior semicircular canal crosses the sacculus from about the (presumed) centre of the dorsal side to the anterior ampulla at its anterolateral corner. The anterior ampulla is connected to the external ampulla by a ventrally flexed utriculus (Figs 2.3, 2.9, 2.10). The position of the anterior ampulla in *Shearsbyaspis* is very different from what has been reconstructed by Stensiö (1963a, 1969) for *Macropetalichthys*, casting doubt on this reconstruction (Fig. 2.11). What was identified by Stensiö as the anterior ampulla is instead an anterolaterally placed utriculus, with the same position and morphology as in *Shearsbyaspis*.

The anterior ampulla in *Macropetalichthys* is likely to have been in the same position as *Shearsbyaspis* but obscured by matrix or obliterated by preparation in the spec-

imen studied by Stensiö (1969, text-fig. 50A, 50B). Thus, it is likely that the anterior semicircular canal of *Macropetalichthys* traversed obliquely towards its anterolateral corner, rather than looping back medially (Fig. 2.11).

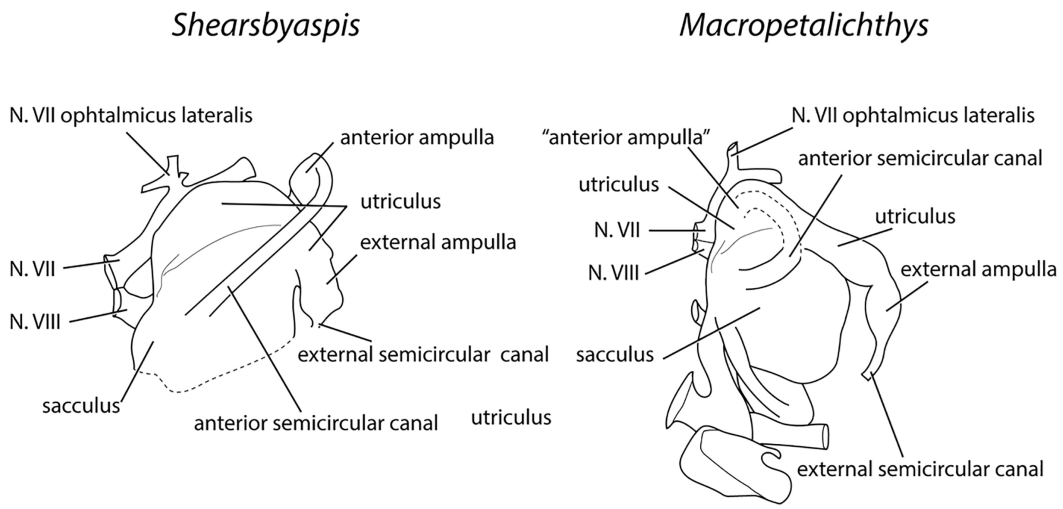

FIGURE 2.11: The morphology of the skeletal labyrinth of *Shearsbyaspis* (left) and *Macropetalichthys* (right) compared. *Macropetalichthys* is redrawn from Stensiö (1969) with original labelling. The "anterior ampulla" is a doubtful interpretation (see text).

2.4 DISCUSSION

2.4.1 **Phylogenetic summary**

The purpose of the present work is not to resolve placoderm relationships, but to add important new phylogenetic data and draw attention to problems with current, competing hypotheses. We are currently preparing a more inclusive analysis of placoderm relationships, but discuss here some of the implications of characters described in this work. We examine the compatibility of a limited, but important subset of phylogenetically informative characters bearing on the question of placoderm relationships. The unrooted trees in Figure 2.12 show several competing scenarios based on recently published hypotheses. Of the topologies considered, those with the lowest transformation cost are the two arrangements indicating the monophyly

of a least a subset of placoderms. This agrees with King et al. (2016) and contrasts with previous, recent numerical hypotheses (e.g. Brazeau 2009; Giles et al. 2015b; Zhu et al. 2016).

A revival of placoderm monophyly needs to account for the newly discovered "placoderm" facial jaw skeletons from the Silurian of China: *Entelognathus* (Zhu et al., 2013) and *Qilinyu* (Zhu et al., 2016). Two competing hypotheses can account for this. One would place *Entelognathus* and *Qilinyu* outside of the main placoderm clade. Given the arthrodire-like configuration of the braincase of *Entelognathus*, this new outgrouping could imply arthrodire-like primitive skull architecture for placoderms as a whole. By consequence, many of the resemblances of "acanthothoracids" and petalichthyids with jawless outgroups could be explained as being secondarily derived. The second hypothesis would place *Entelognathus* and *Qilinyu* as close sister groups of the gnathostome crown (as in current phylogenies). However, this could similarly imply an arthrodire-like morphotype for not only placoderms, but also jaw-bearing gnathostomes as a whole. The phylogenetic interpretation of petalichthyids in these competing scenarios (as either primarily or secondarily "osteostracan" like) is central to reconstructing cranial transformations in early gnathostomes.

2.4.2 Anatomical comparisons with the other early gnathostomes and their potential phylogenetic significance

PARASPHENOID — Parasphenoid bones have previously only been convincingly observed in arthrodire placoderms and osteichthyans. Reports of a parasphenoid in *Bothriolepis* (Young, 1986; Dennis-Bryan, 1995) are unsubstantiated. Its presence was only inferred in personal comments and never formally described in spite of the large amount of available specimens of this taxon. Dupret et al. (2017a,b) reported the presence of a parasphenoid in *Romundina*, although they argued that it does not seem to be formed of dermal bone so that the real nature of the material surrounding the hypophysial fenestra is unclear. A parasphenoid is probably present in *Kosoraspis*

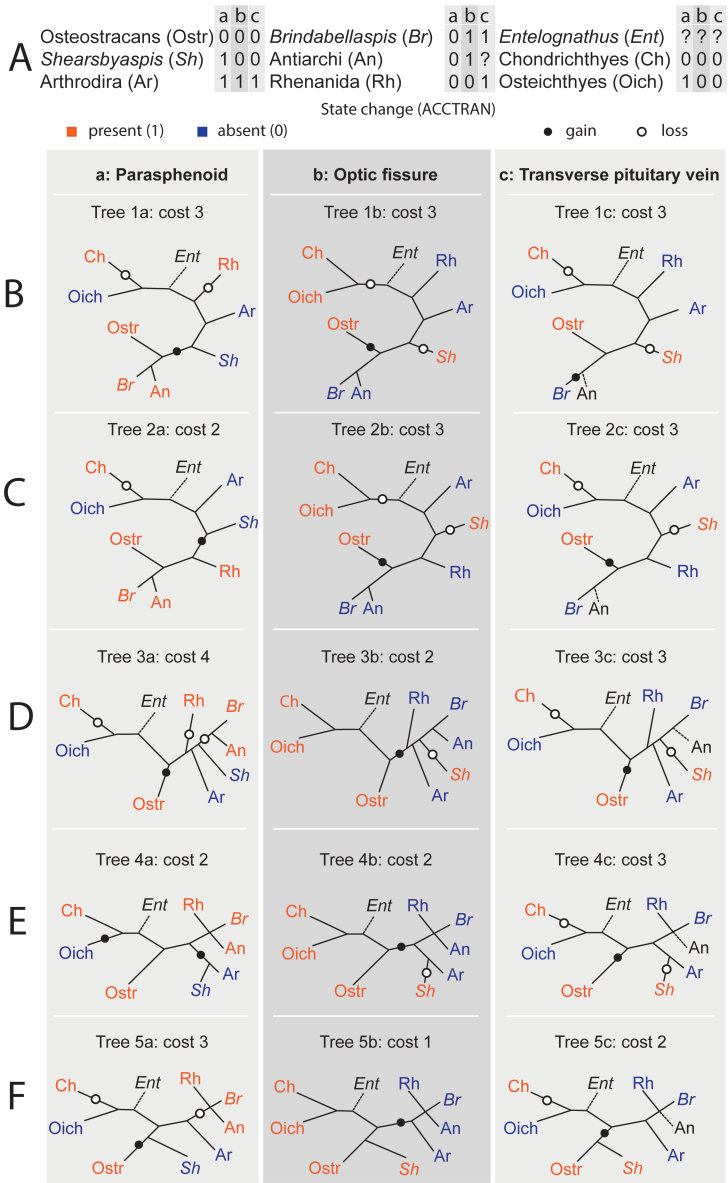

FIGURE 2.12: The distribution of the parasphenoid, the optic fissure and of the transverse pituitary vein on different unrooted topologies showing the evolutionary cost for each topology. A, data matrix with the scoring of the characters for each examined taxa. B, topology 1 represents the most parsimonious output for the distribution of: 1a, parasphenoid; 1b, optic fissure; 1c, transverse pituitary vein. C, topology 2 represents the character distribution with a paraphyletic Placodermi as found in Giles et al., 2015. D, topology 3 tests the result with a monophyletic Placodermi as found by King et al. (2016). E, topology 4 presents a monophyletic Placodermi with *Shearsbyaspis* resolved as sister to arthrodires. F, topology 5 presents a monophyletic subset of placoderms with *Shearsbyaspis* resolved as sister to the rest of the placoderms.

Gross (1959). It is absent in other members of the "Acanthothoracida". As the monophyly of this group has not been consistently recovered (e.g. Giles et al. 2015b; King

et al. 2016; Zhu et al. 2016), the phylogenetic interpretation of the parasphenoid in *Kosoraspis* is unclear.

Given the restricted distribution of parasphenoids, the lack of known petalichthyid examples, and hypotheses of placoderm paraphyly, the observation of a parasphenoid in *Shearsbyaspis* is surprising. Some caution must be exercised in making phylogenetic hypotheses about the parasphenoid in early vertebrates. Interpreting genuine absences can be problematic. In taxa lacking an interdigitating suture between the basicranium and the parasphenoid, the parasphenoid may easily become detached post mortem and therefore be unpreserved or unassociated with the braincase (Goujet, 1984b; Carr and Hlavin, 2010; Zhu and Zhu, 2013). However, we consider here the immediate phylogenetic implications of a parasphenoid in *Shearsbyaspis* given its unexpected observation and the fact that for many taxa (e.g. antiarchs) there is sufficient sampling to presume that this bone is absent. However, the presence of a parasphenoid in *Kosoraspis* (Gross, 1959) might indicate that the distribution of this bone was more widespread in placoderms and not unique to petalichthyids and arthrodires.

The simplest interpretation for the parasphenoid character, if considered in isolation, would be the partitioning of *Shearsbyaspis*, arthrodires and osteichthyans together to the exclusion of all other taxa (Fig. 2.12B, tree 1a). Such a placement would imply at least some placoderms within the gnathostome crown group (as the bone is absent in chondrichthyans). We consider such a hypothesis to be unlikely based on present evidence (as it is not supported by any contemporary phylogenetic analyses). However, it cannot be overlooked simply because of this.

A second alternative accommodates a gnathostome stem- group position for placoderms and places *Shearsbyaspis* together in a split with arthrodires (Fig. 2.12E, tree 4a). This would require only one additional step. Such a placement is consistent with earlier hypotheses suggesting close relationships of arthrodires and petalichthyids, although these were drawn under the presupposition of placoderm monophyly (Goujet and Young, 1995, 2004). Indeed, the earliest known petalichthyids

(quasipetalichthyids) (Zhu, 1991; Pan et al., 2015) bear a strong external resemblance to early arthrodires, such as *Bryantolepis* (Elliott and Carr, 2010) and *Wuttagoonaspis* (Ritchie, 1973). This would be consistent with convergent similarities between osteostracan and macropetalichthyid neurocranial morphology.

OPTIC FISSURE — Several placoderm groups display nasal capsules separated from the rest of the braincase by a perichondrally fissure passing through the canal for the optic nerve canal. It completely subdivides the braincase into postethmoid and rhinocapsular portions. This fissure, termed the optic fissure, has been identified in arthrodires (Stensiö, 1969; Young, 1979; Goujet, 1984a), "acanthothoracids" (Ørvig, 1975; Young, 1980; Olive et al., 2011), rhenanids (Stensiö, 1950, 1969), and inferred to have been present in antiarchs (Young, 1984; Lukševičs, 2001). In petalichthyids the nasal capsules are usually not preserved, suggesting the presence of separate cartilages containing the nasal capsules (Zhu, 1991). This has been proposed as a possible placoderm synapomorphy by Brazeau and Friedman (2014). There is no such fissure observed in *Shearsbyaspis* or *Macropetalichthys* (Stensiö, 1925, 1963b,a, 1969). Thus, the absence of a distinct optic fissure division separates petalichthyids from nearly all other placoderms (Fig. 2.12F, tree 5b).

However, a rhinocapsular division has been inferred in quasipetalichthyids, although it has not been directly observed (Zhu, 1991; Pan et al., 2015). Furthermore, we observe a ridge inside the orbit of *Shearsbyaspis*, corresponding with the external signature of the partially closed fissure in *Brindabellaspis* (Young, 1980, 1986). Furthermore, the division is apparently absent in eubrachythoracid arthrodires (Dennis-Bryan and Miles, 2079, 1983). The latter is probably a derived condition, but shows that the presence of a fissure is not necessarily universal among non-petalichthyid placoderms. These considerations raise caution about interpreting the phylogenetic signal of this absence in petalichthyids and further data from quasipetalichthyids in particular will help to resolve this problem.

HYPOPHYSEAL DUCT — In modern vertebrates, the hypophysis displays two very different morphologies. In cyclostomes, it projects anteriorly connecting with the nasal capsules. In crown-group gnathostomes, it is independent from the nasal capsules and primitively projects posteriorly or posteroventrally as a duct. Fossil jawless fishes appear to exhibit the cyclostome condition, possessing an anteriorly-oriented hypophysis, either connected with the nasal capsules, as in osteostracans (Janvier, 1985a), or as a separate anteroventrally - oriented hypophyseal duct, as in the galeaspid *Shuyu* (Gai et al., 2011; Gai and Zhu, 2012). In placoderms, the hypophyseal duct is projected either anteroventrally, as in *Romundina* (Dupret et al., 2017a) or *Brindabellaspis* (Young, 1980), or ventrally, as in arthrodires (Stensiö, 1969; Goujet, 1984a). Dupret et al. (2017a) suggested that this represents a morphocline documenting the stepwise transformation of the hypophyseal duct from anteriorly directed to posteriorly directed. In this scenario, *Shearsbyaspis* could be interpreted as exhibiting a shared primitive state with jawless fishes and some placoderms (Fig. 2.12F). Alternatively, the conditions in either *Shearsbyaspis* or arthrodires could be secondarily derived, if petalichthyids are considered to be a proximate sister group of arthrodires (Fig. 2.12E).

TRIGEMINAL-PITUITARY MORPHOLOGY AND THE POSTEROVENTRAL MYODOME. — The posteroventral myodome and associated canals in *Shearsbyaspis* and *Macropetalichthys* strongly resembles conditions in osteostracans. In these taxa, (Fig. 2.13A, B) the main trunk of the trigeminal and abducens nerves, and the pituitary vein canals, enter the orbit via the deep posteroventral myodome (Stensiö, 1963a, 1969; Janvier, 1981, 1985a). The opening of these three canals deep within the posteroventral myodome is not observed in other placoderms (Young, 1979; Goujet, 1984a; Young, 1980; Olive et al., 2011; Dupret et al., 2017a) and crown-gnathostomes (Gardiner, 1984b; Basden and Young, 2001; Maisey, 2005) (Fig. 2.13D-H).

In addition, petalichthyids, osteostracans and galeaspids (Gai et al., 2011) are distinct from non-petalichthyid placoderms by having two separate canals for the

pituitary vein (Fig. 2.13A-C). This is opposed to the condition in other placoderms (rhenanids: Stensiö 1969; *Brindabellaspis*: Young 1980; *Romundina*: Dupret et al. 2017a; and arthrodires: Stensiö 1969; Goujet 1984a) where the pituitary canal is represented by a transverse canal spanning the width of the interorbital space (Fig. 2.13F-H). A fully enclosed, horizontal canal for the pituitary vein has been reported in the early osteichthyan *Ligulalepis* (Basden and Young, 2001), but not in early chondrichthyans. This suggests that a single transverse pituitary vein canal may represent the primitive condition for crown-gnathostomes.

The morphology of the pituitary vein and trigeminal nerve in association with the posteroventral myodome is parsimoniously interpreted as a shared primitive condition of osteostracans and macropetalichthyids (Fig. 2.12). However, we note that this phylogenetic arrangement would require the placement of macropetalichthyids as the sister group of other gnathostomes in which this part of the neurocranium is documented. This situation would conflict with existing phylogenetic hypotheses that place *Brindabellaspis* as a more distant relative of the gnathostome crown, relative to macropetalichthyids. This highlights some of the internal character conflicts arising from placoderm paraphyly.

FACIAL NERVE, HYOMANDIBULAR ATTACHMENT AND THE SIMILARITIES BETWEEN PLACODERMS AND JAWLESS FISHES. — Arguments for placoderm paraphyly are based in large part on the disposition of the facial nerve canals, hyomandibular articulation relative to the orbit, and the morphology of the braincase surrounding the orbit (Brazeau, 2009; Brazeau and Friedman, 2014). It has been argued by these authors that petalichthyids and *Brindabellaspis* resemble jawless osteostracans with respect to these characters. By contrast, arthrodires are interpreted as more closely resembling crown-group gnathostomes (see Brazeau and Friedman 2014 for details). Recently, however, these characters were critically examined by King et al. (2016), who noted that they are morphologically related to the relative position of the jaws, and that some of these characters could therefore be expected to co-vary. We agree

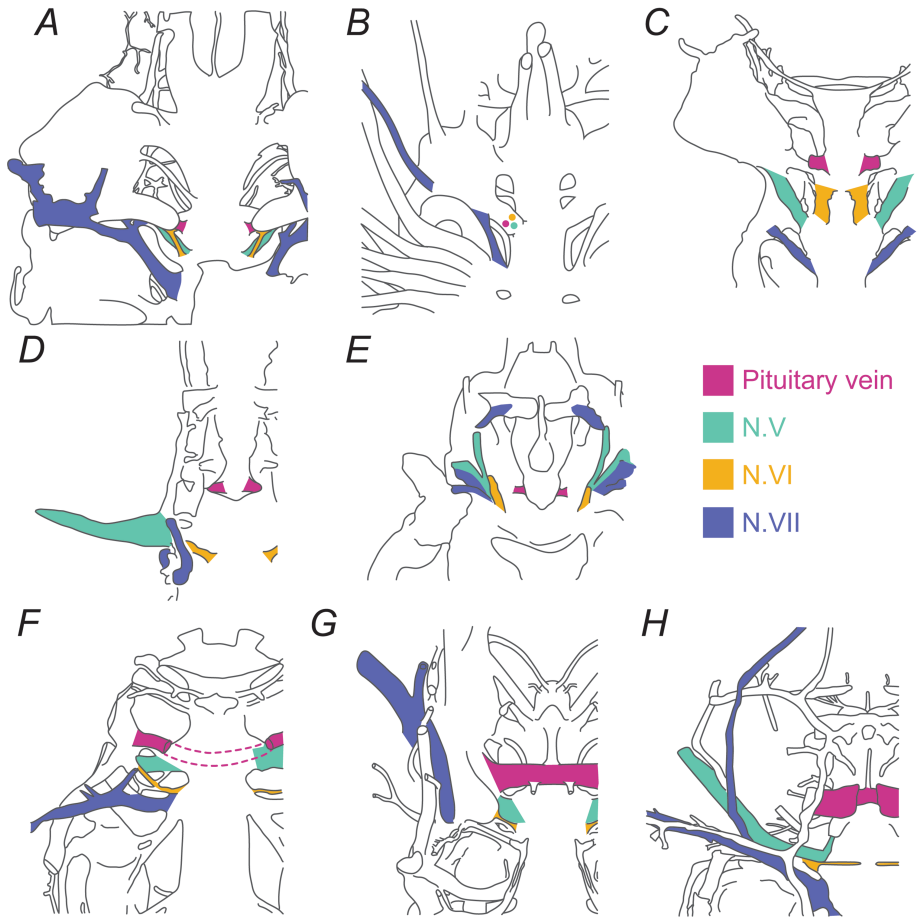

FIGURE 2.13: Endocranial cavities of several gnathostomes, in ventral view, highlighting the morphology of the trigeminal, abducens and facial nerves and of the pituitary vein. A, *Shearsbyaspis*, a petalichthyid placoderm. B, *Norselaspis*, an osteostracan (after Janvier, 1981). C, *Shuyu*, a galeaspid (after Gai et al. 2011). D, *Cladodoides*, a chondrichthyan (after Maisey, 2005). E, *Lawrenciella*, an osteichthyans (after Hamel and Poplin 2008). F, *Kujdanowiaspis*, an arthrodire placoderm (after Goujet 1984a). G, *Brindabellaspis*, an "acanthothoracid" placoderm (after Young 1980). H, *Romundina*, an "acanthothoracid" placoderm (after Dupret et al. 2014). Not to scale.

with these assessments and add further details to the partitioning of these characters based on our examination of *Shearsbyaspis* and in light of recently published information on *Romundina* (Dupret et al., 2017a).

The character concerning the course of the facial nerve was removed from the matrix of King et al. (2016) on the grounds that it was redundant with respect to the position of the hyoid arch. However, we can show that it is not entirely redundant, though our new formulation does not necessarily corroborate recent hypotheses of placoderm paraphyly. Existing datasets, including that of King et al. (2016), divide

total group gnathostomes into two character states: those with an anteriorly situated hyomandibular articulation (lateral or anterior to the posterior orbital wall) and those with an articulation situated posterior to the level of rear orbital wall. King et al. (2016) argued that the exposed course of the facial nerve within the orbit is correlated with the former state, an argument that follows logically from the relative position of the articulation and the associated nerve foramen. However, we note that in *Romundina*, the facial nerve division is exposed within the rear wall of the orbit, in spite of a posteriorly situated hyomandibular attachment. In effect, with respect to hyomandibular articulations and the course of the facial nerve, *Romundina* has been coded as resembling arthrodire and crown gnathostome conditions. By contrast, petalichthyids (i.e. *Macropetalichthys*) have been coded as resembling conditions in osteostracans and *Brindabellaspis*.

However, if we examine the respective morphologies in greater detail, and in light of the anatomy observed in *Shearsbyaspis*, we can demonstrate that these contrasts are incorrect. The course of the facial nerve in *Shearsbyaspis* resembles *Macropetalichthys*, where the hyomandibular branch traverses the rear wall of the orbit, before entering the transverse otic process and exiting next to the hyomandibular articulation. However, as in arthrodires and crown gnathostomes, the palatine branch does not enter the orbital space, nor does the common trunk of the facial nerve breach this wall. Instead, the palatine branch extends downward through the orbital floor, and exists from the palatal surface of the braincase, behind the anteroposterior level of the hypophysis. By contrast, the palatine branch in *Romundina* traverses anteriorly on the dorsal surface of the subocular shelf. Indeed, the division of the palatine and hyomandibular branches can be reasonably inferred to have occurred within the orbital cavity (Dupret et al. 2017a, text-figs D-E). In this respect, the trunk of the facial nerve enters the orbital cavity, and *Romundina* resembles *Brindabellaspis*, despite the differences in the extension of the transverse otic process in these taxa.

We therefore argue that the morphology and division of the facial nerve has phylogenetic value, and that this can be shown to be (at least partially) independent

of the position of the hyomandibula. However, the contrasts implied by examining these characters in further detail suggests closer similarities between petalichthyids and arthrodires than either share with *Brindabellaspis* or *Romundina*. We would therefore suggest inclusion of a modified version of this character that better accounts for the new knowledge from *Shearsbyaspis* and *Romundina*.

2.5 CONCLUSION

We have presented the updated cranial morphology of *Shearsbyaspis oepiki* Young, 1985 based on computed tomography analysis. The new data presented here, augment our understanding of the morphology of petalichthyids. Given the centrality of this group to questions of placoderm relationships, our new data have shed light on the characters that have been the basis of arguments for placoderm paraphyly. We showed that while *Shearsbyaspis* has some interesting resemblances with osteostracans, in the relative position of the pituitary and trigeminal nerve foramina, and the absence of an optic fissure, it presents important characters (such as a parasphenoid) that stand in contrast with this. Additionally, the morphology of *Shearsbyaspis* invited critical reinvestigation of the diversity of facial nerve branching in early gnathostomes. We found that this variable is not strictly correlated with the position of the articulation of the hyomandibula on the braincase wall. However, accurate representation of its variation has not been presented in existing morphological datasets to date. Finally, the character compatibility examples we present raise questions about placoderm paraphyly on a character-based level. Given the importance of this new data, we advocate that the best tests of placoderm relationships will come in the form of more inclusive analyses and better investigations of less well understood placoderm groups, such as petalichthyids. In particular, further knowledge of the so called quasipetalichthyids (Liu, 1973; Zhu, 1991; Liu, 1991; Pan et al., 2015) will add further information on the status of petalichthyids as a whole. These taxa share some significant features in common with petalichthyids that warrant consideration

of their belonging in a clade together. However, quasipetalichthyids are both the earliest known petalichthyid relatives and bear strong resemblances to certain arthrodires (Zhu, 1991; Pan et al., 2015). More information on the morphology of the skull of quasipetalichthyids could illuminate questions such as whether the optic fissure was lost in petalichthyids, or represents a shared primitive absence with non-placoderms.

2.6 ACKNOWLEDGEMENTS

We thank E. Bernard (NHMUK) for collection assistance and permitting us to CT scan the specimen in this work. D. Sykes and F. Ahmed (NHMUK) are thanked for assistance with CT scanning and reconstruction of the tomography data.

CHAPTER 3

NEW INFORMATION ON THE ENDOCRANIAL MORPHOLOGY OF *Ellopetalichthys scheii* KJÆR 1915 (PLACODERMI, MIDDLE DEVONIAN), WITH REMARKS ON THE MORPHOLOGY AND FUNCTION OF THE INNER EAR AND SHOULDER/NECK REGION IN PLACODERMS

3.1 INTRODUCTION

Petalichthyid placoderms exhibit a unique combination of characters from both jawless and jawed vertebrates resulting in them being key in the investigation of early vertebrate evolution (Janvier, 1996b,a; Brazeau, 2009; Brazeau and Friedman, 2014) (see chapter 2). However, despite their importance, the anatomy of this group is still poorly known, as there are very few studies on complete and three-dimensionally preserved specimens (Stensiö 1925, 1963a, 1969; Young 1978, 1985; Pan et al. 2015 and chapter 2 of this thesis). For example, the morphology of the labyrinth and the endolymphatic duct are only known for *Macropetalichthys* (Stensiö, 1969), but the morphological reconstruction is not entirely correct (refer to thesis chapter 2). Moreover, some aspect of petalichthyids endocranial morphology, for example the anatomy of their neck joint, have been considered important for their systematic but are still poorly understood (see introduction of chapter 1 for a review of petalichthyids systematic).

In this chapter, I present the first description of the internal morphology of *Ellopetalichthys scheii* using micro-CT data. *Ellopetalychthys scheii* is a petalichthyid placoderm that was first described from a partially complete, three-dimensionally preserved specimen collected from Ellesmere Island in the Canadian Arctic Archipelago

(Kiær, 1915). Kiær (1915) originally assigned it to a new species of *Macropetalichthys* (*M. scheii*) but it was later redescribed by Ørvig (1957) as *Ellopetalichthys*, based on differences in the size of the orbit, the extension of the supraorbital sensory canal, and the morphology of the ossifications in the posterior part of the endocranium.

Ørvig (1957) also showed that, unlike *Macropetalichthys*, only the posterior portion of the endocranium in *Ellopetalichthys* is ossified and that the ethmoid, orbital, and otic regions may be reduced or absent. However, this is because he was unable to observe the anterior ventral side of the specimen, which is surrounded by the matrix. In fact, my scan reveals that in *Ellopetalichthys* several features of the neurocranium are ossified, as the course of some nerve and the morphology of the brain cavity, the labyrinth, the orbital wall and the occipital joint. Some of those features, as the posterior part of the labyrinth, the endolymphatic duct and the morphology of the articular joint and occipital fossae, are not preserved in *Shearsbyaspis* (see chapter 2) and therefore this study of *Ellopetalichthys* represents an important complement to our dataset on petalichthyid braincases, helping to have a better picture of petalichthyids neurocranial anatomy.

In this work I focus in particular on the morphology and function of the labyrinth of petalichthyids, on the systematic value of the petalichthyid and placoderm neck joints, as well as and the importance of associating vagal and spinal nerve foramina on the ventral neurocranial surface as indicators to reconstruct placoderm branchial and muscular morphology. Those neurocranial features, like the labyrinth and the cranial nerves, are ubiquitous among the gnathostomes lineages and thus represent a vital source of information that allow for comparison between taxa with otherwise very different external morphology. As the holotype of *Ellopetalichthys* possess completely preserved labyrinth and endolymphatic cavities, this allow us to reappraise and review the morphology of the inner ear of Petalichthyida and compare it with that of the other early gnathostomes. In addition, the excellent preservation of the occipital area of *Ellopetalichthys* permits to investigated in more details the neck joint anatomy of petalichthyids, allowing to reconstruct the position of the branchial and

neck musculature for those animals, as well as the possible degree of movement of their head, leading to a better understanding of their ecological adaptations. Moreover, the distribution of the different types of neck joint have been used to investigate the systematic of placoderms (e.g., Denison 1975, 1978; Miles and Young 1977; Young 1979, 1986; Dupret 2004; Dupret and Zhu 2007) but still a poor understanding exists on the polarity and evolution of the neck joint in early jawed vertebrates, as well as of the primitive condition of the spinal nerve at the origin of the head-shoulder division. This new data on *Ellopetalichthys* and my review on the inner ear and neck morphology, musculature and neuroanatomy of early gnathostomes provide important evidences that can help to resolve current debates regarding the evolution of neck muscles and labyrinth anatomy in stem-gnathostomes, as well as for understanding petalichthyid systematics and their ecological adaptations.

3.2 MATERIAL AND METHODS

The holotype of *Ellopetalychthys scheii* Kiær 1915 is held in the collections of the Natural History Museum at the University of Oslo and catalogued as A13047. It consists of an incompletely preserved dermal skull-roof and exposed posterior part of the endocranium. The most anterior part of the skull is missing but the rest is well preserved and three-dimensional. It was collected from the upper part of the Bird Fiord Formation (Mayr, 1994), Late Givetian in age, in Goose Fiord of Ellesmere Island in the Canadian Arctic.

The specimen was scanned at the Imaging and Analysis Centre at the Natural History Museum in London using a Nikon Metrology HMX ST 225 X-ray micro-CT scanner. The fossil was scanned at 165 kV and 170, with a 0.1 mm thick copper filter (voxel size $26,8$ μm), to create 6284 X-ray projections. The resulting tomographic dataset was segmented and rendered in 3D using the software Mimics 18.01 (Materialise Technologielaan, Leuven, Belgium). The 3D models produced with Mimics were then imported into Blender for scientific image preparation.

3.3 DESCRIPTION

3.3.1 **Skull roof and sensory line**

The dermal skull roof of *Ellopetalichthys* is partially preserved, showing some of the underlying endocranial ossification (Fig. 3.1A-B, D). Not much more about the dermal skull roof morphology can be added than what have been previously assessed (Kiær, 1915; Ørvig, 1957). The skull is anteroposteriorly elongated, with a convex profile, and possesses large orbits that open dorsolaterally (Fig. 3.1A-B, D). The dorsal side of the skull roof has been heavily eroded so that only the cast of the dermal cover can be observed in many areas. The original ornamentation is present where the dermal surface is preserved and consists of radiating ridges with low tubercles similar to that of *Macropetalichthys*.

The data presented here corroborate the reconstruction provided by Kiær (1915) and Ørvig (1957) for the sensory line pattern in *Ellopetalichthys* (Fig. 3.1). Sensory line canals pass through tubes along the inner dermal bone surface, and open externally through a single row of pores situated in the lateral side (Ørvig 1957, plate 1), although it is not possible to segment these features due to low resolution of the scan. Overall, the sensory line pattern of *Ellopetalichthys* (Fig 3.1) resembles that of *Macropetalichthys rapheidolabis* , with anastomotic supraorbital and posterior pit line canal (Fig. 1.3). The supraorbital canals extend from the median anterior portion of the skull towards the centre of the skull roof, where they connect with the posterior pit on the nuchal plate (Fig 3.1). The infraorbital canals extend from the anterior lateral tip of the skull and joins the main lateral line. The latter projects posteromedially joining with the posterior pit line on the anterior paranuchal (Fig. 3.1). After that, the main lateral line extends posteriorly towards the end of the skull (Fig. 3.1).

My data reveal for the first time the positions of the endolymphatic duct openings (Fig. 3.1B-C). These are located mesially to the connection of the posterior pit line

and the main sensory line, as in most of the petalichthyids. They signal the position of the anterior paranuchal plate.

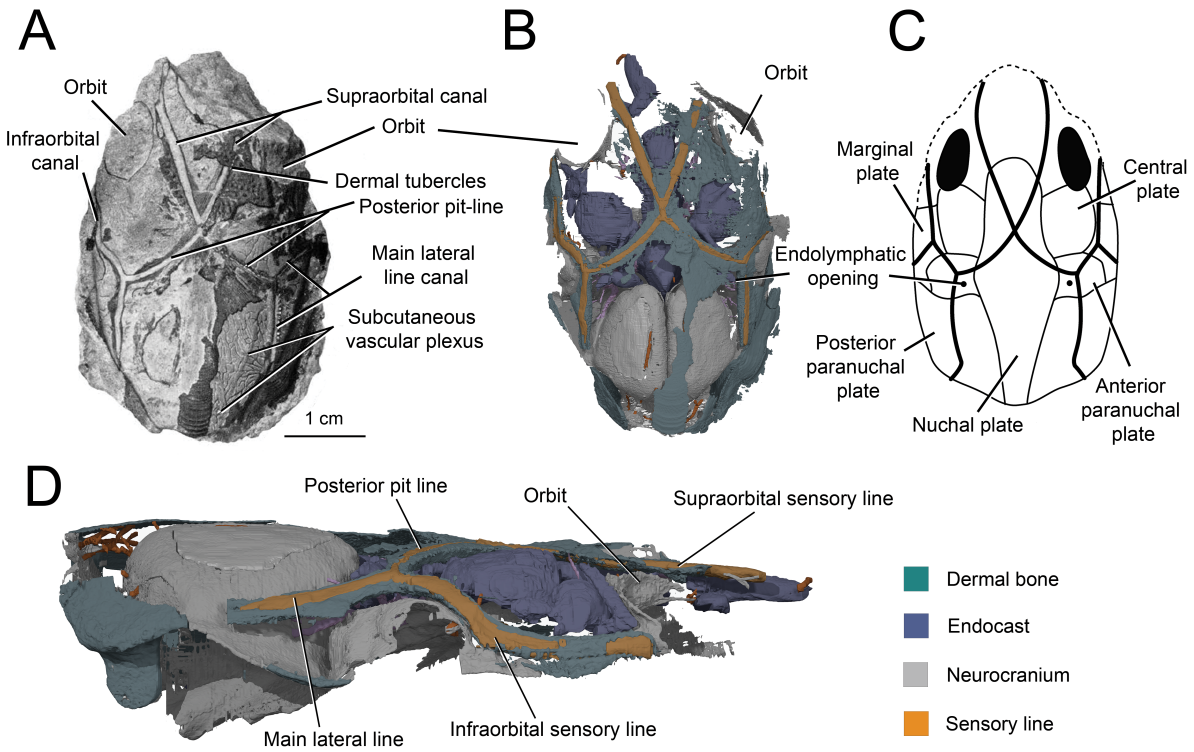

FIGURE 3.1: Skull roof and sensory lines of A13047. A, original photograph in dorsal view (from Ørvig 1957). B, 3D model in dorsal view; C restoration of the dermal skull roof pattern and sensory line of *Ellopetalichthys*, based on this study and Ørvig (1957); D, 3D model in right lateral view. Scale bars represent 10 mm.

3.3.2 **Endocranium**

The posterior portion of the endocranium has been exposed and was briefly described by Kiær (1915) and Ørvig (1957). Much of this portion of the endocranium is covered by matrix, but the CT data reveal the partial morphology of the orbital wall, the skeletal labyrinth and part of the endocavity (Figs 3.1-3.5). This shows that *Ellopetalichthys* possesses a perichondrally ossified braincase, similar to other petalichthyids (Stensiö 1925, 1963a, 1969; Young 1978, 1985 and chapter 2). Although not completely preserved, it is also possible to observe parts of the branchial cham-

ber and the postorbital articulation, as well as nerve and vascular canals of the endocranial cavity and the skeletal labyrinth (Figs 3.2-3.4).

ORBITAL REGION — The orbits are dorsolaterally oriented (Figs 3.1A-B, D; 3.2), as in most of the other petalichthyids. Only the dorsolateral and posterior wall of both the orbit can be partially reconstructed (Figs 3.1-3.4), although the preservation of this area is very limited making it difficult to observe the presence and disposition of foramina for many nerves and blood vessels. Part of the posterior wall of the posteroventral myodome (cf. *Shearsbyaspis*, chapter 2) is visible for the right orbit (Figs 3.2-3.3; my6) and it is pierced by a small canal, although it is difficult to identify which nerve or blood vessel this represents.

POSTORBITAL REGION — The postorbital endocranial region is not very well preserved due to erosion but some of the perichondral bone is preserved on the lateral side of the occipital ossification (Figs 3.1-3.5). The paravagal fossa (Figs 3.3-3.4) is very large and it is enclosed by a bifurcated vagal process (Figs 3.3-3.4). The paravagal process is pierced by a large foramen for the exit of the anterior branch of the vagus nerve (Figs 3.3-3.4 N. Xa). Anteriorly, it is possible to observe a small foramen, probably for the glossopharyngeal nerve (Figs 3.3-3.4 N.IX?). A deep groove on the lateromesial surface of the paravagal fossa shows the course of the lateral dorsal aorta (Figs 3.3-3.4).

OCCIPITAL REGION — The CT data presented here partially corroborate Ørvig's 1957 original interpretation of the occipital region of *Ellopetalichthys*, but also offers new details about the morphology of this area (Figs. 3.1-3.6). According to Ørvig (1957), the occipital area of *Ellopetalichthys* consists of two distinct elements: a flat and broad anterior median bone (Ørvig 1957, text-fig. 7; Oc.a), and a long and narrow, stalk-like posterior ossification (Ørvig 1957, text-fig. 7; Oc.a). However, my data show that these two elements are not discrete but are instead ossified into a single

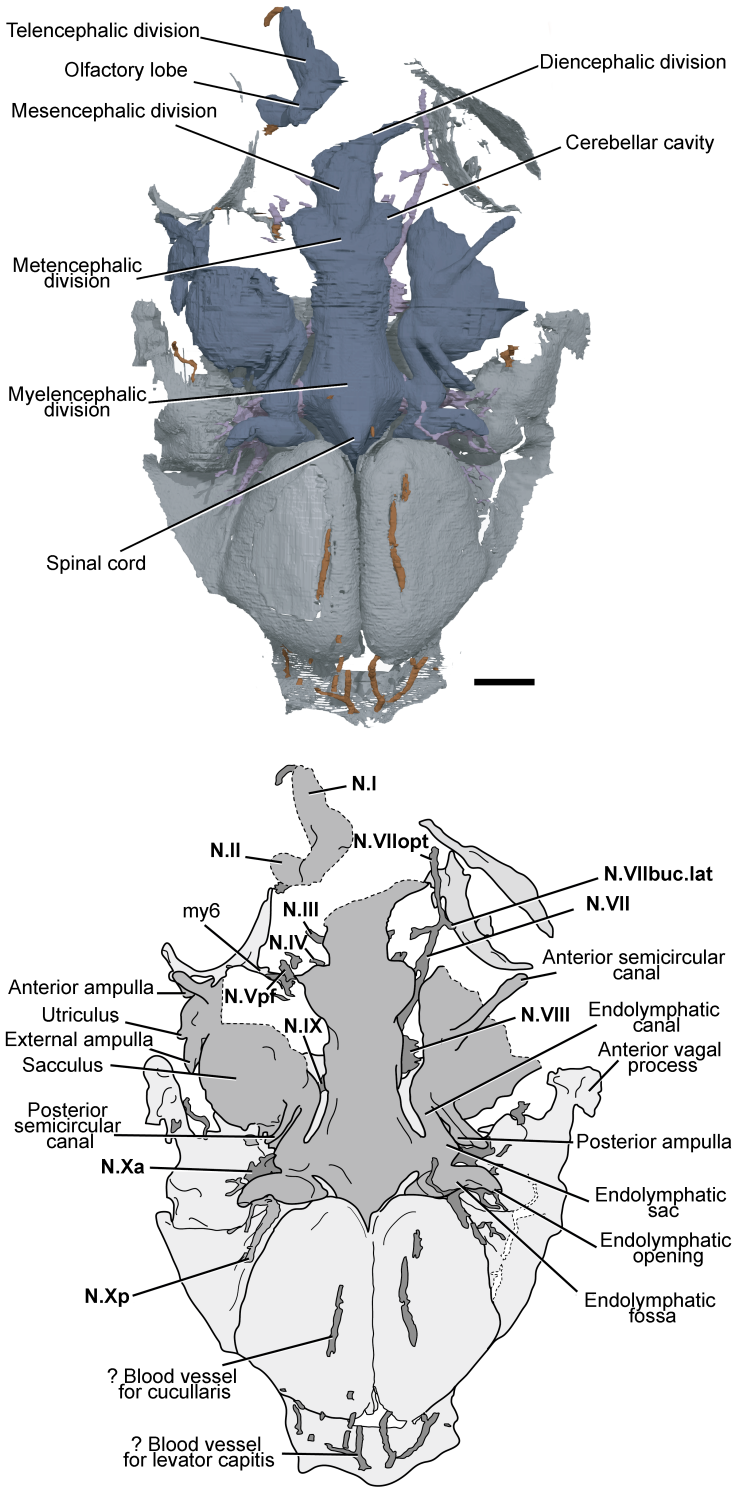

FIGURE 3.2: 3D model (top) and line drawing (bottom) of the endocavity and braincase of A13047, dorsal view. Abbreviation given in the text. Scale bar represents 0.5 cm.

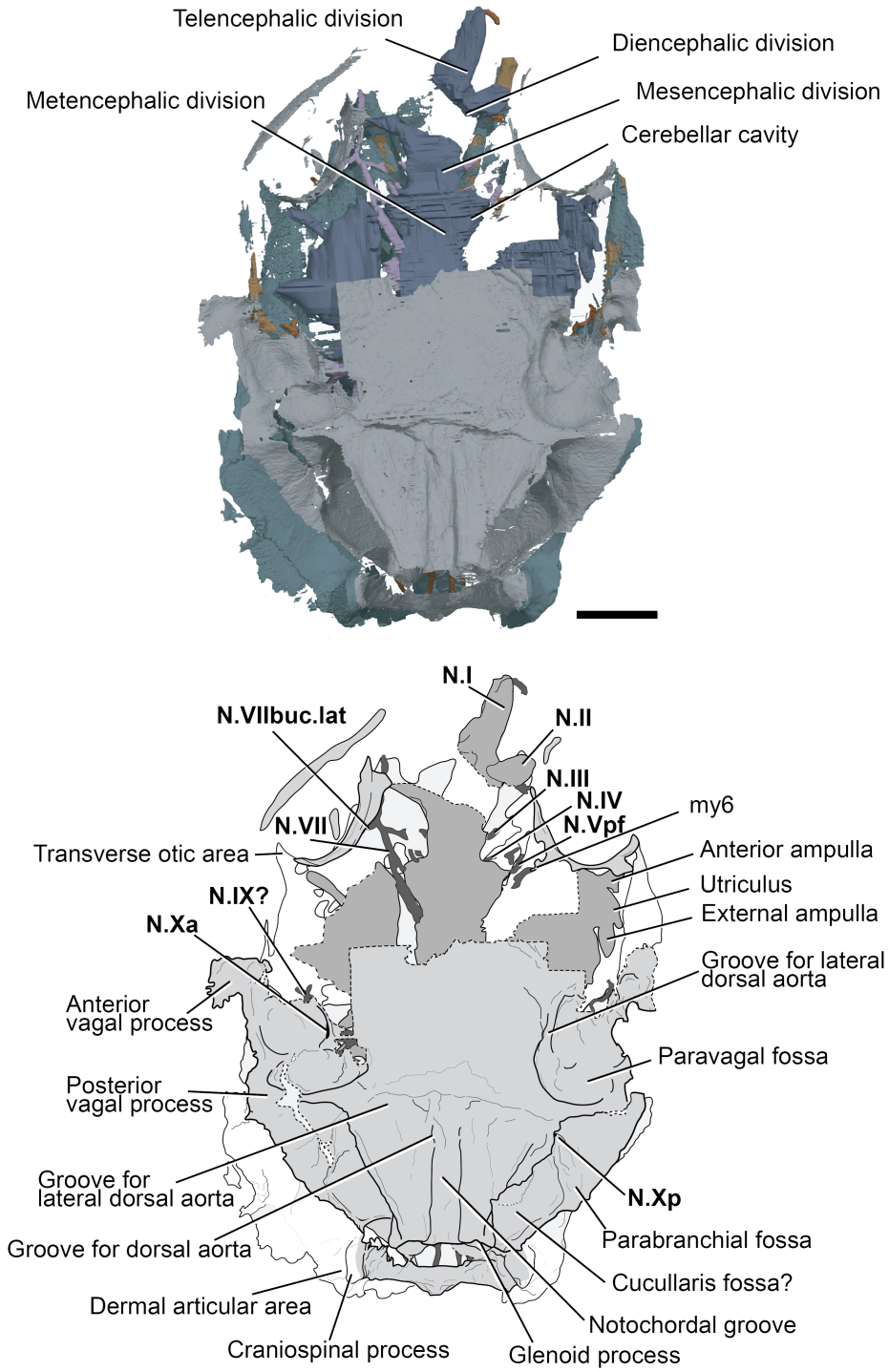

FIGURE 3.3: 3D model (top) and line drawing (bottom) of the endocavity and braincase of A13047, ventral view. Abbreviation given in the text. Scale bar represents 5 mm.

piece that is also attached to the rest of the braincase (Figs. 3.2-3.4), as in *Wijdeaspis* (Young, 1978).

Ventrally, the occipital area shows two long and stalk shaped parachordals. These are flanked on either side by a flat perichondral layer that constitutes the ventral surface of the large occipital fossa (Figs 3.3-3.4), so that the cucullaris fossa and parabranchial fossa (see discussion section for the use of these terms) are surrounded dorsolateroventrally by perichondral tissue (Figs 3.3-3.5). Additionally, the occipital fossae are separated by two distinct layers of perichondral bone (Fig. 3.6). Anteriorly, they are delimited by the posterior vagal process (Figs 3.3-3.4).

In dorsal view, the mesial posterior part of the occipital fossa is not part of the neck articulation but instead, there is an additional layer of perichondral bone that exists posteriorly to it (Figs 1D, 2). This corresponds to the lateral articular surface described by Young (1978) for *Wijdeaspis* (text-figs 1, 4). A series of canals extend between the two perichondral layers (Figs 3.1D, 3.2), and may represent blood vessels for the muscles located in the occipital fossa).

In posterior view, the morphology of the occipital area and neck joint of *Ellopetalichthys* is typical for petalichthyids, with dorsoventrally extended craniospinal process ("para-articular processes" for Young 1978) and anteriorly oriented dermal articular area (”para-articular fossa” for Young 1978). The glenoid processes are only partially preserved and are situated on the mesial side of the occipital area, between the craniospinal process (Figs 3-5). The dorsomesial surface of this area is not fully preserved, but part of the lateral articular surface (*sensu* Young 1978) is visible and is attached to the dorsal dermal component of the neck joint (Figs 3.3-3.5).

Several grooves and foramina for nerves and blood vessels are located on the perichondral bone surrounding the occipital fossa of *Ellopetalichthys*. Two deep grooves extend anteroposteriorly on the mesial dorsal surface of the fossa (Fig. 3.2) and could have contained blood vessels supplying the cucullaris muscles (see below). On the ventral side, the two stalk-shaped parachordals flank a deep groove for the notochord (Figs 3-5). On the mesial sides of the parachordals, lateral to the notochord

groove, there are haemal grooves compared to that found in *Wijdeaspis* (Young 1978, text-figs 1,2,4) and *Macropetalichthys* (Stensiö 1969, text-fig 22 A), which signal the course of the dorsal aorta (Fig. 3.3). From there, the groove extends laterally towards the posterior vagal process (Fig. 3.3).

In general, the occipital morphology of *Ellopetalichthys* is more similar to *Wijdeaspis* then to *Macropetalichthys*. With the latter, *Ellopetalichthys* differs in having a cucullaris fossa roofed by perichondral bone instead of dermal bone. Additionally, it has two distinct layers of perichondral bone separating the cucullaris fossae instead of a single "intercucullaris fossa" (Stensiö, 1969). Between *Ellopetalichthys* and *Wijdeaspis* differences exist in the shape of the posterior vagal process (supravagal crista for Young 1978), transversal in *Ellopetalichthys* and curved in *Wijdeaspis*. Also, *Ellopetalichthys* shows the presence in of a perichondral layer near the parachordal, partially enclosing the ventral side of the occipital fossa, while this is not enclosed in *Wijdeaspis*. Finally, the morphology of the lateral articular fossa of the occipital joint are different between the two taxa, more dorsoventrally elongated in *Ellopetalichthys*.

3.3.3 **Endocranial cavity**

The endocranial cavity is almost completely preserved, only missing the area anterior to the orbit and some nerve canals (Fig 3.1-3.4). As some area of the endocavities are preserved either on the left or on the right side of the specimen, a mirrored reconstruction has been produced to facilitate anatomical interpretations (Fig. 3.6). The overall morphology of the endocavity of *Ellopetalichthys* is platybasic and resembles *Macropetalichthys* and *Shearsbyaspis*, with an elongated and narrow profile that wider at the level of the trigeminal and vagus nerves (Fig. 3.6).

The telencephalic area is incomplete, but some traces of the olfactory lobe are preserved on the right side of the specimen (Figs. 3.2, 3.6). The diencephalic division is fairly complete (Figs 3.2-3.3, 3.6), with large canals for the optic tract. The mesencephalic division is almost complete, extending from behind the optic tract until

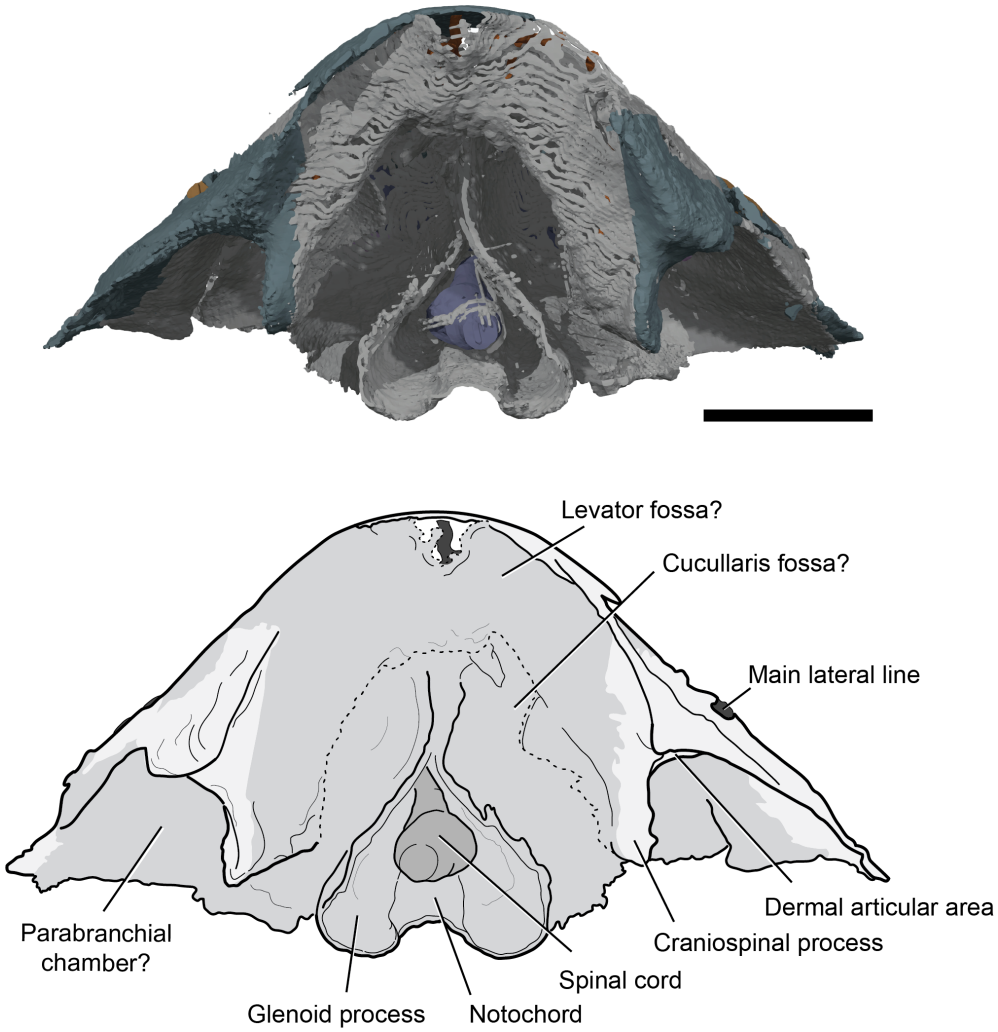

FIGURE 3.4: 3D model (top) and line drawing (bottom) of the occipital region of A13047, posterior view. Scale bar represents 5 mm.

the cerebellar cavities (Figs 3.2-3.3, 3.6). Its ventral side cannot be seen, leaving no information about the hypophysial duct (Fig. 3.3).

The cerebellar cavities of the metencephalon are well developed, showing two very distinct lobes on the dorsal side (Figs. 3.2-3.3, 3.6). The myelencephalic portion of the endocavity is entirely preserved dorsally, as a tubular area that is expanded laterally in its posterior portion where it gives origin to the vagus nerve canals (Figs 3.2, 3.6). The spinal cord canal, the posterior most part of the endocavity, becomes narrower and longer as it exits the braincase (Figs 3.4-3.5).

3.3.4 **Cranial nerves**

Only a small portion of the olfactory tract is preserved, on the right side of the specimen (Figs 3.2-3.4, 3.6; N.I) and consists of a large tubular canal, which would have probably extended anteriorly following the elongation of the skull (Fig. 3.1D). Although not completely preserved on either side of the specimen, the optic tract canal morphology can be reconstructed using the partial preservation of the left anterior and right posterior perichondral wall (Figs 3.2-3.3, 6; N. II). Among the nerves for the eye muscles, only the oculomotor nerve canal is visible, exiting from the lateral wall of the metencephalic cavity (Figs 3.2-3.3, 3.6; N.III). The canal for the profundus branch of the trigeminal nerve is preserved on the left side of the specimen, branching from the anteroventral edge of the cerebellar cavity (Figs 3.2-3.3, 3.6; N. Vpf). Both of these nerves lack information about how they exit on the orbital wall, as this area is not fully preserved.

The facial nerve is only partially preserved (Figs 3.2-3.3, 3.6; N. VII). It originates behind the cerebellar cavities, passing anterolaterally along the anterior surface of the saccular cavity. The only two branches that can be reconstructed are the ramus buccalis lateralis (Figs 3.2-3.3, 3.6; N. VII buc.lat) and the ramus ophthalmicus superficialis (Figs 3.2-3.6; N. VIIopt). Their division from the main canal of the facial nerve can be seen on the left side (Figs 3.2-3.3, 3.6). The ramus buccalis lateralis is a short canal entering the orbit through a small foramen on the lateral wall of the orbit, while the superficial ophthalmic branch canal extends anterodorsally towards the snout, following the supraorbital sensory line (Figs 3.1-3.3, 3.6).

The acoustic (N.VIII) and glossopharyngeal (N.IX) nerves are partially preserved and exit from the anterior myelencephalic portion of the endocavity (Figs 3.2-3.3, 3.6). The acoustic nerve extends laterally to meet the labyrinth (Figs 3.2-3.4, 3.6; N. XIII) and the glossopharyngeal nerve extends posteroventrally, passing below the labyrinth (Fig. 3.4; N.IX). The entire course of the glossopharyngeal nerve is not

preserved, but a small portion of the posterior portion of it is visible, exiting on the anterior area of the paravagal fossa (Fig 3.4; N.IX?).

The vagus nerve is very well preserved on both sides and has a complex morphology. From the vagal recess two branches bifurcate with an anterior branch extending transversally towards the paravagal fossa (Fig 3.2-3.4, 3.6; N.Xa) and a posterior branch extending posterolaterally towards the posterior vagal process and opening in the occipital (parabranchial) fossa (Figs 3.2-3.4, 3.6; N.Xp). Several small canals branch out from both the anterior and posterior branch of the vagus nerve, projecting dorsolaterally to innervate the main sensory line canals (Figs. 3.2-3.4, 3.6).

3.3.5 **Labyrinth cavity**

Both the labyrinth cavities are visible, even if incompletely preserved (Figs 3.2-3.4, 3.6). The left labyrinth preserves the anatomy of the anterior semicircular canal, sacculus, posterior semicircular canal, and ampulla. The right labyrinth shows the anatomy and position of the anterior ampulla, external utriculus, external ampulla, and part of the posterior semicircular canal. The good preservation of the main inner ear on the both sides of the specimen allows for the reconstruction of the overall anatomy of the inner ear of *Ellopetalichthys* (Fig. 3.6). In general, the labyrinth appears as a very deep and large cavity that is at least as big as the orbit, and is almost in contact with the posterior orbital wall, anteriorly, and the paravagal fossa posteriorly (Figs 3.1-3.4).

The anterior ampulla is placed just behind the posterior orbital wall (Figs. 3.2, 3.6). The anterior semicircular canal extends from the centre of the dorsal side of the sacculus to towards the anterior ampulla. The external ampulla extends parallel to the sacculus and connects with the anterior ampulla by a ventrally bent utriculus (Figs 3.2-3.3, 3.6). The posterior ampulla is located at the posteromesial end of the sacculus, near the canal for the vagus nerve (Figs 3.2, 3.6). The posterior semicircular canal crosses the sacculus at the level of the origin of the glossopharyngeal nerve

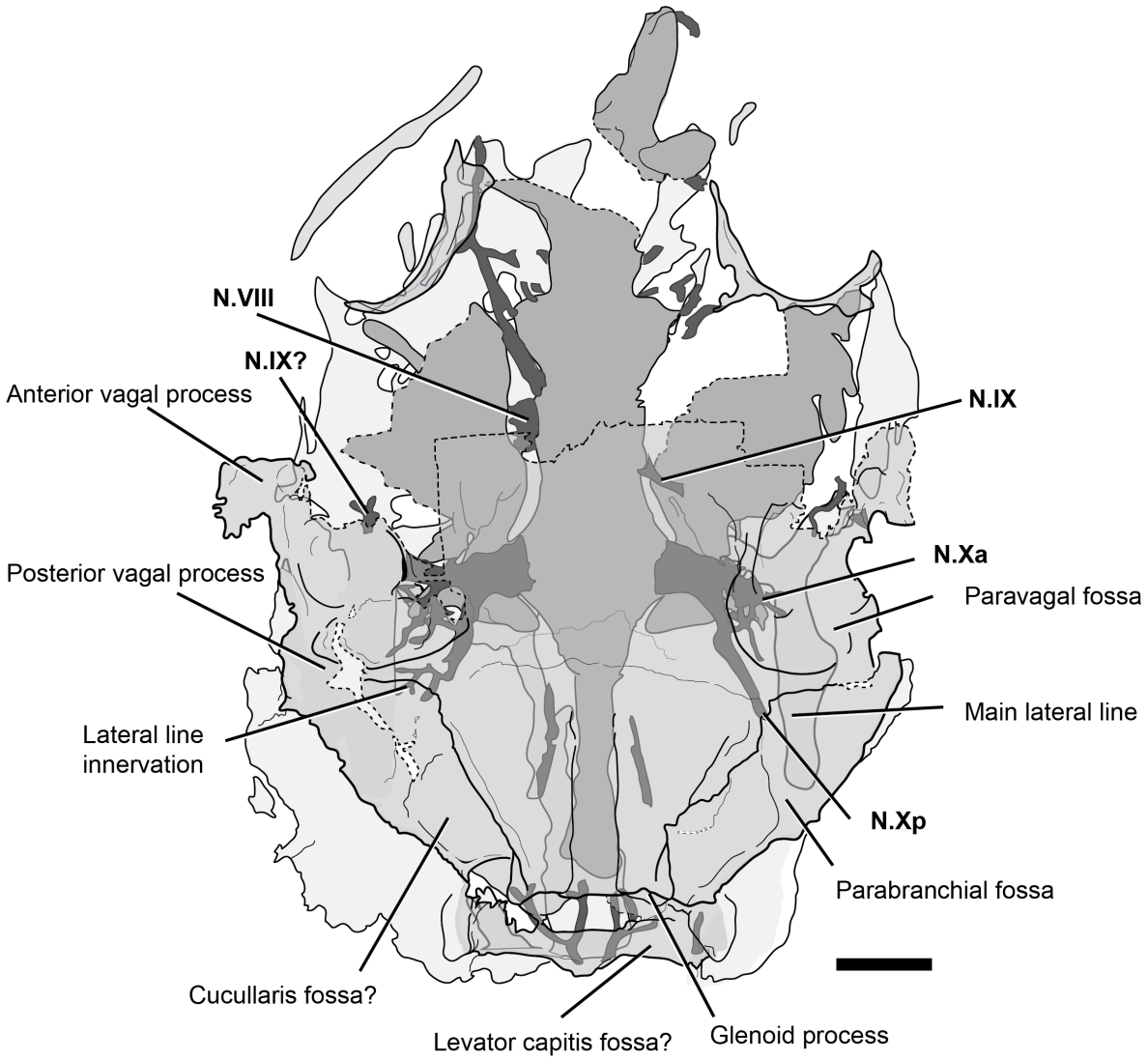

FIGURE 3.5: Line drawing of the endocavity and braincase of A13047, ventral. Transparency has been applied to show the relationships between some nerve canals and endocranial fossae. Abbreviation for nerves given in the text.Scale bar represents 5 mm.

and continues laterally to the posterior ampulla. The posterior semicircular canal is shorter than the anterior one. The anterior and posterior semicircular canals are not in contact so that a crus commune is absent (Figs 3.2, 3.6).

The endolymphatic morphology is very complex, with an endolymphatic canal connected to the inner ear via an endolymphatic sac (Figs 3.2, 3.6). A short canal that probably represents the anterior portion of the endolymphatic canal exits from the inner ear and following the curvature of the vagal recess. Here, the canal enlarges

laterally into an anteroposteriorly elongated endolymphatic sac that passes dorsally to the canal for the vagus nerve. This sac then extends in a posterolaterally directed canal that twists dorsodistally and enlarges in a laterally expanded endolymphatic fossa (Figs 3.2, 3.6). The latter opens to the outside with a distinct foramen on the skull roof (Fig. 3.1B-C).

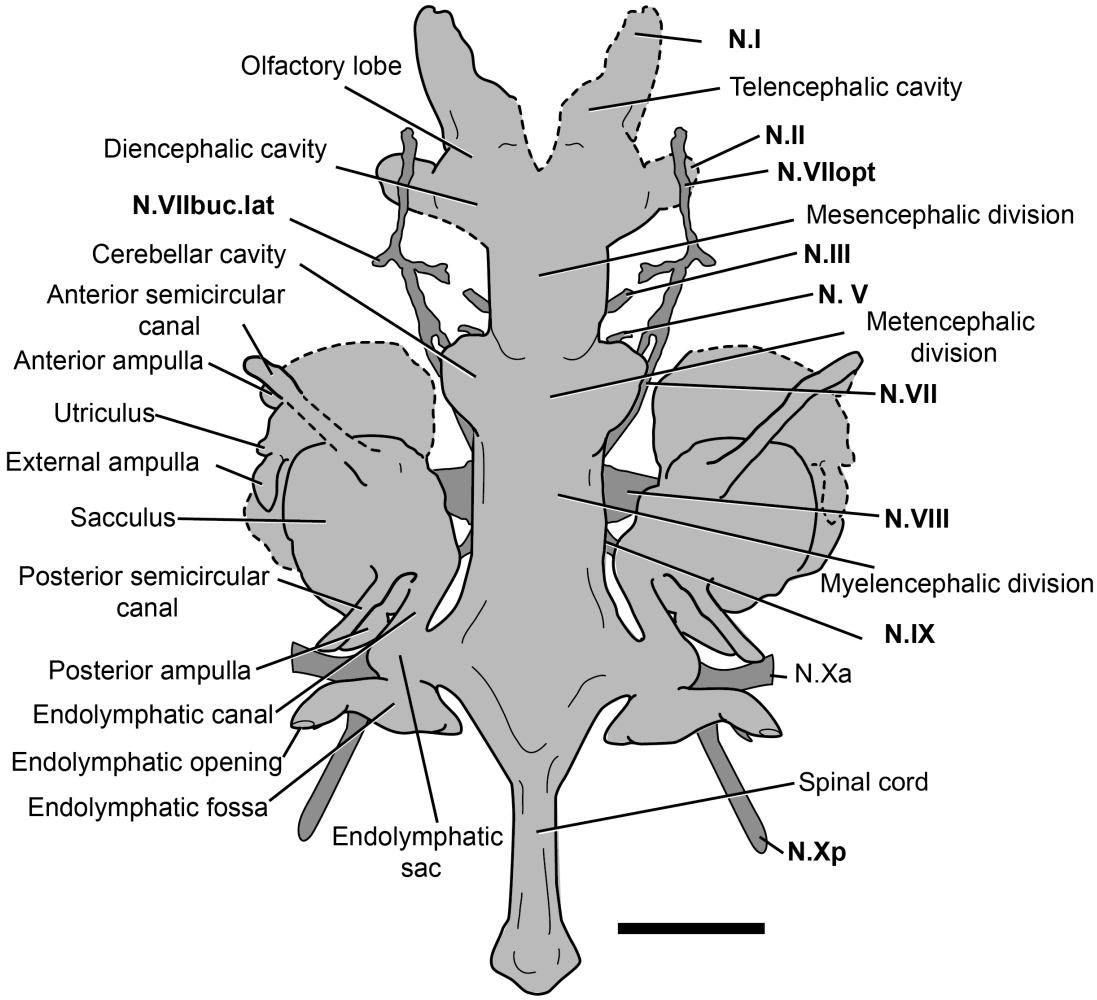

FIGURE 3.6: Line drawing reconstruction of the endocavity of A13047, dorsal view. Abbreviation for nerves given in the text. Scale bar represents 1 cm.

3.4 DISCUSSION

This study of *Ellopetalichthys* represent the first investigation of the inner ear and neck morphology of a petalichthyid carried out with the help of modern computed tech-

niques. It provides for the first-time detailed information about the innervation and internal anatomy of the occipital region of the neurocranium in a petalichthyid, as well as of the posterior part of the labyrinth and endolymphatic duct. Those features were not clearly resolved in *Macropetalichthys*, which detailed description have been so far took as the example for petalichthyid internal morphology. Thus, the data presented here allows to refine previous interpretation on the inner ear and occipital morphology of *Macropetalichthys*. In the following discussion, I revise the anatomy of the inner ear of petalichthyids and compare it with the conditions present in other early vertebrates. Moreover, I discuss some of these morphological features of *Ellopetalichthys* that can gives us a better understanding of the different type of neck joints in early vertebrate, their potential primitive and derived conditions and their systematic value. In addition, since the occipital region of *Ellopetalichthys* preserves several details of the vascular, neural and muscular anatomy, it permits a thorough analysis of the functionality of the peculiar neck joint in petalichthys, helping to shade some light on their possible ecology. Finally, the excellent preservation of the vagal canals helps to discuss some hypothesis about the primitive condition of the neck innervation in early jawed vertebrates, as well as the real nature of the occipital fossae on the neurocranium of petalichthyids and other placoderms.

3.4.1 **The inner ear morphology of petalichthyids - revision and comparison**

To date, only the inner ear morphology of *Macropetalichthys* was known in good detail, showing the position and anatomy of the sacculus, utriculus, ampullae, semicircular canals and endolymphatic duct (Stensiö, 1969). The anterior morphology of the inner ear is now also known for *Shearsbyaspis oepiki* (chapter 2), which demonstrated that some of Stensiö's (1969) interpretations concerning the position of the anterior ampulla and anterior semicircular canal were mistaken (Fig. 2.11). However, only the anterior part of the inner ear is preserved in *Shearsbyaspis* (chapter 2). The

good preservation of the whole labyrinth cavity in *Ellopetalichthys* thus offers a third comparative specimen to review petalichthyid inner ear morphology (Fig. 3.7).

The position of the anterior ampulla and anterior semicircular canals are the same in *Ellopetalichthys* and *Shearsbyaspis* (Fig. 3.7; a. ampulla, a. semi.c), which reinforces the idea that Stensiö's (1969) reconstructions of these features in *Macropetalichthys* were not accurate. This suggests that the anterior ampulla in petalichthyids is placed in a very anterolateral position (external placement) near the transverse otic process. The anterior semicircular canal is very long, narrow and straight, without the curvature hypothesised by Stensiö (1969). The anteromesial portion of the sacculus bears a large utriculus (Fig. 3.7), which mesial edge is followed by the course of the facial nerve so closely that the limit between these two structures are very difficult to discern in the tomographic dataset.

The position of the posterior ampulla and posterior semicircular canal in *Ellopetalichthys* is instead very similar to that of *Macropetalichthys*, supporting Stensiö's (1969) interpretations (Fig. 3.7; p. ampulla, p. semi.c). The ampulla is in a symmetrical diagonal position with respect to the anterior ampulla and is very close to the canal for the vagus nerve. The posterior semicircular canal is shorter than the anterior semicircular canal but it has a similar morphology, extending straight from the medial portion of the sacculus and bending sharply downward to connect to the ampulla.

The posterior and anterior semicircular canals are not connected together so that a crus commune and a sinus superior are absent in macropetalichthyids (Fig. 3.7). A connection between these two semicircular canals is present in *Romundina* (Dupret et al., 2017a), arthrodires (Goujet, 1984a), and possibly antiarchs (Zhu and Janvier, 1996), among placoderms, in addition to lampreys, heterostracans, galeapids, osteostracans, osteichthyans, and non-elasmobranch chondrichthyans (see review in Maisey 2001b and chapter 4 of this thesis, figure 4.9). The dorsal endocranial roof of the early petalichthyid *Diandongpetalichthys* bears impressions of ridges created by the connecting anterior and posterior semicircular canals that are comparable to what is observed in the other vertebrates (Zhu 1991, text-fig. 2), suggesting that the

morphology observed in the macropetalichthyids is apomorphic. A crus commune is absent in elasmobranchs and it adapted, together with other inner ear features, to low-frequency phonoreception (Maisey, 2007; Maisey and Lane, 2010). However, there is not enough evidence to hypothesise the same adaptation for the macropetalichthyids.

The external ampulla is preserved in *Ellopetalichthys*, *Shearsbyaspis*, and *Macropetalichthys* (Fig. 3.7; e. ampulla), and is connected with the anterior ampulla by a well-developed utriculus that is dorsally bulbous and curved and ventrally tubular. Although the utricular morphology between the external and anterior ampulla was not reconstructed accurately in *Macropetalichthys*, the external ampulla occupies the same position, lateral to the sacculus and posterodorsally to the ampulla in all three of the taxa. The external semicircular canal is not well preserved in *Ellopetalichthys* and *Shearsbyaspis* but partially preserved in *Macropetalichthys*, suggesting a similar morphology (Fig. 3.7; e. semi.c).

Ellopetalichthys and *Macropetalichthys* share a similar endolymphatic duct morphology that is unique to the two taxa. The endolymphatic duct (Fig. 3.7; d. end) is a long, straight tube that projects posteriorly and expands into an endolymphatic sac (Fig. 3.7; sac.end). This is further connected with a transverse, externally projected fossa (Fig. 3.7; f. end) that opens with an endolymphatic pore (Fig. 3.7; o.end) on the posterior paranuchal plate (Fig. 3.1B-C). In *Ellopetalichthys*, the endolymphatic fossa is longer and oriented perpendicular to the duct and not slightly posteriorly oriented like in *Macropetalichthys*. Even if usually compared with the endolymphatic sacs present in *Brindabellaspis* (Young 1980, text-fig. 10) and *Minicrania* (Zhu and Janvier, 1996) (text-figs 6-7), the endolymphatic duct of petalichthyids project lateroexternally and on the paranuchal plate, instead of lateromesially and on the nuchal plate, like in those non-petalichthyid taxa (see chapter 4 for a more thorough review on placoderms endolymphatic morphology).

The inner ear morphology of petalichthyids is complex and differs substantially from that of the other vertebrates, for example, in the anatomy of the endolymphatic

sacs and in the position of the ampullae. However, the earliest members of the Petalichthyida, the quasipetalichthyids, seems to possess a condition similar to that of other gnathostomes, both in the anatomy of the semicircular canal and the endolymphatic duct (Zhu, 1991; Dupret, 2008). This suggests that the complex inner ear morphology observed in *Ellopetalichthys*, *Shearsbyaspis*, and *Macropetalichthys* could be a specialization of the macropetalichthyids, which differ from the quasipetalichthyids by having a flatter morphology with enclosed dorsolaterally placed eyes, possibly related to a demersal adaptation.

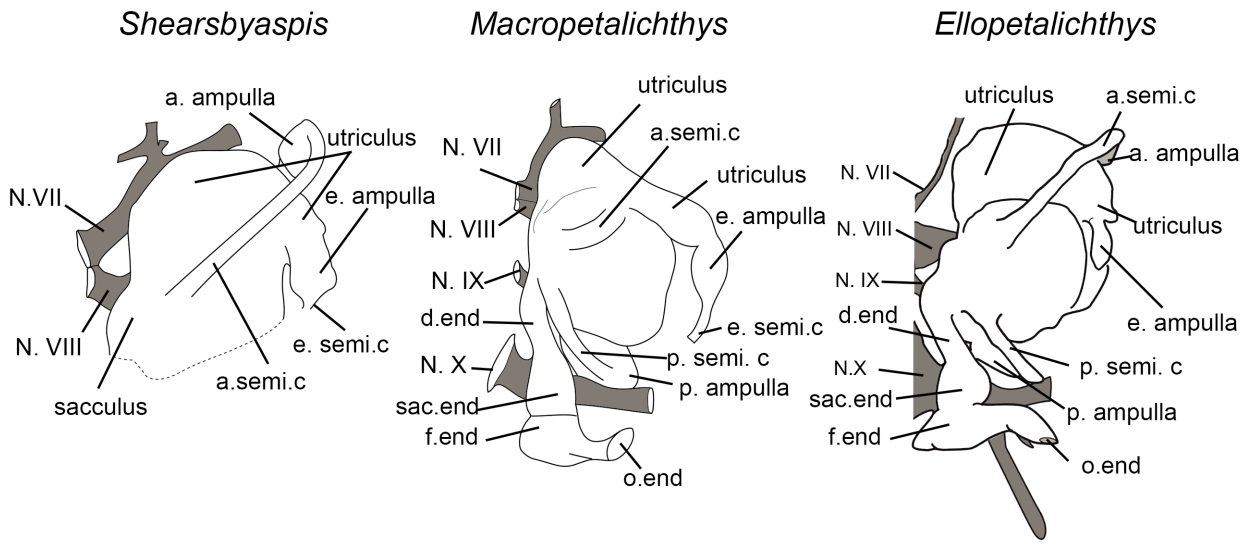

FIGURE 3.7: The morphology of the skeletal labyrinth of *Shearsbyaspis* (left), *Macropetalichthys* (center) and *Ellopetalichthys* compared. *Macropetalichthys* is redrawn from Stensiö (1969) with label changed after chapter 2 and this chapter. Abbreviations: a.ampulla, anterior ampulla; a.semi.c, anterior semicircular canal; d.end, endolymphatic duct; e.ampulla, external ampulla;, e.semi.c, external semicircular canal; f.end, endolymphatic fossa; o.end, endolymphatic opening; p.ampulla, posterior ampulla; p.semi.c, posterior semicircular canal; sac.end, endolymphatic sac; N. VII, facial nerve; N.VIII, acoustic nerve; N. IX, glossopharyngeal nerve; N. X, vagus nerve. Not in scale.

3.4.2 **The occipital joint in placoderms**

Most petalichthyids possess a cranial joint articulation with a longitudinal dermal articular area that rests parallel to the length axis of the skull and with vertical

oriented craniospinal processes (Figs 3.8-3.9). This peculiar articular joint, usually called a "spoon-like" articulation, is well preserved in *Wijdeaspis* (Young, 1978). *Macropetalichthys* (Stensiö, 1925, 1963a, 1969), *Ellopetalichthys* (Ørvig 1975 and this chapter), and *Diandongpetalichthys* (Zhu, 1991) (Fig 3.9). In *Ellopetalichthys*, *Wijdeaspis*, and *Macropetalichthys*, it is also possible to observe the two very peculiar long and narrow parachordals (Fig. 3.9). This type of articulation has not been recognised in other petalichthyids (Zhu, 1991), although similar lateroventically oriented craniospinal processes are visible in *Eurycaraspis* (Liu, 1991) and *Pauropetalichthys* (Pan et al., 2015) (Fig. 3.9).

The occipital joint of petalichthyids is different from that of the other placoderms (Figs 3.8-3.9), Additionally, different groups of placoderms exhibit different type neck joints. Phlyctaenioid arthrodires have a glenoid condyle on the anterior dorsolateral plate of the should girdle that articulate with a transverse articular fossa on the paranuchal plate of the cephalic armour, a condition referred as the ginglymoid neck joint (e.g., Long 1984; Forey and Gardiner 1986; Gardiner and Miles 1990; Goujet 1984a,b; Dupret 2004; Dupret et al. 2009; Zhu et al. 2016). A similar condition is present in antiarchs, called reversed ginglymoid, with the difference being that in this group the articular fossa is on the dermal shoulder girdle and the cephalic armour possess a transverse condyle articulating with it (e.g., Stensiö 1969; Miles and Young 1977; Zhang 1980a; Young 1984; Zhu 1996. Still other placoderms, for example actinolepids arthrodires, *Wuttagoonaspis* and "acanthothoracids", present an articulation constituted by overlapping surfaces between dermal bones, which is referred to as the sliding joint articulation (e.g. Ritchie 1973; Denison 1978; Young 1980; Goujet 1984a,b; Forey and Gardiner 1986; Dupret 2004; Dupret et al. 2009; Olive et al. 2011). Rhenanids lack a proper cervical joint, probably related to the extensive tesserated area constituting their skull (Gross, 1963; Goujet, 1984a). Ptyctodonts are usually considered (and coded, e.g., Zhu et al. 2016) as having an articulation similar to that of petalichthyids, as they possess a lateroventrally oriented occipital process (Miles and Young, 1977; Trinajstic et al., 2012). However, their occipital articulation

shows differences from the typical "spoon-like" articular joint that is present in macropetalichthyids and *Diandongpetalichthys*, and is instead more similar to what can be seen in early petalichthyids like *Eurycaraspis* (Liu, 1991) and *Pauropetalichthys* (Pan et al., 2015).

The distribution of these different cranial articulations has been used to investigate the systematics of placoderms, especially within arthrodires (e.g., Denison 1975, 1978; Miles and Young 1977; Young 1979, 1986; Dupret 2004; Dupret and Zhu 2007). On the other hand, as discussed in chapter 5, many recent comprehensive analyses on early gnathostomes do not thoroughly investigate the anatomy of the articular joint. For example, Giles et al. (2015b) and King et al. (2016) do not have a character that considers all of the types of occipital articulations, focusing only between ginglymoid and not ginglymoid. Other studies (Dupret et al., 2014; Zhu et al., 2016) mistakenly code *Romundina* as having a spoon-like articulation instead of the sliding type (Ørvig, 1975; Goujet, 1984b). Osteichthyans possess a sliding joint articulation (e.g., Zhu et al. 2009) but osteostracans and galeaspids do not possess any trunk-head division. Moreover, the two maxillate placoderms, *Entelognathus* and *Qilinyu*, which usually fall in a phylogenetic position between placoderms and crown-gnathostomes, have very different occipital joint morphology between each other (Zhu et al., 2013; Giles et al., 2015b; Zhu et al., 2016). *Qilinyu* shows a transversely extending condyle on the shoulder girdle which articulates with a fossa on the skull roof, a condition reminiscent to the ginglymoid articulation (Zhu et al., 2016). *Entelognathus* was previsouly regarded as possessing a sliding neck joint (Zhu et al., 2013). However, Zhu et al. (2016) show that this taxon lacks a clear dermal articular surface along the posterior margin of the skull so that a dermal neck joint seems to be absent. As a result, the polarity of this character in these placoderms is difficult to assess, thereby preventing an outgroup comparison. As such, the plesiomorphic state for the occipital articulation in jawed vertebrates remains unclear.

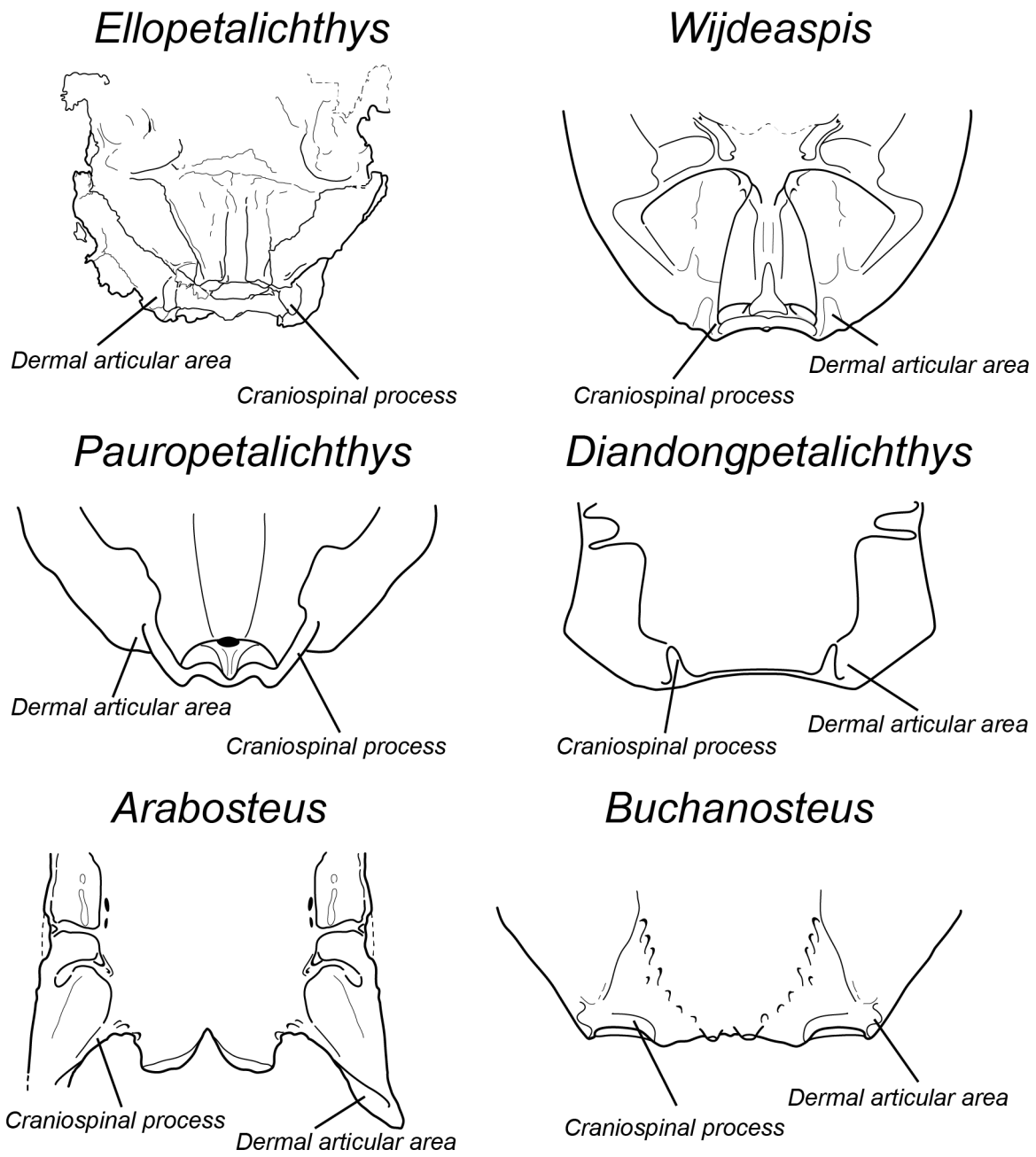

FIGURE 3.8: Occipital region of the petalichthyids *Ellopetalichthys* ("spoon-like" neck joint) and *Wijdeaspis* ("spoon-like" neck joint) (after Young 1978), the quasipetalichthyids *Pauropetalichthys* (possibly "spoon-like" neck joint) (after Pan et al. 2015) and *Diandongpetalichthys* ("spoon-like" neck joint) (after Zhu 1991), the "acanthothoracid" *Arabosteus* (sliding neck joint) (after Olive et al. 2011) and the phlyctaenioid arthrodire *Buchanosteus* (ginglymoid neck joint) (after Young 1979). Ventral view. Not to scale.

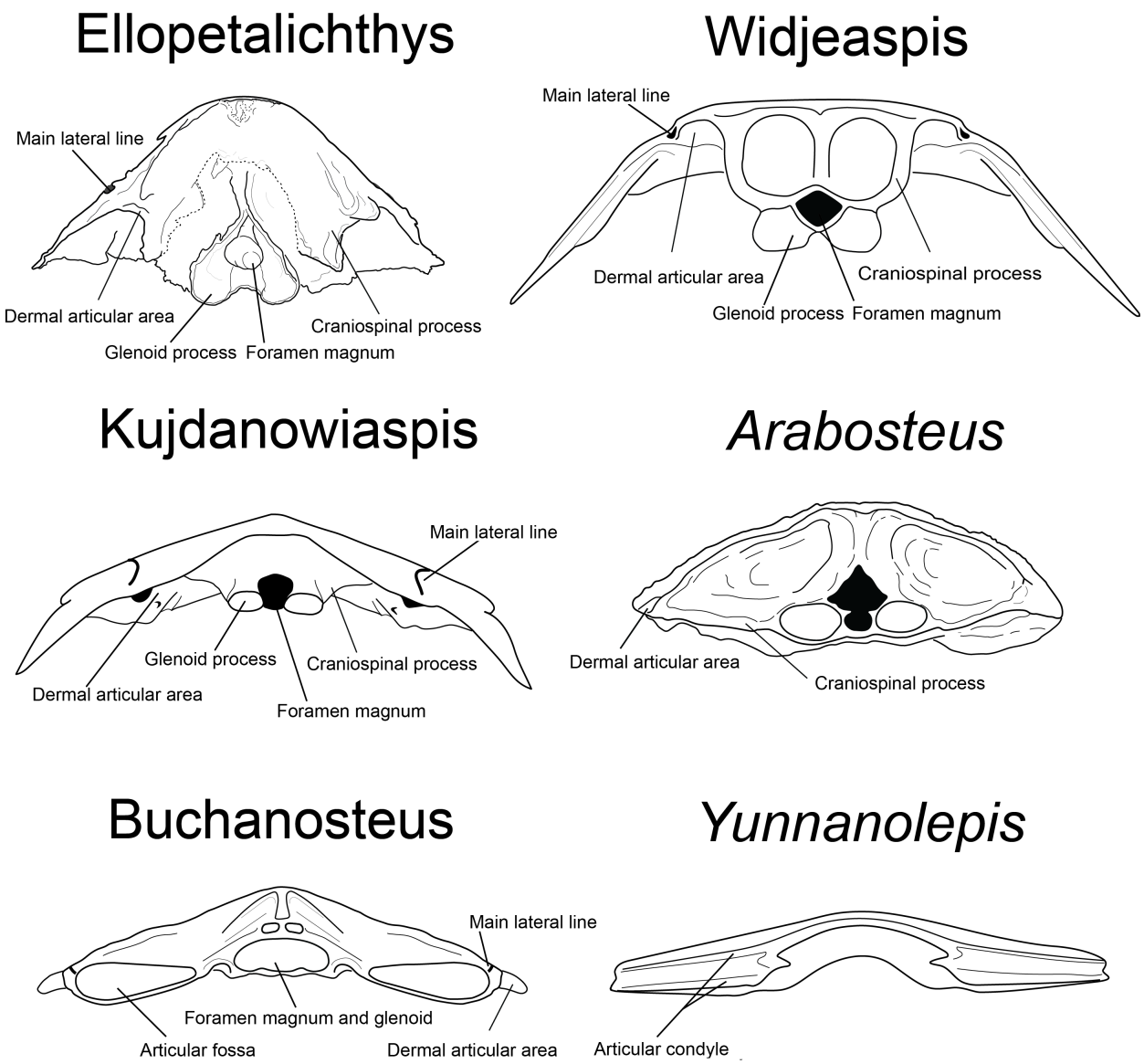

FIGURE 3.9: Occipital region in posterior view of of the petalichthyids *Ellopetalichthys* (spoon-like neck joint) and *Wijdeaspis* (spoon-like neck joint) (after Young, 1978), the actinolepid arthrodire *Kujdanowiaspis* (sliding neck joint) (after Stensiö 1969), the "acanthothoracid" *Arabosteus* (sliding neck joint) (after Olive et al. 2011), the phlyctaenioid arthrodire *Buchanosteus* (ginglymoid neck joint) (after Young 1979) and the antiarch *Yunnanolepis* ("reverse-ginglymoid" neck joint) (after Zhang, 1980). Not to scale.

3.4.3 The petalichthyid "spoon-like" neck joint: functional implications

The function of the unique morphology of the neck joint of petalichthyids is not fully understood and has always been a conundrum for palaeontologists (Young,

1978). Miyashita (2016) suggested that the head-shoulder separation and the origin of distinctive neck musculature probably occurred approximately at the same time as the origin of jaws, making this a significant anatomical and functional transition to understand. Therefore, investigating the different types of neck joints and muscle attachments in stem-vertebrates can provide important clues about the evolution between jawless and jawed vertebrates (see review in Ericsson et al. 2013). Attachment sites for neck musculature are usually present on the surface of the dermal shoulder girdle and skull of placoderms, and include sites for the large levator and the cucullaris muscles (refer to Trinajstic et al. 2013). However, inferring neck musculature in placoderms is problematic, as the muscle attachment sites for these neck muscles appears different from modern jawed vertebrates (Trinajstic et al., 2013; Edgeworth, 1935). In fact, in modern osteichthyians and elasmobranchs the cucullaris muscle is superficial in origin (it attaches to the vertebral column by epaxial muscle by fascia) rather than being attached to bone surfaces. Exception are holocephalans, where the muscles have chondrocranial attachments. For this reason, Trinajstic et al. (2013) used holocephalan neck anatomy as a model to reconstruct the neck musculature for eubrachythoracid placoderms.

Placoderm neurocrania exhibit several fossae that housed neck and/or branchial musculature (Johanson, 2003; Carr et al., 2009) (Fig. 3.10). These fossae are delimited by endocranial processes, which have been recently homologised by Giles et al. (2015b), and possess several foramina and grooves for nerves and blood vessels serving the different soft tissues (Fig. 3.10). In holocephalans, branchial and neck muscles have different innervation, with the cucullaris muscles being innervated by the spinal accessory nerve (SAN), instead of the vagal (N. X) nerve. If we accept a holocephalan model for reconstructing the neck muscles in placoderms, the foramina for the branchial cranial motor nerves (branches of the trigeminal, facial, glossopharyngeal, and vagus nerve) should then be used to discern neck muscle fossae from branchial fossae on placoderm neurocrania.

Major fossae in placoderm braincases include the hyoidean fossa, located between the transverse otic process and the vagal process; the paravalgal fossa, located between the anterior and posterior vagal process in taxa that possess a bifurcated vagal process; and the so-called "cucullaris fossa" (*sensu* Goujet 1984a), between the vagal process and the craniospinal process (Fig. 3.10). The hyoidean and paravagal fossae are innervated by two branchial motor nerves, the glossopharyngeal (N.IX) and the anterior branch of the vagus nerve (N. Xa), respectively, and contained muscles associated with the gill basket (Fig. 3.10). Neck musculature in placoderms is usually interpreted as associated with cucullaris fossa. However, the so-called "cucullaris fossa" (*sensu* Goujet 1984a) in placoderms is pierced anteriorly by the posterior branch of vagus nerve (Xp). Carr et al. (2009) pointed out that using the term cucullaris fossa for placoderms is misleading, because that fossa instead represents the confluence of the parabranchial fossa (containing gill muscles) and a true cucullaris fossa (containing neck muscles) (Fig. 3.10). For this reason, here I refer to that fossa as the occipital fossa.

The occipital fossa (parabranchial plus cucullaris) in placoderms is pierced by both the posterior branch of the vagus nerve and a series of foramina for the craniospinal nerves (Fig. 3. 10). Several papers from embryological studies have suggested that the accessory nerve is not a special branch of the vagal nerve but instead a highly modified spinal nerve in stem-gnathostomes not contained in the vagal bundle (Kusakabe et al., 2011; Tada and Kuratani, 2015). The suggestion that the occipital fossa in placoderms contained both a branchial area and the cucullaris muscle may support this hypothesis, because it implies that the cucullaris muscle was not innervated by a vagal branch, innervating the branchial area, but instead by one (or more) of the spinal nerve. In *Brindabellaspis* the first spinal nerve that enters in the parabranchial fossa differs from the other spinal nerve in not having a dorsally oriented branch (Young 1980, text-fig. 12), which could represent an independent spinal nerve for the innervation of the cucullaris muscle. In petalichthyids, the posterior branch of the vagus nerve seems to be very distant to the possible insertion of

the cucullaris muscles (see below). These features suggest that the cucullaris muscle in placoderms was probably innervated by a spinal nerve that was not contained in the vagus bundle. If this is the case, then this spinal nerve may represent the ancestor of the spinal accessory nerve.

As I discussed before, in holocephalan the cucullaris muscle is innervated by the accessory spinal nerve. This means that the position of those nerve canals can help to discern the relative position of the cucullaris and the parabranchial fossa. Unfortunately, very little information is available about the spinal nerve in petalichthyids. A foramen for a spinal nerve has been reported in *Wijdeaspis* on the internal side of the occipital fossa (Young 1978, text-fig 5). Based on the course of the parachordal stalk and the endocranial cavity, the spinal nerve would have been placed on the external surface of the parachordals, medially to the occipital chamber. The posterior branch of the vagus nerve, serving gills muscles, is not evident in *Wijdeaspis*, but it is very clear in *Ellopetalichthys*, where it enters laterally to the occipital fossa and not medially near the parachordals (Figs 3.3-3.4). This may imply that the branchial area in the occipital (thus parabranchial) fossa would have been placed on the external side in respect of the area representing the cucullaris fossa, with the latter being located along the parachordal. This is supported by the fact that the cucullaris muscle is usually located laterally to the dermal articulation, which is medial in petalichthyids compared to the lateral position in the other placoderms. Additionally, the dorsal surface of each occipital fossa possesses a deep groove, potentially indicating the course of a blood vessel for the cucullaris muscles (Fig. 3.2).

The position of muscles in petalichthyids is related to the position of the articulation between the skull and the thoracic armour. The cucullaris muscle would have inserted medially, lateral to the parachordal and external to the dermal articular joint. The levator capitis would probably insert on the lateral articular facets, which are located medially to the dermal articular joint, located approximately at the posterior edge of the paranuchal plate. This central position of the neck muscles is combined with the peculiar spoon-shaped occipital joint, suggesting that the lateral posterior

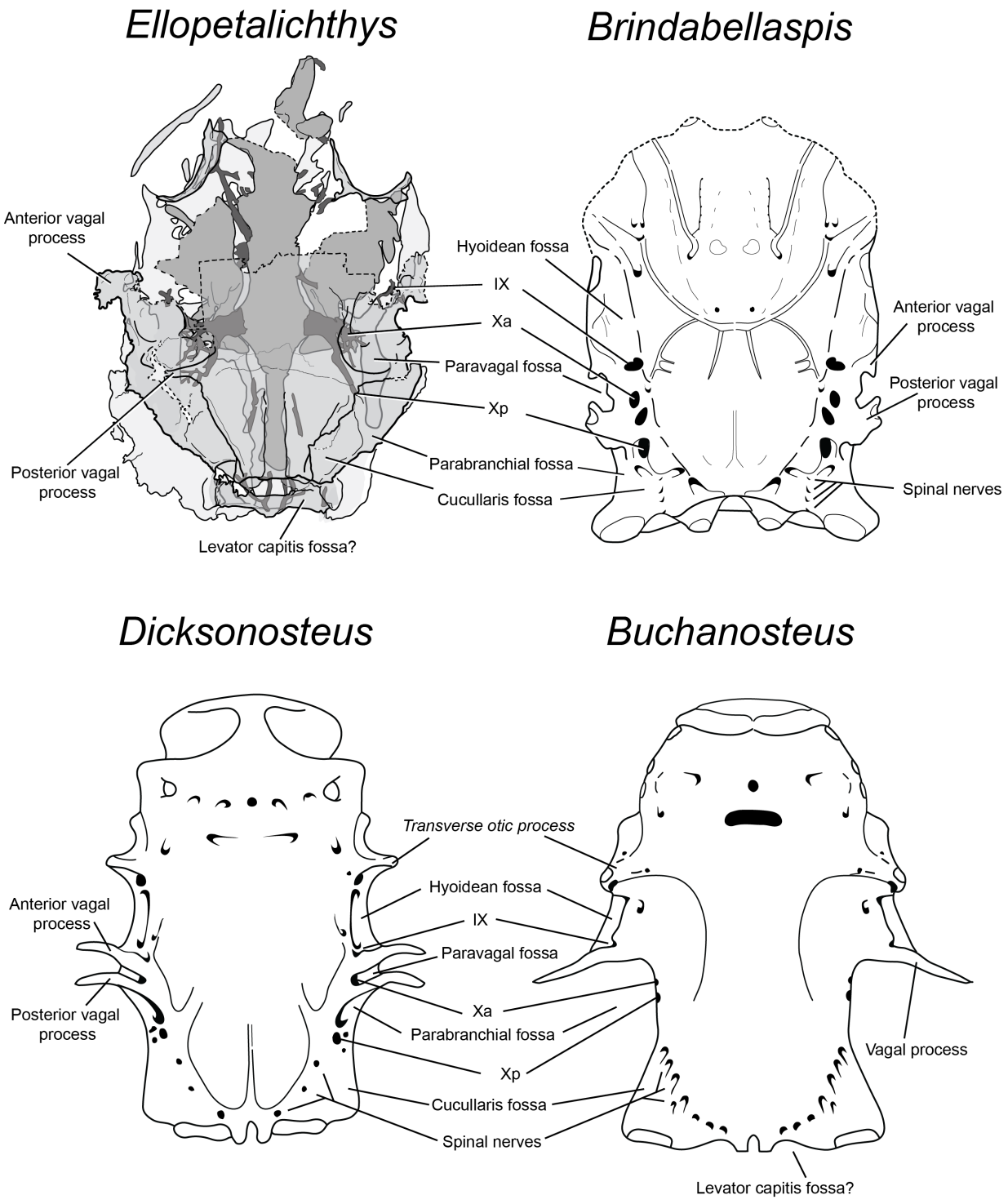

FIGURE 3.10: Braincase in ventral view of of the petalichthyids *Ellopetalichthys*, the "acanthothoraicic" *Brindabellaspis* (after Young, 1980) and the arthrodires *Dicksonousteus* (after Goujet 1984a) and *Buchanosteus* (after Young 1979). Not to scale.

edges of the cephalic armour of petalichthyids would have possessed a high degree of relative side to side movements.

Young (1978) dismissed the hypothesis that the occipital articulation in petalichthyids could have been very mesial and movable, due to the comparison of the ginglymoid articulation in brachythoracid arthrodires. He stated that the main lateral line canals, which connect to the thoracic armour lateral line, might be an indicator for the position of the axis of rotation. In brachythoracids, the glenoid process, the foramen magnum, the main sensory line canal, and the dermal articular surface are placed in a transversal plan between each other and indicate the position of the rotation axis (Fig. 3.9). In petalichthyids, the dermal articular areas in the latter are mesial to the lateral line, instead of lateral to it, and the foramen magnum and glenoid process are situated in a lower position and are not transversal with respect of the lateral line (Fig. 3.9). For this reason, he states that a mesial neck articulation for petalichthyids would have been too far removed from the dermal articular component. However, a direct comparison between arthrodire and petalichthyid neck joints implies that they had the same head function. This does not seem to be the case, as petalichthyids possess a flat and wide skull, which is radically different from skull shape of brachythoracid arthrodires. Moreover, the vertical dermal articular component in petalichthyids extends dorsally from the level of the glenoid process to the lateral line, so that these two structures would not become displaced during rotation. It is, thus, reasonable to hypothesise that the neck articulation in petalichthyids would have been very medial and be capable of a high degree of lateral movement.

Although a vertical articular joint is also present in the quasipetalichthyids, it is only the macropetalichthyids that have this particular mesial neck morphology. Young (1978) suggested that the enlarged occipital fossa of the macropetalichthyids could be interpreted as a specialisation related to increased development of the occipital musculature. In addition to a large occipital fossa, the macropetalichthyids also possess a very large paravagal fossa compared to that of arthrodires (Goujet

1984a). Moreover, petalichthyids possess a large area between the palatoquadrate and the hyomandibular attachment which is related to a well-developed pseudobranch (spiracle) (see chapter 2). All of these characteristics indicate the presence of a very well developed occipito-branchial musculature and, as this musculature is antagonist to the hypobranchial musculature, of a well-developed hypobranchial musculature. As these muscles play a significant role in expanding the oral cavity, this may suggest a demersal ambush predation strategy, also consistent with the general anatomy of the macropetalichthyids, which also possess a flat body, dorsally oriented eyes, elongated snout and large spiracular area.

3.5 CONCLUSION

My examination of *Ellopetalichthys* represents the first description of the neurocranial anatomy for this taxon, including details on the orbital wall, brain cavity, cranial nerve, inner ear and occipital joint morphology. It provides new evidence on the inner ear morphology of petalichthyids. This allowed to revise previous investigations on petalichthyids inner ear anatomy, which is demonstrated to differ substantially from that of other early vertebrates, especially in the morphology of the endolymphatic duct and the position of the ampullae and semicircular canals. This seems to suggest that the macropetalichthyids possess a unique and probably derived condition for the inner ear. This study has also revealed details on the occipital articulation of *Ellopetalichthys* that were previously inaccessible, as the innervation of the occipital fossae. By comparing the course of the vagus nerve and the area for gills and neck muscles attachment in placoderms and living gnathostomes, I suggested that the cucullaris muscle in placoderm was innervated by a spinal nerve that was not related to the vagus bundle and thus that this nerve might have represented the ancestor of the spinal accessory nerve, which innervate this area in modern jawed vertebrates. Moreover, a comparison between of the occipital joint in petalichthyids and arthrodiran placoderm allowed to make hypotheses about the degree of move-

ments and rotation of the placoderm neck joint, which was found to be well suited for lateral movements and for a wide expansion of the oral and branchial cavities, offering some insight on the possible ecological adaptation of these animals.

CHAPTER 4

COMPUTED TOMOGRAPHIC INVESTIGATION OF THE ENDOCRANIUM OF *Kolymaspis sibirica* BYSTROW 1956 (VERTEBRATA: PLACODERMI) WITH REMARKS ON THE ENDOCRANIAL ANATOMY OF "ACANTHOTHORACID" PLACODERMS

4.1 INTRODUCTION

Placoderms, armoured fishes with a fossil record spanning from the Lower Silurian to the Late Devonian, are usually considered the sister group or grade of modern gnathostomes (Young, 1986; Goujet, 2001; Goujet and Young, 2004; Friedman, 2007; Brazeau, 2009; Davis et al., 2012; Zhu et al., 2013; Long et al., 2015; Giles et al., 2015b; Brazeau and Friedman, 2015; King et al., 2016). Among placoderms, the group called "Acanthothoracida" has been historically referred to as comprising a series of taxa showing a peculiar mix of apomorphic characters (e.g. distinct morphology of the premedian plate) (Goujet and Young, 1995, 2004) and plesiomorphic features shared with the jawless sister groups of jawed vertebrates, the osteostracans and the galeaspids, such as dorsally placed eyes and nasal capsules. For this reason, they have often been considered as the emblem for the morphologically primitive condition of jawed vertebrates (Goujet, 1984b; Janvier, 1996a; Young, 2010; Dupret et al., 2014, 2017a).

"Acanthothoracids" have historically been recognized as a monophyletic group, sister to the flat-bodied rhenanids (Young, 1980, 1986), or as a non-monophyletic grade with some taxa aligned with the rhenanids and other with the antiarchs (Goujet, 1984b; Goujet and Young, 2004). Either way, they have been considered as sister

to the other placoderms and thus regarded as highly informative about the primitive gnathostomes morphology and evolution (Dupret et al., 2017a) because of their proximal position to the point of origin of jaw. Nevertheless, the various "acanthothoracid" taxa show different morphology and studies have failed to propose unambiguous synapomorphies for "Acanthothoracida", so that the affinity of the group is still not very clear and has been questioned before (Goujet, 1984b; Janvier, 1996a; Goujet and Young, 2004; Brazeau, 2009). This is mainly due because very few "acanthothoracids" are known from well-preserved endocranial material, making it difficult to investigate their affinity and their morphology.

Well known "acanthothoracids" include *Brindabellaspis* (Young, 1980), *Romundina* (Ørvig, 1975; Dupret et al., 2010, 2014, 2017a), *Kimaspis* (Mark-Kurik, 1973), *Radotina* (Gross, 1959; Stensiö, 1969; Vaškaninová and Ahlberg, 2017) and *Arabosteus* (Olive et al., 2011). However, among those taxa only *Brindabellaspis* and *Romundina* have been studied in a comprehensive way, with information regarding both the neurocranial and endocavities anatomy. This has so far prevented thorough tests of "acanthothoracids" relationship, with *Brindabellaspis* and *Romundina* representing the only two "acanthothoracids included in broad phylogenetic analysis on early jawed vertebrates (Brazeau, 2009; Davis et al., 2012; Zhu et al., 2013; Dupret et al., 2014; Giles et al., 2015b; Zhu et al., 2016; King et al., 2016). Acquiring a larger sample of neurocranial morphology from other "acanthothoracids" is therefore crucial to understand the anatomical diversity and phylogenetic significance of this group of early gnathostomes.

Here, I redescribe the morphology of the "acanthothoracid" *Kolymaspis sibirica*, from the Kolyma Basin, Siberia (Fig. 1). Originally it was described by Bystrow in 1956, but at that time only the external morphology was known and he considered it to be an ostracoderm. Later, it was recognized as a jawed vertebrate and aligned to "acanthothoracid" placoderms (Obruchev, 1964). Lately, because it possesses a combination of characters present in the "acanthothoracids" *Brindabellaspis* (Young, 1980) and *Romundina* (Ørvig, 1975), *Kolymaspis* was hypothesised to be either sister

to *Brindabellaspis* or *Romundina* by Young (1980: fig. 27A). However, the lack of endocranial information was indicated by Young (1980) as an obstacle to resolve these competing hypotheses.

In this study, I provide the first description of the endocavities of *Kolymaspis* using micro-CT scan data. This data reveal for the first time the anatomy of the braincase and brain cavities of *Kolymaspis*, as well as the course of some canals for nerves and blood vessels. The CT data also allows to revise previous interpretation of the sensory line anatomy and cranial circulation of this animal. In addition, I review some character that have recently been the centre of debate on placoderms monophyly, as the position of the nostrils and the morphology of the facial nerve. Moreover, I discuss some similarities between some "acanthothoracids" and other placoderms group, for example in the morphology of the endolymphatic duct, as well as revaluating previous interpretation on the preorbital region of *Brindabellaspis* thanks to the similarities between this taxon and *Kolymaspis*. As only few "acanthothoracids" endocrania have been studies in details (Ørvig, 1975; Young, 1980; Olive et al., 2011; Dupret et al., 2014, 2017a), this work provides a precious help to evaluate the morphology of "acanthothoracids" in a broader context.

4.2 METHODS

Kolymaspis sibirica (specimen number 7656) is known from a single specimen collected from a bituminous limestone level near the Kolyma River in the Magadan Oblast, in eastern Siberia, Russia. The precise age of the locality is unknown but it is supposed to be between late Silurian and Early Devonian (Bystrow, 1956). The specimen consists of an almost complete skull roof with most of the underlying neurocranial ossification preserved. It was originally enclosed in limestone but was mechanically prepared by Bystrow in 1956. During the preparation process, other fragments of armour were found but are now unfortunately lost.

The fossil was originally held in the collections of the FN Chernyshev Central Research Geological Museum in St. Petersburg, Russia but was stolen from the collections in the late 1980s. The specimen eventually resurfaced in the collections of a private collector who recognised it as a holotype and donated it back to the Geological Museum in St. Petersburg.

Specimen 7656 was scanned at the Imaging and Analysis Centre at the Natural History Museum in London using a Nikon Metrology HMX ST 225 X-ray micro-CT scanner. The scan was made with a voxel size of 70.2 μm using a voltage of 210 kV and a current of 150 A. A $2,5$ mm thick copper filter and 6284 projections were used. The resulting tomography data were segmented and rendered in 3D using the software Mimics 18.01 and then imported into Blender for scientific image preparation (Garwood and Dunlop, 2014).

4.2.1 Abbreviation list

Dermal skull roof: Pm, premedian plate; PrO, preorbital plate; PtO, postorbital plate; RP, rostropineal plate. **Sensory line system**: ioc, infraorbital sensory line; mpl, middle pit line; a.ppl, anterior posterior pit line; p.ppl, posterior posterior pit line; pmc, postmarginal canal; soc, supraorbital sensory canal. **Orbital wall**: e.s, eyestalk; gr.Vmd, groove for mandibular branch of trigeminal nerve; gr.Vmax, groove for maxillary branch of trigeminal nerve; gr.VII buc.lat, groove for ramus buccalis lateral of trigeminal nerve; my3a, myodome associated with cranial nerve IIIa; my3av, anteroventral myodome associated with cranial nerve III, my3p, myodome associated with cranial nerve IIIp; my4, myodome associated with cranial nerve IV; my6, myodome associated with cranial nerve VI; no, nasal opening; o.f, optic fissure; VIIhm+j.v., communal foramen for facial nerve and jugular vein. **Nerves (in figure, roman number alone refers to foramen)**: N.II, canal for optic nerve; N. IIIa, p, canals for anterior and posterior branch of the oculomotor nerve; N.IV, canal for abducens nerve; N.V2,3 canal for the root of the maxillary and mandibular branch

of the trigeminal nerve; N.Vmax, canal for the maxillary branch of the trigeminal nerve; N. Vpf, canal for the profundus branch of the trigeminal nerve; N.VII, facial nerve canal; N.VIIbuc.lat, canal for the buccalis lateralis branch of the facial nerve; N.VIIhm, canal for the hyomandibular branch of the facial nerve; N.VIIpal, canal for the palatine branch of the facial nerve; N.Xp, canal for the posterior branch of the vagus nerve. **Vascular system**: ac.v, anterior cerebral vein; opht.a, ophtalmic magna artery; v.pit, pituitary vein.

4.3 DESCRIPTION

Overall, the skull has a convex and antero-posteriorly elongated profile, with large and dorsolaterally directed orbits (Figs 4.1A, 4.2-6). The dermal skull roof is nearly complete, and the rostropineal plate and rhinocapsular ossification are in place (Figs 1A, 2-4, 6). An S-shaped depression is present on the central portion of the skull roof (Figs 4.1A, 4.2), but it is likely to be the result of a diagenetic distortion as it is asymmetrical and the skull roof in this area has been dorsoventrally compressed. The dermal ornamentation consists of large stellate tubercles in the rostral area of the skull (Fig 4.1C), and of smaller and less complex tubercles in the posterior dermal area (Fig 4.1D).

4.3.1 **Skull roof and sensory line**

The skull roof plate boundaries are difficult to identify. The sensory canals and pit lines are clearly visible on the external surface (Figs 4.1A, 4.2, 4.4). A large premedian plate sits anterior to the rostropineal plate and forms the anterior margin of the orbit (Figs 4.1A, 4.2-4, 4.6A). It has an anteroventrally bent profile, and possesses complex vascular and sensory system that is connected with branches of the underlying nervous and circulatory systems (Figs 4.5-7).

The rostropineal plate (Figs 4.1-4, 4.6A) is trapezoidal in shape, narrowest at its anterior where it bears lateral notches for the nasal openings. This plate bears the

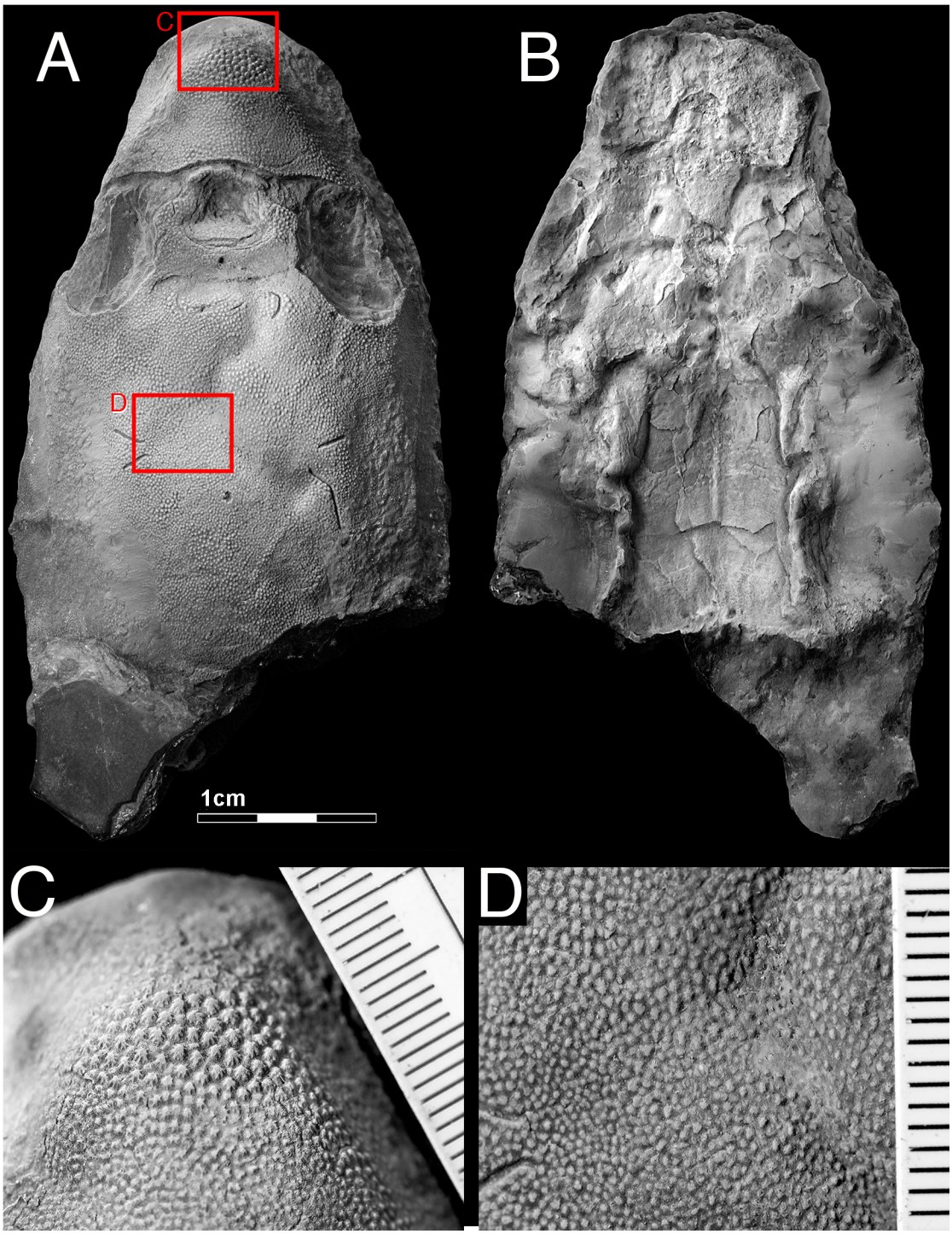

FIGURE 4.1: Photographs of 7656. A, dorsal view; B, dorsal view; C close-up on the ornamentation of the premedian plate; D, close-up on the ornamentation of the central area of the skull roof.

pineal foramen in its posterior portion (Fig. 4.1-2). The plate shows no sutural connections to the neighbouring dermal bones. The central portion of this plate has been taphonomically compressed dorsoventrally, so that now it shows a slight central depression.

There are two very short, mesially curved supraorbital sensory canals situated after the posterior end of the rostropineal plate (Fig. 4.2). A pair of sensory pits are located lateral to the suborbital sensory line and may represent cutaneous sensory organ (Fig. 4.2), similar to the cutaneous sensory organs described in other "acanthothoracids" (Ørvig, 1975; Young, 1980; Dupret et al., 2017a). A pair of groove visible near the cutaneous sensory pit mark the plate boundary between the preorbital and the postorbital plates (Fig. 4.2A).

The main lateral sensory line extends anteriorly from the posterior end of the skull (Figs 4.2, 4.4, 4.6A), with the infraorbital sensory continuing towards to the lateral process of the postorbital plate (Figs 4.2, 4.4, 4.6A). The central sensory line is not present, making it impossible to distinguish between the main lateral line and the infraorbital sensory lines. The central region of the skull roof bears the grooves for the middle pit line (Fig. 4.2) and the anterior posterior pit line (Figs 4.2, 4.4). These short sensory line canals usually are on the central plates. However, it is difficult to discern the exact shape and position of the central plates. On the right side of the specimen, the anterior posterior pit line joins the posterior posterior pit line forming a single sinusoidal posterior pit line (Fig. 4.2). This is reminiscent of the posterior pit line reconstructed for *Hagiangella goujeti* (Dupret et al. 2011, text-fig 2).

The postmarginal sensory line (Figs 4.2, 4.4, 4.6A) is a small canal that connects laterally with the main lateral sensory line and is related with the anterior paranuchal plate. It is located where the posterior posterior pit line joins the main lateral sensory line and projects laterally toward the margin of the skull. Another small canal connected with the main lateral sensory line is present in the posteriormost part of the skull and probably represents the occipital sensory line (Fig 4.2). The lateral

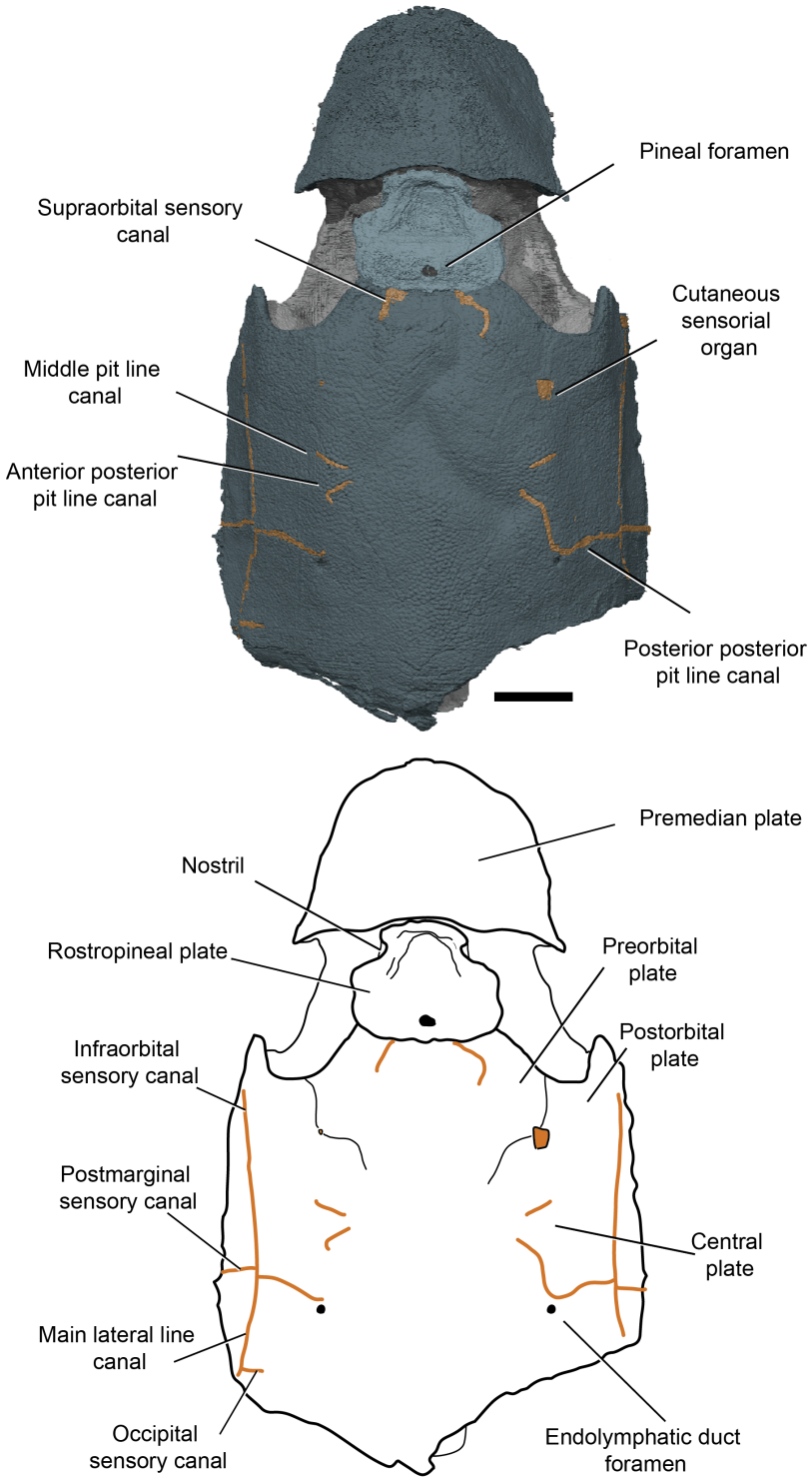

FIGURE 4.2: 3D model (top) and line drawing (bottom) of the skull roof and braincase of 7656, dorsal view. Scale bar represents 10 mm.

posteriormost part of the skull roof also carries the articular joint (Fig. 4.2B) that connects with the thoracic armour, and can thus be identified as the postnuchal plate.

The endolymphatic duct opens as a pore just next to the edge of the posterior posterior pit line (Fig. 4.2). Unfortunately, any plate margins surrounding it are indiscernible.

4.3.2 **Endocranium**

PREORBITAL REGION — The preorbital region of the endocranium (Figs. 4.3, 4.5-7) is covered by the premedian plate and contains many canals for blood vessels and nerves (Figs 4.5-7). The lateral walls of the preorbital region (Figs 4.2-4) are not fully preserved and were probably covered by the dermal suborbital plate. The ventral surface of the preorbital region is pierced by several foramina (Fig. 4.8) for which precise identities cannot be given; however, the CT scan shows that they belong to a very well-developed network of canals (Fig. 4.5-7). A paired row of foramina, similar to that present in *Brindabellaspis* (Young 1980, text-fig 7), indicates the position of the palatine artery (Fig. 4.7-8).

ORBITAL AREA — The orbital wall and subocular shelf are well preserved on both sides of the specimen (Figs 4.2-5). The nasal capsules are placed inside the rhinocapsular ossification and are confluent with the orbits (Fig. 4.3-4). The eyestalk attachment is a rhombic opening located on the mesial wall of the orbit, surrounded by an everted rim (Fig. 4.3-4). The most dorsal portion of the mesial wall of the orbit, above the eyestalk, is formed by both the rhinocapsular ossification and the dorsal portion of the main endocranial ossification (Fig. 4.3-4). Two openings are bounded by these two ossifications, along the optic fissure (Fig. 4.3-4). These include the anterior opening for the optic nerve canal (Fig. 4.3-4; II) and the posterior opening for the anterior cerebral vein (Fig. 4.3-4).

Posterodorsally to the eyestalk is the deep recess that forms the myodome for the oculomotor-innervated extrinsic eye muscle (Fig 4.3-4; my3a), in addition to a

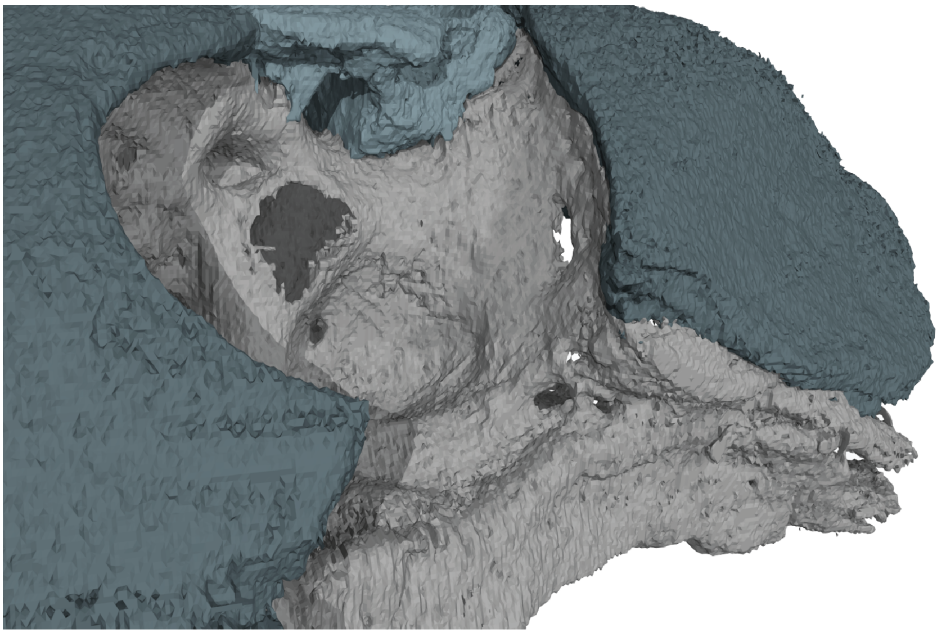

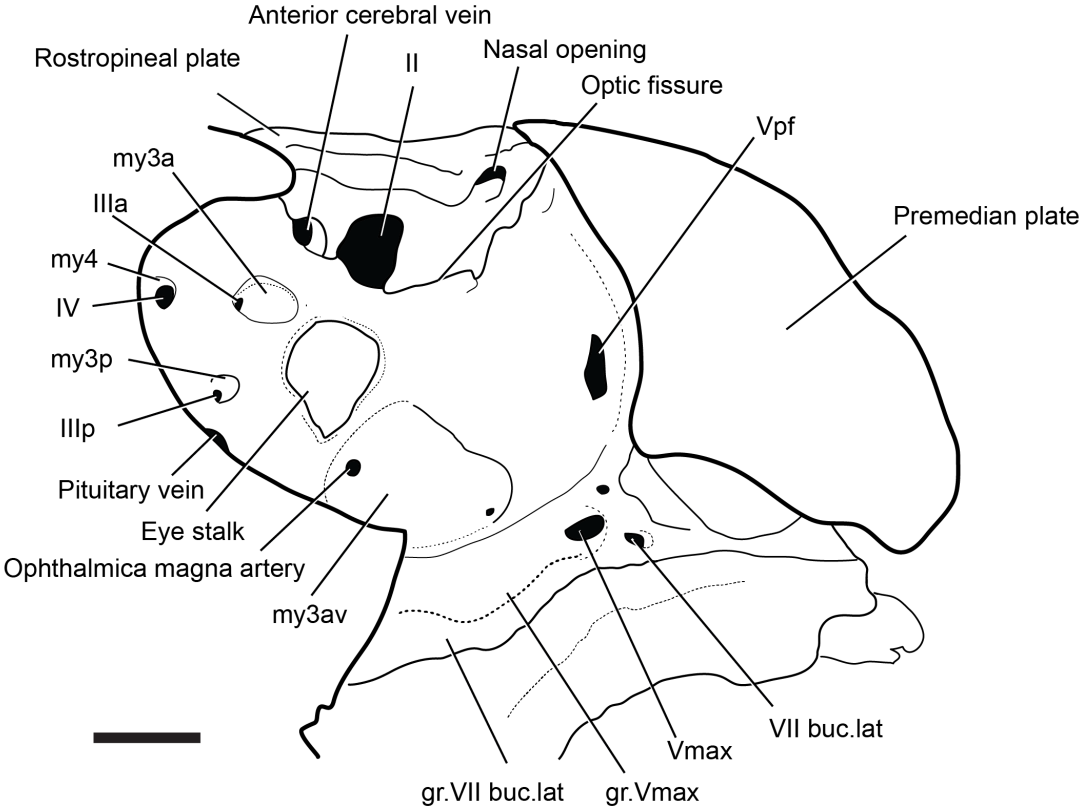

FIGURE 4.3: 3D model (top) and line drawing (bottom) of the orbital region of 7656, anterolateral view. Abbreviations in abbreviation list. Scale bar represents 5 mm.

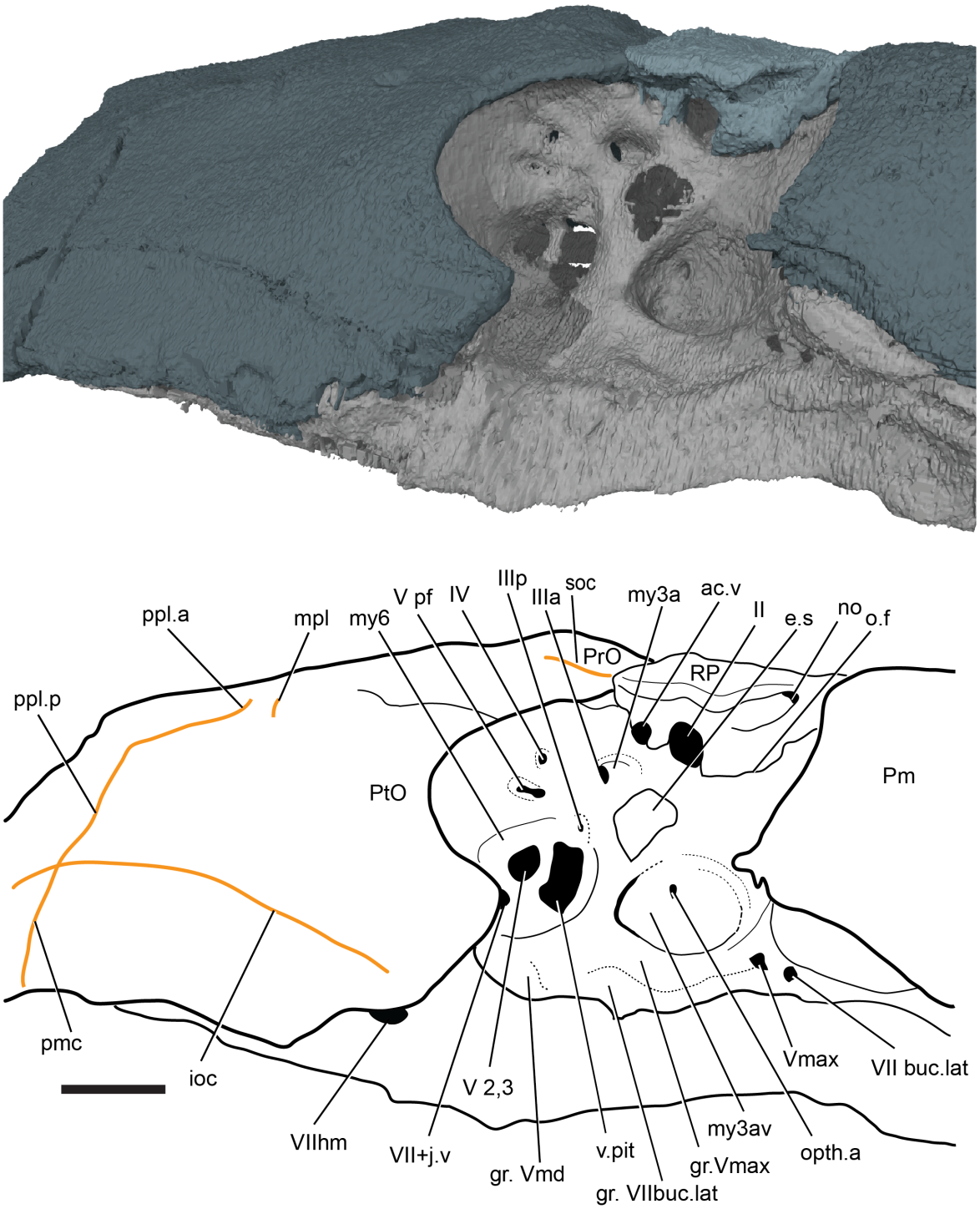

FIGURE 4.4: 3D model (top) and line drawing (bottom) of the orbital region of 7656, posterolateral view. Abbreviations in abbreviation list. Scale bar represents 5 mm.

rounded foramen connected with the canal for the oculomotor nerve (Fig. 4.3-4; IIIa). A very small foramen is situated immediately posterior to the eyestalk and represents the opening for the posterior branch of the oculomotor nerve (Fig. 4.3-4; IIIp). This foramen is in proximity to a shallow recess (Fig. 4.3-4; my3p), probably for the attachment of the internal rectus extraocular muscle. The foramen for the profundus nerve (Fig. 4.4; V pf) opens posterodorsally, at the same level as the myodome for the oculomotor nerve (Fig. 4.3-4; N.III). Dorsally, in a small recess there is a very small foramen for the trochlear nerve (Fig. 4.3-4; my4, IV), usually innervating the posterior (superior) oblique muscle. The myodome for the anterior (inferior) oblique muscle is positioned anteroventrally to the eyestalk (Fig. 4.3-4; my3av), and is related to the anterior branch of the oculomotor nerve. Inside this recess there is a small foramen for the ophthalmica magna artery (Fig. 4.3-4; opht.a) that connects mesially with the hypophysial artery (Fig. 4.4-7).

The posteroventral myodome (Fig. 4.4; my6) is located on the posteroventral wall of the orbit and marked by a large recess that houses several foramina. The abducens nerve (N. VI) usually opens inside this myodome, although neither the foramen nor the canal for this nerve can be observed from these data. A large foramen on the anterior portion of this myodome is the opening for the pituitary vein canal (Fig. 4.4; v.pit). Posterior to the pituitary vein foramen is the foramen for the main division of the trigeminal nerve (Fig. 4.4; V 2,3) and another foramen for the jugular vein and the ramus oticus lateralis of the facial nerve (Fig. 4.4; VII+j.v).

A groove extends from the external edge of the orbit to the posteroventral myodome along the dorsal surface of the subocular shelf (Figs 4.3-5; gr.Vmax). This groove leads to a foramen on the anterior orbital wall that is connected with a canal extending toward the anterior part of the skull (Figs 4.5-7; N. Vmax). Given its position, it could be associated with the groove for the passage of the maxillary branch of the trigeminal nerve (see below).

Two pairs of foramina on the ventral side of the subocular shelf (Fig. 4.8, VIIpal), associated with paired grooves, are identified as the passage for the palatine branch

of the facial nerve (Figs 4.5-7; N. VII pal). Mesially to them are a pair of foramina that flank the depression for the hypophysial foramen (Fig. 4.8), indicating the opening for the paired hypophysial artery (Figs 4.7-8).

The anterior surface of the orbital wall is pierced by a large foramen (Fig. 4.3; Vpf) for the passage of the profundus nerve, which innervates the dorsal portion of the snout (Figs 4.5-7; N. pf). Other foramina pierce this wall more dorsally, connecting with canals extending towards the snout and the premedian plate (Figs 4.5-7).

POSTORBITAL REGION — The ventral surface of the endocranium is transversely concave over its entire length (Fig. 4.8). The lateral edges of this area are not very well resolved in the CT data, due to low contrast with the surrounding matrix, while the central and posterior parts are fairly well resolved (Figs 4.1, 4.8). Nevertheless, comparison between the original description by Bystrow (1956) and the CT data provide enough information to reconstruct some of the anatomy associated with the arterial and branchial system and endocranial processes.

The transverse otic process ("anterior postorbital process" of other authors, for example Young 1980) is located just posterior of the orbit, although not well preserved. The vagal process ("posterior postorbital process" for Young 1980) is also not very well preserved compared to that of other placoderms but it is nonetheless possible to identify its relative position (Figs 4.1B, 4.8). The vagal process shows a small bifurcation (Figs 4.1B, 4.8), as present in other "acanthothoracids" (Ørvig, 1975; Young, 1980; Olive et al., 2011; Dupret et al., 2014, 2017a). However, the vagal process in *Kolymaspis* is reduced so that the hyoidean fossa (Fig. 4.8) and the parabranchial fossa (Figs 4.8, 4.9B) are confluent. The craniospinal process ("supravagal process" for Young 1980) (Figs 4.8-9) is only partially preserved in the left side of the specimen (right side in ventral view). It extends postero-transversally as in the other "acanthothoracids" but it is short and without the posterior projection present in other member of the group.

The ventral surface of the endocranial postorbital region is marked by a series of branching grooves and foramina, showing the course of blood vessels (Fig. 4.8). The foramina for the paired hypophysial vein (Fig. 4.8), flanks a keyhole shaped opening of uncertain identification. Posteriorly, there is another pair of foramina for the posterior part of the supraorbital branch of the orbital artery (initially identified as the internal carotid by Bystrow 1956) (Figs 4.7-8).

Anteriorly to those foramina, a pair of anteriorly projected grooves probably indicate the course of the internal carotids (Fig. 4.8). A paired deep groove extends posteriorly from the orbital artery until the anterior vagal process, marking the course of the dorsal arterial commissure (Fig. 4.8). These grooves are connected posteriorly to another pair of grooves that extends towards the occipital area, identified as the grooves for the lateral dorsal aorta (Figs 4.8, 4.9B). Small foramina are present at the ends of this groove (Figs 4.8, 4.9B) that connect with canals for the spino-occipital nerves (Figs 4.5-7). External to the groove for the dorsal aorta there is a foramen located in the peribranchial fossa that marks the position for the opening for a posterior branch of the vagus nerve (Figs 4.8, 4.9B).

OCCIPITAL REGION — The occipital region is well preserved (Figs 4.8-9). The left side shows a deep fossa for the attachment of the neck muscles (Fig. 4.9) and the area for the foramen magnum (Figs 4.8-9). On the external side, the dermal articular area (Figs 4.8-9) for the attachment with the thoracic plate is formed by both the craniospinal process (Figs 4.8-9) and the posterior edge of the paranuchal plate (Figs 4.8-9).

On the posterior side of the craniospinal process there is a small foramen for the spinocranial nerve (Fig. 4.9). The occipital condyles are not preserved, but symmetrical cavities are present on both sides of the foramen magnum which may represent the insertion points for unossified paired glenoid condyles (Fig. 4.9A), as suggested for *Brindabellaspis* (Young, 1980). The cavity for the anterior portion of the

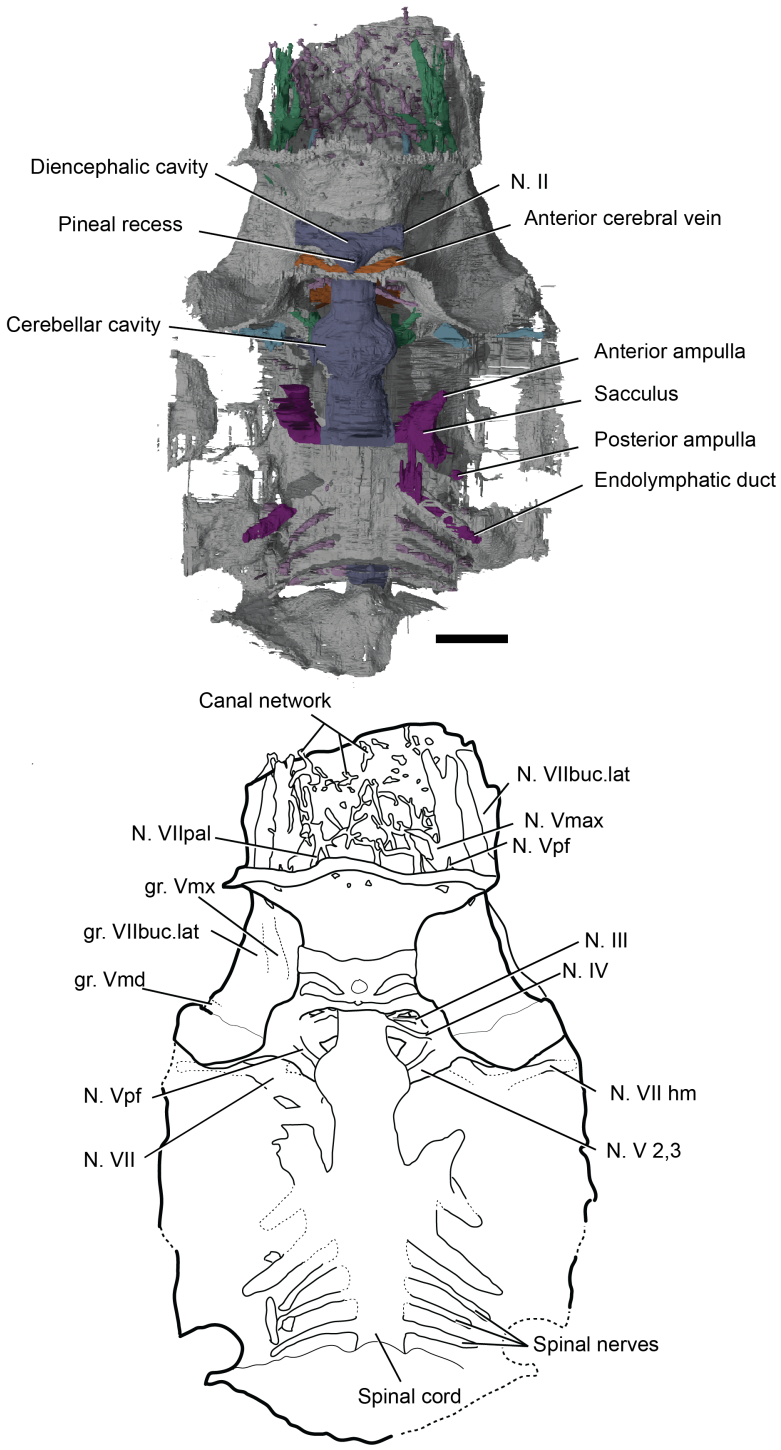

FIGURE 4.5: 3D model (top) and line drawing (bottom) of the endocavity of 7656, dorsal view. Abbreviation in abbreviation list. Scale bar represents 10 mm.

notochordal canal is also not preserved, but could have been located in the unossified area ventromedial to the foramen magnum.

4.3.3 **Endocranial cavity**

The thin perichondral bone surrounding the endocranial cavity is partially preserved in *Kolymaspis*. The area around the labyrinth and the hindbrain cavity are difficult to identify from the CT data because of the low-contrast between the thin perichondral bone and the rock. However, they are visible, possibly owing to a differential mineral infill compared to the interperichondral space.

The endocranial cavity is tubular, expanding laterally at the level of the cerebellar cavity (Figs 4.5, 4.7). It extends anteriorly until the end of the orbital area and the rhinocapsular ossification, so that the preorbital ossification only contains the extension of the trigeminal nerves and a well-developed canal network (Figs 4.5-7). The telencephalic cavity is difficult to identify, as it is very short, not very well developed, and lacks distinct olfactory lobes. The upper part of the diencephalic cavity (Figs 4.5, 4.6C) is anterodorsally elongate, bearing the optic tract (Figs 4.5, 4.7; N. II) and the anterior cerebral vein (Figs 4.5, 4.6B, 4.7). It expands dorsally forming a well-pronounced pineal recess (Figs 4.5, 4.6B).

The lower portion of the endocranial cavity is developed dorsoventrally (Fig. 4.6), with the floor of the cavity sloping towards the ventral braincase to form the canals for the hypophysial artery (Figs 4.6C-7) and the hypophysial duct (Figs 4.6C-7). Posteriorly the width of the endocavity increases, forming the two rounded lobes of the cerebellar cavity (Figs 4.5, 4.6C). Behind this point, the endocavity is tubular, narrowing toward the spinal area, and slopes downward towards the posterior end of the braincase (Fig. 4.6C). The rear of the endocavity cavity is preserved as a small portion of the spinal cord (Figs 4.5, 4.7), opening to the external surface via the foramen magnum (Figs 4.8-9).

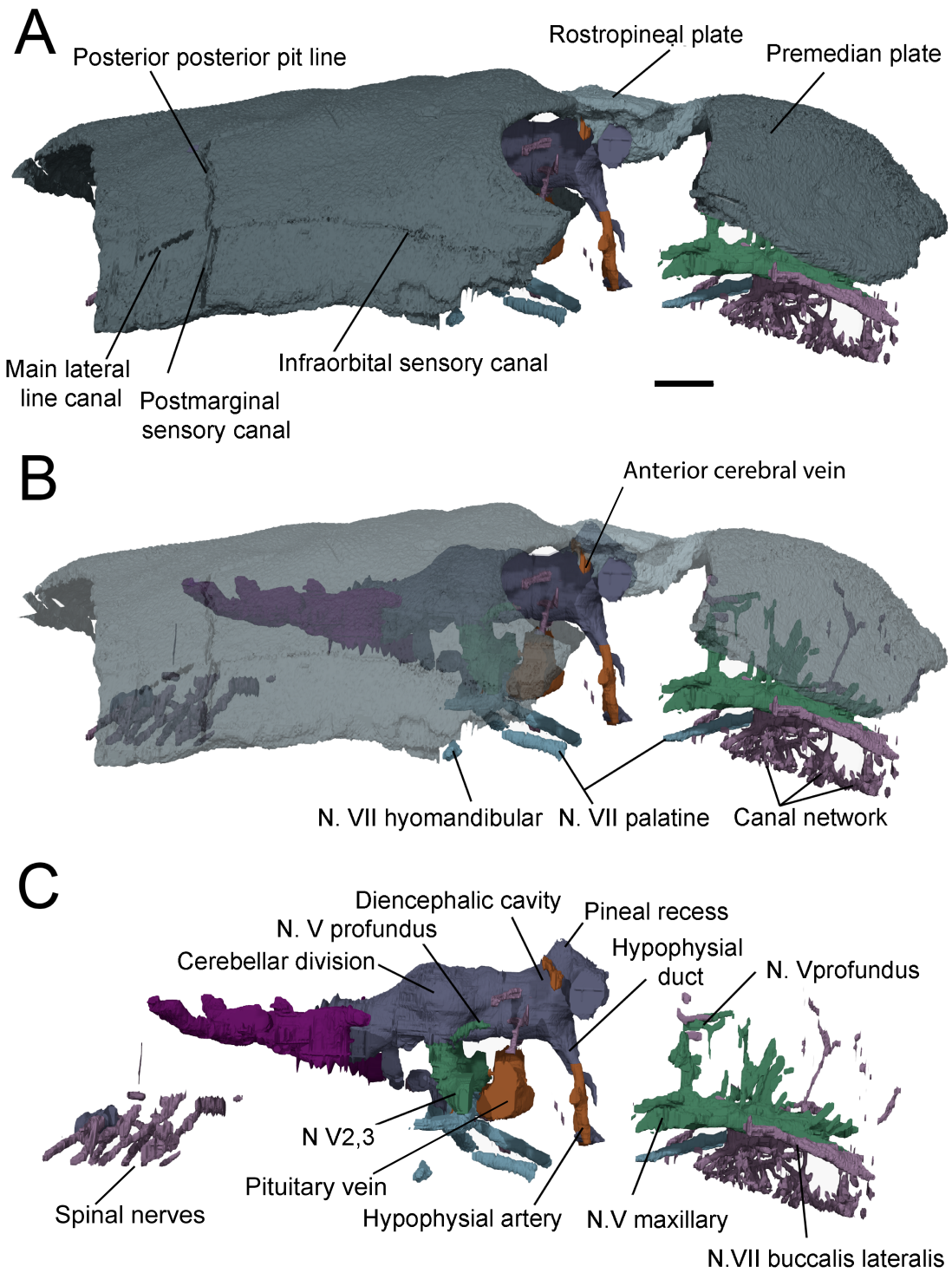

FIGURE 4.6: 3D models of the skull roof and endocast of 7656, right lateral view. A, complete view; B, right view with transparent skull roof; C, endocavities only. Scale bar 5mm

CRANIAL NERVES —

Oculomotor, trochlear and abducens nerves The oculomotor nerve (N.III) canals are well-preserved on both sides of the specimen (Figs 4.5, 4.7; N.III). They originate from the lateral diencephalic cerebral wall, extend toward the orbit and divide into two separate canals. The dorsal canal exits via a foramen located slightly dorso-posteriorly to the eye-stalk (Figs 4.3-4; IIIa), while the ventral canal extends further and exits dorsoanteriorly to the pituitary vein canals (Figs 4.3-4; IIIp). Both of these foramina are surrounded by depressions interpretable as myodomes for the superior rectus (Figs 4.3-4; my3a) and internal rectus eye-muscle (Figs 4.3; my3p), respectively. Another myodome possibly associated with the oculomotor nerve is located antero-ventrally to the eyestalk and probably represents the point of insertion of the anterior oblique eye-muscle (Figs 4.3-4; my3av).

The trochlear nerve is preserved as a tiny canal that is only visible on the right-side of the specimen (Figs 4.5, 4.7; N. IV). It is positioned dorsally to the oculomotor nerve canal, extends postoventrally toward the orbital wall, and opens in a shallow depression that is located dorsal to the foramen for the profundus nerve (Fig. 4.4, IV).

A separate abducens canal cannot be identified. Although, given the morphology of the posteroventral myodome, this nerve must have entered the orbit via that deep recess (Fig. 4.4; my6).

Trigeminal nerve The profundus (Vpf) and main (V 2,3) canals for the trigeminal nerves are well-preserved (Figs 4.5-7). The profundus nerve canal (Vpf) arises from the lateroventral wall of the cerebellar region (Figs 4.5; N.Vpf, 4.6C) and opens in the posterodorsal corner of the orbit (Fig. 4.4; Vpf). This nerve probably passes along the dorsal wall of the orbit and pierces on the anterodorsal corner of it (Fig. 4.3; Vpf.a). From here, a small canal bends anteroventrally and joins other sensorial canals in the snout (Fig. 4.6C).

The main canal of the trigeminal nerve is positioned ventral to the origin of the profundus canal (Figs 4.5-7; N.V 2,3) and emerges from the ventral face of the cerebellar cavity to open into the posteroventral myodome (Fig. 4.4; V 2,3). There are two grooves on the orbital floor of this opening that mark the courses of the maxillary and mandibular branches of the trigeminal nerve (Figs 4.3-5; gr.Vmd, gr.Vmax). The mandibular branch groove (Figs 4.4-5; gr.Vmd) bends toward the external edge of the orbit after leaving the posteroventral myodome, keeping parallel to the hyomandibular branch of the facial nerve. It then exits the orbit through a distinct semicircular groove on the posterior external wall of the orbit (Fig. 4.5; gr.Vmd), near the lateral process of the postorbital plate. The maxillary branch groove (Figs 4.3-5; gr. Vmax) extends toward the snout, passing along the ventrolateral wall of the orbit. This groove then pierces the anterior wall of the orbit (Figs 4.3-4; Vmax) and continue towards the snout, connecting with a series of wide, interconnected vascular premedian canals (Figs 4.5-7; N.Vmax). It is likely that these premedian canals represent an anastomotic complex of sensorial and vascular canals, which will be examined further in the discussion.

Facial nerve The facial nerve canal (Fig 4.5, 4.7; N. VII) can only be partially identified. The main body of the facial nerve is located posterior to the orbit and divides into the palatine hyomandibular branches (Figs 4.5-7; N. VIIhm; N. VIIpal). The palatine branch bends ventrally to exit the braincase beneath the orbit (Figs 4.6-8, VIIpal, N.VIIpal). It continues along the ventral neurocranial surface before entering the braincase (Fig. 4.8; VIIpal), joining the anterior trigeminal canals for innervating the snout and the mouth (Figs 4.5-7; N.VIIpal). The hyomandibular branch of the facial nerve (Figs 4.5-7; N.VIIhm) extends towards the external (lateral) side of the braincase, parallel to the posterior wall of the orbit, and exits the braincase near the transverse otic process (Fig. 4.4; VIIhm).

Part of the facial nerve is preserved as a short canal entering the orbit via a foramen in the posteroventral surface of the orbital wall (Fig. 4.4; VII+jug). This

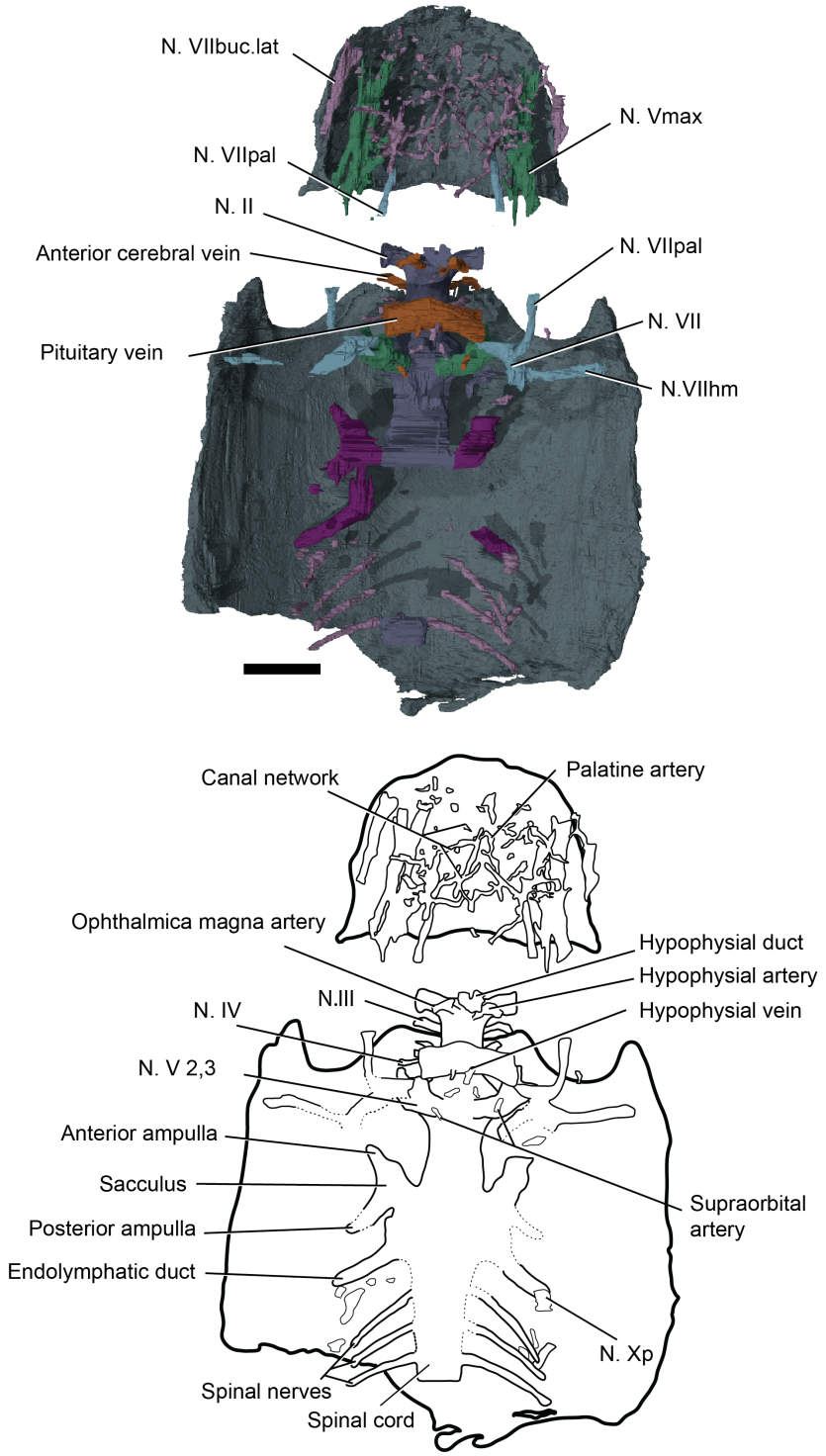

FIGURE 4.7: 3D model (top) and line drawing (bottom) of the endocavity of 7656, ventral view. Abbreviation in abbreviation list. Scale bar represents 10 mm.

canal was probably shared with the jugular vein and possibility represents the ramus buccalis lateralis. The course of the ramus buccalis lateralis in the orbital and preorbital region is evidenced by a small groove present on the lateral side of the orbital wall (Figs 4.3-5; gr.VIIbuc.lat) and leads to a foramen (Figs 4.3-4; VIIbuc.lat) for a canal that extends anteriorly along the lateral edge of the premedian plate (Figs 4.5-7; N.VIIbuc.lat).

Acoustic nerve, glossopharyngeal, and vagus nerves The canals for the acoustic and the glossopharyngeal nerves are not preserved. A possible canal for the posterior branch of the vagus nerve (Fig. 4.7; N.Xp) is located posteroventral to the endolymphatic duct, while some grooves for the external course of this canal are visible on the peribranchial fossa (Figs 4.8-9; Xp). However, it is not possible to reconstruct more specific details of this nerve from the CT dataset.

Spino-occipital nerves At least three spino-occipital nerve canals are preserved in the specimen (Figs 4.5-7). The first two canals project towards the lateral external side of the skull, exiting on the lateroventral surface of the neurocranium (Figs 4.8-9). The third spino-occipital nerve canal exits in the occipital region on the external side of the unmineralised area for the glenoid process (Fig. 4.9).

CRANIAL VESSELS —

Arteries A brief description of the arterial system of *Kolymaspis* is provided by Bystrow (1956, text-fig 3A), but Young (1980) showed that some of these interpretations were not correct. The 3D reconstructions of the vascular organisation allow to refine both interpretations. Two prominent ridges associated with a shallow groove that extends from the posterior end of the ventral endocranial surface to the vagal process, signalling the passage for the lateral dorsal aorta (Figs 4.8-9).

Other grooves extend toward the external side of the neurocranium on the vagal process, in the hyoidean and peribranchial fossa, presumably for branches of the

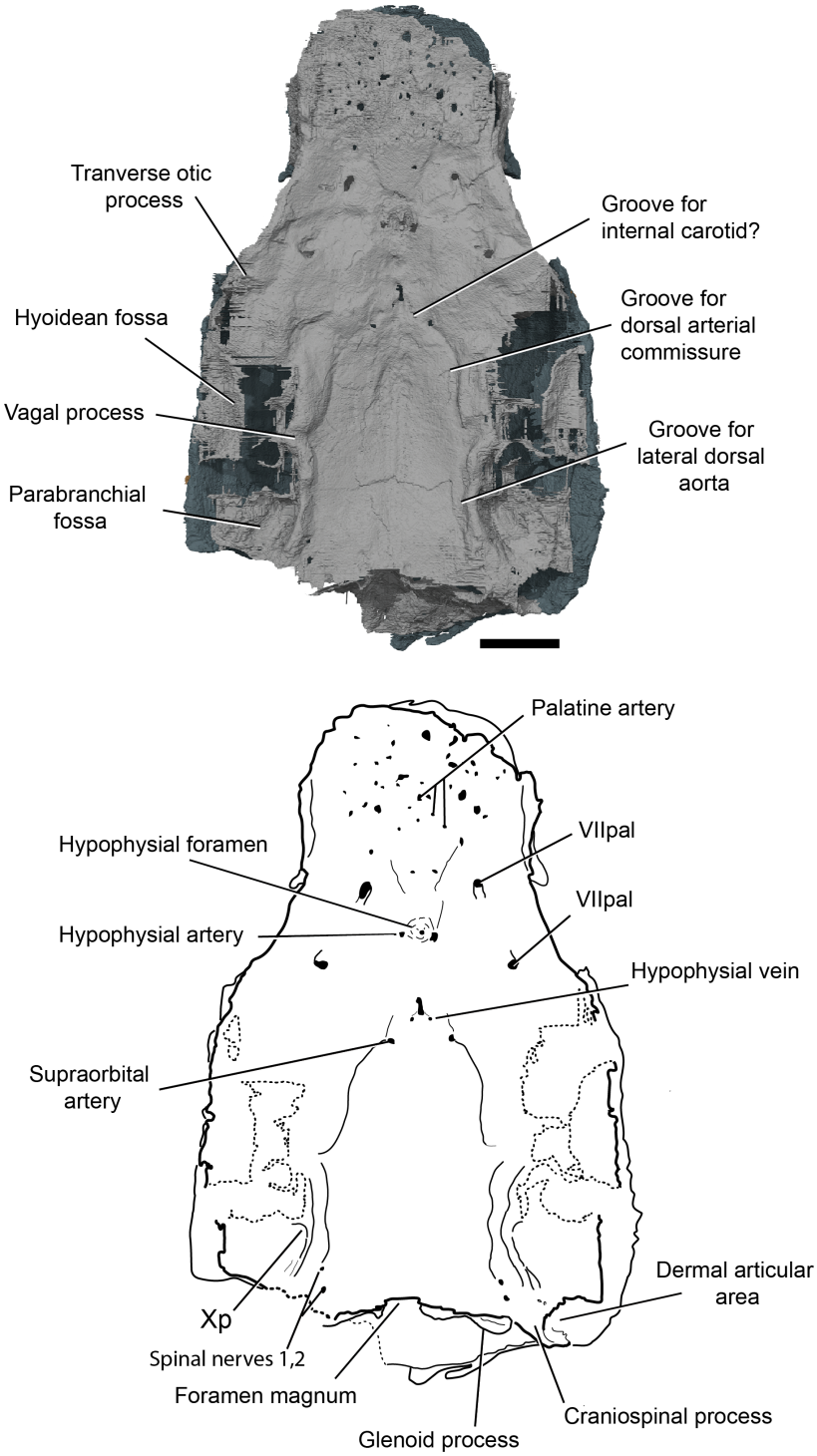

FIGURE 4.8: 3D model (top) and line drawing (bottom) of the skull roof and braincase of 7656, ventral view. Scale bar represents 10 mm.

epibranchial arteries (Figs 4.1B, 4.8). Anterior to the vagal process there is another prominent ridge and associated groove (Fig. 4.8) extending anteromesially that represents the course of the dorsal aorta (or the anterior extension of the lateral dorsal aorta), as suggested by Young (1980). Mesially to the anterior end of the dorsal aorta, there are two foramina, which are connected to two small canals that project towards the ventral orbital floor (Fig. 4.8), possibly representing the supraorbital artery canals (Fig. 4.7).

Two unidentified grooves are present anterior to the canal for the dorsal aorta, which possibly indicates the course of the internal carotid (Fig. 4.8). This area is similar to that of *Brindabellaspis* (Young, 1980), where an aortic fenestra represents the area of connection of the major arterial blood vessels (Young 1980, text-fig 15B). Around the hypophysial foramen (Fig. 4.8), two foramina are associated with the exit for the paired hypophysial artery canals (Fig. 4.8). This vessel was likely connected externally with the efferent pseudobranchial and the internal carotid artery, as suggested for *Brindabellaspis* (Young, 1980). In the endocavity, a short canal projecting laterally from the hypophysial artery canal exits the ventral myodome and represents the arteria ophthalmica magna (Figs 4.3-4, 4.7; opth.a).

The course of the palatine artery is signalled by a series of foramina on the ventral surface of the preorbital portion of the endocranium (Fig. 4.8). The canal for this artery is visible in the preorbital space (Fig. 4.7, connected with the canal for the palatine branch of the facial nerve and other unidentified canals. Many other vascular canals are connected with the maxillary branch of the trigeminal nerve but cannot be identified further.

Veins The venous system in *Kolymaspis* cannot be reconstructed as well as the arterial system due to incomplete resolution of the tomography scans. However, some of the major venous canals can be identified, as the anterior cerebral vein, the pituitary vein, the hypophysial vein, as well as the foramen for the jugular vein.

The anterior cerebral vein consists of a pair of canals that extend from right behind the pineal gland (Figs 4.5-7) and projects laterally to exit through a foramen posterior to the optic tract opening (Figs 4.3-4, ac.v). This canal is composed of the dorsal wall of the neurocranium and the ventral wall of the rhinocapsular ossification, so that the optic fissure passes through the opening for this vein (Figs 4.3-4; o.f).

The pituitary vein canal is a large, gently bowed cylinder along its entire course, and traverses the brain cavity ventrally (Figs 6-7). It opens into the orbit as a large foramen on the anterior wall of the posteroventral myodome (Figs 4.3-4; v.pit). A vertical perichondral ossification, only preserved on the left orbit, divides the foramen into two partitions, possibly indicating that this area is a venous sinus instead of containing only the pituitary vein. No clear canal for the hypophysial vein can be observed. A small canal projects posteriorly from the right side of the pituitary vein canal, and evidence of a similar canal is present on the left side of the pituitary canal (Fig. 4.7). These small posteriorly projecting canals are likely to represent a paired posterior hypophysial vein.

The course of the jugular vein can only be partially reconstructed as only its orbital foramen is preserved. This foramen opens with the facial nerve in the posterior ventral wall of the orbit (Fig. 4.4; VII+jug). From here, this vein would most likely have turned mesially to connect with the pituitary vein.

4.3.4 **Labyrinth cavity**

Both labyrinth cavities are preserved in Kolymaspis but their accurate morphology is unclear. It is possible to identify the relative positions of the left anterior, right anterior and posterior ampullae (Figs 4.5, 4.7), as well as the right mesial portion of the sacculus (Figs 4.5, 4.7). None of the nerves surrounding the labyrinth (N.VII, N.VIII and N.IX) can be reconstructed from this data, although it seems that the labyrinth was not as closely situated to the orbital cavity as in *Brindabellaspis* (Young,

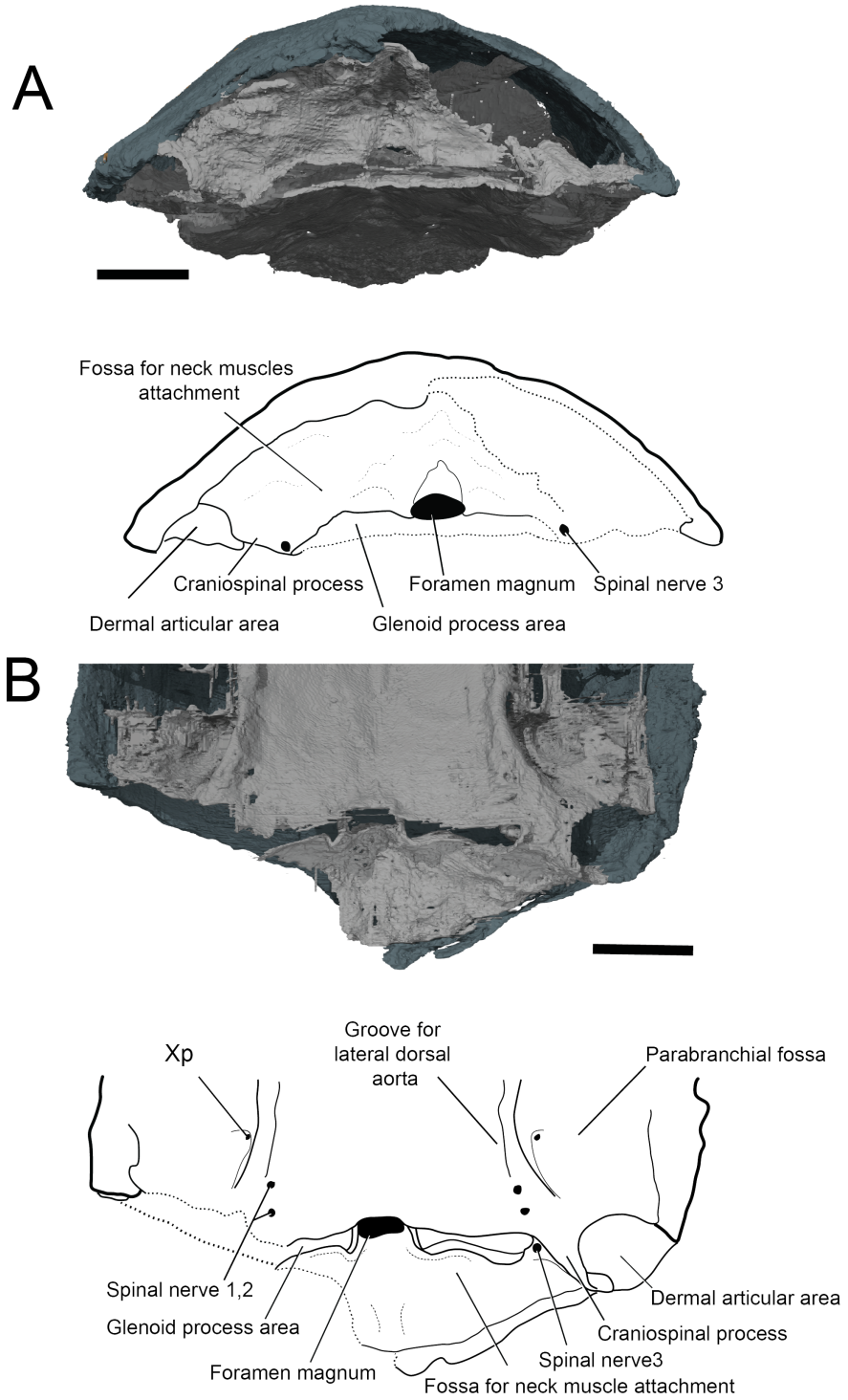

FIGURE 4.9: 3D model (top) and line drawing (bottom) of the occipital area of 7656. A, posterior view; B, ventral view. Abbreviations in abbreviation list. Scale bar represents 10 mm.

1980). The endolymphatic duct (Figs 4.5, 4.7) is enclosed in a very long and narrow canal, which projects posterodorsolaterally and opens on the dorsal skull roof with a distinct foramen (Fig. 4.2).

4.4 DISCUSSION

This work on the neurocranial morphology of *Kolymaspis* provide the first description of the sensory line system and endocranial cavities of this taxon. The anatomical features of *Kolymaspis* revealed by this CT investigation have never been seen before and include information of both the ethmoid region, brain cavity and skeletal labyrinth, expanding substantially our understanding of the endocranial morphology of "Acanthothoracida". This allows for a comparative reappraisal of "acanthothoracids" anatomy as a whole, because the endocranial anatomy of *Kolymaspis* exhibits a combination of characters present in other "acanthothoracids" as well as in arthrodires and antiarchs. In the following discussion, I highlight and discuss some of these morphological features of *Kolymaspis* that can gives better understanding of "acanthothoracids" facial morphology, relationships and their potential primitive and derived conditions. In addition, these characters are reviewed in the broader context of early gnathostomes evolution, comparing the conditions present in the different group of early gnathostomes with the aim of investigate the primitive condition for the ancestor of modern gnathostomes.

4.4.1 **The distribution of the premedian plate and its phylogenetic implication**

The premedian plate is an unpaired median bone present in some subgroups of placoderms (for reviews, see Denison 1978; Goujet 1984b; Dupret et al. 2017a). It sits on the ethmoid portion of the neurocranium anterior to the orbit and the nostril-bearing rostropineal plate, forming the snout. On the dermal surface of the premedian plate there is a sensory line canal or groove called the ethmoid commissure, consisting of the ethmoidal section of the infraorbital canal (Denison, 1978; Goujet, 1984b). The

premedian plate is thus defined by either its location on the neurocranium and/or the presence of the ethmoid commissure sensory line.

A premedian plate is present in antiarchs, many "acanthothoracids", and rhenanids (Gross, 1963; Stensiö, 1969; Ørvig, 1975; Denison, 1978; Young, 1980; Goujet, 1984b; Dupret et al., 2017a) (Fig. 4.10). In antiarchs and "acanthothoracids" it is a large plate that covers the ethmoid extension of the neurocranium, constitutes the anterior edge of the orbit and possess a single ethmoid commissure (Fig. 4.10). A large premedian plate is present in the snout area of *Kolymaspis*, although it is not possible to observe the presence or absence of an ethmoid commissure (Figs 4.1-3, 4.6A). Two types of small premedian plates have been reported in rhenanids, which are present either as a prenasal area covered by a small dermal plate with an ethmoid commissure (e.g., *Gemuendina*, Gross 1963) (Fig. 4.10) or as a tessellated area bearing the ethmoid commissure and the supraorbital commissure (*Jagorina* and *Asteronotus*, Stensiö 1969). Thus, the premedian plate was suggested as a unique feature that united antiarchs, "acanthothoracids", and rhenanids (Goujet, 1984b). Interestingly, a premedian plate is absent in the "acanthothoracid" *Tlamaspis* (Vaškaninová and Ahlberg, 2017) despite it possesses an elongated nasal region (my phylogenetic analysis suggests this might represent a plesiomorphic feature; see chapter 5 for discussion).

The presence of a premedian plate has never been reported in ptyctodonts or arthrodires. Recently, Dupret et al. (2017a) argued that the dermal element covering the internasal wall between the external nares in the arthrodires *Buchanosteus* and *Kujdanowiaspis* represents a possible vestigial premedian plate. For this reason, they hypothesise that a premedian plate is retained in arthrodires as an element that has shrunk and rotated to the internasal area due to the ventral rotation of the nares.

Zhu et al. (2013, 2016) identified a small prenasal element as a premedian plate for the "maxillate" placoderms *Entelognathus* and *Qilinyu*. Dupret et al. (2017a) argued against this identification in both taxa, as the connection of the supposed premedian plate to the ethmoidal endocranial extension or to the rostronasal capsule is uncertain in *Entelognathus*, and the one in *Qilinyu* is situated between the nostrils but not

anterior to them, which is morphologically more similar to the internasal projection of the rostral plate.

The identification of the plate covering the internasal wall in arthrodires and maxillate placoderms being homologous to the premedian plate in antiarchs, "acanthothoracids" and rhenanids presents some incongruence and is thus debatable. Antiarchs and "acanthothoracids" have both an internasal plate and a premedian plate (Fig. 4.10), thus raising doubt on the homology of these two elements (i.e., test of conjunction, Patterson 1982). Moreover, the internasal plate in antiarchs, *Entelognathus*, *Qilinyu*, arthrodires, and "acanthothoracids" form the mesial edge of the nostril, while the premedian plate is placed anteriorly and is not part of the nasal opening (Fig 4.10). I, therefore, dismiss the homology between the internasal plate and the premedian plate, as well as the presence of this plate in arthrodires and those maxillate "placoderms".

For the reasons given above, the presence of a distinct premedian plate covering the ethmoidal extension of the endocranium remains a feature unique to antiarchs, rhenanids and most of the "acanthothoracids". Goujet (1984b) used this character as a synapomorphy for a clade that united these three groups but this is not supported by any recent analyses (Giles et al., 2015b; Zhu et al., 2016; King et al., 2016) (but see chapter 5). However, this is due to both rhenanids and "acanthothoracids" usually acting as wildcards in phylogenetic investigations of stem-gnathostomes (cf. topologies in Giles et al. 2015b; Zhu et al. 2016; King et al. 2016).

4.4.2 The premedian plate as a sensory area of the snout

The prenasal region of *Kolymaspis* is composed of the premedian plate and the canals for blood vessels and nerves that innervate this area and the ventral endocranial surface of the snout (Figs 4.5-8, 4.11A-C). Comparable features are present in *Brindabellaspis* (Young, 1980) (Fig. 4.11D-F) and *Romundina* (Ørvig, 1975; Dupret et al., 2014, 2017a), but are not complete, making the exact identification of these endocavities

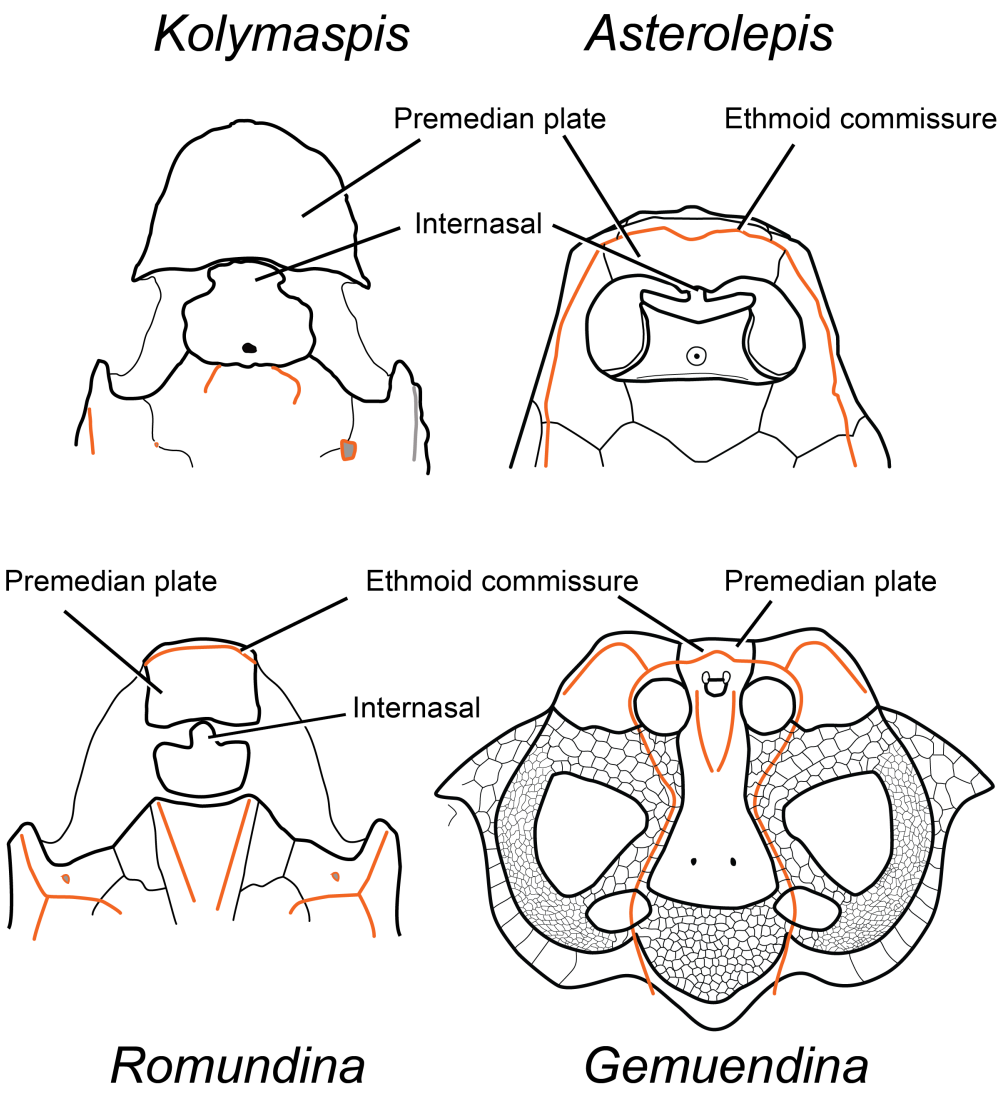

FIGURE 4.10: The morphology of the premedian plate and ethmoid commissure in the "acanthothoracid" *Kolymaspis*, the antiarch *Asterolepis* (after Lukševičs 2001), the "acanthothoracid" *Romundina* (after Ørvig 1975; Dupret et al. 2010) and the rhenanid *Gemuendina* (after Gross 1963; Denison 1978). All in dorsal view. Not in scale.

uncertain. The nearly complete preservation of the preorbital endocast morphology of *Kolymaspis* then makes it a good comparative specimen for identifying these canals and foramina in the other "acanthothoracid" taxa.

Brindabellaspis has two preorbital canals (called c. prod and c.prov by Young 1980; text figs 5,6,10,11,12) extending from the anterior wall of the orbit towards the snout (Fig. 4.11D-F). Young (1980) suggested that these preorbital canals contained the pro-

fundus (Vpf) and ophthalmicus superficialis (V op.sup) branches of the trigeminal nerve, and the ophthalmicus lateralis branch of the facial nerve (VII op.lat), based on a comparison with *Macropetalichthys* (Stensiö, 1963a, 1969). However, Young (1980) could not provide exact individual assignments, as the courses of the nerve canals in the snout region were only partially preserved. Moreover, some of the assignments become even more doubtful when the possible function of these nerves is considered.

Firstly, the ophthalmicus lateralis branch of the facial nerve is a sensory branch innervating the supraorbital section of the sensory line. In *Kolymaspis* (Figs 4.1A, 4.2), like in *Brindabellaspis* (Young 1980, text-fig 1; soc) and *Romundina* (Ørvig 1975, text-fig 1; soc), the supraorbital sensory line terminates at the anterior edge of the preorbital plates, before the snout (Fig. 4.11D-F). Instead, the preorbital canals that Young (1980) assigned to the ophthalmicus lateralis continue forward towards the snout (Young 1980, text-fig 10, 11,12). In contrast, the ophthalmicus lateralis branch in both *Macropetalichthys* (Stensiö 1969, text-fig 48) and *Shearsbyaspis* (chapter 2, figs 2.3, 2.4, 2.10), follows the course of the supraorbital sensory line and projects anteriorly, extending to the tip of the snout. Because the preorbital canals in *Brindabellaspis* do not match the course of the supraorbital sensory line, it is then unlikely they could have contained the ophthalmicus lateralis branch of the facial nerve. These preorbital canals, instead, connect with several small branches to the premedian plate (Fig. 4.11F) and seem to be related to the innervation of the dermal surface of the snout (Young 1980, text-fig. 6, 10, 12), which is usually carried out by the profundus and ophthalmicus superficialis branches of the trigeminal nerve. It is then possible that these canals in *Brindabellaspis* correspond to these two branches of the trigeminal nerve (Fig. 4.11F).

The preorbital canals of *Kolymaspis* project ventrally toward the palate (Figs 4.6, 4.11C), creating a different course in the snout to that of *Brindabellaspis*. This may suggest that the snout of *Kolymaspis* was is innervated by a different set of nerves. A wide groove on the subocular shelf extends anteriorly towards the snout from the

opening for the trigeminal nerve canal in the posteroventral myodome (Figs 4.3-5; gr.Vmax). This groove is connected with a large preorbital canal via a big foramen in the same position as the one indicated in *Brindabellaspis* by Young (1980) for the foramen for the maxillary branch of the trigeminal nerve (Young 1980, text-fig 10-11; gr.mx). I suggest then that the maxillary branch of the trigeminal nerve in *Kolymaspis* would extend inside the preorbital wall and that the largest preorbital canals of *Kolymaspis* contained the maxillary branch of the trigeminal nerve (Fig 4.11B-C).

The maxillary branch of the trigeminal nerve usually extends towards the snout together with the ramus buccalis lateralis of the facial nerve. In *Brindabellaspis* and *Romundina*, the buccalis lateralis has been suggested to exit the orbit with the maxillary branch of the trigeminal nerve, passing laterally in a small groove on the preorbital space (Young, 1980; Dupret et al., 2014). In *Kolymaspis*, a small groove is present on the lateral side of the orbital wall (Figs 4.3-5; gr.VII buc.lat) and it is connected to an anteriorly projected canal that extends towards the snout, paralleling to the maxillary branch of the trigeminal (Figs 4.5-7; VIIbuc.lat). This canal is then identified as the canal for the ramus buccalis lateralis of the facial nerve (Fig 4.11B-C). In *Kolymaspis*, however, this canal, as well as the maxillary branch of the trigeminal, is invested in the neurocranium and extends inside the preorbital interperichondral space (Fig. 4.11A-C), unlike in *Brindabellaspis* (Young, 1980) and *Romundina* (Dupret et al., 2014, 2017b).

The preorbital space of *Kolymaspis* does not show any large canals innervating the dorsolateral surface of the premedian plate, as in *Brindabellaspis* (Young 1980, text-fig 1, 5, 8, 10; cav.pro). It is therefore difficult to assess the course of the profundus and ophthalmicus superficialis branches of the trigeminal nerve, which would normally innervate the skin of the snout. However, the preorbital canals of *Kolymaspis* are very large and divide into smaller canals, some of which are connect to the premedian plate (Figs 4.11A-C). This suggests that the large preorbital canals in *Kolymaspis*, as well as containing the motorial maxillary branch of the trigeminal, may also have contained sensorial canals of the trigeminal nerve.

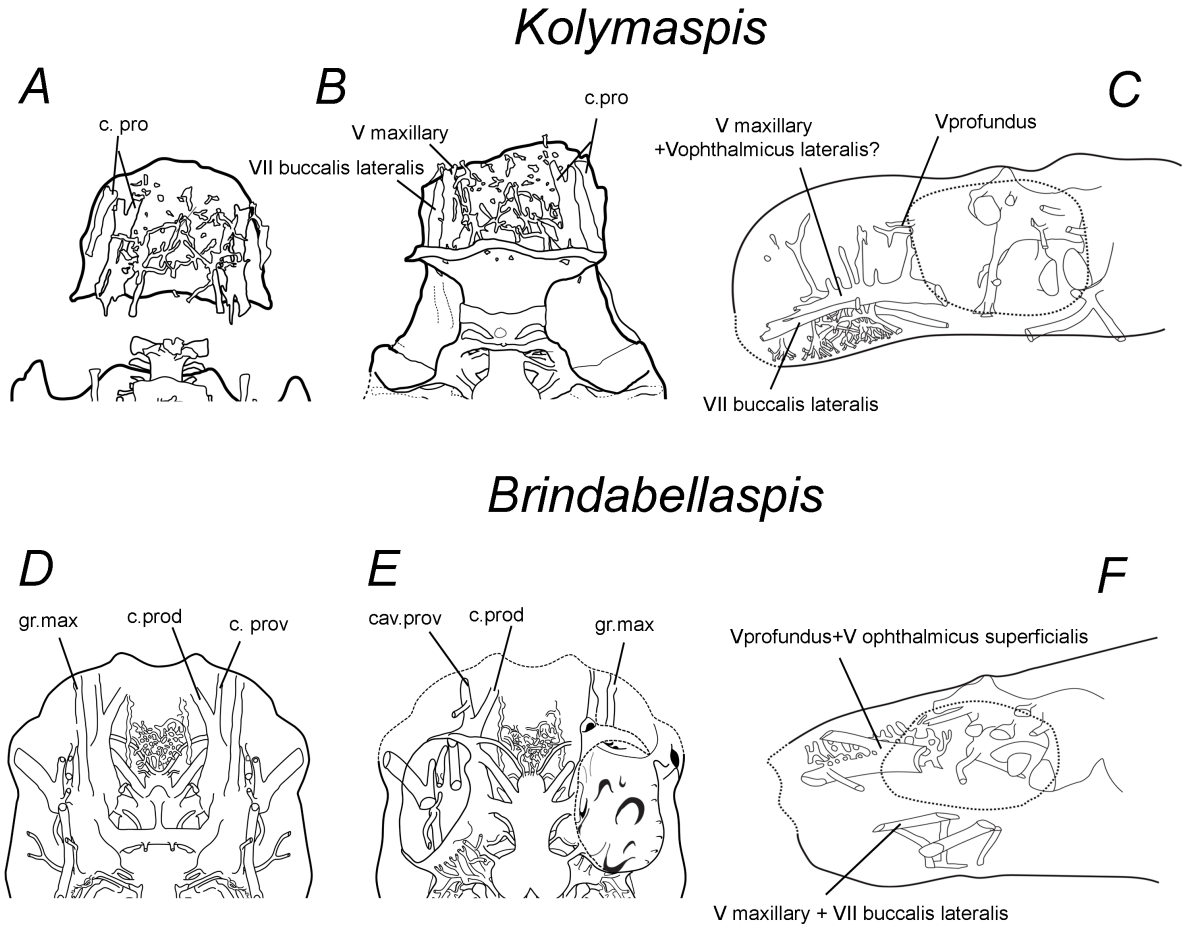

FIGURE 4.11: The morphology of the canals of the preorbital region in *Kolymaspis* (A,B,C) and *Brindabellaspis* (D, E, F) (after Young, 1980). Not in scale. A, ventral view; B, dorsal view; C, lateral view; D, ventral view with original labelling by Young (1980); E, dorsal view with original labelling from Young (1980); F, lateral view with the new labelling after this work. Abbreviations: c.pro, preorbital canals; c.prod, dorsal preorbital canal; c. prov, ventral preorbital canal; gr.max, groove for the maxillary branch of the trigeminal nerve; V maxillary, maxillary branch of the trigeminal nerve; V ophthalmicus superficialis, ramus ophthalmicus superficialis of the trigeminal nerve; V profundus, profundus branch of the trigeminal nerve; VII buccalis lateralis, ramus buccalis lateralis of the facial nerve.

Together with these canals containing innervation for the snout, the premedian region of *Kolymaspis* has a very intricate complex of anastomotic canals (Figs 4.5-7, 4.11A-C) that open on the ventral ethmoidal endocranial surface as a series of foramina and grooves (Fig. 4.8). These canals and related foramina are also evident on the endocavity and braincase of *Brindabellaspis* (Young 1980, text-fig 5,7,10-11).

From an anatomical and sensorial perspective, the snout of these "acanthothoracids" possesses a similar morphology with the rostrum and snout area of modern sturgeons, catfishes, and rays (Northcutt et al., 2000; Wueringer and Tibbetts, 2008; Song and Song, 2012). It is then possible that the presence of this sensorial elongated rostrum, together with the dorsal position of the eyes, could be related to a specialized ecological adaptation of the "acanthothoracids" as benthic predators preying on bottom-dwelling organisms.

4.4.3 The facial nerve in "acanthothoracid" placoderms

In chapter 2, I discuss the debates relating to the phylogenetic value of the morphology and division of the facial nerve. In gnathostomes, the hyomandibular and palatine branches of the facial nerve either divide in the preorbital region, as observed in *Shearsbyaspis* (chapter 2), arthrodires (Young, 1979; Goujet, 1984a; Dupret, 2010) and crown-gnathostomes (e.g. Gardiner 1984b; Maisey 2005; or they divide within or anteriorly the orbit, as observed in *Romundina* (Dupret et al., 2014, 2017a), *Brindabellaspis* (Young, 1980) and osteostracans (Janvier, 1981, 1985a). Our current knowledge of facial nerve morphology thus implies a similarity between jawless fish and "acanthothoracids" (based on *Brindabellaspis* and *Romundina*), which contrasts with *Shearsbyaspis*, arthrodires and crown-gnathostomes.

The data on *Kolymaspis* provides new insights into the morphology of the facial nerve in "acanthothoracids" and may help to resolve the polarity of this character. In *Kolymaspis*, the transverse otic process is similarly positioned to its course in *Romundina*, arthrodires, and *Shearsbyaspis*. The facial nerve divides into the hyomandibular and palatine branches without entering the orbital wall (Figs 4.5-7). The hyomandibular branch then exits near the transverse otic process behind the orbital wall, while the palatine branch extends forward to exit the braincase. *Kolymaspis* is, therefore, different from both *Shearsbyaspis*, where the hyomandibular branch enters the orbit; and *Romundina*, where both the hyomandibular and palatine branches

enter the orbit. It, instead, shows the same morphology as arthrodires and crown-gnathostomes. Therefore, it can show that the extension of the snout and position of the jaw articulations can be decoupled phylogenetically from the position of the hyomandibular articulation and course of the facial nerve (*contra* King et al. 2016).

4.4.4 The primitive condition of the endolymphatic duct in jawed vertebrates

The morphology of the endolymphatic duct in "acanthothoracids" was originally known from only *Romundina* (Dupret et al., 2014, 2017a) and *Brindabellaspis* (Young, 1980), both of which are very different. In *Romundina*, the endolymphatic duct is a short and very slightly oblique posterodorsolaterally oriented tube, in a fashion similar to arthrodires (Goujet, 1984a; Dupret, 2010) (Fig. 4.12). *Brindabellaspis* has a short, horizontally oriented endolymphatic duct that extends posterodorsally until it expands into a large swelling called the endolymphatic sac (Young, 1980) (Fig. 4.12). From there the endolymphatic duct extends dorsomedially and connects to another transversally oriented swelling that opens with a small pore just lateral to the midline on the nuchal plate (Fig. 4.12). These striking differences in the morphology of this structure have created an obstacle in trying to polarize this character in "acanthothoracids".

The 3D data reveal that the endolymphatic duct of *Kolymaspis* is a long and posterodorsolaterally oriented tube, which is more morphologically similar to what is observed in *Romundina* (Figs 4.5, 4.7, 4.12). This shows that the endolymphatic duct of *Kolymaspis* is not only more similar to that of *Romundina* than to *Brindabellaspis*, but also resembles the posterodorsolaterally projected duct of arthrodires (Goujet, 1984a; Dupret, 2010), and suggests that the endolymphatic duct in *Brindabellaspis* could be a specialised condition. It could then be that simple, posterodorsally oriented tube-like endolymphatic duct morphology, present in rhenanids (Stensiö, 1963a, 1969) and early petalichthyids (Liu, 1991; Zhu, 1991), as well in galeaspids (Gai et al., 2011), osteostracans (Stensiö, 1969; Janvier, 1981, 1985a), *Janusiscus* (Giles et al., 2015b) and

osteichthyans (Gardiner, 1984b; Giles and Friedman, 2014), represents the primitive condition for gnathostomes in general (Fig. 4.12).

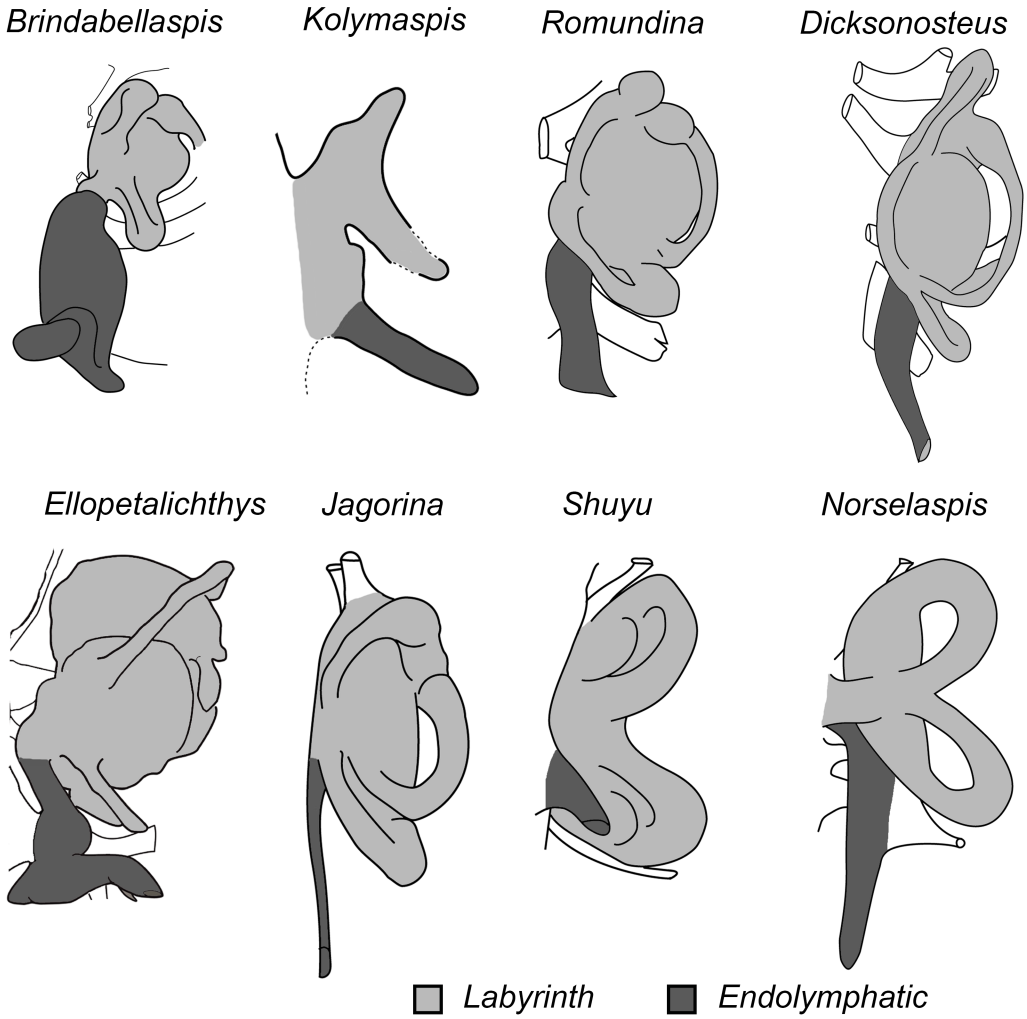

FIGURE 4.12: The morphology of the skeletal labyrinth of several stem gnathostomes. From left to right, top to bottom: the "acanthothoracid" placoderm *Brindabellaspis* (after Young 1980), the "acanthothoracid" placoderm *Kolymaspis*, the "acanthothoracid" placoderm *Romundina* (after Dupret et al. 2017), the arthrodiran placoderm *Dicksonosteus* (after Goujet, 1984a), the petalichthyid placoderm *Ellopetalichthys* (from chapter 3), the rhenanid placoderm *Jagorina* (after Stensiö 1969), the galeaspid *Shuyu* (after Gai et al. 2011) and the osteostracan *Norselaspis* (after Janvier, 1981). Not to scale.

Although the morphology of the endolymphatic duct in *Brindabellaspis* is so different from the other "acanthothoracids", there are many features that are similar to what is observed in the antiarchs. The endolymphatic duct of the antiarch *Minicrania*

(Zhu and Janvier, 1996), for example, is characterized by a medially oriented pair of transverse swellings in the posterior portion of the endolymphatic duct that meet on the midline of the skull roof and open on the middle of the nuchal plate (Zhu and Janvier 1996, text-figs 2, 6-7) The anterior portion of the endolymphatic duct is not present in *Minicrania*, so it is not possible to infer if it has the large endolymphatic sac like in *Brindabellaspis*, although this transverse portion of the endolymphatic duct partially overlaps the endocavity (Zhu and Janvier 1996, text-figs 2, 6-7). Similar features are evident on the visceral surface of the skull roof in many other antiarchs, including *Chuchinolepis* (Ritchie et al., 1992) and *Wufengshania* (Pan et al., 2017).

An endolymphatic duct that expands into an endolymphatic sac is also present in the petalichthyids, such as *Macropetalichthys* (Stensiö, 1925, 1963a, 1969) and *Ellopetalichthys* (chapter 3, Figs 3.2, 3.6). Here, however, the morphology of the endolymphatic sac is very different (Fig. 4.12), as they project laterally, diverging from each other, and opening on the paired paranuchal plates. This suggests that the endolymphatic complexes of petalichthyids and *Brindabellaspis* (and antiarchs), despite having a similar system of endolymphatic sacs, seem to be two independently developed structures. Furthermore, the earliest member of the petalichthyids from China (Liu, 1991; Zhu, 1991) seems to possess a simpler endolymphatic duct that is composed of a short and vertical tube (as noted by Dupret 2008), more similar in morphology to that of jawless fish, arthrodires, and crown gnathostomes. As the complex endolymphatic duct morphology observed in antiarchs, *Brindabellaspis*, and "derived" petalichthyids differs substantially from the simple tubular morphology of the jawless stem-gnathostomes, this calls into question whether the endolymphatic morphology of those placoderm taxa is actually primitive for jawed vertebrates or a derived feature.

4.4.5 "Acanthothoracid" orbitonasal morphology

So far, the presence of nasal openings in the orbit has been poorly investigated in phylogenetic analyses, with the only one published by King et al. (2016), where this character is considered as an autapomorphy of *Brindabellaspis*. However, having nasal openings as part of the orbit is a feature that is much more widespread among placoderms but has been so far neglected. The orbitonasal morphology of *Kolymaspis* is very similar to that of *Brindabellaspis*, showing nasal capsules that open laterally in the anterodorsal corner of the orbit (Fig. 4.13). This anatomy is very reminiscent to that of antiarchs (Fig. 4.10), where the nasal capsules are placed in the anterior corner of the rostropineal plate and form part of the orbital opening (e.g. Lukševičs 2001). Similarly, the morphology of the rostropineal plate of *Romundina* (Ørvig 1975, plate 5), indicates that a comparable condition existed even in this taxon (Fig. 4.10), despite the nasal cavity opens anteriorly instead of opening laterally as in *Brindabellaspis* and *Kolymaspis*. Finally, nasal opening in the orbit are evident for the arthrodire *Parabuchanosteus* (Fig. 4.13), where the terminal portion of the nasal cavity opens ventrally with nasal capsules that are, in fact, inside the orbit (Young, 1979). This morphology is related to the presence of a rhinocapsular ossification, which constitutes the anterodorsal edge of the orbit and bears the nasal capsule. Moreover, many placoderms exhibit ossified sclerotic capsules that bear a process that form one of the lateral edge of the nostril, (e.g. Lukševičs 2001, text-figs 4,6; Young 2010, text-fig 5), indicating the presence of a peculiar orbitonanasal complex. This may suggest that this orbitonasal morphology is a unique feature of a subgroup of placoderms.

The orbitonasal morphology of "acanthothoracids" and antiarchs is usually compared with that of galeaspids and osteostracans (Dupret et al., 2014, 2017a). In these jawless and placoderm groups, the nasal capsules are placed between the orbits, as opposed to anteroventrally to the orbit as seen in most of other placoderms and in crow-gnathostomes. However, as showed above, in many "acanthothoracids" and antiarchs the nasal capsules are not only dorsally placed, but are in fact part of the

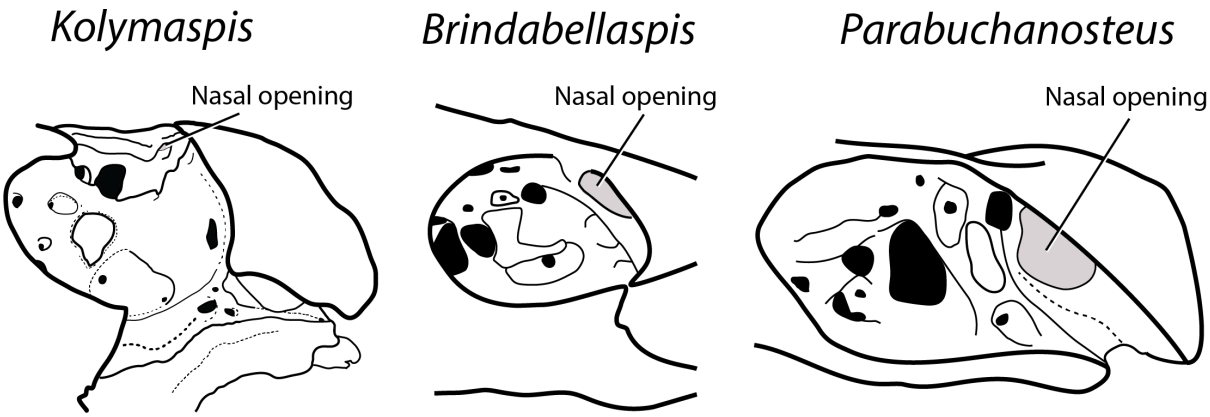

FIGURE 4.13: The position of the nasal capsules inside the orbit in the "acanthothoracid" *Kolymaspis*, the "acanthothoracid" *Brindabellaspis* (after Young 1980) and the arthrodire *Parabuchanosteus* (after Young 1979). Not to scale.

orbit, thus different from the condition in jawless fishes. Moreover, osteostracans lack paired nasal opening, possessing instead a single nasohypophysial complex similar to that of lampreys. Additionally, the jawless heterostracans, the sister lineage to the clade including galeaspids, osteostracans and jawed vertebrates, have paired olfactory bulbs and anteriorly place nasal opening (Janvier and Blieck, 1979). This rises questions about the primitive condition for jawed vertebrates eye and nostril being represented by those jawless fishes with dorsally placed nostrils, and galeaspids and osteostracans have been considered as "derived" forms from a generalized stem-gnathostome condition by some authors (Gai et al., 2011). As a consequence, the position of the nasal capsules and eyes in "acanthothoracids" and antiarchs might not represent the plesiomorphic condition for jawed vertebrates, being instead convergent with those of galeaspids and osteostracans. All the observations above should be considered when comparing the nasal morphology of jawless fishes and those placoderms with dorsally placed eyes, as the position is not sufficient evidence to homologize this character.

4.5 CONCLUSION

Kolymaspis sibirica displays an interesting combination of dermal and endocranial characters present in other genera assigned to the "Acanthothoracida", between the long snouted *Brindabellaspis* and the short snouted *Romundina*. For example, *Kolymaspis* and the long-snouted "acanthothoracid" *Brindabellaspis* share a similar occipital joint morphology, with poorly mineralized glenoid articulation and lacking the posterior projection of the paranuchal plate present in other acanthothoracids like *Romundina*, *Arabosteus* and *Kimaspis*. In addition, they resemble antiarchs in having nasal capsules opening in the orbit and a well-developed premedian plate, suggesting a close affinity between those taxa. On the other hand, *Kolymaspis* is more similar to *Romundina* in the configuration of the sensory line system, rostropineal plate and dermal ornamentation. However, our current knowledge seems insufficient to allow us to understand the relationship of the members of this group. The characters used to support "Acanthothoracida" monophyly, as dorsolaterally placed orbit or the possession of three paranuchal plate, are in fact all much more general gnathostome traits or are not present in many outgroups, making them of uncertain significance. Indeed, several recent studies have failed to report unique features that support the monophyly of "acanthothoracids" (Goujet, 1984b; Brazeau, 2009; Davis et al., 2012; Zhu et al., 2013; Dupret et al., 2014; Giles et al., 2015b; Zhu et al., 2016; King et al., 2016) and the group is often considered as an ensemble of generalized placoderms (Janvier, 1996a).

Goujet 1984b reviewed the characters of the group and suggested that "Acanthothoracida" may constitutes a grade of forms of early branching members of rhenanids and antiarchs. At that time, very little information about "acanthothoracids" endocranial anatomy was available and this statement was supported mainly by the lack of potential synapomorphies and similarities between some "acanthothoracid" to either rhenanids or antiarchs. This revision of acanthothoracid morphology based on the new information on *Kolymaspis* has reinforced the hypothesis that some char-

acters, such as the presence of premedian plate with an ethmoid commissure, may indeed reunite rhenanids, antiarchs, and "acanthothoracids", with some of these "acanthothoracids" also sharing a unique orbitonasal and endolymphatic ducts with antiarchs. However, many of those characters are only comparable among placoderms and present equivocal polarizations when put in a broad gnathostomes context.

Moreover, this new data shows that the anatomy of the facial nerve and endolymphatic duct of *Kolymaspis* is more similar to that of the other stem-gnathostomes rather than other "acanthothoracids" like *Romundina* and *Brindabellaspis*. These evidences provide support to the hypothesis that the facial configuration of those "acanthothoracids" and of antiarchs represents a highly specialized morphology rather than exhibiting the plesiomorphic condition for jawed gnathostomes, thus challenging previous hypothesis. Nevertheless, the lack of endocranial information about antiarchs and the other members of "Acanthothoracida", a major obstacle in comparing this groups with the rest of the gnathostomes, especially if placoderms are considered paraphyletic. These problems impede a clear understanding "acanthothoracids" relationships and thus of their impact on the study of the architecture of the ancestor of jawed vertebrate.

CHAPTER 5

PHYLOGENETIC ANALYSIS OF PLACODERMS WITH A PARTICULAR ATTENTION OF THE RELATIONSHIPS OF PETALICHTHYIDS AND "ACANTHOTHORACIDS"

5.1 INTRODUCTION

Placoderms are the only known stem-group jawed vertebrates with jaws and their phylogenetic relationships have become central to the question of how gnathostomes evolved. Recent discoveries and investigations have raised questions about the phylogenetic relationships of placoderms as a whole, and consequently their impact on understanding of early gnathostome anatomical conditions (Brazeau, 2009; Zhu et al., 2013; Dupret et al., 2014; Long et al., 2015; Zhu et al., 2016; King et al., 2016; Dupret et al., 2017a). Competing views on placoderm monophyly imply radically different hypotheses about the origin of the gnathostome face and reproductive biology (review in Brazeau and Friedman 2014, 2015).

Among placoderms, petalichthyids and "acanthothoracids" have taken a central position in the debate on placoderm paraphyly, owing to their similarities with the jawless outgroups of jawed vertebrates (Janvier, 1996b; Brazeau, 2009; Brazeau and Friedman, 2014; Dupret et al., 2014, 2017a). Nevertheless, their phylogenetic relationships with the other placoderms and the other early gnathostomes are still debated (see chapter 1).

Two major groups are found within Petalichthyida, the macropetalichthyids (Eastman, 1898) and the quasipetalichthyids (Liu, 1991) (see chapters 1-3). Some macropetalichthyids exhibit features that recall the osteostracans, the jawless sister group of gnathostomes (Stensiö 1925, 1963a, 1969, chapters 2 and 3 of this thesis). This

fact has been central to arguments in favour of placoderm paraphyly (Janvier, 1996b; Brazeau, 2009; Brazeau and Friedman, 2014). By contrast, some quasipetalichthyids (Zhu, 1991; Pan et al., 2015) present features, such as the morphology of the endocranial processes, the presence of a central sensory line and the anatomy of ethmoidal region of the skull, which could nest them with the arthrodires, the group most commonly considered a close sister group to the jawed vertebrate crown group (Giles et al., 2015b).

Previously, the monophyly of Petalichthyida has been based on probably plesiomorphic dermal bone characters and tested only including a few petalichthyid taxa and only using arthrodires as an outgroup (Zhu, 1991; Pan et al., 2015). As a result, many of the proposed synapomorphies for the group (e.g. sensory line openings with pores instead of grooves or the absence of contact between the preorbitals), are found among other placoderm groups, sometimes allied with petalichthyids, but not considered part of the group itself (for instance, ptyctodonts). This casts doubts on the monophyly of Petalichthyida as "traditionally defined". Furthermore, it raises question about whether their osteostracan-like traits can be said to be general traits of the placoderms, or secondarily derived.

"Acanthothoracid" placoderms have been hypothesised to exhibit the primitive condition for jawed vertebrates, as they possess shared similarities with galeaspids and osteostracans, such as dorsally placed eyes and nostrils (Brazeau 2009; Zhu et al. 2013; Dupret et al. 2014; Zhu et al. 2016; Dupret et al. 2017a and chapters 1 and 4). However, some recent phylogenetic analyses have resolved "Acanthothoracida" as non-monophyletic, with the two best-known taxa, *Brindabellaspis* and *Romundina*, placed far apart (Giles et al., 2015b; King et al., 2016).

In those studies, *Brindabellaspis* has been resolved as the sister group of other jawed vertebrates while *Romundina* has been placed closer to the more crownward placoderms such as arthrodires. Moreover, recent analyses have included only a few representatives of the "Acanthothoracida" (Brazeau, 2009; Davis et al., 2012; Zhu et al., 2013; Dupret et al., 2014; Giles et al., 2015b; Zhu et al., 2016; King et al., 2016).

This is because most of the "acanthothoracid" taxa are only now for few endocranial details or are disarticulated or poorly preserved. Nevertheless, some of these "acanthothoracids" show important features of their endocranial anatomy and orbital anatomy (Gross 1958, 1959; Olive et al. 2011; Vaškaninová and Ahlberg 2017, chapter 4) or present unique dermal skull roof configuration (Gross 1950, 1958; Vaškaninová and Ahlberg 2017), so that they can be useful to investigate the anatomical diversity of the group. Investigating a more inclusive sample for "acanthothoracids" could thus help illuminating the uncertainty about this group.

The question of petalichthyids and "acanthothoracids" monophyly and relationships to other placoderms and early gnathostomes is therefore pivotal in understand the role of placoderm characters in our hypotheses on gnathostomes bodyplan evolution. However, the uncertainty about the phylogenetic relationships of those groups of placoderms represents a major obstacle and has led to different competing hypothesis about the primitive condition for jawed vertebrates. For these reasons, here I test the relationship of petalichthyids, "acanthothoracids" and ultimately early jawed gnathostomes, by performing phylogenetic analyses on a novel data matrix that include a broad sample of petalichthyids and "acanthothoracids" placoderms. Using this extended dataset, I aim to test the monophyly of placoderms under different phylogenetic methods, as well as investigating the monophyly and relationships of petalichthyid and "acanthothoracid" placoderms. In particular, this analysis includes almost all known petalichthyids and quasipetalichthys with the exclusion of *Neopetalichthys* (Liu, 1973), for which poor preservation limits interpretation and character coding. In addition, it includes most of the best known "acanthothoracids", many of which are known for a wide array of endocranial character and are thus comparable in a broad gnathostomes sample.

In this chapter, I present the results from this novel phylogenetic investigation and discuss the implications of them in the context of vertebrate evolution. Special attention is given to the affinity of *Kolymaspis* in relation to the other "acanthothoracids", as these are currently still obscure, and to the relationship between

the "quasipetalichthyids" and the rest of petalichthyids placoderms. These should shed some lights on the significance of the similarities between those group (i.e. petalichthyids and "acanthothoracid") with osteostracans and galeaspids, a key topic in understanding the plesiomorphic condition at the origin of jawed vertebrates.

5.2 DATA AND METHODOLOGY

5.2.1 **Taxon selection**

The data matrix produced here has three aims, which include investigating the monophyly and character polarity of petalichthyid placoderms, "acanthothoracid" placoderms and of jawed vertebrates as a whole. For this reason I initially updated the data matrix of King et al. (2016), as it includes a wide samples of placoderm taxa and a thorough revision of previous stem-gnathostomes data matrices. The original dataset included 5 petalichthyids and 2 "acanthothoracids", for a total of 34 placoderm taxa.

I expanded the dataset by adding 9 petalichthyid taxa, specifically *Shearsbyaspis* (Young, 1985), *Ellopetalichthys* (Ørvig, 1957), *Pauropetalichthys* (Pan et al., 2015), *Guangxipetalichthys* (Zhao and Zhu, 2010; Ji and Pan, 1997), *Sinopetalichthys* (P'an et al., 1975; Zhao and Zhu, 2010), *Notopetalichthys* (Woodward, 1941), *Pampetalichthys* (Zhu and Wang, 1996; Zhu, 2000), *Epipetalichthys* (Zhu and Wang, 1996; Zhu, 2000), *Widjeaspis* (Young, 1978). I also added 8 "acanthothoracids", *Sudaspis* (Gross, 1959; Vaškaninová and Ahlberg, 2017), *Radotina kosorensis* (Gross, 1950, 1958; Vaškaninová and Ahlberg, 2017), *Radotina tessellata* (Gross, 1950, 1958; Vaškaninová and Ahlberg, 2017), *Kimaspis* (Mark-Kurik, 1973), *Kosoraspis* (Gross, 1958, 1959), *Tlamaspis* (Gross, 1959; Vaškaninová and Ahlberg, 2017), *Kolymaspis* (Bystrow, 1956) and *Arabosteus* (Olive et al., 2011). Other placoderms added also include *Asterolepis* (Lukševičs, 2001),*Minicrania* (Zhu and Janvier, 1996), *Chuchinolepis* (Thanh and Janvier, 1990), *Mulgaspis* (Ritchie, 2004) and *Qilinyu* (Zhu et al., 2016). *Anglaspis* (Watson, 1954; Blieck and Heintz, 1983) was added as an outgroup (see below). Two osteostracans, *Aceraspis*

(Heintz, 1939) and *Dartmuthia* (Patten, 1931; Janvier, 1985b) have been added to increase the sample of osteostracans anatomical diversity.

The extended dataset presented here include 1 heterostracan, 7 galeaspids and 13 osteostracans as outgroups. 121 ingroup taxa include 54 placoderms, *Qilinyu*, *Entelognathus*, *Janusiscus*, *Ramirosaurezia*, 25 osteichthyans, 22 "acanthodians" and 14 non-acanthodians chondrichthyans. Petalichthyids diversity is sampled including 14 taxa (out of 19 described, some of which have been excluded due to poor preservation). The sampled "acanthothoracids" now include most "acanthothoracids" for which good endocranial material is preserved. The antiarchs *Chuchinolepis* and *Minicrania*, which usually fall near the root of antiarchs (Zhu, 1996; Pan et al., 2017) have been included to investigated the polarity of the characters within the antiarchs. All taxa from the original matrix have been kept.

5.2.2 **Characters and coding**

This character list derives principally from the dataset published by King et al. (2016) and consists of 485 characters (originally 497). However, extensive revisions have been applied for character coding and states. Some characters have been deleted as problematic in their formulation (discussion in the appendix). 15 new characters have been added to the original dataset, 10 of which are of new formulation. Other characters have been reformulated, merged or split, and sometimes ordered. Brief comments on newly formulated, modified or deleted character states or coding are included in the character list below and in the appendix. Characters order has been structured as much as possible as originally presented by King et al. (2016). Original sources for character descriptions are specified and listed in the bibliography if they differ from King et al. (2016).

The character data entry and formatting were performed in Mesquite (version 3.31) (Maddison and Maddison, 2017). All characters were treated as unordered unless specified.

5.2.3 Outgroup selection, scoring and constraints

Outgroups, which are set at the root of the tree, affect character polarity and ingroup relationships, making them vitally important for phylogenetic analysis. However, justification is rarely given for outgroup selections. Most recent phylogenetic analysis use galeaspids and/or osteostracans as outgroup to investigate jawed vertebrates relationships (Brazeau, 2009; Davis et al., 2012; Zhu et al., 2013; Dupret et al., 2014; Long et al., 2015; Giles et al., 2015b; King et al., 2016; Zhu et al., 2016). Among these, most have adopted the practice of coding Galeaspida and Osteostraci as composite single terminals, which are scored based on data from several species (Brazeau, 2009; Davis et al., 2012; Zhu et al., 2013; Dupret et al., 2014; Long et al., 2015; Zhu et al., 2016). This method has the advantage of requiring less computing and decreases the time for running the analysis. However, many studies have criticized the use of composite terminals, arguing that they may cause less accurate results by homogenizes the interspecific various within the group, and instead suggesting scoring several taxa within a group as an alternative (Prendini, 2001; Brusatte, 2010). Among those investigating stem-gnathostomes, King et al. (2016) has so far been the only study to adopt this method. Here, I maintained this approach, retaining all the galeaspids and osteostracans included in the original matrix.

Galeaspids and osteostracans may represent groups with their own derived morphology and not necessarily exhibit the primitive condition for the ancestor of jawed vertebrates (refer to Gai et al. 2011 and discussion in chapters 2 and 4). The use of those groups as outgroups for jawed vertebrate phylogeny have the problem of potentially biasing the ancestral states of the origin of jawed vertebrates. For example, characters as dorsally placed eyes or dorsally placed nasal opening are usually considered primitive for jawed vertebrates (e.g Dupret et al. 2014). However, this condition is not present in some other, probably more rootwards, stem-gnathostomes, such as some heterostracans, where the eyes and potentially the nasal openings are laterally and anteriorly placed, respectively. To avoid assuming *a priori*

the primitive state at the origin of jawed vertebrates, I introduced an heterostracans in the outgroup. I choose *Anglaspis maccoulloughi*, from the Early Devonian of the UK and France, as it is known from relatively complete material which shows external and internal anatomy (Wills, 1935; Watson, 1954), as well as for its histology (Keating et al., 2015). *Anglaspis* was then constrained to be sister to all other taxa in the matrix (Janvier, 1996b, 2008; Donoghue et al., 2000).

5.2.4 **Phylogenetic analysis**

PARSIMONY ANALYSIS — The data matrix is large and contains many taxa for which a high percentage of the characters cannot be coded, due to inapplicability or missing data. This raised concerns, as the parsimony analysis yielded a high number of equally parsimonious trees, causing a very long computing time during tradition heuristic searches. In order to resolve this issue, I decided to use a different approach and performed a Parsimony Ratchet. The Parsimony Ratchet (or "Island Hopper") is a search strategy developed by Nixon (1999) with the aim of finding the shortest tree in a shorter time for those large datasets that will require a prolonged computing time with traditional heuristic searching methods. The Ratchet has the advantage of sampling many more tree islands compared to traditional heuristic search by sampling fewer trees from each island, and maximizing the starting point for each iteration by keeping one (arbitrary) MPT from previous iteration.

Practically, the Parsimony Ratchet computes a single connected search comprising many short heuristic searches on many islands, instead of performing more thorough independent visits on fewer islands, as in the traditional heuristic search. Initially, it creates a random starting tree and then perform two searches for each iteration, one selecting and reweighting a randomly chosen (but with a fixed count) subset of characters, and another with the character returned to their original weight. The best tree found for each search is then kept and used by the next search iteration as a starting tree. In this way, the Ratchet search are "guided" through new island

of tree space which are not randomly chosen but rather constitute neighbour island that can be reach by alterating the shape of the tree landscape (Sikes and Lewis, 2001). In this analysis, I selected to reweight 25% of the character for each iteration.

There is a chance that a single Parsimony ratchet will not find the shortest tree (Nixon, 1999). However, multiple ratchets can be performed and has been demonstrated that executing multiple runs with fewer iteration will usually recover the shortest tree (Nixon, 1999). Here, I used PRAP2, an implementation that prepares the file to be suitable for a Parsimony Ratchet performed in the software PAUP* (Swafford, 2003). 10 runs of 300 iterations were performed, as advised by (Sikes and Lewis, 2001). I also performed another parsimony analysis on the same dataset using TNT (Goloboff et al. 2008), to test for congruence in the shortest tree found betweem these two different very fast tree-searching algorithms.

Strict and majority rule (50% bootstrap) consensuses were computed and Mesquite (version 3.31) (Maddison and Maddison, 2017) was used to trace the character transformation on those cladograms.

BAYESIAN ANALYSIS — A recent study by (King et al., 2016) recovered very different results when the same dataset was analysed with Parsimony and Bayesian analysis, especially concerning the relationships of placoderms. This highlights the importance of using different phylogenetic methods of inference. Many recent study on stem-gnathostomes indeed include both these analytical methods.

Here, the full dataset has been analysed with Bayesian MCMC analysis using MrBayes 3.2 (Ronquist and Huelsenbeck, 2003). *Anglaspis* was set as the outgroup, with galeaspids and osteostracans constrained as monophyletic and osteostracans as the sister to jawed vertebrates. The analyses used the Lewis stochastic model for standard datatype (Lewis, 2001) with coding set to 'variable' and a gamma parameter to account for rate variation across traits. The search was run for twenty million generations (ngen=20000000), employing two independent runs (nruns=2) each including four Markov chains (nchains=4). Trees were sampled for each run every 1000

generations (samplefreq=1000), and a majority rule consensus of the sampled trees was computed from this output, with the "Burn-in" (discarded generations) fraction set at 0.25.

5.3 CHARACTER LIST

Each alteration to the original data matrix of (King et al., 2016) is listed below and is accompanied by a brief justification. The original character number is given in bold and squared brackets. The full character list is given in the appendix.

Histology

Ideally, histological characters can be coded only if histological sections have been made. For that reason, coding has been revised and changed to "?" when no histological section has been published. Presence or absence of perichondral and endochondral bone can be coded based on CT sections. Presence of enamel and enameloid has been reported based on the shininess of the dermal surface but this might be misleading and it is bad practice. Histological data for stem-gnathostomes are from Donoghue and Sansom (2002); Donoghue et al. (2006a); Giles et al. (2013); Keating et al. (2015).

1) [1] **Tessellate prismatic calcified cartilage**: **(0) absent (1) present**

2) [2] **Prismatic calcified cartilage**: **(0) single-layered (1) multi-layered**

3) [3] **Perichondral bone**: **(0) present (1) absent**

Score changed from ? to 0 in *Parayunnanolepis* and from ? to 1 in *Pterichthyodes* (Giles et al., 2015b).

4) [4] **Extensive endochondral ossification**: **(0) absent (1) present**

Score changed from ? to 0 in *Parayunnanolepis* (Giles et al., 2015b). *Dicksonosteus* and *Macropetalichthys* are changed from ? to 0 according to character discussion in Giles et al. (2015b).

5) [5] **Pore canal network**: **(0) absent (1) present**

   Character formulation changed following Lu et al. (2016) and scoring changed consequently.

6) [6] **Three-layered exoskeleton**: **(0) absent (1) present**

7) [7] **Cephalic dermoskeletal bone**: **(0) cellular (1) acellular**

8) [8] **Perforated horizontal lamina in the sensory line canals and vascular system**: **(0) absent (1) present**

9) [9] **Galeaspidin**: **(0) absent (1) present**

10) [10] **Dentine**: **(0) absent (1) present**

    Score for *Lunaspis* changed from ? to 0 and subsequent related characters to inapplicable. Score changed from ? to 1 for *Yunnanolepis*, both according to Giles et al. (2013).

11) [11] **Bone cell lacunae in body scale bases** : **(0) present (1) absent**

12) [12] **Dentine kind**: **(0) mesodentine (1) semidentine (2) orthodentine**

    Score changed from 1 to ? for *Brindabellaspis* as there is no indication of semidentine (Burrow and Turner, 1998)

13) [13] **Main dentinous tissue forming fin spine**: **(0) osteodentine (1) orthodentine**

14) [14] **Resorption and redeposition of odontodes**: **(0) lacking (1) partially developed (2) developed**

15) [15] **Enamel(oid) present on dermal bones and scales**: **(0) absent (1) present**

    Score for *Lunaspis* and *Macropetalichthys* has been change from ? to 0 and subsequent related characters to inapplicable (Giles et al., 2013; Gross, 1935).

Score for *Diandongpetalichthys* and *Quasipetalichthys* has been changed from 0 to ? as no histological section are published.

16) [16] **Enamel**: **(0) single-layered (1) multi-layered**

17) [17] **Enamel layers**: **(0) applied directly to one another (1) separated by layers of dentine**

18) [18] **Superficial glassy layer of dermal armour**: **(0) absent (1) present**

Neurocranium and associated dermal ossifications

19) [19] **Precerebral fontanelle**: **(0) absent (1) present**

Score change from ? to 0 for *Shuyu* (Gai et al., 2011) and *Buchanosteus* (Young, 1979). Score changed from 0 to ? for *Entelognathus*, *Wuttagoonaspis* and *Diandongpetalichthys*, as the dorsal endocranial surfaces is unknown.

20) [20] **Nasal opening(s)**: **(0) dorsal, placed between orbits (1) ventral and anterior to orbits**

This character is here intended as the topological placement of the nares. For this reason, this has been coded for taxa where, despite not having the nares preserved, the location of the nasal openings can be tracked with confidence (e.g. antiarchs, where the nares are associated with the orbitonasal space or petalichthyids where the nasal capsule are in front of the skull). For this reason, state has been changed from ? to 0 for *Microbrachus* (Long et al., 2015).

21) [21] **Olfactory tracts**: **(0) short, with olfactory capsules situated close to telencephalon cavity (1) elongate and tubular (much longer than wide)**

22) [22] **Extended preorbital region between eyes and nasal capsule**: **(0) absent (1) present**

This character is related to the anterior expansion of the neurocranium between the eyes and anteriorly placed nasal capsules, as exhibit by petalichthyids, *Debeerius* and *Chondrenchelys*. This is opposed to the condition in taxa that have an anteriorly expanded preorbital region but with nasal capsule close to (or between) the eyes, like *Brindabellaspis*, antiarchs and osteostracans. Taxa where the orbit and the nares are placed close to each other are scored 0 even if no neurocranial remain are preserved (for example in jawless fishes) because of topological reason. In King et al. (2016) the states were labelled incorrectly as 0 indicate absence and 1 presence. Change has been made here.

23) [23] **Pronounced sub-ethmoidal keel**: **(0) absent (1) present**

Score changed from 0 to ? in *Diandongpetalichthys* has the neurocranial ethmoid region is not preserved. Score changed from 0 to ? for *Lunaspis* has no endocranial information are available.

24) [24] **Position of myodome for superior oblique eye muscles**: **(0) posterior and dorsal to foramen for nerve II (1) anterior and dorsal to foramen**

Score changed from 0 to ? for *Diandongpetalichthys* and *Lunaspis* as no information on the myodome has been published.

25) [25] **Endoskeletal cranial joint**: **(0) absent (1) present**

26) [26] **Spiracular groove on basicranial surface**: **(0) absent (1) present**

27) [27] **Spiracular groove on lateral commissure**: **(0) absent (1) present**

28) [29] **Supraorbital shelf broad with convex lateral margin**: **(0) absent (1) present**

29) **NEW Orbit dorsal or facing dorsolaterally** [30] : **(0) present (1) absent**

Originally, this was a single character regarding the presence or absence of orbit facing dorsally or dorsolaterally and surrounded laterally by endocranium (as defined by Brazeau 2009). However, this was a problematic character as

some taxa, like ptyctodonts, possess laterally facing orbit that are only partially surrounded by endocranium, a condition not taken in account by the original definition of the character. Here, two separate characters have been created, one taking in account the position of the orbit (ch. 23), and the other taking in account the degree of the extension of the endocranium in relation to the orbit (ch.24). In the latter, three states are considered: absence, partially surrounded orbit, surrounded orbit. New coding has been applied to *Diandongpetalichthys* and *Pauropetalichthys*, now scored as 0. Those taxa were previously scored as absent for this character because the orbit are not surrounded by endocranium. However, the orbit seems to be facing dorsolaterally in both taxa, as can be inferred by the internal margin of the orbit (Zhu, 1991; Pan et al., 2015).

30) **NEW Orbits, surrounded laterally by endocranium** [30] : **(0) absent (1) partially surrounded (2) surrounded**

Explanation of states in the character above.

31) [31] **Extended prehypophysial portion of sphenoid**: **(0) absent (1) present**

Score changed from ? to 0 in *Macropetalichthys* and from 0 to ? for *Lunaspis*.

32) [32] **Narrow interorbital septum**: **(0) absent (1) present**

Score changed from 0 to ? for *Diandongpetalichthys*, *Quasipetalichthys* and *Lunaspis* as there are no published information about this region of the braincase. Score changed from 0 to ? for *Acanthodes* and *Howqualepis* as there are not enough information to infer that character.

33) [33] **Hyoid ramus of facial nerve (N. VII) exits through posterior jugular opening**: **(0) absent (1) present**

Score changed to 0 to 1 for *Ligulalepis*, as showed by Basden and Young (2001).

34) [34] **Glossopharyngeal nerve (N. IX) exit**: **(0) foramen situated posteroventral to otic capsule and anterior to metotic fissure (1) through metotic fissure**

Inapplicable for taxa lacking a metotic fissure.

35) [35] **Short otico-occipital region of braincase (0) absent (1) present**

Score changed from 0 to ? for *Diandongpetalichthys* as there are no published information about this region of the braincase.

36) [36] **Ethmoid region elongate with dorsoventrally deep lateral walls**: **(0) absent (1) present**

Score changed from 0 to ? for *Lunaspis* and *Diandongpetalichthys* as there are no published information about this region of the braincase.

37) [37] **Relationship of cranial endocavity to basisphenoid**: **(0) endocavity occupies full depth of sphenoid (1) endocavity dorsally restricted**

38) [38] **Ascending basisphenoid pillar pierced by common internal carotid**: **(0) absent (1) present**

39) [39] **Canal for efferent pseudobranchial artery within basicranial cartilage**: **(0) absent (1) present**

40) [40] **Canal for lateral dorsal aorta within basicranial cartilage**: **(0) absent (1) present**

41) [41] **Entrance of internal carotids**: **(0) through separate openings flanking the hypophyseal opening or recess (1) through a common opening at the central midline of the basicranium**

Score changed from - to ? in *Macropetalichthys*.

42) [42] **Position of basal/basipterygoid articulation**: **(0) same anteroposterior level as hypophysial opening (1) anterior to hypophysial opening**

43) [43] **Postorbital process articulates with palatoquadrate**: **(0) absent (1) present**

44) [44] **Labyrinth cavity**: **(0) separated from the main neurocranial cavity by a cartilaginous or ossified capsular wall (1) skeletal capsular wall absent**

Score changed from 0 to ? for *Diandongpetalichthys*.

45) [45] **Basipterygoid process (basal articulation) with vertically oriented component**: **(0) absent (1) present**

46) [46] **Pituitary vein canal**: **(0) dorsal to level of basipterygoid process (1) flanked posteriorly by basipterygoid process**

47) [47] **External (horizontal) semicircular canal**: **(0) absent (1) present**

48) [48] **Sinus superior**: **(0) absent, indistinguishable from union of anterior and posterior canals with saccular chamber (1) present**

49) [49] **External (horizontal) semicircular canal**: **(0) joins the vestibular region dorsal to posterior ampulla (1) joins level with posterior ampulla**

50) [50] **Posterior dorsal fontanelle**: **(0) absent (1) present**

Score changed from ? to 0 for *Chondrenchelys* (Finarelli and Coates, 2014).

51) [51] **Shape of posterior dorsal fontanelle**: **(0) approximately as long as broad (1) much longer than wide, slot-shaped**

52) [52] **Dorsal ridge**: **(0) absent (1) present**

The dorsal part of the neurocranium in *Shearsbyaspis*, *Ellopetalichthys* and *Kolymaspis* is not visible and probably fused with the visceral dermal surface, so for these taxa this character has been tentatively coded as inapplicable.

53) [53] **Endolymphatic ducts orientation**: **(0) posteriodorsally angled tubes (1) tubes oriented vertically through median endolymphatic fossa**

Originally this character distinguished the condition present in elasmobranchs, where the endolymphatic duct are oriented vertically opening through a median endolymphatic fossa, to that of the other gnathostomes, where the endolymphatic ducts have separated openings (Schaeffer, 1981; Coates and Sequeira, 1998; Maisey, 2001a). With this definition, all placoderms are considered sharing the same condition and coded as having posteriodorsally angled tubes. However, different endolymphatic morphologies exist among the different group of placoderms (see discussion in chapter 3 and 4). For example, in petalichthyids, *Brindabellaspis* (Young, 1980), *Minicrania* (Zhu and Janvier, 1996) and possibily *Kolymaspis*, the duct enlarges in an endolymphatic sacs before narrowing again and exits on the dermal surface. Instead, in arthrodire and rhenanids, as well as osteichthyes and jawless fishes, the endolymphatic duct is essentially a straight oblique tube with no endolympatic sac. Hence, I created another character (ch. 54, below) to deal with presence of endolympahtic sacs. The presence of endolymphatic sacs is dealt with the subsequent character. It is also worth to notice that the endolymaphatic sacs in *Brindabellaspis* and *Minicrania* are different from that of petalichthyids and *Kolymaspis* as they bend towards the midline on the skull, opening on the nuchal plates, instead of being laterally projected and opening on the paranuchal plate. This condition is considered in character 206.

54) **NEW Endolymphatic sacs**: **(0) absent (1) present (2) medially oriented endolymphatic fossae (3) laterally oriented endolymphatic fossae**

55) [54] **Ventral cranial fissure**: **(0) absent (1) present**

Score changed from ? to 0 for *Chondrenchelys* (Finarelli and Coates, 2014).

56) [55] **Metotic (otic-occipital) fissure**: **(0) absent (1) present**

57) [56] **Vestibular fontanelle**: **(0) absent (1) present**

Score changed from ? to 0 for *Psarolepis* (Lu et al., 2016) and *Chondrenchelys* (Finarelli and Coates, 2014)

58) [57] **Occipital arch wedged in between otic capsules**: **(0) absent (1) present**

59) [58] **Spino-occipital nerve foramina**: **(0) two or more, aligned horizontally (1) one or two, dorsoventrally offset**

60) [59] **Ventral notch between parachordals**: **(0) absent (1) present or entirely fused**

Score chaged from 0 to 1 in *Macropetalichthys* (Stensiö, 1969) and same score applied to *Ellopetalichthyis* (chapter 3) and *Wijdeaspis* (Young, 1978), where the notorchordal notch is clearly visibile with an open floor. Score changed from 0 to 1 for *Kujdanowiaspis* and *Diksonosteues* (Goujet, 1984a). Tentatively, this character has been scored present in *Norselaspis* (Janvier, 1981), where a little opening is present on the floor of the notochordal tunnel. The lower part of the occipital ossification of *Kolymaspis* is not preserved enough to score this character. Score changed from 0 to 1 for *Janusiscus* (Giles et al., 2015b) and *Ramirosuarezia* (Pradel et al., 2009).

61) [60] **Parachordal shape**: **(0) forming a broad, flat surface as wide as the otic capsules (1) mediolaterally constricted relative to the otic capsules**

King et al. (2016) used the original states description from this character (from Davis et al. 2012) which was: (0) broad, flat (1) keeled with sloping lateral margins. However, as pointed out by Giles et al. (2015b), the parachordal might be considered laterally compressed respect of the otic capsules, and the parachordal base being placed more ventrally. For this reason, here we use their character state descriptions.

62) [61] **Hypotic lamina (and dorsally directed glossopharyngeal canal)**: **(0) absent (1) present**

63) [62] **Eye stalk or unfinished area on neurocranial wall for eye stalk**: **(0) absent (1) presence**

64) **NEW Eye stalk position**: **(0) positioned laterally on the orbital wall (1) positioned ventrally on the subocular shelf wall**

Character states have been created to highlight the difference between an eye stalk positioned ventrally on the subocular shelf as opposed to on the lateral wall of the orbit. This is an important distinction between taxa that possess similar orientation fo the orbit that have a different position for the eyestalk. As an example, *Brindabellaspis* and *Shearsbyaspis* both possess dorsolaterally placed eyes but the eye stalk in placed laterally or ventrally on the orbital wall, respectively (see chapter 2).

65) [63] **Articulation facet with hyomandibular**: **(0) single-headed (1) double-headed**

66) [64] **Basicranial fenestra**: **(0) absent (1) present**

Score changed from ? to 0 for *Brindabellaspis* (Young, 1980).

67) [65] **Lateral cranial canal**: **(0) absent (1) present**

68) [66] **Midline canal in basicranium for dorsal aorta**: **(0) absent (1) present**

Score changed from ? to 0 for *Romundina* (Dupret et al., 2017a).

69) [67] **Rostral tubuli**: **(0) absent (1) present**

70) [68] **Unconstricted cranial notochord**: **(0) absent (1) present**

71) [69] **Processus descendens of sphenoid**: **(0) absent (1) present**

In King et al. (2016), the definition of this character was based on Zhu et al. (2009) (ch. 41, "descending process of sphenoid, with its posterior extremity lacking periostegeal lining"). However, this definition is confusing and incorporates different features. Here, I used the definition provided by Friedman

(2007) relative to the absence or presence of a descending process on the sphenoid. A descendens process on the sphenoid has been reported for *Guyu* (Qiao and Zhu, 2010).

72) [70] **Opercular suspension on braincase**: **(0) absent (1) present**

73) [71] **Vomeral area with grooves and raised areas**: **(0) absent (1) present**

74) [72] **Ethmoid articulation for palatoquadrate**: **(0) placed on postnasal wall (1) extends posteriorly to the level of N.II**

75) [73] **Optic fissure**: **(0) absent (1) present**

Score changed from ? to 0 for *Macropetalichthys* as there is no trace of the fissure on the braincase. Score changed from 0 to ? for *Diandongpetalichthys* and *Bothriolepis* sp Gogo, as there are not enough information on the braincase to estimate the presence or absence of this character. Score achanged from 1 to ? for *Materpiscis*, as a definite assessment on the presence of an optic fissure can be done as the braincase is a series of non articulated ossifications (*contra* Trinajstic et al. 2012).

76) [74] **Buccohypophysial canal in parasphenoid**: **(0) single (1) paired**

Score changed from - to ? in *Macropetalichthys*. (Stensiö, 1969) was not able to provide clear information about the buccohypophysial region in *Macropetalichthys*. However, the presence of a parasphenoid with an opening for the buccohypophysial canal in *Shearsbyaspis* suggests that it is possible that also *Macropetalichthys* possesses this feature.

77) [75] **Transverse otic process**: **(0) present (1) absent**

As the transverse otic process has been homologised to the anterior postorbital process (Giles et al., 2015b), score changed from inapplicable to present in *Macropetalichthys*. For the same reason, it is scored as present for *Diandongpetalichthys* and *Eurycaraspis*.

78) [76] **Jugular canal**: **(0) long (invested in otic region along length of skeletal labyrinth) (1) short (restricted to region anterior of skeletal labyrinth) (2) absent (jugular vein uninvested in otic region)**

As explained by Giles et al. 2015b, this character is composed as a compound because there are no further dependent characters and thus equivalent to atomize it and use inapplicability.

Although part of the canal is clearly invested in both *Shearsbyaspis* and *Kolymaspis*, this region is not preserved enough to see the entire length of the canal and the character has been scored as unknown. Score changed from ? to 2 for *Chondrenchelys* (Finarelli and Coates, 2014).

79) [77] **Postorbital process**: **(0) absent (1) present**

80) [78] **Canal for jugular in postorbital process**: **(0) absent (1) present**

Score changed from ? to 1 for *Chondrenchelys* (Finarelli and Coates, 2014).

81) [79] **Series of perforations for innervation of supraorbital sensory canal in supraorbital shelf**: **(0) absent (1) present**

82) [80] **Subcranial ridges**: **(0) absent (1) present**

83) [81] **Horizontal semicircular canal in dorsal view**: **(0) medial to path of jugular vein (1) dorsal to jugular vein**

84) [82] **Synotic tectum**: **(0) absent (1) present**

85) [83] **Shape of median dorsal ridge anterior to endolymphatic fossa**: **(0) developed as a squared-off ridge or otherwise ungrooved (1) bears a midline groove**

86) [84] **Branchial ridges**: **(0) present (1) reduced to vagal process (2) absent (articulation made with bare cranial wall)**

87) [85] **Craniospinal process ("supravagal process" in Stensiö)**: **(0) absent (1) present**

Score changed from ? to 0 for *Chondrenchelys* (Finarelli and Coates, 2014).

88) [86] **Stalk-shaped parachordal/occipital region**: **(0) absent (1) present**

89) [87] **Paired occipital facets**: **(0) absent (1) present**

90) [88] **Size of aperture to notochordal canal**: **(0) much smaller than foramen magnum (1) as large, or larger, than foramen magnum**

91) [90] **Medial recess of the posteroventral mydome**: **(0) absent (1) present**

Some osteostracans show a deep median recess in the posteroventral myodome (Sansom, 2008). This character was supposed to be unique to osteostracans but has now been observe in *Shearsbyaspis* (see chapter 2). For this reason, I argue that now can be scored as present in this taxon and absent in other taxa where the morphology of the posteroventral myodome in well known.

92) **NEW: Abducens, trigeminal nerves and pituitary vein**: **(0) opening via different foramina on the orbital wall (1) sharing the same foramen on the orbital wall**

Explanation for this character is discussed in chapter 2 and figure 2.13.

93) **NEW: Pituitary vein in a transverse canal connecting the orbit**: **(0) absent (1) present**

Explanation for this character is discussed in chapter 2 and figure 2.13.

94) [28] **Subpituitary fenestra**: **(0) absent (1) present**

Score changed from ? to 0 for *Romundina* based on (Dupret et al., 2017a). The area is not fully preserved but as the pituitary vein extends completely enclosed in a transverse canal, the subpituitary fossa must not have been present.

95) [91] **Number of "sel" canals**: **(0) five (1) less than 5**

96) [92] **'sel' 1 canal bifurcation**: **(0) between orbit and field (1) adjacent to lateral field (2) adjacent to orbit**

97) [93] **Marginal vein**: **(0) absent (1) present**

98) [94] **Profundus nerve (Young 1980)**: **(0) emerges from the cranial cavity separately from the trigeminal nerve (1) emerges together with the trigeminal nerve**

Score changed from ? to 0 for *Romundina* according to (Dupret et al., 2017a).

99) [95] **Transverse otic process**: **(0) Not extending in front of orbits (1) extending in front of orbits**

Score changed from ? to 0 for *Romundina* according to (Dupret et al., 2017a). Score changed from ? to 0 for *Brindabellaspis* as this process is connected with the hyomandibular attachment.

100) [96] **Nasal capsules in anterolateral corners of orbit**: **(0) no (1) yes**

King et al. (2016) introduced this character as an autapomorphy of *Brindabellaspis*. However, this character is not unique to *Brindabellaspis* but is instead present in antiarchs, many "acanthothoracids", for example in *Kolymaspis* and *Romundina*, and possibily in some arthrodires, such as *Parabuchanosteus* (see discussion in chapter 3). By contrast, petalichthyids and rhenanids, among placoderms, are scored absent as the nares are separated from the orbit. This character is independent from character 14, as the position of the nasal opening to the orbit (i.e. dorsal or ventral) are not necessarily related to the inclusion of the nasal capsules in the orbit. *Parabuchanosteus* has nasal capsule in the anterolateral corners of the orbit but they nasal opening are ventral, for example, and rhenanids and osteostracans has dorsally placed nasal capsules but those are not included in the orbital wall.

101) [97] **Vagal process**: **(0) forked (1) unforked**

According to Giles et al. (2015b), the two bifurcations of the vagal process constitute the anterior and posterior limit of the paravagal fossa. A paravagal fossa is present in both *Macropetalichthys* (Stensiö, 1969) and *Brindabellaspis* (Young, 1980), and for this reason the score for this character has been changed from inapplicable to 0 (forked). *Kolymaspis* has a very poorly developed vagal process but there are two small ridges so can be coded 0. *Minicrania* shows an anterior and posterior supravagal process (Zhu and Janvier, 1996) and here is tentatively coded has possessing a bifurcated vagal process.

102) [99] **Rostral processes**: **(0) absent (1) present**

103) [100] **Median rostral dorsal process of the braincase**: **(0) absent (1) present**

104) [103] **Expanded articular area anterior to basipterygoid process**: **(0) absent (1) present**

105) [104] **Hyomandibular facets where they straddle the jugular vein**: **(0) narrowly separated (1) widely separated**

106) [106] **Posttemporal fossae**: **(0) absent (1) present**

107) [107] **Rostral organ**: **(0) absent (1) present**

108) [108] **Prespiracular dental plate**: **(0) absent (1) present**

109) [109] **Suprapterygoid process**: **(0) absent (1) present**

110) [110] **Processus supraorbitalis lateralis**: **(0) absent (1) present**

111) [111] **Anterolateral fenestra in roof of otoccipital**: **(0) absent (1) present**

112) [112] **Ventral cranial fissure connects with vestibular fontanelles**: **(0) absent (1) present**

113) [113] **Bar across spiracular groove**: **(0) absent (1) present**

114) [114] **Hypophysial opening in braincase**: **(0) absent (1) present**

Score changed from 0 to ? for *Macropetalichthys* as the morphology of the hypophysial region was not properly recovered by Stensiö (1969).

115) **NEW: Hypophysial organ projection**: **(0) anterior (1) anteroventral (2) posteroventral**

An anteriorly projected hypophysial duct is reported for galeaspid *Shuyu* (Gai et al., 2011) and evident in *Shearsbyaspis*. The hypophysial duct is anteroventrally projected in *Romundina* (Dupret et al., 2014, 2017a), *Brindabellaspis* (Young, 1980), *Kolymaspis*, *Dicksonosteus* (Goujet, 1984a), *Jagorina* (Stensiö, 1969) and some osteichthyans (e.g. Holland 2014; Giles and Friedman 2014), while is posteroventral in some chondrichthyans (e.g. Maisey 2005, 2007). Osteostracans are scored as inapplicable as they do not possess an hypophysial duct as the hypophysis opens dorsally within the nasal opening. States have been ordered.

116) [115] **Pineal opening in braincase**: **(0) absent (1) present**

117) [159] **Pineal opening perforation in dermal skull roof**: **(0) present (1) absent**

Score changed from 0 to 1 for *Quasipetalichthys* (Liu, 1973), *Eurycaraspis* (Liu, 1991) and *Cowralepis* (Ritchie, 2005).

118) [116] **Ventral rounded processes on preotic part of braincase**: **(0) absent (1) present**

119) [117] **Periotic process**: **(0) absent (1) present**

120) [118] **Dorsal otic ridge forming horizontal crest**: **(0) absent (1) present**

121) [119] **Perilymphatic fenestrae**: **(0) absent (1) present**

122) [120] **Notochord short, ending at the occipital cotylus**: **(0) absent (1) present**

123) [124] **Accessory processes extend from ventral surface of nasal capsule**: **(0) absent (1) present**

124) [125] **Internal carotid meets efferent pseudobranchial in orbit**: **(0) absent (1) present**

125) [126] **Jugular vein passes through cranioquadrate passage**: **(0) absent (1) present**

126) [127] **Anterior margin of ventral fissure**: **(0) straight (1) sinusoidal**

127) [128] **Bulbous otic and auxiliary condyles for palatoquadrate articulation**: **(0) absent (1) present**

128) [129] **Basal fenestra opening into floor of orbit**: **(0) absent (1) present**

129) [130] **Nasal sacs**: **(0) unpaired (1) paired**

130) [131] **Median dermal bone of palate (parasphenoid)**: **(0) absent (1) present**

Score changed from 0 to ? for *Macropetalichthys*. Presence of parasphenoid in *Romundina* (Dupret et al., 2017a) is unconvincing and thus score has been changed from 1 to ?. The braincase morphology and "texture" of the hypophysial area are similar between *Romundina* and *Kolymaspis*, where a dermal parasphenoid is not presence. Here this feauture scored ? but potentially 0 for the fact that the parasphenoid is a dermal bone and not just a more ossified area around the hypophysial opening (discussion in chapter 2).

131) [132] **Ascending process of parasphenoid**: **(0) absent (1) present**

Given the neurocranial morphology of the placoderm palate seems to be reasonable to code this character as inapplicabile, as there would not be space for accommodate the ascending process of the parasphenoid. Score change to inapplicable for those taxa which absence or presence of a parasphenoid can be scored.

132) [133] **Shape of parasphenoid denticulated field**: **(0) broad rhomboid or lozenge-shaped (1) broad, splint-shaped (2) slender, splint-shaped**

133) [134] **Parasphenoid denticulated field with multifid anterior margin**: **(0) absent (1) present**

134) [135] **Parasphenoid**: **(0) protruding forward into ethmoid region of endocranium (1) behind ethmoid region**

Score changed from 1 to ? for *Romundina* as the presence of a parasphenoid in this taxon is doubful.

135) [136] **Denticulated field of parasphenoid**: **(0) without spiracular groove (1) with spiracular groove**

136) [137] **Parasphenoid denticle field**: **(0) terminates at or anterior to level of foramina for internal carotid arteries (1) extends posterior to foramina for internal carotid arteries**

137) [138] **4 carotid foramina in parasphenoid**: **(0) absent (1) present**

138) [139] **Parotic dental plates**: **(0) absent (1) present**

Hyoid arch and gill skeleton

139) [140] **Basihyal**: **(0) present (1) absent, hyoid arch articulates directly with basibranchial**

140) [141] **Interhyal**: **(0) absent (1) present**

141) [142] **Foramen in hyomandibular**: **(0) absent (1) present**

142) [143] **Gill arches**: **(0) largely restricted to region under braincase (1) extend far posterior to braincase**

Score changed for from ? to 0 for *Chondrenchelys* (Finarelli and Coates, 2014)

143) [144] **Hypohyal**: **(0) absent (1) present**

144) [145] **Endoskeletal urohyal**: **(0) absent (1) present**

145) [146] **Disposition of the interbranchial ridges of the oralobranchial chamber roof**: **(0) oligobranchiate (1) orthobranchiate (2) nectaspidoform**

146) [147] **Number of branchial fossae**: **(0) 5-7 (1) 9-17 (2) more than 20**

147) [148] **Basibranchial elements**: **(0) unpaired (1) paired**

148) [149] **Sublingual rod**: **(0) absent (1) present**

149) [150] **Dense array of hyoid arch rays covers gill area**: **(0) absent (1) present**

Dermal skull bone

150) [151] **Dermal skull roof**: **(0) includes large dermal plates (1) consists of undifferentiated plates or tesserae (2.) include both large dermal plates and tesserae**

I created state 2 to represent the condition in rhenanids and certain "acanthothoracids", where the skull roof is composed by both tesserae and dermal plates (Gross 1950, 1958; Goujet 1984b; Vaškaninová and Ahlberg 2017).

151) [152] **Tesserae morphology**: **(0) large interlocking polygonal plates (1) microsquamose, not larger than body tesserae**

152) [153] **Extent of dermatocranial cover**: **(0) complete (1) incomplete (scale-free and elsewhere)**

153) [154] **Endolymphatic ducts open in dermal skull roof**: **(0) present (1) absent**

Unknown for *Shearsbyaspis*, although from the visceral side in CPC24622 it seems that an endolymphatic duct foramen could have been present. Score changed from ? to 1. for *Cowralepis* (Ritchie, 2005). Changed from 1 to 0 for *Eurycaraspis* (Pan et al., 2015).

154) [155] **Endolymphatic ducts with oblique course through dermal skull bones**: **(0) absent (1) present**

155) [156] **Series of paired median skull roofing bones that meet at the dorsal midline of the skull (rectilinear skull roof pattern)** : **(0) absent (1) present**

Score changed from 0 to - for *Cowralepis* and *Gavinaspis* as they possess a median unpaired plate instead of paired but separate plates as considered in state 0

156) [157] **Consolidated cheek plates**: **(0) absent (1) present**

157) [159] **Enlarged postorbital tessera separate from orbital series**: **(0) absent (1) present**

158) [160] **Bony hyoidean gill-cover series (branchiostegals)**: **(0) absent (1) present**

159) [161] **Branchiostegal plate series along ventral margin of lower jaw**: **(0) absent (1) present**

160) [162] **Branchiostegal ossifications**: **(0) plate-like (1) narrow and ribbon-like**

Score changed from ? to 1 for *Porolepis* (Lu et al., 2016)

161) [163] **Branchiostegal ossifications**: **(0) ornamented (1) unornamented**

162) [164] **Imbricated branchiostegal ossifications**: **(0) absent (1) present**

163) [165] **Opercular cover of branchial chamber**: **(0) complete or partial (1) separate gill covers and gill slits**

164) [166] **Shape of opercular (submarginal) ossification**: **(0) broad plate that tapers towards its proximal end (1) narrow, rod-shaped**

165) [167] **Gular plates**: **(0) absent (1) present**

166) [168] **Size of lateral gular plates**: **(0) extending most of length of the lower jaw (1) restricted to the anterior third of the jaw (no longer than the width of three or four branchiostegals)**

167) [169] **Median gular**: **(0) present (1) absent**

168) [170] **Dermal intracranial joint**: **(0) absent (1) present**

169) [171] **Posterior nostril**: **(0) associated with orbit (1) not associated with orbit**

In King et al. (2016) this character has been coded for some placoderm probably based on the position of the nasal opening. Posterior nostril (excurrent) and anterior (incurrent) nostril are known for crown-gnathostomes but never reported in placoderms, so that we do not know if those opening are posterior nostril or single nostrils. In fact, the score of this character in placoderm is equal to that of character 90 (ch. 96 in King et al. 2016), which take in account the position of the nasal capsules in relationship with the orbit. Nevertheless, this character is not necessarily related to the position of the nasal capsule in relation to the orbit and here the score for placoderms has been changed to ?.

170) [172] **Number of marginal bones alongside paired median skull roofing bones over the otico-occipital division of braincase**: **(0) single (1) two or more**

171) [173] **Type of dermal neck-joint**: **(0) sliding, dermal shoulder girdle plate articulate with cephalic flat flange (1) ginglymoid, dermal shoulder girdle condyle articulates with cephalic fossa (2) reversed ginglymoid, dermal shoulder girdle plate articulates with cephalic transverse condyle (3.) spoon-like, with transverse articular area**

The different type of placoderm neck-joints (discussion in chapter 3) were not thoroughly taken in account in King et al. (2016), where the only distinction was between ginglymoid and overlap (sliding) joint, with taxa like *Macropetalichthys* scored as having the same state as arthrodires. Other author (Dupret

et al., 2014; Zhu et al., 2016) instead divided this characters taken in account also the difference between the spoon-like articulation of petalichthyids and the "reversed ginglymoid" articulation for antiarchs. Here, I used the latter approach, creating a multi-state character with the same definition of Zhu et al. (2016). Character 174 of King et al. (2016), concerning the distinction between the "conventional" and "reversed" ginglymoid condition has been deleted as these are now integrated in the new character states. All taxa has been checked and scored consequently.

172) [175] **Posterior expansion of maxilla (maxilla cleaver-shaped)**: **(0) present (1) absent**

173) [176] **Contribution by maxilla to posterior margin of cheek**: **(0) present (1) absent**

174) [177] **Large unpaired median skull roofing bone anterior to the level of nasal capsules - premedian plate**: **(0) absent (1) present**

Discussion on the diagnosis, presence and absence of a premedian plate in chapter 4.

175) [178] **Number of nasals**: **(0) many (1) one or two**

176) [179] **Mesial margin of nasal**: **(0) not notched (1) notched**

177) [180] **Dermintermedial process**: **(0) absent (1) present**

178) [181] **Position of posterior nostril**: **(0) external, far from jaw margin (1) external, close to jaw margin**

179) [182] **Supraorbital (sensu Cloutier and Ahlberg 1996, including posterior tectal of Jarvik)**: **(0) absent (1) present**

180) [183] **Supraorbital, preorbital and nasal**: **(0) unfused (1) fused**

181) [184] **Tectal (sensu Cloutier and Ahlberg 1996, not counting the posterior tectal of Jarvik)**: **(0) absent (1) present**

182) [185] **Lateral plate**: **(0) absent (1) present**

183) [186] **Location of pineal foramen/eminence**: **(0) level with posterior margin of orbits (1) well posterior of orbits**

184) [187] **Parietals (preorbitals of placoderms) surround pineal foramen or eminence**: **(0) yes (1) no**

Score changed from 0 to 1 for *Gavinaspis* (Dupret and Zhu, 2007) and from 0 to ? for rhenanids as they don't have consolidate preorbital plates.

185) **Canal-bearing bone of skull roof extends far past posterior margin of parietals**: **(0) no (1) yes**

From Lu et al. (2016), character 238. The presence of a posteriorly expanded supraorbital has been revealed by Lu et al. (2016) to be one of the key character uniting actinopterygians.

186) [188] **Complete enclosure of spiracle by skull roof bones**: **(0) absent (1) present**

187) [189] **Paranuchal number**: **(0) one pair (1) two pairs (2) three pairs**

A new state (2) has been create to represent the condition in some "acanthothoracids", for example *Romundina*, *Arabosteus* (Olive et al., 2011) and *Sudaspis* (Vaškaninová and Ahlberg, 2017), which show the presence of an anterior, median and posterio paranuchal plates.

188) **NEW Posterior projection on posterior paranuchal plate**: **(0) absent (1) present**

Posterior projections are present on the posterior paranuchal plates on certain 'acanthothoracids' (*Romundina* (Ørvig, 1975), *Arabosteus*, *Kimaspis*, *Kosoraspis* and *Tlamaspis*.

189) **NEW Unpaired median skull roofing bone in contact with unpaired plate bearing pineal eminence or foramen**: **(0) absent (1) present**

This character is a new formulation of Dupret et al. (2009) character 34. It is about the condition presents in many placoderms where a median impaired bone (nuchal plate) is in contact with the unpaired bone bearing the pineal foramen or eminence. This is opposed to some other placoderms and osteichthyans where the median impaired bone (extrascapular in osteichthyans) is not in contact with the pineal plate so that the preorbitals (parietals in sarcopterygian, frontal in actinopterygian) are in contact.

190) [191] **Number of extrascapulars**: **(0) uneven (1) paired**

191) [192] **Dermal neck-joint between paired main-lateral-line-bearing bones of skull and shoulder girdle**: **(0) absent (1) present**

192) [193] **Foramina (similar to infradentary foramina) on cheek bones**: **(0) absent (1) present**

193) [194] **Lacrimal posteriorly enclosing posterior nostril**: **(0) absent (1) present**

194) [195] **Most posterior major bone of cheek bearing preopercular canal (preopercular) extending forward, close to orbit**: **(0) absent (1) present**

195) [196] **Number of cheek bones bearing preopercular canal posterior to jugal**: **(0) one (1) two**

196) [197] **Bone bearing both quadratojugal pit-line and preopercular canal**: **(0) absent (1) present**

197) [198] **Dermohyal**: **(0) absent (1) present**

198) [199] **Premaxillae with inturned symphysial processes**: **(0) absent (1) present**

199) [200] **Premaxilla forming part of orbit**: **(0) absent (1) present**

200) [201] **Ventral margin of maxilla**: **(0) straight (1) curved**

201) [202] **Large dermal plates forming outer dental arcade**: **(0) only with denticles (1) with large monolinear tooth row**

202) [203] **Presupracleithrum**: **(0) absent (1) present**

203) [204] **Number of sclerotic plates**: **(0) four or less (1) more than four**

204) [205] **Dermal ornamentation**: **(0) smooth (1) ridges (2) tuberculate**

In *Shearsbyaspis* the ornamentation consists of low ridges with irregularly developed tubercles. As the main ornamentation consists of ridges, it has been scored as 1. Score changed from 1 to 2 for *Glyptolepis*, from 2 to inapplicable for *Onychoselache*, from 2 to 0 for *Psarolepis* according to (Lu et al., 2016)

205) [206] **Cranial spines**: **(0) absent (1) present, multicuspid (2) present, monocuspid**

As explained by Giles et al. 2015b, this character is composed as a compound because there are no further dependent characters and thus equivalent to atomize it and use inapplicability.

206) [207] **Endolymphatic duct relationship to median skull roof bone (i.e. nuchal plate)**: **(0) within median bone (1) on bones flanking the median bone (e.g. paranuchals)**

Score change from - to 1 for *Eurycaraspis* (Pan et al., 2015).

207) [208] **Dermal plate associated with pineal eminence or foramen**: **(0) contributes to orbital margin (1) plate bordered laterally by skull roofing bones**

208) [200] **Broad supraorbital vaults**: **(0) absent (1) present**

209) [210] **Suture between paired skull roofing bones (centrals of placoderms; postparietals of osteichthyans)**: **(0) straight (1) sinusoidal**

Score changed from 0 to - for *Wuttagoonaspis* as it has either a centronucal plate or the centrals are not in contact (Dupret, 2008).

210) [211] **Medial processes of paranuchal wrapping posterolateral corners of nuchal plate**: **(0) absent (1) present**

Originally (Giles et al., 2015b) this character presented 4 states, considering absence and presence of this process, as well as the condition where the paranuchal plate was separated from the nuchal by central plates (as in ptyctodonts) and the situation where a nuchal plate is absent (as in osteichthyans). King et al. (2016) removed the last character states as they followed Zhu et al. (2013) convention that homologize the median extrascapular in osteichthyans with the nuchal plate in placoderm.

Here, I removed the state related to the contact between paranuchal and nuchal (state 2 in Giles et al. 2015b; King et al. 2016). This character is about the presence or absence of the process, not the relationships between different plates. Ptyctodonts have then been scored as inapplicable. Presence (1) is scored for *Quasipetalichthys*, *Eurycaraspis* and *Pauropetalichthyids* among petalichthyids (Liu, 1973, 1991; Pan et al., 2015). In these taxa, the process is not as developed as in brachitoracid arthrodires but still a little projection is present on the internal side of the paranuchal plates.

Score changed from - to 0 for *Romundina* and *Diandongpetalichthys*.

211) [212] **Paired pits on ventral surface of nuchal plate**: **(0) absent (1) present**

212) [213] **Sclerotic ring**: **(0) absent (1) present**

213) [214] **Cheek plate**: **(0) undivided (1) divided (i.e., squamosal and preopercular)**

214) [215] **Subsquamosals in taxa with divided cheek**: **(0) absent (1) present**

215) [216] **Preopercular shape**: **(0) rhombic (1) bar-shaped**

216) [217] **Premaxilla**: **(0) extends under orbit (1) restricted anterior to orbit**

217) [218] **Median rostral extension of the headshield**: **(0) absent (1) present**

218) [219] **Lateral fields**: **(0) absent (1) present**

219) [220] **Division of lateral fields**: **(0) absent(1) divided once (2) divided twice**

220) [221] **Lateral fields extend posterior to pectoral sinus**: **(0) absent (1) present**

221) [222] **Lateral fields extend onto cornua**: **(0) absent (1) present**

222) [223] **Median fields**: **(0) absent (1) present**

223) [224] **Median field separation from pineal plate or foramen**: **(0) absent (1) present**

224) [225] **External endolymphatic duct openings' location in relation to median field**: **(0) internal (1) external**

225) [226] **Median dorsal opening**: **(0) absent (1) present**

226) [227] **External nasal opening**: **(0) single median (1) paired**

227) [228] **Nasohypophyseal opening shape**: **(0) unconstricted (1) constriction between nasal and hypophysial divisions (2) split into nasal and hypophysial divisions**

228) [229] **Cornual extensions**: **(0) absent (1) present**

King et al. (2016) homologized the posterolateral extensions of the headshield present in osteostracans and in galeaspids. However, in osteostracans these extensions are related with the presence of pectoral sinus for the attachment of the pectoral fins (see Sansom, 2008). The posterolateral extensions of the headshield in galeaspids are instead non associated with paired pectoral fins and thus probably not homologous (see Zhu and Gai, 2006). For this reason, here

I split the character and coding as presented in King et al. (2016), introducing a separated character for the posterolateral extension of Galeaspida (from Zhu and Gai 2006 character 14).

229) **Corners**:**(0) absent (1) present**

From Zhu and Gai (2006), character 14.

230) [230] **Fused scale rows on posterior of headshield**: **(0) absent (1) present**

231) [231] **Dorsal spinal process of headshield**: **(0) absent (1) present**

232) [232] **Oralobranchial covering**: **(0) minute scales (1) tesserae (2) dermal plates (3) one or two massive dermal plates**

233) [234] **Spines on corners**: **(0) absent (1) present**

234) [233] **Shape of median dorsal opening**: **(0) transverse slit-like (1) oval-like (2) slender longitudinal oval**

235) [235] **Headshield enclosed posteriorly behind oralobranchial chamber**: **(0) no (1) yes**

236) [236] **Enlarged tubercles form symmetrical pattern on posterior part of headshield**: **(0) absent (1) present**

237) [237] **T-shaped rostral plate**: **(0) absent (1) present**

238) [238] **Single median element carrying the central, middle and posterior pit line**: **(0) absent (1) present**

This character was originally from Dupret et al. (2009) (ch. 17) and related to the fact that, while in most of placoderm there are two central plates flanking a median nuchal plate, in *Wuttagoonaspis*, *Gavinaspis* and phyllolepids there is a single median element, named centronuchal plate, supposed to be constituted by the fusion of central plates and the nuchal plate. King et al. (2016) changed

the name of the character as related the presence of absence of a centronuchal plates. However, we think that the name of this element should not assume fusion (or reduction) of different plates, as this is a speculative pattern. Instead, sensory lines can be used as reference point to separate dermal plates in discrete elements. Here, we reformulate the character to assess the presence of a single median element carrying the central, middle and posterior pit sensory line.

239) [239] **Postnuchal plates**: **(0) absent (1) present**

240) [240] **Cutaneous sensory organ on suborbital plate**: **(0) absent (1) present**

241) [241] **Cutaneous sensory organ on postsuborbital plate**: **(0) absent (1) present**

242) [242] **Cutaneous sensory organ on skull roof posterior to orbits**: **(0) absent (1) present**

243) [244] **Sclerotic ring incorporated into skull roof**: **(0) absent (1) present**

244) [245] **Rostrocaudal groove on the inner surface of the premedian plate**: **(0) absent (1) present**

245) [246] **Preorbital depression**: **(0) absent (1) present**

246) [247] **Preorbital recess**: **(0) absent (1) present**

247) [248] **Preorbital recess**: **(0) restricted to premedian plate (1) extends onto lateral plates**

248) [249] **Nuchal plate**: **(0) without orbital facets (1) with orbital facets**

249) [250] **Submarginal articulation**: **(0) absent (1) present**

250) [251] **Prelateral plate**: **(0) absent (1) present**

251) [252] **Posterior descending lamina of skull roof**: **(0) absent (1) present**

252) [254] **Mesial lamina on the internal surface of marginal plate**: **(0) absent (1) present**

Character has been reformulated to specify that the lamina is present on the internal surface of the plate. See Long (1997) (text-fig. 4 mes.lam).

253) [255] **Nostrils enclosed in dermal skull roof**: **(0) yes (1) no**

Scored as 0 for taxa that possess nostril inside orbital margin.

254) [257] **Lacrimal**: **(0) absent (1) present**

255) [258] **Pineal and rostral** : **(0) contact (1) separated**

Reformulated from Dupret et al. (2009) (ch. 7). This character highlights the difference between possessing pineal and rostral plates in contact or without contact. This is less arbitrary than infer the fusion between the pineal and the rostral, as in the original formulation of the character, as this can depend on the ontogeny of the specimen.

256) [259] **Snout region fragmented into mosaic of small plates**: **(0) no(1) yes**

257) [260] **Choana**: **(0) absent (1) present**

258) [261] **B-bone**: **(0) absent (1) present**

259) [262] **Number of supraorbitals**: **(0) one (1) two (2) many**

Ordered character

260) [263] **Series of bones lateral to supratemporal (postmarginal plate in placoderms)**: **(0) absent (1) single bone (2) two bones**

State 2 is an autapomorphy of *Guyu*. It is composed as a compound because it is not related to any other character and thus mathematically equivalent as atomizing it and add inapplicability.

261) [267] **Pore clusters**: **(0) absent (1) present**

262) [268] **Westoll lines**: **(0) absent (1) present**

263) [269] **Prerostral plate**: **(0) absent (1) present**

264) [270] **Relative size of cosmine pores**: **(0)small (1) large**

265) [271] **Interparietal**: **(0) absent (1) present**

266) [272] **Premaxilla contributes to posterior nostril**: **(0) absent (1) present**

267) [273] **Supratemporal (marginal) in contact with postparietal (central)**: **(0) absent (1) present**

In King et al. (2016) some taxa were coded as 2 but no character state description was associated with that state. Here, state 2 has been deleted and taxa have been recoded. Antiarchs do not have marginal and central plates so they should be coded as inapplicable. Score has been changed from 0 to 1 for *Wuttagoonaspis*, as the two plates are clearly in contact (Dupret, 2008).

268) [274] **Supratemporal (marginal) contact with nasal (postnasal)**: **(0) absent (1) present**

If the supratemporal of osteichthyes is the marginal plate in placoderms and the nasal is the placoderm postnasal, as intended by King et al. (2016), then most of the placoderm can be scored from unknown to 0. Score changed consequently.

269) [275] **Notch in anterior margin of jugal**: **(0) absent (1) present**

270) [276] **Quadratojugal**: **(0) present (1) absent**

271) [277] **Number of paired extrascapulars**: **(0) one pair (1) two pairs**

This character takes in account the fact that some taxa (i.e. *Moythomasia* Gardiner 1984b) possess a paired median extrascapular and a paired lateral extrascapular. (King et al., 2016) considered *Romundina* as having two paired of

extrascapular because of the presence of a medial paranuchal plate, following Zhu et al. (2013) scheme of the posterior paranuchal being homologous with the extrascapular. The same condition is present in *Arabosteus* (Olive et al., 2011). However, I think that the condition in *Romundina* and *Arabosteus* is different from that of *Moythomasia*, as the nuchal plate is still a single unit and so there are not two paired (because of the meaning of paired) extrascapulars. For this reason, score for *Romundina* has been changed from 1 to 0. Same criterion has been applied to rhenanids, now scored 0.

272) [278] **Accessory operculum**: **(0) absent (1) present**

273) [279] **Dermal bone (sarcopterygian postorbital) between jugal (suborbital) and intertemporal (postorbital)**: **(0) absent (1) present**

274) [280] **Lacrimal notch**: **(0) absent (1) present**

275) [282] **Orbital process of maxilla**: **(0) absent (1) present**

Sensory Lines

276) [283] **Sensory line network**: **(0) preserved as open grooves (1) pass through canals enclosed within dermal bones**

277) [284] **Jugal portion of infraorbital canal joins supramaxillary canal**: **(0) present (1) absent**

This feature is also evident in rhenanids, which are similar to *Romundina* in the disposition of the infraobital and supramaxillary sensory line (e.g. Young 1986, text-fig. 11). Score has thus been changed from ? to 0 for *Jagorina* and *Gemuendina*.

278) [286] **Course of ethmoid commissure**: **(0) middle portion through median rostral (1) sutural course (2) through bone center of premaxillary**

279) [287] **Position of anterior pit-line**: **(0) on paired median skull roofing bones over the otico-occipital division of braincase (1) on paired median skull roofing bones over the sphenoid division of braincase**

280) [288] **Middle and posterior pit-lines on postparietal (centrals)**: **(0) posteriorly situated (1) mesially situated**

281) [289] **Position of middle and posterior pit lines**: **(0) close to midline (1) near the central portion of each postparietal (centrals)**

Score changed to ? to 1 for *Eurycaraspis* (Liu, 1991).

282) [290] **Course of supraorbital canal**: **(0) between anterior and posterior nostrils (1) anterior to both nostrils**

283) [291] **Course of supraorbital canal**: **(0) straight (1) lyre-shaped**

Score changed to inapplicable for those antiarchs that lack a supraorbital sensory canal.

284) [293] **Contact between otic (main lateral line) and supraorbital canals**: **(0) not in contact (1) in contact**

Many taxa were scored with unknown although the sensory line pattern is pretty clear. Score changed from ? to 0 for *Diandongpetalichthys*, *Quasipetalichthys*, *Lunaspis*, *Holonema*, *Incisoscutum*, *Compagnopiscis*, *Eastmanosteus*, *Austroptyctodus*, *Rhamphodopsis*, *Campbellodus*.

285) [294] **Contact of supraorbital and infraorbital canals**: **(0) not in contact rostrally (1) in contact rostrally**

Character state names were inverted, now have been corrected.

286) [295] **Otic canal**: **(0) pass through skull roof (1) follows edge of skull roof**

287) [296] **Infraorbital canal follows premaxillary suture**: **(0) no (1) yes**

288) [297] **Sensory canal or pit-line on maxilla**: **(0) absent (1) present**

289) [298] **Course of mandibular canal**: **(0) not passing through most posterior infradentary (1) passing through most posterior infradentary**

290) [299] **Course of mandibular canal**: **(0) passing through dentary (1) not passing through dentary**

291) [300] **Supraorbital canals and posterior pitlines convergence**: **(0) absent (1) converge without contact (2) converge with contact**

This character was originally proposed by Long et al. (2015) (ch. 258) and referred to the pattern of the sensory line on the nuchal plate of placoderms, where the supraorbital canals and posterior pit lines either not converge towards each others, converge without contact or converge with contact. The character was modified by King et al. (2016) in "Supraorbital canals and posterior pitlines cross as an X" to avoid referring to a specific plate. Also, they included another character related to the posterior extension of the supraorbital canal (ch. 292 in King et al. 2016). However, here I eliminated that character because of the ambiguity in it formulation (see below) and thus restored the original character from Long et al. (2015), with the original states.

292) [301] **Sensory canals/grooves**: **(0) contained within the thickness of dermal bones (1) contained in prominent ridges on visceral surface of bone**

Score changed from 0 to 1 for *Diandongpetalichthys* (Zhu, 1991) and *Eurycaraspis* (Liu, 1991).

293) [302] **Anterior pit line of dermal skull roof**: **(0) absent (1) present**

Score changed from 0 to 1 for *Cheirolepis* (Pearson and Westoll, 1979; Arratia and Cloutier, 1996).

294) [303] **Otic canal extends through postparietals (centrals)**: **(0) absent (1) present**

This character refers to the course of the otic branch of the infraorbital sensory line canal on the postparietals (centrals in placoderms). Thus, can be coded for placoderms that show the position of the centrals and the otic infraorbital canals. Rescored consequently.

295) [304] **Infra-orbital sensory line**: **(0) Crosses lateral field (1) does not cross lateral field**

296) [305] **Festooned pattern of sensory canals**: **(0) absent (1) present**

297) **Median transverse canals**: **(0) two or more (1) one**

Character 30 of Zhu and Gai (2006), uniting eugaleaspidiform and polybranchi-aspidid galeaspids

298) [306] **Multiply branched sensory canal system associated with the posterior end of the supraorbital canal**: **(0) absent (1) present**

299) [307] **Supraorbital sensory canals**: **(0) absent (1) present**

Score changed from 0 to 1 for *Romundina* (Dupret et al., 2017a; Ørvig, 1975) and for *Rhamphodopsis* (Miles, 1967). *Entelognathus* do not show any supraorbital sensory canal so score changed from 1 and 0. Changed from ? to 1 for *Jagorina* (Stensiö, 1969).

300) [308] **Branching end of lateral transverse canals**: **(0) absent (1) present**

301) [310] **Median dorsal canal**: **(0) absent (1) present**

302) [311] **Infraorbital and otic sensory line grooves run along mesial margin of marginal plate**: **(0) no (1) yes**

Score changed from ? to 0 for *Diandongpetalichthys* (Zhu, 1991).

303) [312] **Central sensory line**: **(0) absent (1) present**

304) [313] **Semicircular pit line**: **(0) absent (1) present**

The semicircular pit line is a sensory line branch of the infraorbital sensory line presents on the lateral plate of some antiarchs. Its absence can be scored for taxa that lack a lateral plate and here coding has been applied consequently.

305) [314] **Horizontal sensory line canal on cheek**: **(0) absent (1) present**

306) [315] **Postmarginal canal**: **(0) absent (1) present**

307) [316] **Preopercular canal**: **(0) absent (1) present**

308) [317] **Preopercular canal meets otic canal**: **(0) absent (1) present**

309) [318] **Supraoral canal**: **(0) absent (1) present**

The supraoral canal passes on the postmarginale plate. This plate is known in *Lunaspis* but does not show any sensory line canal. For this reason, score has been changed from ? to 0 for this taxon (Gross, 1961)

310) [319] **Extension of otic canal beyond infraorbital canal ("P" canal)**: **(0) absent (1) present**

311) **NEW Ethmoid commissure**: **(0) absent (1) present**

The ethmoid commissure is usually considered an osteichthyan character (Zhu et al., 2001; Zhu and Yu, 2002b; Friedman, 2007). Nevertheless, an ethmoidal portion of the infraorbital sensory line identified as the ethmoid commissure is present in some antiarchs (Stensiö, 1969; Zhang, 1980b; Zhu, 1996), rhenanids (Gross, 1963; Stensiö, 1969) and some "acanthothoracids" (e.g. *Romundina* Ørvig 1975; Dupret et al. 2010. However, this is usually dismissed and placoderms are scored as lacking an ethmoid commissure (e.g. Friedman 2007, where *Bothriolepis* is scored as lacking an ethmoid commissure). Here, I considered this condition to be present in those placoderm and a character concerning the presence or absence of an ethmoid commissure (originally from Zhu et al. 2001)

is created. Same score is applied for both placoderms and osteichthyans that show an ethmoidal portion of the infraorbital canal.

312) **[320] Ethmoid commissure fused into midline canal**: **(0) absent (1) present**

Coding has been changed based on the character above. Taxa that do not possess an ethmoid commissure are now scored inapplicable.

313) **[321] Posterior pitline and postmarginal canal**: **(0) absent (1) present**

314) **[322] Supraorbital canal joins infraorbital canal**: **(0) anterior to supraoral canal (1) posterior to supraoral canal**

315) [323] **Sensory line commissure across extrascapular bones (nuchal and paranuchal)**: **(0) absent (1) present**

316) [324] **Sensory line canal**: **(0) passes between or beneath scales (1) passes over scales and/or is partially enclosed or surrounded by scales (2) perforates and passes through scales**

317) [325] **Dorsal branch of main lateral line canal on Posterior Dorsolateral plate**: **(0) absent (1) present**

318) [326] **Sharp downward bend in Posterior Dorsolateral plate sensory line**: **(0) absent (1) present**

Dentition and Jaws

319) [327] **Oral dermal tubercles borne on jaw cartilages**: **(0) absent (1) present**

320) [328] **Tooth whorls**: **(0) absent (1) present**

321) [329] **Bases of tooth whorls**: **(0) single, continuous plate (1) some or all whorls consist of separate tooth units**

322) [330] **Enlarged adsymphysial tooth whorl**: **(0) absent (1) present**

323) [331] **Teeth ankylosed to dermal bones**: **(0) absent (1) present**

324) [332] **Dermal jaw plates on biting surface of jaw cartilages**: **(0) absent (1) present**

325) [333] **Maxillary and dentary tooth-bearing bones**: **(0) absent (1) present**

326) [334] **Large otic process of the palatoquadrate**: **(0) absent (1) present**

327) [335] **Insertion area for jaw adductor muscles on palatoquadrate**: **(0) ventral (1) lateral**

328) [336] **Oblique ridge or groove along medial face of palatoquadrate**: **(0) absent (1) present**

329) [337] **Fenestration of palatoquadrate at basipterygoid articulation**: **(0) absent (1) present**

330) [338] **Perforate or fenestrate anterodorsal (metapterygoid) portion of palatoquadrate**: **(0) absent (1) present**

331) [339] **Pronounced dorsal process on Meckelian bone or cartilage**: **(0) absent (1) present**

332) [340] **Preglenoid process**: **(0) absent (1) present**

333) [341] **Jaw articulation located on rearmost extremity of mandible**: **(0) absent (1) present**

334) [342] **Acrodin**: **(0) absent (1) present**

335) [343] **Plicidentine**: **(0) absent (1) present**

336) [344] **Number of coronoids**: **(0) more than three (0) three**

337) [345] **Fangs of coronoids (sensu stricto)**: **(0) absent (1) present**

338) [346] **Tooth-bearing median rostral**: **(0) absent (1) present**

339) [347] **Teeth of dentary**: **(0) reaching anterior end of dentary (1) not reaching anterior end**

340) [348] **Marginal denticle band on coronoids**: **(0) broad band, at least posteriorly (1) narrow band with 2-4 denticle rows**

341) [349] **Infradentary**: **(0) absent (1) present**

Score changed from 0 to ? for *Macropetalichthys* and *Eurycaraspis* as the morphology of the jaws is still unknown.

342) [350] **Infradentary foramina**: **(0) absent (1) present**

343) [351] **Large ventromesially directed flange of symphysial region of mandible**: **(0) absent (1) present**

344) [352] **Flange-like extension of mandible composed of prearticular and Meckelian ossification**: **(0) absent (1) present**

345) [353] **Strong ascending flexion of symphysial region of mandible**: **(0) absent (1) present**

346) [354] **Parasymphysial plate**: **(0) detachable tooth whorl (1) long with posterior corner, sutured to coronoid, denticulated or with tooth row (2) absent**

347) [355] **Anterior end of prearticular**: **(0) far from jaw symphysis (1) near jaw symphysis**

348) [356] **Prearticular - dentary contact**: **(0) present (1) absent**

349) [357] **Meckelian bone exposed immediately anterior to first coronoid**: **(0) yes (1) no**

350) [358] **Dermal plates on mesial (lingual) surfaces of Meckel's cartilage and palatoquadrate**: **(0) absent (1) present**

351) [359] **Biconcave glenoid on lower jaw**: **(0) absent (1) present**

352) [360] **Vomerine fangs**: **(0) absent (1) present**

353) [362] **Metapterygoid with developed medial ventral protrusion**: **(0) absent (1) present**

354) [364] **Deep, high supragnathal bone with durophagous occlusal surface**: **(0) absent (1) present**

355) [365] **Enamel(oid) on teeth**: **(0) absent (1) present**

356) [366] **Distribution of tooth whorls**: **(0) upper and lower jaws (1) lower jaws only (2) upper jaws only**

357) [367] **Pair of tooth plates (anterior supragnathals or vomers) on ethmoidal plate**: **(0) absent (1) present**

358) [368] **Extent of infradentaries**: **(0) along much of ventral margin of dentary (1) restricted to posterior half of dentary**

359) [370] **Autopalatine and quadrate**: **(0) comineralized (1) separate mineralizations**

360) [371] **Palatoquadrate fused with neurocranium**: **(0) absent (1) present**

361) [372] **Fused anterior supragnathals**: **(0) absent (1) present**

362) [373] **Posterior superognathal with vertical pipe-like ridges**: **(0) absent (1) present**

363) [374] **Strongly curved infragnathals with wide flat non-biting region**: **(0) absent (1) present**

364) [375] **Posterior process of vomers**: **(0) absent (1) present**

365) [376] **Number of fang pairs on ectopterygoid**: **(0) none (1) one (2) two**

Character states has been renamed, rescored and ordered.

366) [377] **Proportions of entopterygoid**: **(0) anterior end level with processus ascendens (1) anterior end considerably anterior to processus ascendens**

367) [378] **Number of dermopalatines**: **(0) one (1) two (2) more than 2**

368) [379] **Enlarged anterior tooth on premaxilla**: **(0) absent (1) present**

369) [380] **Number of tooth rows on outer dental arcade**: **(0) one (1) two**

370) [381] **Number of infradentaries**: **(0) one (1) two (2) more than 2**

371) [382] **Coronoids**: **(0) absent (1) present**

372) [383] **Number of fang pairs on posterior coronoid**: **(0) none (1) one (2) two**

373) [384] **Teeth radial rows on prearticular**: **(0) absent (1) present**

374) [385] **Labial pit**: **(0) absent (1) present**

375) [386] **Retroarticular process**: **(0) absent (1) present**

376) [388] **'Symplectic' articulation**: **(0) absent (1) present**

377) [389] **Processus ascendens of palatoquadrate**: **(0) absent (1) present**

378) [390] **Grooved, curved upper toothplates attached to median labial element**: **(0) absent (1) present**

379) [391] **Two divergent processes extending from anterior of palatoquadrate**: **(0) absent (1) present**

380) [392] **Extramandibular dentition**: **(0) absent (1) present**

381) [393] **Bilateral series of labial cartilages**: **(0) absent (1) present**

Paired fins and girdle

382) **Paired fins**: **(0) absent (1) present**

From Sansom (2009), character 63.

383) **Paired fins relation to cephalic shield**: **(0) continuous (1) delimited at pectoral sinus**

From Sansom (2009), character 65.

384) [394] **Pelvic fins**: **(0) absent (1) present**

385) [395] **Intromittent organ for internal fertilization ('claspers')**: **(0) absent (1) present**

Both chondrichthyans and some groups of placoderms show the presence of intromittent organ for fertilization (claspers). In chondrichthyans they are supported by cartilage and attached to the posterior extremity of the pelvic fin metaptyerygium. In placoderms it has been suggested that claspers were independent from the pelvic fins, and thus not homologous to that of chondrichthyans, as they do not show any articulation with the pelvic girdle and are positioned more posteriorly (Trinajstic et al., 1979). For this reason, Long et al. 2015 proposed the distinction of two separated characters to describe the differences between placoderm claspers and chondrichthyans claspers, instead of the single character used, for example, by Brazeau (2009) and Dupret et al. (2014). However, the hypothesis that the claspers in placoderms and chondrichthyans are non-homologous is assumed a priori. Moreover, this is controversial because, despite being placed more posteriorly than in chondrichthyans, biologically those intromittent organs must have be part of the reproductive apparatus and thus in the proximity of the pelvic girdle. For this reason, here

we dismiss the validity of the two separated characters for claspers and reintroduce a single character for the presence or absence of claspers (Brazeau 2009, ch. 119). Score changed from present to unknown for *Pterichthyodes* as there are not evidence for distinct male and female "genital plates" so is not possible to evaluate if those plates corresponds to claspers.

386) [396] **Dermal pelvic clasper**: **(0) absent (1) present**

The original definition of the character, "intromittent organ with one large J-shaped element" (Long et al., 2015), has been change in favour of the definition adopted by Brazeau (2009). The latter does not consider the shape of the bone, which is not necessarely homologous, but rather the fact that in ptyctodonts and the antiarch *Microbrachius* (Long et al. 2015) the pelvic claspers are part of the dermal coverage, thus different from the condition of arthrodires, where the claspers are only internally ossified, and of chondrichthyes, where they are cartilaginous.

387) [398] **Scapular process of shoulder endoskeleton**: **(0) absent (1) present**

388) [399] **Ventral margin of separate scapular ossification**: **(0) horizontal (1) deeply angled**

389) [400] **Cross sectional shape of scapular process**: **(0) flattened and strongly ovate (1) subcircular**

390) [401] **Flange on trailing edge of scapulocoracoid**: **(0) absent (1) present**

391) [402] **Scapular process with posterodorsal angle**: **(0) absent (1) present**

392) [403] **Endoskeletal postbranchial lamina on scapular process**: **(0) present (1) absent**

393) [404] **Mineralisation of internal surface of scapular blade**: **(0) mineralised all around (1) unmineralised on internal face forming a hemicylindrical cross-section**

394) [405] **Coracoid process**: **(0) absent (1) present**

395) [406] **Procoracoid mineralisation**: **(0) absent (1) present**

396) [407] **Fin base articulation on scapulocoracoid**: **(0) stenobasal (1) eurybasal**

397) [408] **Perforate propterygium**: **(0) absent (1) present**

398) [409] **Endoskeletal supports in pectoral fin**: **(0) multiple elements articulating with girdle (1) single element ("humerus") articulating with girdle**

399) [410] **Triradiate scapulocoracoid**: **(0) absent (1) present**

400) [411] **Subscapular foramen**: **(0) absent (1) present**

401) [412] **Pectoral propterygium**: **(0) absent (1) present**

402) [413] **Scapular infundibulum**: **(0) absent (1) present**

403) [414] **Number of basals in polybasal pectoral fins**: **(0) three or more (1) two**

404) [415] **Number of mesomeres in metapterygial axis**: **(0) five or fewer (1) seven or more**

405) [416] **Biserial pectoral fin endoskeleton**: **(0) absent (1) present**

406) [417] **Filamentous extension of pectoral fin from axillary region**: **(0) absent (1) present**

407) [418] **Entepicondyle on humerus**: **(0) present (1) absent**

408) [419] **Horizontal plate of scapulocoracoid**: **(0) absent (1) present**

409) [420] **Distal articulation of propterygium**: **(0) with fin rays (1) with a second enlarged element ((2)) no articulation**

410) [421] **Macromeric dermal shoulder girdle**: **(0) present (1) absent**

411) [422] **Dermal shoulder girdle composition**: **(0) ventral and dorsal (scapular) components (1) ventral components only**

412) [423] **Dermal shoulder girdle forming a complete ring around the trunk**: **(0) absent (1) present**

413) [424] **Pectoral fenestra completely encircled by dermal shoulder armour**: **(0) present (1) absent**

414) [425] **Median dorsal plate**: **(0) absent (1) present**

415) [426] **Pronounced internal crista (keel) on median dorsal surface of shoulder girdle**: **(0) absent (1) present**

416) [427] **Pectoral fins covered in macromeric dermal armour**: **(0) absent (1) present**

417) [428] **Pectoral fin base has large, hemispherical dermal component**: **(0) absent (1) present**

418) [429] **Paired fin spines**: **(0) absent (1) present**

419) [430] **Anocleithrum**: **(0) element developed as postcleithrum (1) element developed as anocleithrum sensu stricto**

420) [431] **Dorsal cleithrum (AL of the Placodermi), ventral cleithrum (AVL of the Placodermi) and pectoral spine (SP of the Placodermi)**: **(0) not fused (1) fused**

421) [432] **Relationship of clavicle to cleithrum**: **(0) ascending process of clavicle overlapping cleithrum laterally (1) ascending process of clavicle wrapping round anterior edge of cleithrum, overlapping it both laterally and mesially**

422) [433] **Pelvic girdle with substantial dermal component**: **(0) yes (1) no**

423) [434] **Pelvic fin spine**: **(0) absent (1) present**

424) [435] **Shape of dorsal blade of dermal shoulder girdle**: **(0) spatulate (1) pointed**

425) [436] **Posterior dorsolateral (PDL) plate or equivalent**: **(0) absent (1) present**

426) [437] **PL and PDL overlap**: **(0) simple (1) insertion**

427) [438] **Left and right Posterior Dorsolateral plate plates contact below the Median Dorsal plate**: **(0) absent (1) present**

428) [439] **PDL plate visible externally**: **(0) absent (1) present**

429) [440] **Posteriorly produced spine on MD plate**: **(0) absent (1) present**

430) [441] **Joint in macromeric armoured pectoral fin**: **(0) absent (1) present**

431) [442] **Cd1 (first dorsal central) and Cd2 (second dorsal central) plates**: **(0) in contact (1) separated**

432) [443] **Clavicles/interolateral plates**: **(0) Large plates, comparable in size to cleithrum (1) paired small semilunar plates (2) unpaired semilunar plates**

433) [444] **Chang;s apparatus**: **(0) absent (1) present**

434) [445] **Number of median dorsal plates**: **(0) one (1) two (2) three**

435) [446] **Anocleithrum sensu stricto**: **(0) exposed (1) subdermal**

436) [447] **Median ventral trunk plates**: **(0) absent (1) present**

437) [448]**Extracleithrum**: **(0) absent (1) present**

438) [449] **Pectoral fin spine small (bivalve-like)**: **(0) absent (1) present**

Axial skeleton and median fins

439) [450] **Number of dorsal fins, if present**: **(0) one (1) two**

440) [451] **Horizontal caudal lobe**: **(0) absent (1) present**

441) [452] **Triphycercal tail**: **(0) absent (1) present**

442) [453] **Caudal radials**: **(0) extend beyond level of body wall and deep into hypochordal lobe (1) restricted to axial lobe**

443) [454] **Supraneurals in axial lobe of caudal fin**: **(0) absent (1) present**

444) [455] **Series of thoracic supraneurals**: **(0) absent (1) present**

445) [456] **Branching radial structure articulating with dorsal fin basal plate**: **(0) absent (1) present**

446) [457] **Dorsal fin spines**: **(0) absent (1) present**

447) [458] **Anal fin spine**: **(0) absent (1) present**

448) [459] **Median fin spine insertion**: **(0) shallow, not greatly deeper than dermal bones / scales (1) deep**

449) [460] **Intermediate fin spines**: **(0) absent (1) present**

450) [461] **Prepectoral fin spines**: **(0) absent (1) present**

451) [462] **Fin spines with ridges**: **(0) absent (1) present**

452) [463] **Fin spines with nodes**: **(0) absent (1) present**

453) [464] **Fin spines with rows of large retrorse denticles**: **(0) absent (1) present**

454) [465] **Synarcual**: **(0) absent (1) present**

455) [466] **Anal fin**: **(0) absent (1) present**

456) [467] **Fringing fulcra**: **(0) absent (1) present**

457) [468] **Longitudinal scale alignment in fin webs**: **(0) absent (1) present**

This character was scored as present for many placoderms in (King et al., 2016) However, this score for placoderms is debatable, as the complete morphology for placoderm fin is known only in rhenanids, which nonetheless do not show

such arrangement (Gross, 1963). Score for placoderms has been here modified as ?, which rhenanids scored as 0. Scoring was also full of problems for the crown-gnathostomes so here it has been checked and extensively rescored.

458) [469] **Differentiated lepidotrichia**: **(0) absent (1) present**

459) [470] **Epichordal lepidotrichia in caudal fin**: **(0) absent (1) present**

460) [471] **Scute-like ridge scales (basal fulcra)**: **(0) absent (1) present**

461) [472] **Fin spine cross-section**: **(0) round or horseshoe shaped (1) Flat-sided, with rectangular profile**

462) [473] **Intermediate spines when present**: **(0) one pair (1) multiple pairs**

463) [474] **Expanded spine rib on leading edge of spine**: **(0) absent (1) present**

464) [475] **Spine ridges**: **(0) converging at the distal apex of the spine (1) converging on leading edge of spine**

465) [476] **Posterior dorsal fin shape**: **(0) base approximately as broad as tall, not broader than all of other median fins (1) base much longer than the height of the fin, substantially longer than any of the other dorsal fins**

466) [477] **Basal plate in dorsal fin** : **(0) absent (1) present**

467) [478] **Basal plate in anal fin**: **(0) absent (1) present**

468) [479] **Spine-brush complex**: **(0) absent (1) present**

469) [480] **Series of median hexagonal scutes anterior to first dorsal fin**: **(0) absent (0) present**

470) [481] **Intermediate spines with finlets**: **(0) absent (1) present**

471) [482] **Median ventral prepectoral spine**: **(0) absent (1) present**

472) [483] **Prepectoral spines form "necklace": (0) absent (1) present**

473) [484] **Longitudinal rows of enlarged keeled scutes: 0. absent 1. present**

Scales

474) [485] **Body scale growth pattern: (0) monodontode (1) polyodontode**

475) [486] **Body scale growth concentric: (0) absent (1) present**

476) [487] **Body scales with peg-and-socket articulation: (0) absent (1) present**

477) [492] **Peg on rhomboid scale: (0) narrow (1) broad**

Changed from ? to 0 in *Styloichthys* (Lu et al., 2016)

478) [488] **Body scale profile: (0) distinct crown and base demarcated by a constriction (neck) (1) flattened**

479) [489] **Body scales with bulging base: (0) absent (1) present**

480) [490] **Body scales with flattened base: (0) present (1) absent**

481) [491] **Flank scales alignment: (0) vertical rows (1) oblique rows or hexagonal/rhombic packing (2) disorganised**

482) [493] **Anterodorsal process on scale: (0) absent (1) present**

483) [494] **Profile of scales with constriction between crown and base: (0) neck similar in width to crown (1) neck greatly constricted, resulting in anvil-like shape**

484) [495] **Basal pore in scales: (0) absent (1) present**

485) [496] **Scales: (0) macromeric (1) micromeric**

5.4 RESULTS

5.4.1 Parsimony analysis

The Parsimony ratchet search (300 heuristic search reiterations) resulted in 183 shortest trees of 1174 steps (CI= 0.440, RI= 0.825, RC= 0.363, HI=0.560). The strict consensus is poorly resolved within "acanthothoracids", petalichthyids and actinopterygians (Fig. 5.1). Majority rule is better resolved but with low bootstrap values for the aforementioned groups. The analysis executed in TNT resulted in 43750 MPTs with a length of 1174 steps, so consistent with that found by the Parsimony Ratchet. Strict consensus trees for both analyses are given in figures 5.1, 5.2, 5.3 and A.1.

PLACODERM MONOPHYLY AND INTRARELATIONSHIPS — In both the Parsimony Ratchet and TNT analyses placoderms, with the exclusion of the maxillate forms *Qilinyu* and *Entelognathus*, are found to be monophyletic and sister to all other jawed gnathostomes. The only unambiguous character supporting placoderm monophyly is the presence of claspers (ch. 385). Placoderm ingroup relationship are resolved as a balanced clade, with two large groups resolved as sister groups (Fig 5.1).

One group includes quasipetalichthyds, macropetalichthyids and ptyctodontids (Fig. 5.2, clade A). Many unambiguous characters support this clade, including the presence of sensory line openings with pores instead of grooves (ch. 276), the absence of a series of paired median skull roofing bones that meet at the dorsal midline of the skull (ch. 155), and an occipital joint articulation with longitudinal articular areas ("the spoon-like" articulation, ch. 171). Within this group, macropetalichthyids and ptyctodontids form monophyletic groups (Fig. 5.2). *Diandongpetalichthys* is resolved as sister to macropetalichthyids by the Parsimony Ratchet, however no unambiguous character supports this relationship. Quasipetalichthyids (with the exclusion of *Diandongpetalichthys*) form a monophyletic clade with ptyctodontids (Fig. 5.2, clade E), with *Pauropetalichthys* representing the sister taxa to two sister groups, one including ptyctodontids and the other uniting *Quasipetalichthys* and

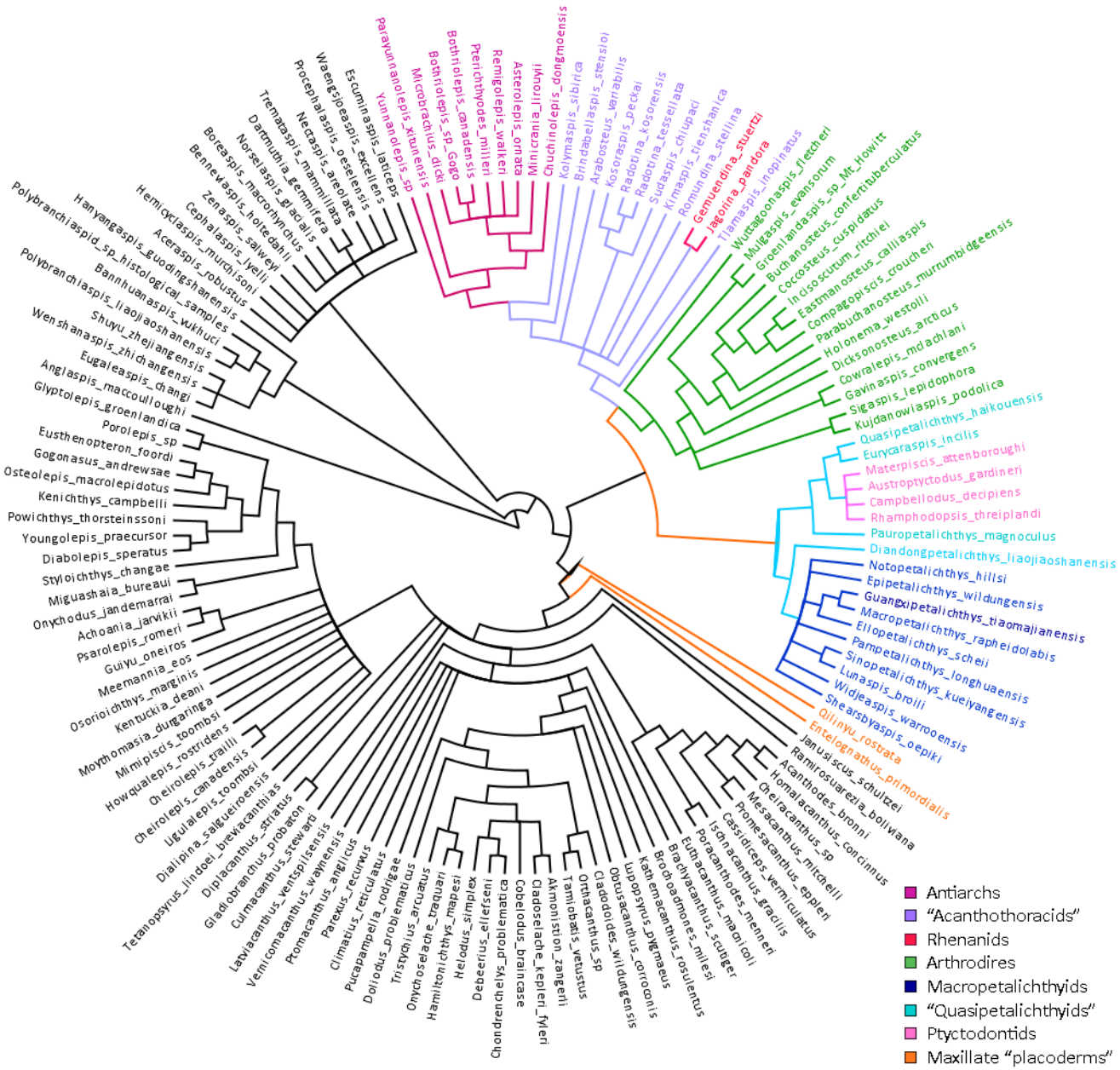

Antiarchs
"Acanthothoracids"
Rhenanids
Arthrodires
Macropetalichthyids
"Quasipetalichthyids"
Ptyctodontids
Maxillate "placoderms"

FIGURE 5.1: Strict consensus tree arising from the parsimony ratchet analysis (183 MPTs, tree lenght 1174)

Eurycaraspis (only in the Parsimony ratchet). Clade E is defined by the presence of a posterior descending lamina (ch. 251).

Another group (Fig. 5.2, clade B) includes a monophyletic Arthrodira (Fig. 5.2, clade C) sister to a clade including Rhenanida, Antiarchi and a paraphyletic "Acanthothoracida" (Fig. 5.2, clade D). They are reunited by the presence of the optic fissure (ch. 75). "Acanthothoracid" taxa are resolved as either sister taxa to antiarchs, in a polytomy with rhenanids or as sister taxa to all other taxa included in this group (Figs 5.1, 5.2). Synapomorphies of clade D include the presence of dorsally placed nasal openings (ch. 20), of posterior projection of the posterior paranuchal (ch. 188) and, with the exclusion of *Tlamaspis*, of a premedian plate (ch. 174). Resolution is low inside Antiarchi, probably caused by the lack of specific characters, although yunnanolepid taxa (*Yunnanolepis*, *Parayunnanolepis* and *Chuchinolepis*) are resolved as sister to all other antiarchs, as in the most recent phylogenetic analysis on the group (Pan et al. 2017). Contrastingly, resolution is instead very high within Arthrodira and similar with what found by specific studies on arthrodires, as Dupret et al. (2009, 2017b). *Wuttagoonaspis* is resolved as sister to all other arthrodires. The only unambiguous synapomorphy of clade B is represented by endolymphatic ducts with oblique course through dermal skull bones (ch. 154).

GNATHOSTOME RELATIONSHIPS — Among the jawed vertebrates outside the placoderms clade, *Qilinyu*, *Entelognathus*, and *Janusiscus* form a paraphyletic array of taxa sister to Crown-Gnathostomata (Figs 5.1, 5.3). *Qilinyu* is resolved as sister to the rest of the jawed vertebrates with the exclusion of placoderms. *Entelognathus* is found to be more closely related to crown-gnathostomes than *Qilinyu*. *Ramirosuarezia* is resolved in a polytomy with Osteichthyes, Chondrichthyes (including some "acanthodians"), the "acanthodians" *Culmacanthus* and *Tetanopsyrus*, and a clade formed by the "acanthodians" *Gladiobranchus* and *Diplacanthus* (Figs 5.1, 5.3). Character optimization shows two equally suboptimal positions for *Ramirosuarezia*, either representing the closest sister taxon to crown gnathostomes or being inside Chondrichthyes,

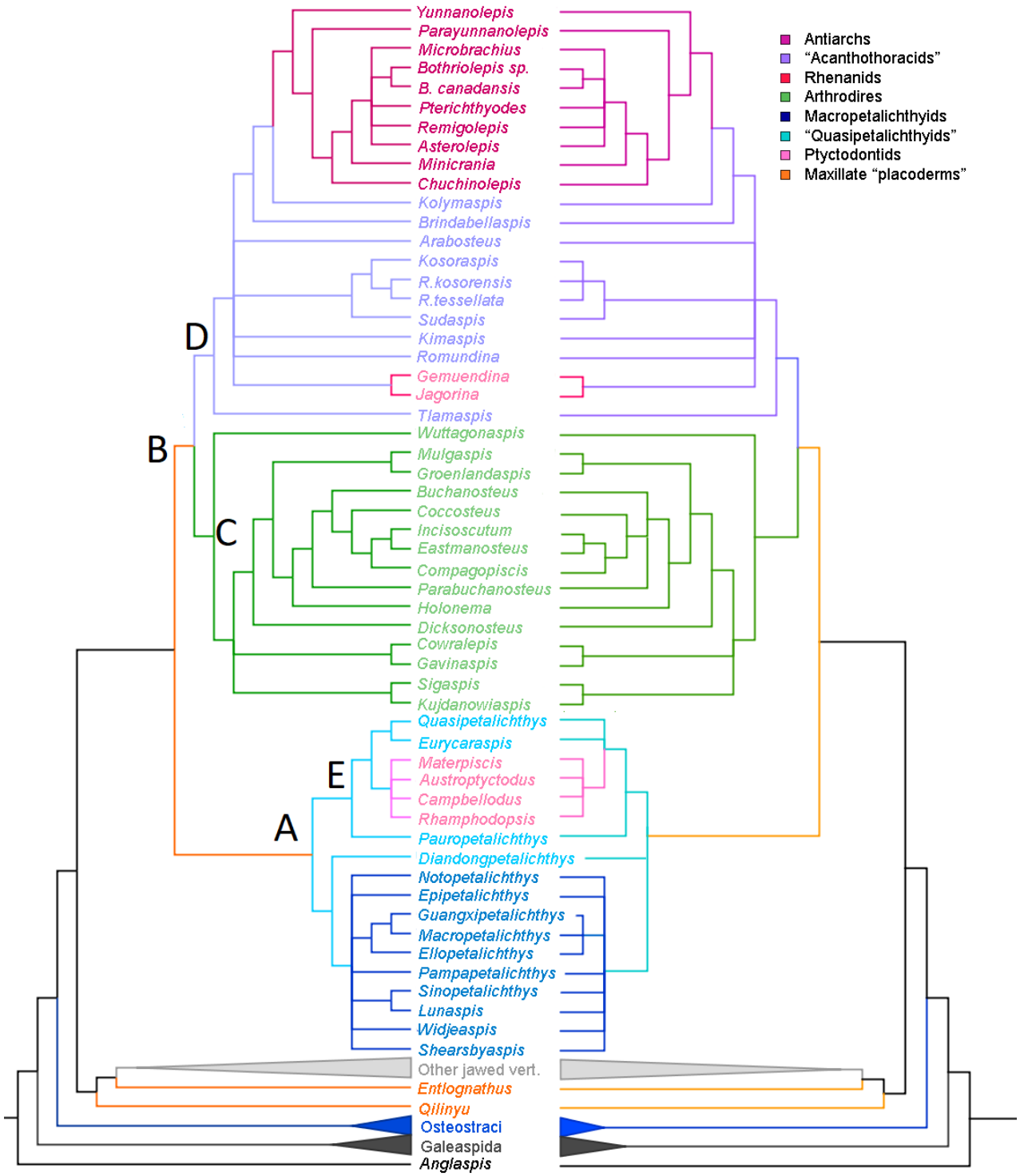

FIGURE 5.2: Strict consensus trees from the Parsimony Ratchet (left) and the TNT analysis (right) for the placoderm clade.

sister to a clade form by the aforementioned "acanthodians". This is one reason why the relationships inside Crown-Gnathostomata have poor resolution.

Problems in the resolution of the osteichthyans are derived by the uncertain placement of *Dialipina*, *Ligulalepis* and *Meemannia*, which form either a clade sister to the other Osteichthyes or result in a paraphyletic array where *Ligulalepis* is sister to *Dialipina* plus the rest of the Osteichthyes and *Meemannia* is sister to all other actinopterygians. Other problems that decrease resolution in this area regard the position of the clade formed by *Guiyu*, *Psarolepis* and *Achoania*, resolved either as sister to all other osteichthyans or sister to the clade formed by sarcopterygians and actinopterygians with the exclusion of *Dialipina* and *Ligulalepis* (plus or minus *Meemannia*). Relationships within sarcopterygians and chondrichthyans are instead better resolved and are consistent with that found by King et al. (2016) and other analyses (e.g. Giles et al. 2015b; Zhu et al. 2016).

5.4.2 **Bayesian analysis**

Bayesian inference gives a result that contrasts substantially to that of parsimony (Fig. 5.4). Bayesian analysis does not recover placoderms monophyly but instead places a polytomy of antiarchs, "acanthothoracids" (with the exclusion of *Tlamaspis*) and rhenanids as the sister groups to all other jawed gnathostomes (Figs 5.4, A.2, A.3). Resolution is very low in this part of the tree. Antiarchi is resolved as monophyletic, as well as Rhenanida, while *Kolymaspis* and *Brindabellaspis* are revolved as sister to antiarchs (Figs 5.A, A.2). The other "acanthothoracids" are not resolved and in a large polytomy with rhenanids and antiarchs. The "acanthothoracid" *Tlamaspis* is excluded from that group and instead placed in a group formed by the rest of the placoderms and crown-gnathostomes (Figs 5.A, A.2). This group includes a polytomy between *Tlamaspis*, arthrodires, petalichthyids (which also include ptyctodontids) and the rest of jawed vertebrates. Bayesian posterior probability for this node is quite high (0.859). Relationships in this group are similar to that of Parsimony analysis but

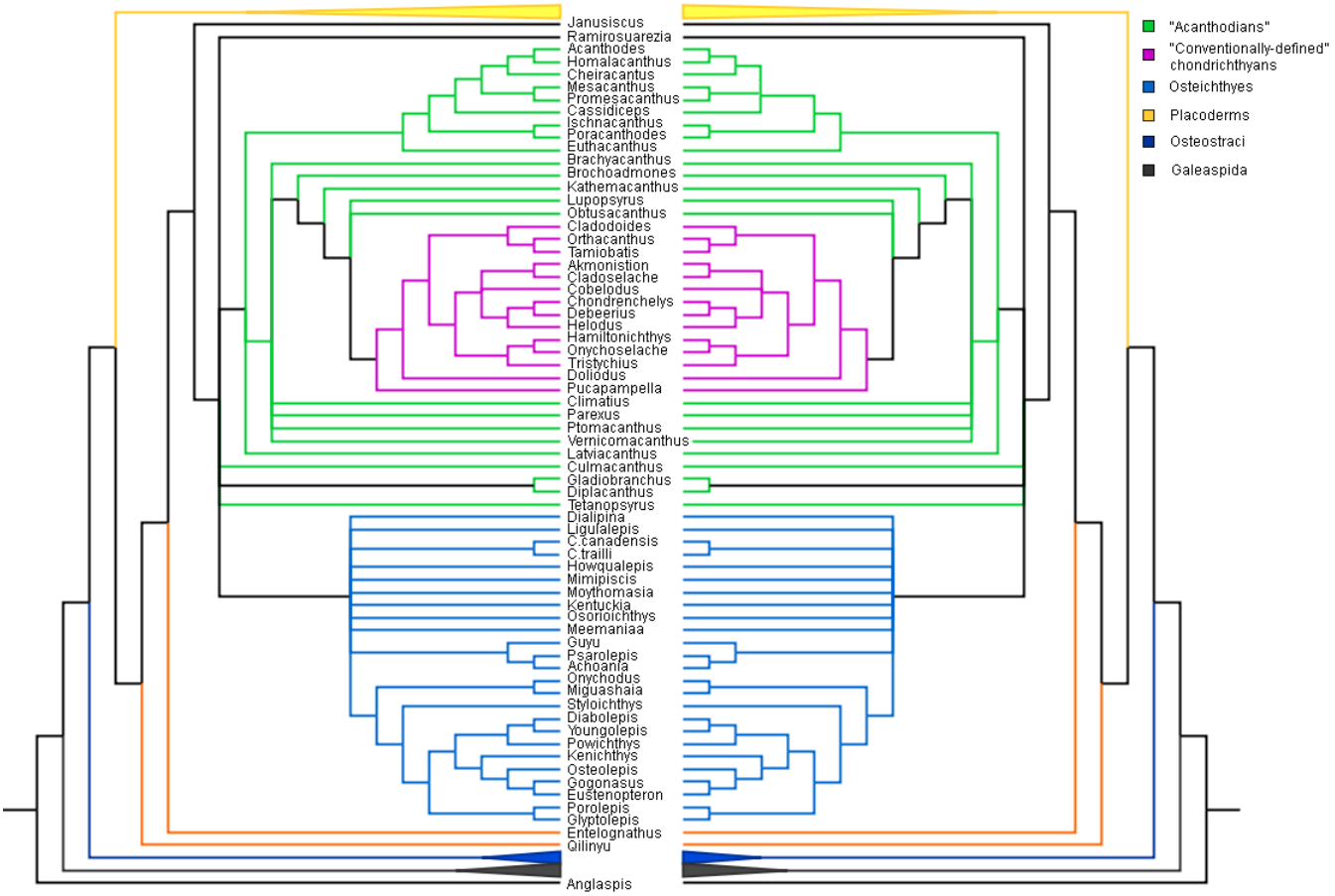

FIGURE 5.3: Strict consensus trees from the Parsimony Ratchet (left) and the TNT analysis (right) for the jawed vertebrate clade with outgroups and "traditional" placoderms collapsed.

some of them have low BPP value (e.g. Arthrodira is only 0.528). The relationships between quasipetalichthyids and ptyctodontids are retained, although with a low support (0.63) (Figs 5.A, A.2).

Qilinyu, *Entelognathus* and *Janusiscus* form an array of sister taxa towards crown-gnathostomes. Difference with the parsimony results includes the different position of *Ramirosuarezia*, which is placed in a clade with some "acanthodians", the resolution of the actinopterygian and the placement of *Guiyu*, *Psarolepis* and *Achoania*, which are resolved as stem-sarcopterygians instead of stem-osteichthyans (Figs 5A, A.4).

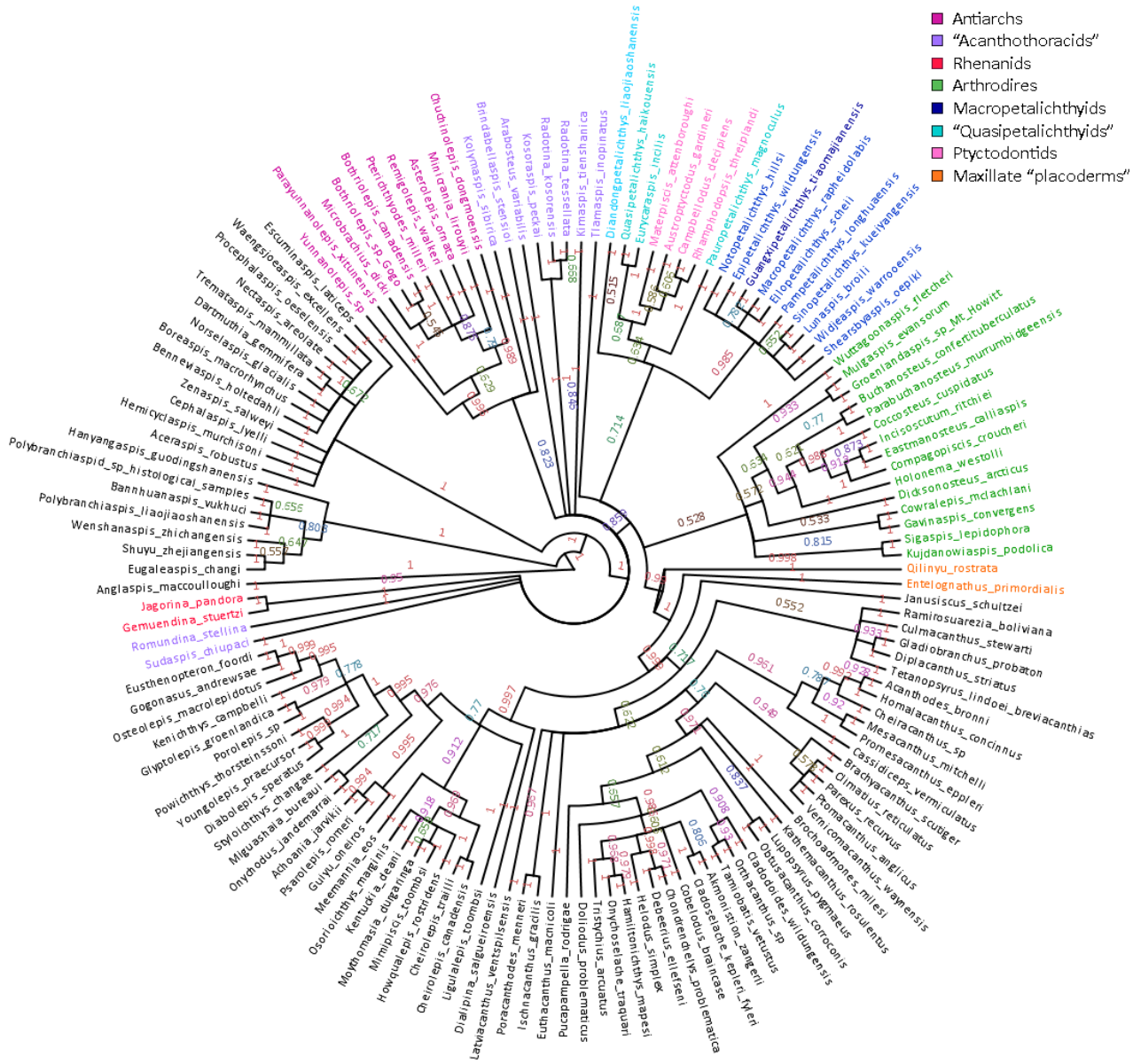

FIGURE 5.4: Majority-rule consensus tree resulting from Bayesian inference analysis. Frequencies of bipartitions among sampled trees (Bayesian posterior probabilities) are indicated for each node.

5.5 DISCUSSION

Previous analyses on placoderms have found consensus between parsimony and bayesian methods (e.g. Brazeau 2009; Zhu et al. 2013, 2016). A recent study published by Qiao et al. (2016) performed several tests on a large dataset of stem-gnathostomes

including a wide sample of placoderms (updated and expanded from the dataset of Long et al. 2015). They found consensus between parsimony and bayesian topologies, which both resolved placoderms as paraphyletic, and thus argued that none of the two methods necessarily perform better or worse than the other. Moreover, they argued that performing different phylogenetic methods on the same dataset is important as they may generate different results for character evolution and thus different perspectives when investigating evolutionary transformations.

Recent simulation studies have suggested that the bayesian inference outperforms parsimony in terms of topological accuracy (O'Reilly et al., 2016). In this study, parsimony and bayesian inference give contrasting results, the first resolving placoderms as monophyletic while bayesian failing to recover placoderm monophyly. These results are however opposed to those of King et al. (2016), where the monophyly of placoderms was found by bayesian but not by parsimony methods. This may imply that the uncertainty about the relationships at the root of jawed vertebrates may not necessarily being methods dependent but instead being related to the amount of missing data and inapplicable characters in early gnathostomes data matrices.

In fact, dataset that incorporate a wide array of groups across the early vertebrate's tree usually incorporate large amount of character that are only scorable for a small percentage of the dataset, being specifically related to a particular group or subset of groups. For this reason, as I showed in chapter 2, it is important to consider character transformation compatibility under the different competing hypotheses, as certain topologies can result in less parsimonious scenarios for individual character evolution when considered in a broader context. In the following discussion, I examine these competing hypotheses in terms of what they imply for some key periods in modern gnathostomes evolution, such as the primitive skull architecture at origin of jaws or the ancestral state for fertilization.

5.5.1 The monophyly of Petalichthyida

Both parsimony and bayesian analyses resolved Petalichthyida as monophyletic with the inclusion of ptyctodontids. Of the characters suggested by Zhu (1991) and Pan et al. (2015) as defining Petalichthyida, only the presence of sensory line opening with pores instead of grooves (ch. 276) is found to represent a unique synapomorphy of this group, however this is dependent on the inclusion of ptyctodontids in Petalichthyida. Other of the proposed characters, such as the presence of supraorbital sensory canal converging with the posterior pit line canals (ch. 291) and the absence of central sensory line (ch. 303), are resolved as plesiomorphic or homoplasic. Additionally, this clade is defined by the presence of a spoon-like articulation (see discussion in chapter 3) which, although not present in ptyctodonts, it is present in macropetalichthyids, *Diandongpetalichthys* and in the early branching member of the group (Fig. 5.2, clade E) formed by quasipetalichthyids and ptyctodontids.

A topology that resolved ptyctodontids as sister to quasipetalicthyids and included in a monophyletic group with macropetalichthyids has only been reported before by King et al. (2016) among recent phylogenetic analyses. Other recent studies have instead resolved ptyctodontids as either sister group to petalichthyids (Brazeau, 2009; Long et al., 2015), closer to crown-gnathostomes than petalichthyids (Zhu et al., 2013, 2016) or related to phyllolepid arthrodires (Davis et al., 2012; Giles et al., 2015b).

The relationships between quasipetalichthyids and ptyctodontids and the monophyly of Petalichthyida have important evolutionary implication. Firstly, it suggests that claspers may have been ancestrally present but lost in petalichthyids, or alternatively yet to be discovered in those forms, as only few petalichthyids are known for postcranial remains. In addition, because taxa such as *Diandongpetalichthys* and *Pauropetalichthys* are found to represent the earliest branching member of this clade, it leads to a primitive 'arthrodire-like' gestalt for the group, thus suggesting that similarities between the macropetalichthyids and jawless fishes are homoplasic. However, quasipetalichthyids are mostly known from their dermal anatomy, while the

similarities between macropetalichthyids and jawless fishes concern endocranial character that are unknown for the quasipetalichtyids as well as for ptyctodontids. This constitutes a major obstacle in understanding the polarities of those character within the group, and caution need to be maintained until better information about endocranial morphology of these taxa is revealed.

5.5.2 **"Acanthothoracids" as a paraphyletic assemblage**

"Acanthothoracida" is here resolved as a paraphyletic assemblage of taxa in both parsimony and bayesian inference (Figs 5.1, 5.2, 5.4). The parsimony analysis recovers some "acanthothoracids" to be more closely related to antiarchs, some others to form a monophyletic group characterized by the presence of tesserae, and some other to represent sister taxa to all other members of this large group (Figs 5.1, 5.2). In general, however, all those form are included in a monophyletic group with antiarchs and rhenanids. Bayesian analysis instead has a lower resolution for "acanthothoracids", which is recovered in an unresolved polytomy at the root of jawed vertebrates (Figs 5.5, 5.6). However, some of the relationships found by the parsimony analysis are retained.

Among "acanthothoracids", *Brindabellaspis* amd *Kolymaspis* are sister to antiarchs due to the possession of endolymphatic sacs (ch. 54) (further discussion in chapter 4) and the absence of posterior projection on the paranuchal plates, a character present in all other "acanthothoracids" and which constitutes a synapomorphy of clade D (Fig. 5.2). The proximity between *Kolymaspis*, *Brindabellaspis* and antiarchs is also found by bayesian inference (Fig. 5.4) with good supported (BPP=0.823).

In the parsimony analyses, the other "acanthothoracids" form a polytomy with rhenanids (Figs 5.1, 5.2, 5.4). *Kosoraspis*, *Radotina kosorensis*, *Radotina tessellata* and *Sudaspis* form a monophyletic clade because of a dermal skull roof constituting by both large dermal plates and tesserae (ch.150). In King et al. (2016) rhenanids were recovered as the earliest branching member of the placoderms clade. In other analyses,

such as Zhu et al. (2016), rhenanids were found near the root of mandibulated gnathostomes. Both this placement implies a micromeric ancestral state for placoderms or possibly for jawed vertebrates. However, both the jawless outgroups and osteichthyans possess a macromeric skeleton and thus this imply a reversal occurred at the root of placoderms. Here, rhenanids and tesserate "acanthothoracids" are resolved nested within a monophyletic placoderm and, as the earliest branching members of this group present a present a dermal skull roof formed by large dermal plates, the micromeric condition of rhenanids and those "acanthothoracids" is recovered as a secondary condition, a scenario more parsimonious considering the macromeric condition of placoderm outgroups.

Tlamaspis is resolved by parsimony analyses at the root of the group formed by the other "acanthothoracid" plus rhenanids and antiarchs, while bayesian inference placed *Tlamaspis* as separated from those group and instead closer to arthrodire and petalichthyids. This is due to the existence in *Tlamaspis* of many characters found in arthrodire, *Qilinyu* and Osteichthyes, as the presence of central plates in contact (ch. 155) and the absence of a premedian plate (ch. 174). Other features similar to those of arthrodire and Osteichthyes, for example the possession of a central sensory line (ch. 303), are present in other members of the group, as *Romundina*, but absent in the more nested taxa. This leads to the hypothesis that the primitive condition for clade D (Fig. 5.2) might have been similar to that of the earliest branching member of clade B and C (Fig. 5.2), and in general "arthrodire-like", and that the unique morphology of antiarchs, *Brindabellaspis* and the more nested taxa are instead derived from that initial condition. The implications of this hypothesis on the reconstruction of the ancestral cranial morphology of jawed vertebrates are discussed below.

5.5.3 **Placoderm monophyly**

In the analysis by King et al. (2016), three character transformations were found to be most parsimonious when placoderms are considered monophyletic rather than

paraphyletic: the acquisitions of an optic fissure, pelvic claspers and paired occipital facets. Among these, only the presence of pelvic claspers was found to support placoderm monophyly in this analysis.

The optic fissure is in fact absent in some placoderms, as discussed in chapter 2. For instance, it has never been reported in petalichthyids, even if very few information is currently available for the quasipetalichthyids. Moreover, here I decided to code the presence of an optic fissure for ptyctodontids as unknown instead of present (*contra* King et al. 2016, which followed Trinajstic et al. 2012), as the braincase of ptyctodonts is always found disarticulated and there is no definite certainty of the presence or absence of an optic fissure in this group. New discovery and investigation of quasipetalichthyids and ptyctodontids need to be carried out to assess the distribution of this character in those group. Nonetheless, the presence of an optic fissure is here resolved as a synapomorphy uniting a subgroup of placoderms, as proposed in chapter 2, comprising arthrodires, rhenanids, acanthothoracids and antiarchs (Fig. 5.2, clade B). This relationships between those placoderms represents a new finding and differs strikingly to previous phylogenetic results (Brazeau, 2009; Davis et al., 2012; Zhu et al., 2013; Long et al., 2015; Dupret et al., 2014; Giles et al., 2015b; Zhu et al., 2016; King et al., 2016), which usually resolved petalichthyids, rather than antiarchs or "acanthothoracids", in a closer proximity to arthrodires. This has important implications as the possession of an optic fissure may be related to the evolution of a unique orbitonasal morphology for those placoderms, as discussed below and in chapter 4.

Paired occipital facets are present in all taxa within placoderms for which the occipital area is known and proposed by King et al. (2016) as a synapomorphy for placoderms. Here, however, it is not resolved as an unambiguous character for placoderms. In addition, this results call attention to the morphology of the neck joint. If placoderms are monophyletic with the relationships found by my analysis, then a sliding joint, shared by the earliest member of clade D (Fig. 5.2), the earliest arthrodires and Osteichthyes could be indicated as the primitive condition for all

jawed vertebrates. Unfortunately, the lack of a head-shoulder division in the jawless outgroup and the little information on that area available for the maxillate 'placoderms', still represent obstacles to a clear understanding on the primitive condition of the occipital facets and neck-joint morphology for jawed vertebrates. Moreover, uncertainty remains in understanding the early evolution of the neck in petalichthyids (*sensu* clade A, fig. 5.2), as even the earliest members of the group show the unique "spoon-like" occipital articulation, which is very different from that of the other jawed vertebrates (as discussed in chapter 3).

Intromitting organs (or claspers) are known in most of the major groups of placoderms, being found in antiarchs, arthrodires and ptyctodonts, and are also present in chondrichthyans. Debates still exist on the homology between the chondrichthyans and the placoderms claspers, primarily based on the fact that some author suggested that the placoderms claspers are not articulated with the pelvic girdle (Trinajstic et al., 1979), as instead in chondrichthyans. However, the hypothesis that these two structures are non-homologus is assumed *a priori* and presents anatomical problems that and is thus controversial (see discussion for character 385).

The presence of claspers in some group of placoderms represent a problematic condition in term of placoderm paraphyly. If placoderms are considered paraphyletic and antiarchs represent the earliest-branching group of the jawed vertebrate lineage, as proposed in several major recent analyses (Brazeau, 2009; Davis et al., 2012; Zhu et al., 2013; Long et al., 2015; Dupret et al., 2014; Giles et al., 2015b; Zhu et al., 2016) and in our bayesian analysis, this requires claspers to be the ancestral condition for jawed vertebrate and implies a reversal from internal to external fertilization for Crown-Gnathostomata. This scenario is considered heterodox, as there are no evidences for reversal from internal to external fertilization in modern group of fish (Blackburn, 2015). Moreover, this scenario depends on the demonstration that the presence of clasper in placoderms is not a specialized feature of a subset of placoderms, if not all.

Clasper in placoderms possess a similar morphology and are ossified, leading to the alternative hypothesis that they are homologous structures and a potential specialization of this group (Long et al., 2015), thus supporting the monophyly of placoderm and leading to a scenario where external fertilization is the ancestral condition for jawed vertebrates, more consistent with the lack of evidence for reversal from internal to external fertilization in vertebrates. Indeed, our parsimony analysis indeed indicates that claspers can potentially constitute a local synapomorphy of placoderms, suggesting that internal fertilization is a secondarily specialization of placoderms. This also imply that the craniofacial similarities between certain groups of placoderms, like antiarchs and petalichthyids, with osteostracans and galeaspids are convergent.

Nevertheless, there are evidences that internal fertilization can be independently acquired (Blackburn, 2015) and thus for multiple independent evolution of clasper in the different group of placoderms. This thus invite to remain cautious about considering clasper as uniting placoderms in a monophyletic group, as little is known about the presence or absence of this feature in the earliest branching placoderms, as *Wuttagoonaspis*, quasipetalichthyids and some "acanthothoracids", as well as in macropetalichthyids. Crucial to this will be investigating the pelvic morphology of those groups, especially given the existence of specimens with fairly complete postcrania, as for *Lunaspis*.

Other characters are uniquely present in placoderms, such as the presence of synarcual or of an opercular suspension on the braincase. However, those features cannot be scored for the jawless outgroup and only among osteichthyans for crown-gnathostomes, making the polarity of those features unclear. Again, the lack of information in the jawless outgroup constitutes the major obstacle to establish the ancestral character condition for jawed vertebrates and thus for placoderms.

5.5.4 The primitive condition of jawed vertebrates

The ambiguities in character polarity at the root of jawed vertebrates reflect a realistic summary of our current knowledge on the early evolution of the group. In fact, most of the best known jawed stem-gnathostomes are from relatively recent deposits, mainly from the Devonian, while the Silurian record for jawed vertebrates is instead still poorly known. However, some example of jawed vertebrates from the Silurian include both Osteichthyes, such as *Guiyu*, as well as "placoderms" that show a facial architecture similar to Osteichthyes. If we consider placoderms to be paraphyletic, then we need to face the problem of having a large gap in terms of nodes on the tree, morphological changes and tempo, between the origin of jaw and the origin on crown gnathostomes. Instead, a monophyletic Placodermi sister to *Qilinyu*and *Entelognathus*, which are then in immediacy with the node of origin of crown-gnathostomes, mitigate this problem and decreases the gap between the appearance of jaws and the origin of modern gnathostomes groups.

This new phylogenetic framework for stem-gnathostomes contrasts with recent hypotheses for the primitive condition of vertebrates (e.g. Dupret et al. 2014; Zhu et al. 2016) but that has been recently suggested by other studies that recovered placoderm monophyly, for instance King et al. (2016). For example, in the monophyletic placoderms found by my analysis, the earliest branching member of the different groups possess a generalized "arthrodire-like" endocranial morphology, also similar to that of the maxillate "placoderms" *Qilinyu* and *Entelognathus*. This implies an "arthrodire-like" morphotype for not only placoderms, but also jaw-bearing gnathostomes as a whole, and indicates that the similarities between groups usually considered sharing facial plesiomorphic architecture with jawless fishes, such as antiarchs, "acanthothoracids" or macropetalichthyids, are instead likely to be derived features, possibly resulting from ecological adaptation.

According to my analysis, antiarchs and macropetalichthyids are nested within the placoderms (Figs 5.1, 5.2), with "acanthothoracids" representing a series of forms

falling between antiarchs and rhenanids. The earliest branching taxa of the different clades within placoderms possess instead several features similar to arthrodires and to generalized gnathostomes, both in neurocranial, dermal skull roof morphology, rather than resembling the jawless outgroup. Likewise, my analysis found the presence of an optic fissure as uniting a subset of placoderm including arthrodire, antiarchs, "acanthothoracids" and rhenanids (Fig. 5.2, clade B). The occurrence of this fissure in those animals, related to the presence of nasal capsules as part of a neurocranial unit independent from the rest of the braincase and thus with a higher degree to which the nasal capsule can move relative to the rest of the braincase, might explains the peculiar orbitonasal morphology of certain placoderms (see discussions in chapter 2 and 4). Those placoderms could therefore not represent the primitive condition for jawed vertebrates, but could instead being viewed as highly specialized forms.

Uncertainty remains regarding the shared primitive features between macropetalichthyids and jawless vertebrates. This is because those similarities are related to endocranial neurocranial features, for example the morphology of the pituitary vein and certain nerves, not known in the early branching petalichthyids as well as in *Qilinyu* and *Entelognathus*. Moreover, the presence of the optic fissure or pelvic clasper are still unknown in petalichthyids *sensu stricto*, a potential weakness to the hypothesis on placoderm monophyly. Gathering those neurocranial information in those forms will thus be key not only to test hypothesis on the monophyly and ancestral condition for placoderms, but also to illuminate the early evolution of jawed vertebrates.

5.6 CONCLUSION

Here I present the first numerical phylogenetic analyses to include diverse petalichthyid, "acanthothoracid" and antiarch placoderms simultaneously. This amied to test the monophyly of placoderms, as well as of certain historical group, as "Acantho-

thoracida" and Petalichthyida. Petalichthyida was found to include ptyctodontids, which are aligned with some members the quasipetalichthyids. "Acanthothoracida" was found to form an array of forms, some of which are aligned with antiarchs, while other with yet unresolved relationships but proximity with rhenanids.

Parsimony and bayesian analyses resulted in competing hypothesis about placoderm monophyly. Placoderms were found to be monophyletic with the exclusion of the maxillate forms under parsimony principle, while bayesian inference failed to recover the monophyly of this group. Despite this disagreement in the results invite to remain cautious, those competing hypotheses can be discussed in term of character compatibility, which seems to favour placoderm monophyly for characters as the presence of claspers or the optic fissure.

Placoderms monophyly indicates a new scenario for the early evolution of jawed vertebrates, implying a primitive architecture similar to those of early arthrodires, maxillate "placoderms" and Osteichthyes. As a consequence, the similarities between jawless outgroups and certain placoderms would be the consequence of convergent evolution. However, uncertainty remain among some character distribution, comprising potential synapomorphies of placoderms, as well as problems in establishing the polarity of clade specific character that are difficult to compare with the outgroups. Future discoveries or reinvestigation of the earliest member of the placoderm group, as well as of both jawless and jawed outgroup, will be key to illuminate the deepest transformations that occurred at the origin of jawed vertebrates.

CHAPTER 6

CONCLUSION

The central goal of this thesis has been to gather information about the internal skull anatomy of some of the most obscure groups within placoderms such as petalichthyids and "acanthothoracids". Those placoderm groups have taken a pivotal position in the debate on placoderm paraphyly, owing to their similarities in their facial architecture with the jawless outgroups of jawed vertebrates. Nevertheless, their endocranial anatomy was poorly known, with only few taxa investigated in great details and included in comparative analysis with the other early gnathostomes.

This thesis re-examined the holotype of petalichthyids *Shearbyaspis oepiki* and *Ellopetalichthys scheii*, and the "acanthothoracid" *Kolymaspis sybirica*. These specimens are preserved in 3D and with extraordinary preservation of the internal endocranial stricture. This allowed the use of X-ray computed tomography (CT) scanning and virtual three-dimensional (3D), non-destructive techniques that were not available when these taxa were originally described and have been applied extremely successfully to the reconstruction of internal cranial anatomy in early fishes. This has revealed novel anatomical details about those placoderms and expanded anatomical accounts for the morphological diversity of petalichthyid and "acanthothoracid" braincases in the form of a set of descriptive morphological chapters.

The investigation of the endocranial anatomy of *Shearsbyaspis* found the first evidence of a parasphenoid in a petalichthyid, a feature otherwise described only in arthrodires and in the "acanthothoracid" *Kosoraspis* among placoderms. It also recovered an unexpected condition in the morphology of the facial nerve, which divides in the palatine and hyomandibular branch before the orbit but have a hyomandibular branch that pass through the orbital wall. This condition differ from

what has been assumed before for petalichthyids and has never observed before in a jawed vertebrate. Other newly observed feature included the presence of a median recess of the posteroventral myodome and of a communal foramen on the orbital wall for the canals for the abducens, trigeminal nerves and pituitary vein, conditions observed before only in jawless osteostracans. In general, the study of the endocranial anatomy of *Shearsbyaspis* has revealed a combination of both derived and plesiomorphic characters never observed before in a placoderm, particularly in its orbital morphology and palatal architecture.

The examination of the neurocranial anatomy of *Ellopetalichthys* provided new evidence on the inner ear morphology of petalichthyids. This allowed to revise previous investigation on petalichthyid inner ear anatomy and having a better understanding of the unique morphology of the endolymphatic duct and sacs of these animals. The study of the well-preserved occipital joint revealed details previously inaccessible to earlier investigators, offering another example of the complex morphology of the occipital articulation of petalichthyids. This has presented important details in the study of the extension, morphology and function of the neck and gills musculature in petalichthyids placoderms, offering some insight about the origin and evolution of the innervation of the occipital area in early vertebrates.

The study of *Kolymaspis* provided the first description of its sensory line system and internal morphology of this animal, expanding substantially our understanding of the endocranial morphology of "Acanthothoracida". The internal anatomy of *Kolymaspis* presented a combination of character between the short and the long snouted "acanthothoracids", as well as many characters present in arthrodires and antiarchs. The morphology of *Kolymaspis* presented many similarities with that of the long snouted "acanthothoracid" *Brindabellaspis* and antiarchs, for example in having nasal capsules opening in the orbit and a well-developed premedian plate. Moreover, this study founds that the anatomy of the facial nerve and endolymphatic duct of *Kolymaspis* is more similar to that of the other stem-gnathostomes rather than other "acanthothoracids'. These evidences have provided support to the hypothesis

that placoderms with this facial configuration represent a highly specialized morphology rather than exhibiting the plesiomorphic condition for jawed gnathostomes, as previously suggested.

The monophyly of Petalichthyida and "Acanthothoracida" was previously assumed based on probably plesiomorphic dermal bone characters but never tested in a global analysis of placoderm taxa. This prevented from having a clear understanding of the anatomy of those groups. For example, within the Petalichthyida, some members such as *Shearsbyaspis* exhibit features that recall the osteostracans while other forms, as the quasipetalichthyids, present features which could nest them with the arthrodires. Given the central role of petalichthyids and "acanthothoracid" placoderms in understanding the role of placoderm characters in our hypotheses on gnathostomes bodyplan evolution, this thesis also attempted to test the monophyly and relationships of Petalichthyida, 'Acanthothoracida' and placoderms as a group.

I performed different phylogenetic analyses on a new large dataset comprising a wide range of early gnathostomes, particularly focusing on the inclusion of an extensive sample of petalichthyid and "acanthothoracid" taxa. Both parsimony and bayesian analysis resolved petalichthyids to constitute a monophyletic clade with the inclusion of ptyctodonts, a configuration found only few times by recent investigations. "Acanthothoracids" were resolved as a non-monophyletic group were the different taxa represent an array of form united with rhenanids and antiarchs. Those results suggested that those groups may represent derived forms instead of exhibiting the primitive condition for jawed vertebrates, as the earlier branching member of both groups were found to share cranial similarities with arthrodires and bony fishes rather than with jawless fishes.

Parsimony and bayesian analysis resulted in competing hypothesis about placoderm monophyly. This highlighted the uncertainty that still persists about the polarity of the characters at the node of the origin of jawed vertebrates, related to large amount of missing data and inapplicable character that characterize the fossil record of early gnathostomes. Nevertheless, through the thesis chapters I compared

the strengths and weaknesses of competing scenarios of placoderm relationships, as they lead to radically different implication for some of the key event in vertebrate evolution, such as the appearance of jaws or modes of reproduction. For instance, the resurrection of placoderms monophyly may indicates a primitive architecture similar to those of early arthrodires, maxillate "placoderms" and bony fishes, while placoderm paraphyly places placoderms with a facial architecture similar to that of jawless fishes at the root of jawed vertebrates and potentially a reversal from internal to external fertilization at the origin of modern gnathostomes. However, the data available seems to not be sufficient to decisively favour one or the other hypothesis. Future tentative of illuminating the deepest evolutionary history of jawed vertebrate thus cannot preclude from the exploration of the cranial anatomy of the earliest member of the different placoderms groups, as well as from new discovery that might populate the morphological gap still existing between jawless and jawed stem-gnathostomes.

BIBLIOGRAPHY

Ahlberg, P. E. (1989). Paired fin skeletons and relationships of the fossil group Porolepiformes (Osteichthyes: Sarcopterygii). *Zoological Journal of the Linnean Society*, 96(2):119–166.

Andrews, M., Long, J. A., Ahlberg, P. E., Barwick, R., and Campbell, K. (2005). The structure of the sarcopterygian *Onychodus jandemarrai* n. sp. from Gogo, Western Australia: with a functional interpretation of the skeleton. *Transactions of the Royal Society of Edinburgh: Earth Sciences*, 96(03):197–307.

Arratia, G. and Cloutier, R. (1996). Reassessment of the morphology of *Cheirolepis canadensis* (Actinopterygii). *Devonian fishes and plants of Miguasha, Quebec, Canada*, pages 165–197.

Basden, A. M. and Young, G. C. (2001). A primitive actinopterygian neurocranium from the Early Devonian of Southeastern Australia. *Journal of Vertebrate Paleontology*, 21(4):754–766.

Basden, A. M., Young, G. C., Coates, M. I., and Ritchie, A. (2000). The most primitive osteichthyan braincase? *Nature*, 403(6766):185–188.

Béchard, I., Arsenault, F., Cloutier, R., and Kerr, J. (2014). The devonian placoderm fish *Bothriolepis canadensis* revisited with three-dimensional digital imagery. *Palaeontologia Electronica*, 17(1):1–19.

Bendix-Almgreen, S. (1975). The paired fins and shoulder girdle in *Cladoselache*, their morphology and phyletic significance. *Colloques International CNRS*, 218:111–23.

Blackburn, D. G. (2015). Evolution of vertebrate viviparity and specializations for fetal nutrition: a quantitative and qualitative analysis. *Journal of Morphology*, 276(8):961–990.

Blieck, A. and Heintz, N. (1983). The cyathaspids of the Red Bay Group (Lower Devonian) of Spitsbergen. *Polar Research*, 1(1):49–74.

Brazeau, M. D. (2009). The braincase and jaws of a Devonian 'acanthodian' and modern gnathostome origins. *Nature*, 457:305–308.

Brazeau, M. D. (2012). A revision of the anatomy of the Early Devonian jawed vertebrate *Ptomacanthus anglicus* miles. *Palaeontology*, 55(2):355–367.

Brazeau, M. D. and de Winter, V. (2015). The hyoid arch and braincase anatomy of *Acanthodes* support chondrichthyan affinity of 'acanthodians'. In *Proceedin of the Royal Society B*, volume 282, page 20152210. The Royal Society.

Brazeau, M. D. and Friedman, M. (2014). The characters of Palaeozoic jawed vertebrates. *Zoological Journal of the Linnean Society*, 170(4):779–821.

Brazeau, M. D. and Friedman, M. (2015). The origin and early phylogenetic history of jawed vertebrates. *Nature*, 520:490–497.

Brazeau, M. D., Friedman, M., Jerve, A., and Atwood, R. C. (2017). A three-dimensional placoderm (stem-group gnathostome) pharyngeal skeleton and its implications for primitive gnathostome pharyngeal architecture. *Journal of Morphology*.

Brusatte, S. L. (2010). Representing supraspecific taxa in higher-level phylogenetic analyses: Guidelines for palaeontologists. *Palaeontology*, 53(1):1–9.

Burrow, C. J., Newman, M. J., Davidson, R. G., and den Blaauwen, J. L. (2013). Redescription of *Parexus recurvus*, an Early Devonian acanthodian from the Midland Valley of Scotland. *Alcheringa: an Australasian Journal of Palaeontology*, 37(3):392–414.

Burrow, C. J. and Turner, S. (1998). Devonian placoderm scales from Australia. *Journal of Vertebrate Paleontology*, 18(4):677–695.

Bystrow, A. (1956). *Kolymaspis sibirica* ng, n. sp., a new representative of the Lower Devonian agnathous vertebrates. *Vestnik Leningradskogo Universiteta Geologiya-Geografiya*, 18:5–13.

Carr, R. K. and Hlavin, W. J. (2010). Two new species of *Dunkleosteus* Lehman, 1956, from the Ohio Shale Formation (U.S.A., Famennian) and the Kettle Point Formation (Canada, Upper Devonian), and a cladistic analysis of the Eubrachythoraci (Placodermi, Arthrodira). *Zoological Journal of the Linnean Society*, 159(1):195–222.

Carr, R. K., Johanson, Z., and Ritchie, A. (2009). The phyllolepid placoderm *Cowralepis mclachlani*: insights into the evolution of feeding mechanisms in jawed vertebrates. *Journal of Morphology*, 270(7):775–804.

Chang, M. (1991). Head exoskeleton and shoulder girdle of *Youngolepis*. In Chang, M.-M., Liu, Y.-H., and Zhang, G.-R., editors, *Early vertebrates and related problems of evolutionary biology*, pages 355–378. Science Press Beijing.

Chang, M.-M. (1995). *Diabolepis* and its bearing on the relationships between porolepiforms and dipnoans. *Bulletin du Muséum national d'histoire naturelle. 4 Séries*, 17:235–268.

Chang, M.-M. and Yu, X.-B. (1984). Structure and phyogenetic significance of *Diabolepis speratus* gen. et sp. nov., a new dipnoan-like form from the Lower Devonian of eastern Yunnan, China. *Proceeding of the Linnean Society New South Wales*, 107:171–184.

Chang, M.-M. and Zhu, M. (1993). A new Middle Devonian osteolepidid from Qujing, Yunnan. *Mem. Assoc. Australas Palaeontol*, 15:183–198.

Clement, G. (2004). Nouvelles données anatomiques et morphologie génerale des Porolepididae (Dipnomorpha, Sarcopterygii). *Revue de Paléontologie*, 9:193–211.

Cloutier, R. (1996). The primitive actinistian *Miguashaia bureaui* Schultze (Sarcopterygii). *Devonian fishes and plants of Miguasha, Québec, Canada. München: Verlag Dr. Friedrich Pfeil*, pages 227–247.

Coates, M. I. (1994). The origin of vertebrate limbs. *Development*, 1994:169–180.

Coates, M. I. and Gess, R. W. (2007). A new reconstruction of *Onychoselache traquairi*, comments on early chondrichthyan pectoral girdles and hybodontiform phylogeny. *Palaeontology*, 50(6):1421–1446.

Coates, M. I., Gess, R. W., Finarelli, J. A., Criswell, K. E., and Tietjen, K. (2017). A symmoriiform chondrichthyan braincase and the origin of chimaeroid fishes. *Nature*, 541(7636):208–211.

Coates, M. I. and Sequeira, S. E. K. (1998). The braincase of a primitive shark. *Transactions of the Royal Society of Edinburgh: Earth Sciences*, 89(02):63–85.

Coates, M. I. and Sequeira, S. E. K. (2001). A new stethacanthid chondrichthyan from the Lower Carboniferous of Bearsden, Scotland. *Journal of Vertebrate Paleontology*, 21(3):438–459.

Coates, M. I., Sequeira, S. E. K., Sansom, I. J., and Smith, M. M. (1998). Spines and tissues of ancient sharks. *Nature*, 396(6713):729–730.

Cope, E. D. (1882). On the phylogeny of Vertebrata. *Proceedings of the American Philosophical Society*, 30:278–281.

Cope, E. D. (1889). Synopsis of the families of Vertebrata. *The American Naturalist*, 23:849–877.

Crane, A. (1877). On Certain Genera of Living Fishes and their Fossil Affinities. *Geological Magazine*, 4:209–219.

Davis, S. P., Finarelli, J. A., and Coates, M. I. (2012). *Acanthodes* and shark-like conditions in the last common ancestor of modern gnathostomes. *Nature*, 486:247–250.

Dean, B. (1899). The so-called Devonian "Lamprey", *palaeospondylus gunni* Trq., with notes on the systematic arrangement of the fish-like vertebrates. *Memoirs of the New York Academy of Sciences*, 2:1–32.

Dean, B. (1901). Palæontological Notes: I. On Two New Arhtrodires from the Cleveland Shale of Ohio. II. On the Characters of *Mylostoma* Newberry. III. Further Notes on the Relationships of the Arthrognathi. *Memoirs of the New York Academy of Sciences*, 2:87–124.

Denison, R. (1978). Placodermi. In Schultze, H.-P., editor, *Handbook of Paleoichthyology. Vol. 2*, page 128. Stuttgart: Gustav Fischer Verlag.

Denison, R. H. (1947). The exoskeleton of *Trematapsis*. *American Journal of Science*, 245(6):337–365.

Denison, R. H. (1951). Evolution and classification of the Osteostraci. *Fieldania, Geology*, 11:157–196.

Denison, R. H. (1975). Evolution and classification of placoderm fishes. *Breviora*, 432:1–24.

Dennis, K. and Miles, R. S. (1981). A pachyosteomorph arthrodire from Gogo, Western Australia. *Zoological Journal of the Linnean Society*, 73(3):213–258.

Dennis-Bryan, K. (1987). A new species of eastmanosteid arthrodire (Pisces: Placodermi) from Gogo, Western Australia. *Zoological Journal of the Linnean Society*, 90(1):1–64.

Dennis-Bryan, K. (1995). Some comments on the placoderm parasphenoid. *Bull. du Muséum Natl. Histoire Nat.*, 17:127–142.

Dennis-Bryan, K. and Miles, R. S. (1983). Further eubrachythoracid arthrodires from Gogo, Western Australia. *Zoological Journal of the Linnean Society*, 77(2):145–173.

Dennis-Bryan, K. and Miles, R. S. (2079). Eubrachythoracid arthrodires with tubular rostral plates from Gogo, Western Australia. *Zoological Journal of the Linnean Society*, 67:297–328.

Dick, J. R. F. (1978). On the Carboniferous shark *Tristychius arcuatus* Agassiz from Scotland. *Transactions of the Royal Society of Edinburgh*, 70(04):63–108.

Dick, J. R. F. and Maisey, J. G. (1980). The Scottish Lower Carboniferous shark *Onychoselache traquairi*. *Palaeontology*, 23:363–74.

Donoghue, P. C. J., Forey, P. L., and Aldridge, R. J. (2000). Conodont affinity and chordate phylogeny. *Biol. Rev. Camb. Philos. Soc.*, 75(2):191–251.

Donoghue, P. C. J. and Sansom, I. J. (2002). Origin and early evolution of vertebrate skeletonization. *Microscopy research and technique*, 59(5):352–372.

Donoghue, P. C. J., Sansom, I. J., and Downs, J. P. (2006a). Early evolution of vertebrate skeletal tissues and cellular interactions, and the canalization of skeletal development. *Journal of Experimental Zoology Part B: Molecular and Developmental Evolution*, 306(3):278–294.

Donoghue, P. C. J., Sansom, I. J., and Downs, P. J. (2006b). Early Evolution of Vertebrate Skeletal Tissues and Cellular Interactions , and the Canalization of Skeletal Development. *Journal of Experimental Zoolog*, 306(B):278–294.

Donoghue, P. C. J. and Smith, M. P. (2001). The anatomy of *Turinia pagei* (Powrie), and the phylogenetic status of the Thelodonti. *Transactions of the Royal Society of Edinburgh: Earth Sciences*, 92:15–37.

Downs, J. P. and Donoghue, P. C. J. (2009). Skeletal histology of *Bothriolepis canadensis* (Placodermi, Antiarchi) and evolution of the skeleton at the origin of jawed vertebrates. *Journal of Morphology*, 270(11):1364–1380.

Dupret, V. (2004). The phylogenetic relationships between actinolepids (Placodermi: Arthrodira) and other arthrodires (phlyctaeniids and brachythoracids). *Fossils and Strata*, 50:40–55.

Dupret, V. (2008). A new wuttagoonaspid (Placodermi, Arthrodira) from the Lower Devonian of Yunnan (South China): origin, dispersal, and paleobiogeographic significance. *Journal of Vertebrate Paleontology*, 28(1):12–20.

Dupret, V. (2010). Revision of the genus *Kujdanowiaspis* Stensiö, 1942 (Placodermi, Arthrodira,"Actinolepida") from the Lower Devonian of Podolia (Ukraine). *Geodiversitas*, 32(1):5–63.

Dupret, V., Phuong, T. H., Thanh, T.-D., Phong, N. D., Janvier, P., and Clément, G. (2011). The skull of *Hagiangella goujeti* Janvier, 2005, a high-crested acanthothoracid (Vertebrata, Placodermi) from the Lower Devonian of northern Vietnam. *Journal of Vertebrate Paleontology*, 31(3):531–538.

Dupret, V., Sanchez, S., Goujet, D., and Ahlberg, P. E. (2017a). The internal cranial anatomy of *Romundina stellina* Ørvig, 1975 (Vertebrata, Placodermi, Acanthothoraci) and the origin of jawed vertebrates - Anatomical atlas of a primitive gnathostome. *PloS one*, 12(2):e0171241.

Dupret, V., Sanchez, S., Goujet, D., Tafforeau, P., and Ahlberg, P. E. (2010). Bone vascularization and growth in placoderms (vertebrata): The example of the premedian plate of *Romundina stellina* ørvig, 1975. *Comptes Rendus Palevol*, 9(6-7):369–375.

Dupret, V., Sanchez, S., Goujet, D., Tafforeau, P., and Ahlberg, P. E. (2014). A primitive placoderm sheds light on the origin of the jawed vertebrate face. *Nature*, 507:500–3.

Dupret, V. and Zhu, M. (2007). The earliest phyllolepid (Placodermi, Arthrodira) from the Late Lochkovian (Early Devonian) of Yunnan (South China). *Geol. Mag.*, 145(02):257–278.

Dupret, V., Zhu, M., and Wang, J.-Q. (2009). The morphology of *Yujiangolepis liujingensis* (Placodermi, Arthrodira) and its phylogenetic significance. *Zoological Journal of the Linnean Society*, 157(1):70–82.

Dupret, V., Zhu, M., and Wang, J.-Q. (2017b). Redescription of *Szelepis* Liu, 1981 (Placodermi, Arthrodira) from the lower devonian of China. *Journal of Vertebrate Paleontology*, page e1312422.

Eastman, C. R. (1898). Some new points in dinichthyid osteology. *The American Naturalist*, 32(382):747–768.

Edgeworth, F. H. (1935). *The cranial muscles of vertebrates*. Cambridge University Press.

Elliott, D. K. and Carr, R. K. (2010). A new species of *Bryantolepis* Camp, Welles, and Green, 1949 (Placodermi, Arthrodira) from the Early Devonian Water Canyon Formation of Northern Utah and Southern Idaho, with comments on the endocranium. *Kirtlandia*, 57:22–35.

Ericsson, R., Knight, R., and Johanson, Z. (2013). Evolution and development of the vertebrate neck. *Journal of Anatomy*, 222(1):67âĂŞ–78.

Finarelli, J. A. and Coates, M. I. (2012). First tooth-set outside the jaws in a vertebrate. *Proceedings of the Royal Society of London B: Biological Sciences:rspb20111107*.

Finarelli, J. A. and Coates, M. I. (2014). *Chondrenchelys problematica* (Traquair, 1888) redescribed: a Lower Carboniferous, eel-like holocephalan from scotland. *Earth and Environmental Science Transactions of the Royal Society of Edinburgh*, 105(01):35–59.

Forey, P. (1980). *Latimeria*: a paradoxical fish. *Proceedings of the Royal Society of London. Series B, Biological Sciences*, pages 369–384.

Forey, P. L. (1984). Yet more reflections on Agnatha-gnathostome relationships. *Journal of Vertebrate Paleontology*, 4(3):330–343.

Forey, P. L. (1998). *History of the Coelacanth Fishes*. Chapman and Hall, London.

Forey, P. L. and Gardiner, B. G. (1986). Observations on *Ctenurella* (Ptyctodontida) and the classification of placoderm fishes. *Zoological Journal of the Linnean Society*, 86:43–74.

Forey, P. L. and Janvier, P. (1993). Agnathans and the origin of jawed vertebrates. *Nature*, 361:129–134.

Friedman, M. (2007). *Styloichthys* as the oldest coelacanth: implications for early osteichthyan interrelationships. *Journal of Systematic Palaeontology*, 5(3):289–343.

Gagnier, P. (1996). Acanthodii. In Schultze, H.-P. and Cloutier, R., editors, *Devonian fishes and plants of Miguasha, Quebec, Canada*, pages 149–164. Verlag Dr. Friedrich Pfeil München.

Gagnier, P.-Y., Hanke, G. F., and Wilson, M. V. H. (1999). *Tetanopsyrus lindoei* gen. et sp. nov., an Early Devonian acanthodian from the Northwest Territories, Canada. *Acta Geologica Polonica*, 49(2):81–96.

Gagnier, P.-Y. and Wilson, M. V. H. (1996). Early Devonian acanthodians from northern Canada. *Palaeontology*, 39(2):241–258.

Gai, Z., Donoghue, P. C. J., Zhu, M., Janvier, P., and Stampanoni, M. (2011). Fossil jawless fish from China foreshadows early jawed vertebrate anatomy. *Nature*, 476:324–7.

Gai, Z. and Zhu, M. (2012). The origin of the vertebrate jaw: Intersection between developmental biology-based model and fossil evidence. *Chinese Science Bulletin*, pages 1–10.

Gardiner, B. G. (1984a). The Relationship of Placoderms. *Journal of Vertebrate Paleontology*, 4(3):379–395.

Gardiner, B. G. (1984b). The relationships of the palaeoniscid fishes, a review based on new specimens of *Mimia* and *Moythomasia* from the Upper Devonian of Western Australia. *Bull. Br. Museum (Natural Hist.) Geol.*, 37:173 – 428.

Gardiner, B. G. and Bartram, A. W. H. (1977). The homologies of ventral cranial fissures in osteichthyans. *Problems in Vertebrate Evolution. Academic Press, London*, pages 227–245.

Gardiner, B. G. and Miles, R. S. (1990). A new genus of eubrachythoracid arthrodire from Gogo, Western Australia. *Zoological Journal of the Linnean Society*, 99(2):159–204.

Gardiner, B. G. and Miles, R. S. (1994). Eubrachythoracid arthrodires from Gogo, Western Australia. *Zoological Journal of the Linnean Society*, 112(4):443–477.

Garwood, R. and Dunlop, J. (2014). The walking dead: Blender as a tool for paleontologists with a case study on extinct arachnids. *Journal of Paleontology*, 88:735–746.

Giles, S., Coates, M. I., Garwood, R. J., Brazeau, M. D., Atwood, R., Johanson, Z., and Friedman, M. (2015a). Endoskeletal structure in *Cheirolepis* (Osteichthyes, Actinopterygii), an early ray-finned fish. *Palaeontology*, 58(5):849–870.

Giles, S. and Friedman, M. (2014). Virtual reconstruction of endocast anatomy in early ray-finned fishes (Osteichthyes, Actinopterygii). *Journal of Paleontology*, 88(4):636–651.

Giles, S., Friedman, M., and Brazeau, M. D. (2015b). Osteichthyan-like cranial conditions in an Early Devonian stem gnathostome. *Nature*, 520:82–85.

Giles, S., Rücklin, M., and Donoghue, P. C. J. (2013). Histology of "placoderm" dermal skeletons: Implications for the nature of the ancestral gnathostome. *Journal of Morphology*, 274(6):627–644.

Goloboff, P. A., Farris, J. S., and Nixon, K. C. (2008). Tnt, a free program for phylogenetic analysis. *Cladistics*, 24(5):774–786.

Goujet, D. (1973). *Sigaspis*, un nouvel arthrodire du Dévonien inférieur du Spitsberg. *Palaeontographica Abteilung A*, pages 73–88.

Goujet, D. (1982). Les affinités des placodermes, une revue des hypothèses actuelles. *Geobios Mémoire Spécial*, 6:27–38.

Goujet, D. (1984a). *Les Poissons placodermes du Spitsberg. Arthrodires Dolichothoraci de la Formation de Wood Bay (Dévonien Inférieur).* Cahiers de Paléontologie (section Vertébrés).Éditions du CNRS. Paris.

Goujet, D. (1984b). Placoderm interrelationships: a new interpretation, with a short review of placoderm classifications. *Proceeding of the Linnean Society New South Wales*, 107:211–243.

Goujet, D. (2001). Placoderms and basal gnathostome apomorphies. In Ahlberg, P. E., editor, *Major events in early vertebrate evolution: palaeontology, phylogeny, genetics and development*, pages 209–222. Taylor & Francis, London.

Goujet, D. and Young, G. C. (1995). Interrelationships of placoderms revisited. *Geobios, Mem. Spec.*, 19:89–95.

Goujet, D. and Young, G. C. (2004). Placoderm anatomy and phylogeny: new insights. In Arratia, G., Wilson, M., and Cloutier, R., editors, *Recent advances in the origin and early radiation of vertebrates*, pages 109–126. München: Verlag Dr. Friedrich Pfeil.

Grogan, E. D. and Lund, R. (2000). *Debeerius ellefseni* (Fam. Nov., Gen. Nov., Spec. Nov.), an autodiastylic chondrichthyan from the Mississippian Bear Gulch Limestone of Montana (USA), the relationships of the Chondrichthyes, and comments on gnathostome evolution. *Journal of Morphology*, 243(3):219–245.

Gross, W. (1931). *Asterolepis ornata* Eichw. und das Antiarchi-problem. *Palaeontographica*, 75A:1–62.

Gross, W. (1935). Histologische studien am aussenskelett fossiler Agnathen und Fische. *Palaeontographica Abteilung A*, 86:1–60.

Gross, W. (1937). Die Wirbeltiere des rheinischen Devons. *Abhandlungen der Preussische Geologische Landesanstalt, Neue Folge*, 76:1–83.

Gross, W. (1950). Die paläontologische und stratigraphische Bedeutung der Wirbeltierfaunen des Old Reds und der marinen altpaläozoischen Schichten. *Abhandlungen der Deutschen Akademie der Wissenschaftenzu Berlin. Mathematisch-naturwissenschaftliche Klasse*, (1):1–130.

Gross, W. (1958). Über die älteste Arthrodiren-Gattung. *Notizblatt des Hessischen Landesamtes für Bodenforschung zu Wiesbaden*, 86:7–30.

Gross, W. (1959). Arthrodiren aus dem Obersilur der Prager Mulde. *Palaeontolographica*, 113(A):1–35.

Gross, W. (1961). *Lunaspis broilii* und *Lunaspis heroldi* aus dem Hunsrückschiefer (Unterdevons, Rheinland). *Notizblatt Hessisches Landesamtes für Bodenforschung zu Wiesbaden*, 89:17–43.

Gross, W. (1963). *Gemuendina stuertzi* Traquair. Neuuntersuchung. *Notizblatt des Hessischen Landesamtes für Bodenforschung zu Wiesbaden*, 91:36–73.

Hamel, M.-H. and Poplin, C. (2008). The braincase anatomy of *Lawrenciella schaefferi*, actinopterygian from the Upper Carboniferous of Kansas (U.S.A.). *Journal of Vertebrate Paleontology*, 28(4):989–1006.

Hanke, G. F. (2008). *Promesacanthus eppleri* n. gen., n. sp., a mesacanthid (Acanthodii, Acanthodiformes) from the Lower Devonian of northern Canada. *Geodiversitas*, 30(2):287–302.

Hanke, G. F. and Davis, S. P. (2008). Redescription of the acanthodian *Gladiobranchus probaton* Bernacsek & Dineley, 1977, and comments on diplacanthid relationships. *Geodiversitas*, 30(2):303–330.

Hanke, G. F. and Davis, S. P. (2012). A re-examination of *Lupopsyrus pygmaeus* Bernacsek & Dineley, 1977 (Pisces, Acanthodii). *Geodiversitas*, 34(3):469–487.

Hanke, G. F., Davis, S. P., and Wilson, M. V. H. (2001). New species of the acanthodian genus *Tetanopsyrus* from northern Canada, and comments on related taxa. *Journal of Vertebrate Paleontology*, 21(4):740–753.

Hanke, G. F. and Wilson (2010). The putative stem-group chondrichthyans *Kathemacanthus* and *Seretolepis* from the Lower Devonian MOTH locality, Mackenzie Mountains, Canada. In Elliott, D., Maisey, J., Yu, X., and Miao, D., editors, *Morphology, Phylogeny and Paleobiogeography of Fossil Fishes, Honoring Meemann Chang. Verlag Dr. Friedrich Pfeil München*, pages 159–182.

Hanke, G. F. and Wilson, M. V. H. (2004). New teleostome fishes and acanthodian systematics. In Arratia, G., Wilson, M. V. H., and Cloutier, R., editors, *Recent Advances in the Origin and Early Radiation of Vertebrates.*, pages 189–216. Verlag Dr. Friedrich Pfeil Munich.

Hanke, G. F. and Wilson, M. V. H. (2006). Anatomy of the Early Devonian acanthodian *Brochoadmones milesi* based on nearly complete body fossils, with comments on the evolution and development of paired fins. *Journal of Vertebrate Paleontology*, 26(3):526–537.

Harris, J. E. (1938). The dorsal spine of *Cladoselache*. *Scientific Publications of the Cleveland Museum of Natural History*, 8:1–12.

Heintz, A. (1939). *Cephalaspida from Downtonian of Norway*, volume 5. Skrifter utgitt av Det Norske Videnskaps-Akademi i Oslo. Matematisk- Naturvidenskapelig Klasse.

Hemmings, S. K. (1978). *The old red sandstone antiarchs of Scotland: Pterichthyodes and Microbrachius*. Palaeontographical Society Monographs 131.

Holland, T. (2013). Pectoral girdle and fin anatomy of *Gogonasus andrewsae* Long, 1985: implications for tetrapodomorph limb evolution. *Journal of morphology*, 274(2):147–164.

Holland, T. (2014). The endocranial anatomy of *Gogonasus andrewsae* Long, 1985 revealed through micro CT-scanning. *Earth and Environmental Science Transactions of the Royal Society of Edinburgh*, 105(01):9–34.

Hussakof, L. (1905). Notes on the Devonian "placoderm", *Dinichthys intermedius* Newb. *Bulletin of the American Museum of Natural History*, 21:27–36.

Hussakof, L. (1906). Studies on the Arthrodira. *Memoire of the American Museum of Natural History*, 3:103–154.

Huxley, T. H. (1861). *Preliminary essay upon the systematic arrangement of the fishes of the Devonian epoch*. Memoirs âĂŞ Geological Survey of the United Kingdom.

Janvier, P. (1975). Les yeux des Cyclostomes fossiles et le problème de l'origine des Myxinoïdes. *Acta Zoologica*, 56(1):1–9.

Janvier, P. (1981). *Norselaspis glacialis* ng, n. sp. et les relations phylogénétiques entre les Kiaeraspidiens (Osteostraci) du Dévonien inférieur du Spitsberg. *Palaeovertebrata*, 11:19–131.

Janvier, P. (1985a). *Les Céphalaspides du Spitsberg*. Cahiers de Paléontologie (section Vertébrés).Éditions du CNRS., Paris.

Janvier, P. (1985b). Les Thyestidiens (Osteostraci) du Silurien de Saaremaa (Estonie). *Annales de Paléontologie*, 71:83–147.

Janvier, P. (1996a). *Early Vertebrates*. Oxford: Clarendon Press.

Janvier, P. (1996b). The dawn of the vertebrates: characters versus common ascent in the rise of current vertebrate phylogenies. *Palaeontology*, 39(2):259–287.

Janvier, P. (2008). Early jawless vertebrates and cyclostome origins. *Zoological Science*, 25(10):1045–1056.

Janvier, P. (2015). Facts and fancies about early fossil chordates and vertebrates. *Nature*, 520:483–489.

Janvier, P., Arsenault, M., and Desbiens, S. (2004). Calcified cartilage in the paired fins of the osteostracan *Escuminaspis laticeps* (Traquair 1880), from the Late Devonian of Miguasha (Québec, Canada), with a consideration of the early evolution of the pectoral fin endoskeleton in vertebrates. *Journal of Vertebrate Paleontology*, 24(4):773–779.

Janvier, P. and Blieck, A. (1979). New Data on the Internal Anatomy of the Heterostraci (Agnatha), with General Remarks on the Phylogeny of the Craniata. *Zoologica scripta*, 8(1-4):287–296.

Janvier, P., Thanh, T. D., and Phuong, T. H. (1993). A new Early Devonian galeaspid from Bac Thai Province, Vietnam. *Palaeontology*, 36:297–297.

Jarvik, E. (1972). Middle and Upper Devonian Porolepiformes from East Greenland with special reference to *Glyptolepis groenlandica* N. Sp.: and a discussion on the structure of the head in the porolepiformes. *Palaeontogr. Abt. A Palaeozool-Stratigr*, 167:180–214.

Jarvik, E. (1980). *Basic structure and evolution of vertebrates*. London: Academic Press.

Jessen, H. (1980). Lower Devonian porolepiformes from the canadian arctic with special reference to *Powichthys thorsteinssoni* jessen. *Palaeontographica Abteilung A*, pages 180–214.

Ji, S. (1996). The biostratigraphy of petalichthyids (Placodermi) in China. *Journal of Stratigraphy*, 20:161–164.

Ji, S. and Pan, J. (1997). The macropetalichthyids (Placodermi) from Guangxi and Hunan, China. *Vertebrata PalAsiatica*, 35(1):18–34.

Johanson, Z. (1997). New *Remigolepis* (Placodermi; Antiarchi) from Canowindra, New South wales, Australia. *Geological Magazine*, 134(06):813–846.

Johanson, Z. (2003). Placoderm branchial and hypobranchial muscles and origins in jawed vertebrates. *Journal of Vertebrate Paleontology*, 23(4):735–749.

Keating, J. N., Marquart, C. L., and Donoghue, P. C. J. (2015). Histology of the heterostracan dermal skeleton: insight into the origin of the vertebrate mineralised skeleton. *Journal of morphology*, 276(6):657–680.

Kiær, J. (1915). Upper Devonian fish remains from Ellesmere Land, with remarks on *Drepanaspis*. *Rep. Second Nor. Arct. Exped. "Fram" 1898-1902*, 33.

King, B., Qiao, T., Lee, M. S. Y., Zhu, M., and Long, J. A. (2016). Bayesian Morphological Clock Methods Resurrect Placoderm Monophyly and Reveal Rapid Early Evolution in Jawed Vertebrates. *Systematic Biology*, page syw107.

Kusakabe, R., Kuraku, S., and Kuratani, S. (2011). Expression and interaction of muscle-related genes in the lamprey imply the evolutionary scenario for vertebrate skeletal muscle, in association with the acquisition of the neck and fins. *Developmental biology*, 350(1):217–227.

Lewis, P. O. (2001). A likelihood approach to estimating phylogeny from discrete morphological character data. *Systematic biology*, 50(6):913–925.

Liu, Y. (1965). New devonian agnathans from Yunnan. *Vertebrata PalAsiatica*, 9(2):125–134.

Liu, Y. (1975). Lower Devonian agnathans of Yunnan and Sichuan. *Vertebrata PalAsiatica*, 13(4):202–216.

Liu, Y.-h. (1973). On the New Forms of Polybranchiaspiformes and Petalichthyida from Devonian of South-west China. *Vertebrata PalAsiatica*, 11(2):132–143.

Liu, Y. H. (1991). On a new petalichthyid, *Eurycaraspis incilis* gen. et sp. nov., from the Middle Devonian of Zhanyi, Yunnan. In Chang, M., Liu, Y., and Zhang, G., editors, *Early Vertebrates and Related Problems of Evolutionary Biology.*, pages 139–177. Science Press, Beijing.

Long, J. A. (1983). A new diplacanthoid acanthodian from the Late Devonian of Victoria. *Memoirs of the Association of Australasian Palaeontologists*, 1:51–65.

Long, J. A. (1984). New Phyllolepids from Victoria and the Relationships of the Group. *Proceeding of the Linnean Society New South Wales*, 107(3):263–308.

Long, J. A. (1985). A new osteolepidid fish from the Upper Devonian Gogo Formation, Western Australia. *Records of the Western Australian Museum*, 12:361–377.

Long, J. A. (1988). New palaeoniscoid fishes from the Late Devonian and Early Carboniferous of Victoria. *Memoirs of the Association of Australasian Palaeontologists*, 7:1–64.

Long, J. A. (1997). Ptyctodontid fishes (Vertebrata, Placodermi) from the Late Devonian Gogo Formation, WesternAustralia, with a revision of the European genus *Ctenurella* Ørvig, 1960. *Geodiversitas*, 19(3):515–555.

Long, J. A., Barwick, R. E., and Campbell, K. S. W. (1997). Osteology and functional morphology of the osteolepiform fish *Gogonasus andrewsae* Long, 1985, from the Upper Devonian Gogo Formation, Western Australia. *Records of the Western Australian Museum. Supplements*, 53:1–89.

Long, J. A., Mark-Kurik, E., Johanson, Z., Lee, M. S., Young, G. C., Min, Z., Ahlberg, P. E., Newman, M., Jones, R., den Blaauwen, J., et al. (2015). Copulation in antiarch placoderms and the origin of gnathostome internal fertilization. *Nature*, 517:196–199.

Long, J. A., Mark-Kurik, E., and Young, G. C. (2014). Taxonomic revision of buchanosteoid placoderms (Arthrodira) from the Early Devonian of south-eastern Australia and Arctic Russia. *Australian journal of zoology*, 62(1):26–43.

Long, J. A., Trinajstic, K., and Johanson, Z. (2009). Devonian arthrodire embryos and the origin of internal fertilization in vertebrates. *Nature*, 457:1124–1127.

Long, J. A., Trinajstic, K., Young, G. C., and Senden, T. (2008). Live birth in the Devonian period. *Nature*, 453(7195):650–652.

Long, J. A., Young, G. C., Holland, T., Senden, T. J., and Fitzgerald, E. M. G. (2006). An exceptional Devonian fish from Australia sheds light on tetrapod origins. *Nature*, 444(7116):199–202.

Lu, J., Giles, S., Friedman, M., den Blaauwen, J. L., and Zhu, M. (2016). The oldest actinopterygian highlights the cryptic early history of the hyperdiverse ray-finned fishes. *Current Biology*, 26(12):1602–1608.

Lukševičs, E. (2001). The orbito-nasal area of *Asterolepis ornata*, a Middle Devonian placoderm fish. *Journal of Vertebrate Paleontology*, 21(4):687–692.

Maddison, W. P. and Maddison, D. R. (2017). Mesquite: a modular system for evolutionary analysis. *Version 3.31*.

Maisey, J., Miller, R., and Turner, S. (2009). The braincase of the chondrichthyan *Doliodus* from the Lower Devonian Campbellton formation of New Brunswick, Canada. *Acta Zoologica*, 90(1):109–122.

Maisey, J. G. (1989). *Hamiltonichthys mapesi*, g. & sp. nov. (Chondrichthyes, Elasmobranchii), from the Upper Pennsylvanian of Kansas. *American Museum novitates. 2931.*, pages 1–42.

Maisey, J. G. (2001a). A primitive chondrichthyan braincase from the Middle Devonian of Bolivia. In Ahlberg, P., editor, *Major events in early vertebrate evolution*, pages 263–288. London and New York: Taylor and Francis.

Maisey, J. G. (2001b). Remarks on the inner ear of elasmobranchs and its interpretation from skeletal labyrinth morphology. *Journal of Morphology*, 250(3):236–264.

Maisey, J. G. (2005). Braincase of the Upper Devonian shark *Cladodoides wildungensis* (Chondrichthyes, Elasmobranchii), with observations on the braincase in early chondrichthyans. *Bulletin of the American Museum of Natural History*, 288:1–103.

Maisey, J. G. (2007). The braincase in Paleozoic symmoriiform and cladoselachian sharks. *Bulletin of the American Museum of Natural History*, pages 1–122.

Maisey, J. G. and Lane, J. A. (2010). Labyrinth morphology and the evolution of low-frequency phonoreception in elasmobranchs. *Comptes Rendus Palevol*, 9(6):289–309.

Mark-Kurik, E. (1973). *Kimaspis*, a new palaeacanthaspid from the Early Devonian of Central Asia. *Eesti NSV teaduste akadeemia toimetised*, 22(4):322–330.

Mayr, U. (1994). Chapter 1, Introduction. In Mayr, U., Packard, J. J., Goodbody, Q. H., Okulitch, A. V., Rice, R. J., Goodarzi, F., and R., S. K., editors, *The Phanerozoic Geology of Southern Ellesmere Island and North Kent Islands, Canadian Arctic Archipelago.*, page 298. Geological Society of Canada Bulletin 470.

M'Coy, F. (1848). On some new fossil fish of the Carboniferous period. *Annals and Magazine of Natural History*, 2:1–10.

Miles, R. S. (1967). Observations on the ptyctodont fish, *Rhamphodopsis* Watson. *Journal of the Linnean Society*, 47:99–120.

Miles, R. S. (1971). The Holonematidae (placoderm fishes), a review based on new specimens of *Holonema* from the Upper Devonian of Western Australia. *Philosophical Transactions of the Royal Society of London. Series B, Biological Sciences*, pages 101–234.

Miles, R. S. (1973a). Articulated acanthodian fishes from the Old Red Sandstone of England, with a review of the structure and evolution of the acanthodian shoulder-girdle. *Bulletin of the British Museum (Natural History): Geology*, 24:113–213.

Miles, R. S. (1973b). Relationships of acanthodians. In Greenwood, P. H., Miles, R. S., and Patterson, C., editors, *Interrelationships of fishes*, pages 63–104. Zoological Journal of the Linnean Society, London.

Miles, R. S. and Westoll, T. S. (1968). Ix.-the placoderm fish *Coccosteus cuspidatus* Miller ex Agassiz from the Middle Old Red Sandstone of Scotland. Part I. Descriptive morphology. *Earth and Environmental Science Transactions of The Royal Society of Edinburgh*, 67(9):373–476.

Miles, R. S. and Young, G. C. (1977). Placoderm interrelationships reconsidered in the light of new ptyctodontids from Gogo Western Australia. In Andrews, S. M., Miles, R. S., and Walker, A. D., editors, *Problems in Vertebrate Evolution*, pages 123–198. London: Academic Press.

Miller, R. F., Cloutier, R., and Turner, S. (2003). The oldest articulated chondrichthyan from the Early Devonian period. *Nature*, 425(6957):501–504.

Miyashita, T. (2016). Fishing for jaws in early vertebrate evolution: a new hypothesis of mandibular confinement. *Biological Reviews*, 91(3):611–657.

Moy-Thomas, J. A. (1935). The Structure and Affinities of *Chondrenchelys problematica* Traquair. *Proceedings of the Zoological Society of London*, 105(2):391–404.

Moy-Thomas, J. A. (1936). On the structure and affinities of the Carboniferous cochliodont *Helodus simplex*. *Geol.Mag*, 73:488–503.

Moy-Thomas, J. A. (1939). *Palaeozoic fishes*. Methuen & Co, London.

Moy-Thomas, J. A. and Miles, R. S. (1971). *Palaeozoic Fishes. 2nd Edition*. Chapman & Hall, London.

Newberry, J. S. (1875). Description of fossil fishes. *Report of the Geological Survey of Ohio*, 2:1–64.

Newman, M. J., Burrow, C. J., Den Blaauwen, J. L., and Davidson, R. G. (2014). The Early Devonian acanthodian *Euthacanthus macnicoli* Powrie, 1864 from the Midland Valley of Scotland. *Geodiversitas*, 36(2):321–348.

Nixon, K. C. (1999). The parsimony ratchet, a new method for rapid parsimony analysis. *Cladistic*, 15:407–414.

Northcutt, R. G., Holmes, P. H., and Albert, J. S. (2000). Distribution and innervation of lateral line organs in the channel catfish. *Journal of Comparative Neurology*, 421(4):570–592.

Obruchev, D. V. (1964). Class placodermi. *Fundamentals of palaeontology*, 11:118–174.

Olive, S., Goujet, D., Lelièvre, H., and Janjou, D. (2011). A new Placoderm fish (Acanthothoraci) from the Early Devonian Jauf Formation (Saudi Arabia). *Geodiversitas*, 33(3):393–409.

O'Reilly, J. E., Puttick, M. N., Parry, L., Tanner, A. R., Tarver, J. E., Fleming, J., Pisani, D., and Donoghue, P. C. J. (2016). Bayesian methods outperform parsimony but at the expense of precision in the estimation of phylogeny from discrete morphological data. *Biology letters*, 12(4):20160081.

Ørvig, T. (1957). Notes on some Paleozoic lower vertebrates from Spitsbergen and North America. *Nor. Geol. Tidsskr.*, 37(3-4):285–353.

Ørvig, T. (1975). Description, with special reference to the dermal skeleton, of a new radotinid arthrodire from the Gedinnian of Arctic Canada. In *Colloque Internatl. CNRS*, volume 218, pages 41–71.

P'an, K. and Wang, S. T. (1978). Devonian Agnatha and Pisces of South China. In Institute of Mineral Resources, C. A. o. G. S. E., editor, *Symposium on the Devonian System of South China.*, pages 298–333. Geological Press, Beijing.

P'an, K., Wang, S. T., and Liu, Y. P. (1975). The lower devonian agnatha and pisces from south china. *Prof Pap Stratigr Paleont,(1)*, pages 135–169.

Pan, Z., Zhu, M., Zhu, Y., and Jia, L. (2015). A new petalichthyid placoderm from the Early Devonian of Yunnan, China. *Comptes Rendus Palevol*, 14(2):125–137.

Pan, Z., Zhu, M., Zhu, Y., and Jia, L. (2017). A new antiarch placoderm from the Emsian (Early Devonian) of Wuding, yunnan, China. *Alcheringa: An Australasian Journal of Palaeontology*, pages 1–12.

Patten, W. (1904). New facts concerning *Bothriolepis*. *The Biological Bulletin*, 7(2):113–124.

Patten, W. (1931). New ostracoderms from oesel. *Science*, 73(1903):671–673.

Patterson, C. (1982). Morphological characters and homology. *Problems of phylogenetic reconstruction*, pages 21–74.

Pearson, D. M. and Westoll, T. S. (1979). The Devonian actinopterygian *Cheirolepis* Agassiz. *Transactions of the Royal Society of Edinburgh*, 70(13-14):337–399.

Pradel, A. (2010). Skull and brain anatomy of a Late Carboniferous Sibyrhynchidae (Chondrichthyes, Iniopterygia) from Kansas and Oklahoma (USA). *Geodiversitas*, 32(4):595–661.

Pradel, A., Maisey, J. G., Tafforeau, P., and Janvier, P. (2009). An enigmatic gnathostome vertebrate skull from the Middle Devonian of Bolivia. *Acta Zoologica*, 90(s1):123–133.

Pradel, A., Tafforeau, P., Maisey, J. G., and Janvier, P. (2011). A new Paleozoic Symmoriiformes (chondrichthyes) from the Late Carboniferous of Kansas (USA) and cladistic analysis of early chondrichthyans. *Plos one*, 6(9):e24938.

Prendini, L. (2001). Species or supraspecific taxa as terminals in cladistic analysis? Groundplans versus exemplars revisited. *Systematic Biology*, 50(2):290–300.

Qiao, T., King, B., Long, J. A., Ahlberg, P. E., and Zhu, M. (2016). Early gnathostome phylogeny revisited: multiple method consensus. *PloS one*, 11(9):e0163157.

Qiao, T. and Zhu, M. (2010). Cranial morphology of the silurian sarcopterygian *Guiyu oneiros* (Gnathostomata: Osteichthyes). *Science China Earth Sciences*, 53(12):1836–1848.

Rayner, D. H. (1952). Iii.-On the Cranial Structure of an Early Palæoniscid, *Kentuckia*, gen. nov. *Transactions of the Royal Society of Edinburgh*, 62(01):53–83.

Regan, C. T. (1904). The phylogeny of the Teleostomi. *Annals and Magazine of Natural History*, 4:329–349.

Ritchie, A. (1973). *Wuttagoonaspis* gen.nov., an unusual arthrodire from the Devonian of Western New South Wales, Australia. *Palaeontographica A (Paleozoology, Stratigraphy)*, 143:58–72.

Ritchie, A. (2004). A new genus and two new species of groenlandaspidid arthrodire (Pisces: Placodermi) from the Early-Middle Devonian Mulga Downs Group of western New South Wales, Australia. *Fossils and Strata*, 50:56–81.

Ritchie, A. (2005). *Cowralepis*, a new genus of phyllolepid fish (Pisces, Placodermi) from the late Middle Devonian of New South Wales, Australia. *Proceedings of the Linnean Society of New South Wales*, 126:215.

Ritchie, A., Wang, S. T., Young, G. C., and Zhang, G. R. (1992). The Sinolepidae, a family of antiarchs (placoderm fishes) from the Devonian of South China and eastern Australia. *Records of the Australian Museum*, 44(3):319–370.

Robertson, G. M. (1939). An Upper Silurian vertebrate horizon, with description of a new species, *Cephalaspis oeselensis*. *Transactions of the Kansas Academy of Science (1903-)*, 42:357–363.

Rogers, S. W. (1999). *Allosaurus*, crocodiles, and birds: evolutionary clues from spiral computed tomography of an endocast. *The Anatomical Record*, 257(5):162–173.

Romer, A. S. (1945). *Vertebrate Paleontology*. University of Chicago Press, Chicago, 2 edition.

Romer, A. S. (1966). *Vertebrate Paleontology*. University of Chicago Press, Chicago, 3 edition.

Ronquist, F. and Huelsenbeck, J. P. (2003). Mrbayes 3: Bayesian phylogenetic inference under mixed models. *Bioinformatics*, 19(12):1572–1574.

Rücklin, M., Donoghue, P. C. J., Johanson, Z., Trinajstic, K., Marone, F., and Stampanoni, M. (2012). Development of teeth and jaws in the earliest jawed vertebrates. *Nature*, 491:748–51.

Sampson, S. D. and Witmer, L. M. (2007). Craniofacial anatomy of *Majungasaurus crenatissimus* (Theropoda: Abelisauridae) from the late Cretaceous of Madagascar. *Journal of Vertebrate Paleontology*, 27(8):32–102.

Sansom, R. S. (2008). The origin and early evolution of the Osteostraci (Vertebrata): a phylogeny for the Thyestiida. *Journal of Systematic Palaeontology*, 6(3):317–332.

Sansom, R. S. (2009). Phylogeny, classification and character polarity of the Osteostraci (Vertebrata). *Journal of Systematic Palaeontology*, 7(1):95–115.

Schaeffer, B. (1975). Comments on the origin and basic radiation of the gnathostome fishes with particular reference to the feeding mechanism. *Colloque International Centre National de la Recherche Scientifique*, 218:101–109.

Schaeffer, B. (1981). The xenacanth shark neurocranium, with comments on elasmobranch monophyly. *Bulletin of the American Museum of Natural History*, 169:3–66.

Schultze, H.-P. (1968). Palaeoniscoidea-Schuppen aus dem Unterdevon Australiens und Kanadas und aus dem Mitteldevon Spitzbergens. *Bulletin of the British Museum (Natural History)*, 16(7):341–368.

Schultze, H.-P. and Cumbaa, S. L. (2001). *Dialipina* and the characters of basal actinopterygians. In Ahlberg, P., editor, *Major events in early vertebrate evolution*, pages 315–332. Oxford University Press Oxford.

Schultze, H.-P. and Zidek, J. (1982). Ein primitiver acanthodier (pisces) aus dem Unterdevon Lettlands. *Paläontologische Zeitschrift*, 56(1-2):95–105.

Sikes, D. S. and Lewis, P. O. (2001). Software manual for PAUPRat: A tool to implement parsimony ratchet searches using PAUP*. *University of Connecticut, Storrs, CT*.

Sollas, I. B. J. and Sollas, W. J. (1914). A Study of the Skull of a *Dicynodon* by means of Serial Sections. *Philosophical Transactions of the Royal Society of London B: Biological Sciences*, 204(303-312):201–225.

Sollas, W. J. (1904). A method for the investigation of fossils by serial sections. *Philosophical Transactions of the Royal Society of London. Series B, Containing Papers of a Biological Character*, 196:259–265.

Song, W. and Song, J. (2012). Morphological structure and peripheral innervation of the lateral line system in the Siberian sturgeon (*Acipenser baerii*). *Integrative zoology*, 7(1):83–93.

Stensiö, E. (1925). On the head of the macropetalichthyids with certain remarks on the head of the other arthrodires. *Publications of the Field Museum of Natural History, Geo- logical Series*, 4:87–197.

Stensiö, E. (1950). La cavité labyrinthique, l'ossification sclérotique et l'orbite de *Jagorina*. In *Paleontologie et transformisme. Sciences d'aujourd'hui.*, pages 9–44. Colloques International CNRS, Paris.

Stensiö, E. (1963a). Anatomical studies on the arthrodiran head. Pt 1. Preface, geological and geographical distribution, and organisation of the arthrodires, the anatomy of the head in the Dolichothoraci, Coccosteomorphi and Pachyosteomorphi. *K. Sven. Vetenskapsakademiens Handl.*, 1:1–419.

Stensiö, E. (1963b). The brain and the cranial nerves in fossil, lower craniate vertebrates. *Skriflter Ulgitt Av Det Nor. Videnskaps-Akademi*, (13):1–120.

Stensiö, E. (1969). Elasmobranchiomorphi Placodermata Arthrodires. In Piveteau, J., editor, *Trait. Paléontologie 4*, pages 71–692. Masson, Paris.

Stensiö, E. A. (1932). *The Cephalaspids of Great Britain*. British Museum (Natural History), London, 220 pp.

Sutton, M. D. (2008). Tomographic techniques for the study of exceptionally preserved fossils. *Proceedings of the Royal Society of London B: Biological Sciences*, 275(1643):1587–1593.

Sutton, M. D., Briggs, D. E. G., Siveter, D. J., and Siveter, D. J. (2001). Methodologies for the visualization and reconstruction of three-dimensional fossils from the Silurian Herefordshire Lagerstätte. *Palaeontologia Electronica*, 4(1):1–17.

Sutton, M. D., Rahman, I., and Garwood, R. (2014). *Techniques for virtual palaeontology*. John Wiley & Sons.

Swafford, D. L. (2003). PAUP*. phylogenetic analysis using parsimony (* and other methods) v.4.0b 10. *Sinauer Associates*.

Tada, M. N. and Kuratani, S. (2015). Evolutionary and developmental understanding of the spinal accessory nerve. *Zoological letters*, 1(1):4.

Taverne, L. (1997). *Osorioichthys marginis*, "paléonisciforme" du Famennien de Belgique, et la phylogénie des Actinoptérygiens dévoniens (Pisces). *Bulletin de l'institut Royal des Sciences Naturelles de Belgique*, 67:57–78.

Thanh, T.-D. and Janvier, P. (1990). Les Vertébrés du Dévonien inférieur du Bac Bo oriental (province de Bac Thai et Lang son, Viêtam). *Bull. Mus. Nat. Paris*, 12:143–223.

Thomson, K. S. (1965). The endocranium and associated structures in the Middle Devonian rhipidistian fish *Osteolepis*. *Proceedings of the Linnean Society of London*, 176(2):181–195.

Trinajstic, K., Boisvert, C., Long, J. A., Maksimenko, A., and Johanson, Z. (1979). Pelvic and reproductive structures in placoderms (stem gnathostomes). *Biological reviews of the Cambridge Philosophical Society*, 67(4):297–328.

Trinajstic, K., Long, J. A., Johanson, Z., Young, G. C., and Senden, T. (2012). New morphological information on the ptyctodontid fishes (Placodermi, Ptyctodontida) from Western Australia. *Journal of Vertebrate Paleontolology*, 32(4):757–780.

Trinajstic, K., Sanchez, S., Dupret, V., Tafforeau, P., Long, J. A., Young, G. C., Senden, T., Boisvert, C., Power, N., and Ahlberg, P. E. (2013). Fossil musculature of the most primitive jawed vertebrates. *Science*, 314(6142):160–164.

Valiukevicius, J. (1992). First articulated *Poracanthodes* from the Lower Devonian of Severnaya Zemlya. *Fossil fishes as living animals. Academy of Sciences of Estonia, Tallinn*, pages 193–214.

Vaškaninová, V. and Ahlberg, P. E. (2017). Unique diversity of acanthothoracid placoderms (basal jawed vertebrates) in the Early Devonian of the Prague Basin, Czech Republic: A new look at *Radotina* and *Holopetalichthys*. *PloS one*, 12(4):e0174794.

Wang, N.-Z., Donoghue, P. C. J., Smith, M. M., and Sansom, I. J. (2005). Histology of the galeaspid dermoskeleton and endoskeleton, and the origin and early evolution of the vertebrate cranial endoskeleton. *Journal of Vertebrate Paleontology*, 25(4):745–756.

Wängsjö, G. (1952). The Downtonian and Devonian vertebrates of Spitsbergen. ix, Morphologic and systematic studies of the Spitsbergen Cephalaspids. Results of Th. Vogt's Expedition 1928 and the English-Norwegian-Swedish Expedition in 1939. *Norsk Polarinstitutt Skrifter*, 97:1–611.

Watson, D. M. S. (1937). The acanthodian fishes. *Philosophical Transactions of the Royal Society of London. Series B, Biological Sciences*, pages 49–146.

Watson, D. M. S. (1954). A consideration of ostracoderms. *Philosophical Transactions of the Royal Society of London B: Biological Sciences*, 238(652):1–25.

Westoll, T. S. (1936). On the structures of the dermal ethmoid shield of *Osteolepis*. *Geological Magazine*, 73:157–171.

White, E. I. (1958). On *Cephalaspis lyelli* Agassiz. *Palaeontology*, 1(2):99–105.

White, E. I. and Toombs, H. A. (1972). *The buchanosteid arthrodires of Australia*. British Museum (Natural History).

Williams, M. E. (1998). A new specimen of *Tamiobatis vetustus* (Chondrichthyes, Ctenacanthoidea) from the Late Devonian Cleveland Shale of Ohio. *Journal of Vertebrate Paleontology*, 18(2):251–260.

Wills, L. J. (1935). Xviii.- Rare and New Ostracoderm Fishes from the Downtonian of Shropshire. *Earth and Environmental Science Transactions of The Royal Society of Edinburgh*, 58(2):427–447.

Woodward, A. S. (1891). *Catalogue of the fossil fishes in the British Museum (Natural History)*, volume 2. British Museum.

Woodward, A. S. (1941). The head shield of a new macropetalichthyids (*Notopetalichthys hillsi*, gen. et sp. nov.) from the Midlle Devonian of Australia. *Annals and Magazine of Natural History*, 8:91–96.

Wueringer, B. E. and Tibbetts, I. R. (2008). Comparison of the lateral line and ampullary systems of two species of shovelnose ray. *Reviews in Fish Biology and Fisheries*, 18(1):47–64.

Young, G. (1985). Further petalichthyid remains (Placoderm fishes, Early Devonian) from the Taemas-Wee Jasper region, New South Wales. *Journal of Australian Geology & Geophysics*, 9:121–131.

Young, G. C. (1978). A new Early Devonian petalichthyid fish from the Taemas/Wee Jasper region of New South Wales. *Alcheringa: An Australasian Journal of Palaeontology*, 2(2):103–116.

Young, G. C. (1979). New information on the structure and relationships of *Buchanosteus* (Placodermi : Euarthrodira) from the Early Devonian of New South Wales. *Zoological Journal of the Linnean Society*, 66:309–352.

Young, G. C. (1980). A new Early Devonian placoderm from New South Wales, Australia, with a discussion of placoderm phylogeny. *Palaeontographica*, 167(A):10–76.

Young, G. C. (1984). Reconstruction of the jaws and braincase in the Devonian placoderm fish *Bothriolepis*. *Palaeontology*, 27(3):635–661.

Young, G. C. (1986). The relationships of placoderm fishes. *Zoological Journal of the Linnean Society*, 88(1):1–57.

Young, G. C. (2008). The relationships of antiarchs (Devonian placoderm fishes) - evidence supporting placoderm monophyly. *Journal of Vertebrate Paleontology*, 28(3):626–636.

Young, G. C. (2009). New arthrodires (Family Williamsaspididae) from Wee Jasper, New South Wales (Early Devonian), with comments on placoderm morphology and palaeoecology. *Acta Zoologica*, 90:69–82.

Young, G. C. (2010). Placoderms (Armored Fish): Dominant Vertebrates of the Devonian Period. *Annual Review of Earth and Planetary Sciences*, 38(1):523–550.

Yu, X. (1998). A new porolepiform-like fish, *Psarolepis romeri*, gen. et sp. nov.(Sarcopterygii, Osteichthyes) from the Lower Devonian of Yunnan, China. *Journal of Vertebrate Paleontology*, 18(2):261–274.

Zhang, G.-R., Wang, J.-Q., and Wang, N.-Z. (2001). The structure of pectoral fin and tail of Yunnanolepidoidei, with a discussion of the pectoral fin of chuchinolepids. *Vertebrata PalAsiatica*, 39:9–19.

Zhang, M. (1980a). Preliminary note on a Lower Devonian antiarch from Yunnan, China. *Vertebrata PalAsiatica [in Chinese with English abstract]*, 28:179–190.

Zhang, M. (1982). *The braincase of Youngolepis, a Lower Devonian crossopterygian from Yunnan, south-western China*. PhD thesis. Swedish Museum of Natural History, Stockholm.

Zhang, M. M. (1980b). Preliminary note on a Lower Devonian antiarch from Yunnan, China. *Vertebrata PalAsiatica*, 18(3):179.

Zhang, M.-M. and Yu, X.-B. (1981). A new crossopterygian, *Youngolepis praecursor*, gen. et sp. nov., from Lower Devonian of Eastern Yunnan, China. *Scientia Sinica*, 24(1):89–99.

Zhao, W., Zhu, M., and Jia, L. (2001). New discovery of galeaspids from Early Devonian of Wenshan, southeastern Yunnan, China. *Vertebrata PalAsiatica*, 40(2):97–113.

Zhao, W. J. and Zhu, M. (2010). Siluro-Devonian vertebrate biostratigraphy and biogeography of China. *Palaeoworld*, 19(1):4–26.

Zhu, M. (1991). New information on *Diandongpetalichthys* (Placodermi: Petalichthyida). In Chang, M.-M., Liu, Y.-H., and Zhang, G.-R., editors, *Early vertebrates and related problems of evolutionary biology*, pages 179–194. Science Press, Beijing.

Zhu, M. (1996). The Phylogeny of Antiarcha (Placodermi, Pisces), with the Description of Early Devonian Antiarchs from Qujing, Yunnan, China. *Bulletin of the American Museum of Natural History. Section C*, 4:2–3.

Zhu, M. (2000). Catalogue of Devonian vertebrates in China, with notes on bio-events. In Blieck, A. and Turner, S., editors, *Palaeozoic Vertebrate Biochronology and Global Marine/Non-Marine Correlation. Final Report of IGCP 328 (1991-1996)*, pages 373–390. Courier Forschun- ginstitut Senckenberg, Frankfurt.

Zhu, M. and Ahlberg, P. E. (2004). The origin of the internal nostril of tetrapods. *Nature*, 432(7013):94–97.

Zhu, M., Ahlberg, P. E., Pan, Z., Zhu, Y., Qiao, T., Zhao, W., Jia, L., and Lu, J. (2016). A Silurian maxillate placoderm illuminates jaw evolution. *Science*, 354(6310):334–336.

Zhu, M. and Gai, Z. (2006). Phylogenetic relationships of galeaspids (Agnatha). *Frontiers of Biology in China*, 2(2):151–169.

Zhu, M. and Janvier, P. (1996). A small antiarch, *Minicrania lirouyii* gen. et sp. nov., from the Early Devonian of Qujing, Yunnan (China), with remarks on antiarch phylogeny. *Journal of Vertebrate Paleontology*, 16(1):1–15.

Zhu, M. and Schultze, H.-P. (1997). The oldest sarcopterygian fish. *Lethaia*, 30(4):293–304.

Zhu, M. and Wang, J. (1996). A new macropetalichthyid from China, with special reference to the historical zoogeography of the Macropetalichthyidae (Placodermi). *Vertebrata PalAsiatica*, 10(34):253–268.

Zhu, M., Wang, J.-Q., and Wang, S.-T. (2010a). A new antarctaspid arthrodire (placoderm fish) from the Lower Devonian of Guangxi, China. *Vertebrata PalAsiatica*, 48(2):100–110.

Zhu, M., Wang, W., and Yu, X. (2010b). *Meemannia eos*, a basal sarcopterygian fish from the Lower Devonian of China–expanded description and significance. In Elliot, D., Maisey, J. G., Yu, X., and Miao, D., editors, *Morphology, phylogeny and paleobiogeography of fossil fishes.*, pages 199–214. München: Verlag Dr. Friedrich Pfeil.

Zhu, M. and Yu, X. (2002a). A primitive fish close to the common ancestor of tetrapods and lungfish. *Nature*, 418:767–770.

Zhu, M. and Yu, X. (2002b). A primitive fish close to the common ancestor of tetrapods and lungfish. *Nature*, 418(6899):767–770.

Zhu, M. and Yu, X. (2009). Stem sarcopterygians have primitive polybasal fin articulation. *Biology Letters*, 5(3):372–375.

Zhu, M., Yu, X., and Ahlberg, P. E. (2001). A primitive sarcopterygian fish with an eyestalk. *Nature*, 410(6824):81–84.

Zhu, M., Yu, X., Ahlberg, P. E., Choo, B., Lu, J., Qiao, T., Qu, Q., Zhao, W., Jia, L., Blom, H., et al. (2013). A Silurian placoderm with osteichthyan-like marginal jaw bones. *Nature*, 502:188–193.

Zhu, M., Yu, X., Choo, B., Wang, J., and Jia, L. (2012). An antiarch placoderm shows that pelvic girdles arose at the root of jawed vertebrates. *Biology Letters*, 8(3):453–456.

Zhu, M., Yu, X., and Janvier, P. (1999a). A primitive fossil fish sheds light on the origin of bony fishes. *Nature*, 397(6720):607–610.

Zhu, M., Yu, X., and Janvier, P. (1999b). A primitive fossil fish sheds light on the origin of bony fishes. *Nature*, 397(6720):607–610.

Zhu, M., Yu, X., Wang, W., Zhao, W., and Jia, L. (2006). A primitive fish provides key characters bearing on deep osteichthyan phylogeny. *Nature*, 441(7089):77–80.

Zhu, M. and Yu, X.-B. (2004). Lower jaw character transitions among major sarcopterygian groups-a survey based on new materials from Yunnan, China. In Arratia, G., Wilson, M. V. H., and Cloutier, R., editors, *Recent Advances in the Origin and Early Radiation of Vertebrates.*, pages 271–286. Verlag Dr. Friedrich Pfeil, München.

Zhu, M., Zhao, W., Jia, L., Lu, J., Qiao, T., and Qu, Q. (2009). The oldest articulated osteichthyan reveals mosaic gnathostome characters. *Nature*, 458:469–74.

Zhu, Y.-A. and Zhu, M. (2013). A redescription of *Kiangyousteus yohii* (Arthrodira: Eubrachythoraci) from the Middle Devonian of China, with remarks on the systematics of the Eubrachythoraci. *Zoological Journal of the Linnean Society*, 169(4):798–819.

APPENDIX A

APPENDIX

A.1 LIST OF TAXA WITH REFERENCES

Taxon	**References**
Acanthodes bronni	(Gross, 1935; Watson, 1937; Miles, 1973a,b; Coates, 1994; Davis et al., 2012; Brazeau and de Winter, 2015)
Aceraspis robustus	(Heintz, 1939)
Achoania jarvikii	(Zhu et al., 2001; Zhu and Yu, 2004, 2009)
Akmonistion zangerli	(Coates and Sequeira, 1998; Coates et al., 1998; Coates and Sequeira, 2001)
Anglaspis maccoulloughi	(Wills, 1935; Watson, 1954; Keating et al., 2015)
Arabosteus variabilis	(Olive et al., 2011)
Asterolepis ornata	(Gross, 1931; Zhu, 1996; Lukševičs, 2001)
Austroptyctodus gardineri	(Long, 1997)
Bannhuanaspis vukhuci	(Janvier et al., 1993)
Benneviaspis holtedahli	(Janvier, 1985a)
Boreaspis macrorhynchus	(Janvier, 1975, 1985a, 2008)

Taxon	**References**
Bothriolepis sp Gogo	(Young, 1984; **?**)
Bothriolepis canadensis	(Downs and Donoghue, 2009; Béchard et al., 2014)
Brachyacanthus scutiger	(Watson, 1937)
Brindabellaspis stensioi	(Young, 1980; **?**)
Brochoadmones milesi	(Hanke and Wilson, 2006)
Buchanosteus confertituberculatus	(Burrow and Turner, 1998; Long et al., 2014)
Campbellodus decipiens	(Long, 1997)
Cassidiceps vermiculatus	(Gagnier and Wilson, 1996)
Cephalaspis lyelli	(Stensiö, 1932)
Cheiracanthus sp	(Watson, 1937; Miles, 1973a)
Cheirolepis canadensis	(Pearson and Westoll, 1979; Arratia and Cloutier, 1996)
Cheirolepis trailli	(Pearson and Westoll, 1979; Giles et al., 2015a)
Chondrenchelys problematica	(Moy-Thomas, 1935; Finarelli and Coates, 2012, 2014)
Chuchinolepis dongmoensis	(Thanh and Janvier, 1990)
Cladodoides wildungensis	(Maisey, 2005)
Cladoselache kepleri	(Harris, 1938; Bendix-Almgreen, 1975; Schaeffer, 1981)
Climatius reticulatus	(Watson, 1937; Miles, 1973a)

Taxon	**References**
Coccosteus cuspidatus	(Miles and Westoll, 1968)
"Cobelodus"	(Maisey, 2007)
Compagopiscis croucheri	(Gardiner and Miles, 1994)
Cowralepis mclachlani	(Ritchie, 2005; Carr et al., 2009)
Culmacanthus stewarti	(Long, 1983)
Dartmuthia gemmifera	(Patten, 1931; Janvier, 1985b)
Debeerius ellefseni	(Grogan and Lund, 2000)
Diabolepis speratus	(Chang and Yu, 1984; Chang, 1995)
Dialipina salgueiroensis	(Schultze, 1968; Schultze and Cumbaa, 2001)
Diandongpetalichthys liaojiaoshanensis	(Zhu, 1991)
Dicksonosteus arcticus	(Goujet, 1984a)
Diplacanthus striatus	(Watson, 1937; Miles, 1973a)
Doliodus problematicus	(Miller et al., 2003; Maisey et al., 2009)
Eastmanosteus calliaspis	(Dennis-Bryan, 1987)
Ellopetalichthys scheii	(Ørvig 1957, chapter 3)
Entelognathus primordialis	(Zhu et al., 2013)
Epipetalichthys wildungensis	(Zhu and Wang, 1996; Zhu, 2000)
Escuminaspis laticeps	(Janvier et al., 2004)
Eugaleaspis changi	(Liu, 1965; Zhu and Gai, 2006)
Eurycaraspis incilis	(Liu, 1973, 1991; Pan et al., 2015)
Eusthenopteron foordi	(Jarvik, 1980)

Taxon	**References**
Euthacanthus macnicoli	(Watson, 1937; Miles, 1973a; Newman et al., 2014)
Gavinaspis convergens	(Dupret and Zhu, 2007; Dupret et al., 2009)
Gemuendina stuertzi	(Gross, 1963)
Gladiobranchus probaton	(Hanke and Davis, 2008)
Glyptolepis groenlandica	(Jarvik, 1972; Ahlberg, 1989)
Gogonasus andrewsae	(Long, 1985; Long et al., 1997, 2006; Holland, 2013, 2014)
Groenlandaspis sp Mt Howitt	(**?**)
Guangxipetalichthys tiaomajianensis	(Zhao and Zhu, 2010; Ji and Pan, 1997)
Guiyu oneiros	(Zhu et al., 2009; Qiao and Zhu, 2010)
Hamiltonichthys mapesi	(Maisey, 1989)
Hanyangaspis guodingshanensis	(Zhu and Gai, 2006)
Helodus simplex	(Moy-Thomas, 1936)
Hemicyclaspis murchisoni	(Stensiö, 1932)
Holonema westolli	(Miles, 1971)
Homalacanthus concinnus	(Gagnier, 1996)
Howqualepis rostridens	(Long, 1988)
Incisoscutum ritchiei	(Dennis and Miles, 1981; Giles et al., 2013)
Ischnacanthus gracilis	(Watson, 1937; Miles, 1973a)
Jagorina pandora	(Stensiö, 1950, 1969; Young, 1986)

Taxon	**References**
Janusiscus schultzei	(Giles et al., 2015b)
Kathemacanthus rosulentus	(Gagnier and Wilson, 1996; Hanke and Wilson, 2010)
Kenichthys campbelli	(Chang and Zhu, 1993; Zhu and Ahlberg, 2004)
Kentuckia deani	(Rayner, 1952; Giles and Friedman, 2014)
Kimaspis tienshanica	(Mark-Kurik, 1973)
Kolymaspis sibirica	(Bystrow 1956, chapter 4)
Kosoraspis peckai	(Gross, 1958, 1959)
Kujdanowiaspis podolica	(Stensiö, 1963a, 1969; Dupret, 2010)
Latviacanthus ventspilsensis	(Schultze and Zidek, 1982)
Ligulalepis toombsi	(Basden et al., 2000; Basden and Young, 2001)
Lupopsyrus pygmaeus	(Hanke and Davis, 2012)
Lunaspis broili	(Gross, 1961)
Macropetalichthys rapheidolabis	(Stensiö, 1925, 1963a,b, 1969)
Materpiscis attenboroughi	(Long et al., 2008)
Meemannia eos	(Zhu et al., 2006, 2010b)
Mesacanthus mitchelli	(Watson, 1937; Miles, 1973a)
Microbrachius dicki	(Hemmings, 1978; Long et al., 2015)
Miguashaia bureaui	(Cloutier, 1996; Forey, 1998)

Taxon	**References**
Mimipiscis toombsi	(Gardiner and Bartram, 1977; Gardiner, 1984a; Giles and Friedman, 2014)
Minicrania lirouyii	(Zhu and Janvier, 1996)
Moythomasia durgaringa	(Gardiner, 1984b)
Mulgaspis evansorum	(Ritchie, 2004)
Nectaspis areolate	(Wängsjö, 1952; Janvier, 1981)
Norselaspis glacialis	(Janvier, 1981, 2008)
Notopetalichthys hillsi	(Woodward, 1941)
Obtusacanthus corroconis	(Hanke and Wilson, 2004)
Onychodus jandemarrai	(Andrews et al., 2005)
Onychoselache traquari	(Dick and Maisey, 1980; Coates and Gess, 2007)
Orthacanthus sp	(Schaeffer, 1981)
Osorioichthys marginis	(Taverne, 1997)
Osteolepis macrolepidotus	(Westoll, 1936; Thomson, 1965; Jarvik, 1980)
Pampetalichthys longhuaensis	(Zhu and Wang, 1996; Zhu, 2000)
Parabuchanosteus murrumbidgeensis	(White and Toombs, 1972; Young, 1979; Burrow and Turner, 1998)
Parayunnanolepis xitunensis	(Zhang et al., 2001; Zhu et al., 2012)
Parexus recurvus	(Watson, 1937; Miles, 1973a; Burrow et al., 2013)

Taxon	**References**
Pauropetalichthys magnoculus	(Pan et al., 2015)
Polybranchiaspis liaojiaoshanensis	(Liu, 1965, 1975)
Polybranchiaspid sp histological samples	(Wang et al., 2005)
Poracanthodes menneri	(Valiukevicius, 1992)
Porolepis sp	(Jarvik, 1972; Clement, 2004)
Powichthys thorsteinssoni	(Jessen, 1980)
Procephalaspis oeselensis	(Robertson, 1939; Denison, 1951; Janvier, 1985b)
Promesacanthus eppleri	(Hanke, 2008)
Psarolepis romeri	(Yu, 1998; Zhu et al., 1999b; Zhu and Yu, 2004, 2009)
Pterichthyodes milleri	(Hemmings, 1978)
Ptomacanthus anglicus	(Miles, 1973a; Brazeau, 2012)
Pucapampella rodrigae	(Maisey, 2001a)
Quasipetalichthys haikouensis	(Liu, 1991, 1973)
Radotina kosorensis	(Gross, 1950, 1958; Vaškaninová and Ahlberg, 2017)
Radotina tessellata	(Gross, 1950, 1958; Vaškaninová and Ahlberg, 2017)
Ramirosuarezia boliviana	(Pradel et al., 2009)
Remigolepis walkeri	(Johanson, 1997)
Rhamphodopsis threiplandi	(Miles, 1967; Long, 1997)
Romundina stellina	(Ørvig, 1975; Dupret et al., 2017a)

Taxon	**References**
Shearsbyaspis oepiki	(Young 1985, chapter 2)
Shuyu zhejiangensis	(Gai et al., 2011)
Sigaspis lepidophora	(Goujet, 1973)
Sinopetalichthys kueiyangensis	(P'an et al., 1975; Zhao and Zhu, 2010)
Styloichthys changae	(Zhu and Yu, 2002a; Friedman, 2007)
Sudaspis chiupaci	(Gross, 1959; Vaškaninová and Ahlberg, 2017)
Tamiobatis vetustus	(Williams, 1998)
Tetanopsyrus lindoei/breviacanthias	(Gagnier et al., 1999; Hanke et al., 2001)
Tlamaspis inopinatus	(Gross, 1959; Vaškaninová and Ahlberg, 2017)
Trematapsis mammillata	(Denison, 1947, 1951; Janvier, 1985b)
Tristychius arcuatus	(Dick, 1978; Coates and Gess, 2007)
Vernicomacanthus waynensis	(Miles, 1973a)
Waengsjoeaspis excellens	(Wängsjö, 1952; Janvier, 1985a)
Wenshanaspis zhichangensis	(Zhao et al., 2001)
Widjeaspis warrooensis	(Young, 1978)
Wuttagoonaspis fletcheri	(Ritchie, 1973; Miles and Young, 1977; **?**)
Youngolepis praecursor	(Zhang and Yu, 1981; Zhang, 1982; Chang, 1991)
Yujiangolepis liujingensis	(Dupret et al., 2009)

Taxon	**References**
Yunnanolepis sp	(Zhang, 1980b; Zhu, 1996)
Zenaspis salweyi	(Stensiö, 1932; White, 1958)

A.2 CHARACTERS REMOVED FROM KING ET AL. 2016

[89] Relative position of jugular groove and hyomandibular articulation: **(0) hyomandibula dorsal or same level (1) jugular vein passing dorsal or lateral to hyomandibula**

Character excluded because the presence of an enclosed jugular canal is already accounted by character 27.

[98] Paravagal fossa: **(0) absent (1) present**

This character is related to the present of a bifurcated vagal process (character 91) and is thus redundant.

[100] Braincase is a series of bilateral ossifications: **(0) no (1) yes**

Removed because of ambiguous formulation of the character.

[102] Tectum orbitale/supraorbital shelf: **(0) absent or very narrow (1) present**

This characater is redundant as the presence of a broad supraorbital shelf is already taken in account by character 24.

[105] Parachordal plates: **(0) separated from the otic capsule (1) sutured or fused with the otic capsule**

This character is related to the metotic fissure (Character 51) and thus redundant.

[121] Hyomandibular articulating with the braincase: **(0) yes (0) no**

This character is relative with the presence of a transverse otic process (anterior postorbital process) (character 71) and thus redundant.

[122] Ethmoidal articulation: **(0) absent (1) present**

Originally from (Pradel et al., 2011). Removed as it is ambiguous if the ethmoid articulation in osteichthyes is homologous to the supposed "ethmoidal articulation" in chondrichthyans and placoderms.

[123] Orbital/palatobasal articulation: **(0) posterior to optic foramen (1) anterior to optic foramen**

The palatobasal articulation has been homologised with the basypterigoid articulation (character 35) by (Giles et al., 2015b) and here we follow this convention.

[174] Type of ginglymoid neck joint: **(0) "conventional" (1) reverse**

Incorporated in character 143.

[243] Parietals or Preorbital plates at anterior edge of skull roof: **(0) no (1) yes**

This character was created by King et al. (2016) to take in account that in some placoderms, such as *Cowralepis*, *Eurycaraspis*, *Quasipetalichthys* and ptyctodonts, the preorbital plates form the anterior edge of the skull roof. They considered this feature in relation of a reduction of the dermal bones of the snout. However, in *Eurycaraspis* and *Quasipetalichtys*, for example, the orbit are still surrounded by dermal bone, as the preorbital plates constitute the anterior margin of the orbit. In ptyctodonts, instead, the anterior margin of the orbit is depleted by dermal bone and the preorbital plate only makes up the lateral edge of the orbit. Given the problem of coding this character as it is currently formulated, it has been removed.

[253] Paraorbital plate separating suborbital from orbit: **(0) absent (1) present**

King et al. (2016) created this character to assess the presence of a dermal plate that is not associated with the palatoquadrate and extends lateral to the orbit. This plate was thought to be present in *Wuttagoonaspis* and possibly *Brindabellaspis*. However, this character might just be an automoporphy of *Wuttagoonaspis* as the supposed ”paraorbital” plates in *Brindabellaspis* are possibly just part of the large premedian plate. Character has been tentatively removed.

[255] Transverse external groove behind pineal opening: **(0) absent (1) present**

A transverse groove behind the pineal opening is present in *Dicksonosteus* (Goujet 1984a) and *Diandongpetalichthys* (Zhu 1991), but it is difficult to assess if this feature represents an anatomical or taphonomic groove.

[264] Foramina on cheek bones: **(0) absent (1) present**

Removed as identical to character 164.

[265] Contact between most posterior major bone of cheek bearing preopercular canal and maxilla: **(0) present (1) absent**

Removed as equivalent to character 145.

[266] Number of branchiostegal rays per side: **(0) 10 or more (1) 2-7 (2) one**

Removed as the states number are arbitrary and thus character formulation is ambiguous.

[281 Cheek plates fragmented into many small plates: **(0) absent (1) present**

Removed as equivalent to 137.

[285] Junction of posterior pitline and main lateral line: **(0) far in front of posterior margin of skull roof (1) close to posterior margin of skull roof**

Some placoderms possess an anterior posterior pit line and a posterior posterior pit line (e.g. Denison 1978). For example, in the original matrix the same scoring was applied for *Kujdanowiaspis* and *Ctenurella* as their posterior pit line is close to the posterior end of the skull. However, *Kujdanowiaspis* possess two pair of posterior pit line (Goujet 1984a), while *Ctenurella* (Forey and Gardiner, 1986) only one. Also, this can be related with the elongation of the occipital region of the skull. This character is thus ambiguous and has been removed.

292] Posterior end of supraorbital canal: **(0) extends back to level of posterior/middle pitlines (1) terminates anterior to level of posterior/middle pit lines ((2)) extends posterior to pit-lines**

In *Romundina* the sopraorbital canal is short but reach the anterior posterior pit line, differently from *Brindabellaspis* or *Lunaspis* where the supraorbital canal is longer and reach the posterior (and only) posterior pit line. Because of the ambiguous definition of the character, it has been removed.

[309] Anterior supraorbital canal: **(0) absent (1) present**

The "anterior supraorbital canal" in *Lunaspis* are of doubtful identification and not necessarily related to the supraorbital canal. For this reason, I think this character is contentious and should be removed.

[361] Contact between palatoquadrate and dermal cheek bones: **(0) continuous contact of metapterygoid and autopalatine (1) metapterygoid and autopalatine contacts separated by gap between commissural lamina of palatoquadrate and cheek bones**

Removed because of ambiguous formulation.

[363] Jaws: **(0) absent (1) present**

As the jawless stem-gnathostomes are constrained to be sister to the jawed-gnathostomes, this character became redundant.

[369] Position of hyomandibula articulation on neurocranium: **(0) Anterior position, suborbital (1) posterior position, behind orbit**

Redundant as the position of the hyomandibular articulation is already considered in character 91.

[387] Submandibulars: **(0) absent (1) present**

This character is problematic because it is not clear how it is possible to distinguish the submandibulars from the branchiostegals (which presence or absence is considered in character 131.

[396] Intromittent organ (clasper) consisting entirely of cartilage, formed from distal part of pelvic fin: **(0) absent (1) present**

Removed following discussion for character 317

[497] Scales with well-developed pores on ganoine surface: **(0) absent (1) present**

The absence of pores is usually considered as a feature of ganoine, so that this character might simply being related with the presence of cosmine. However, the terms "cosmine" and "ganoine" probably indicate a compound of different tissue and need to be used carefully (see Lu et al. 2016).

A.3 SUPPLEMENTARY FIGURES

Antiarchs
"Acanthothoracids"
Rhenanids
Arthrodires
Macropetalichthyids
"Quasipetalichthyids"
Ptyctodontids
Maxillate "placoderms"

FIGURE A.1: Strict consensus tree resulting from TNT analysis.

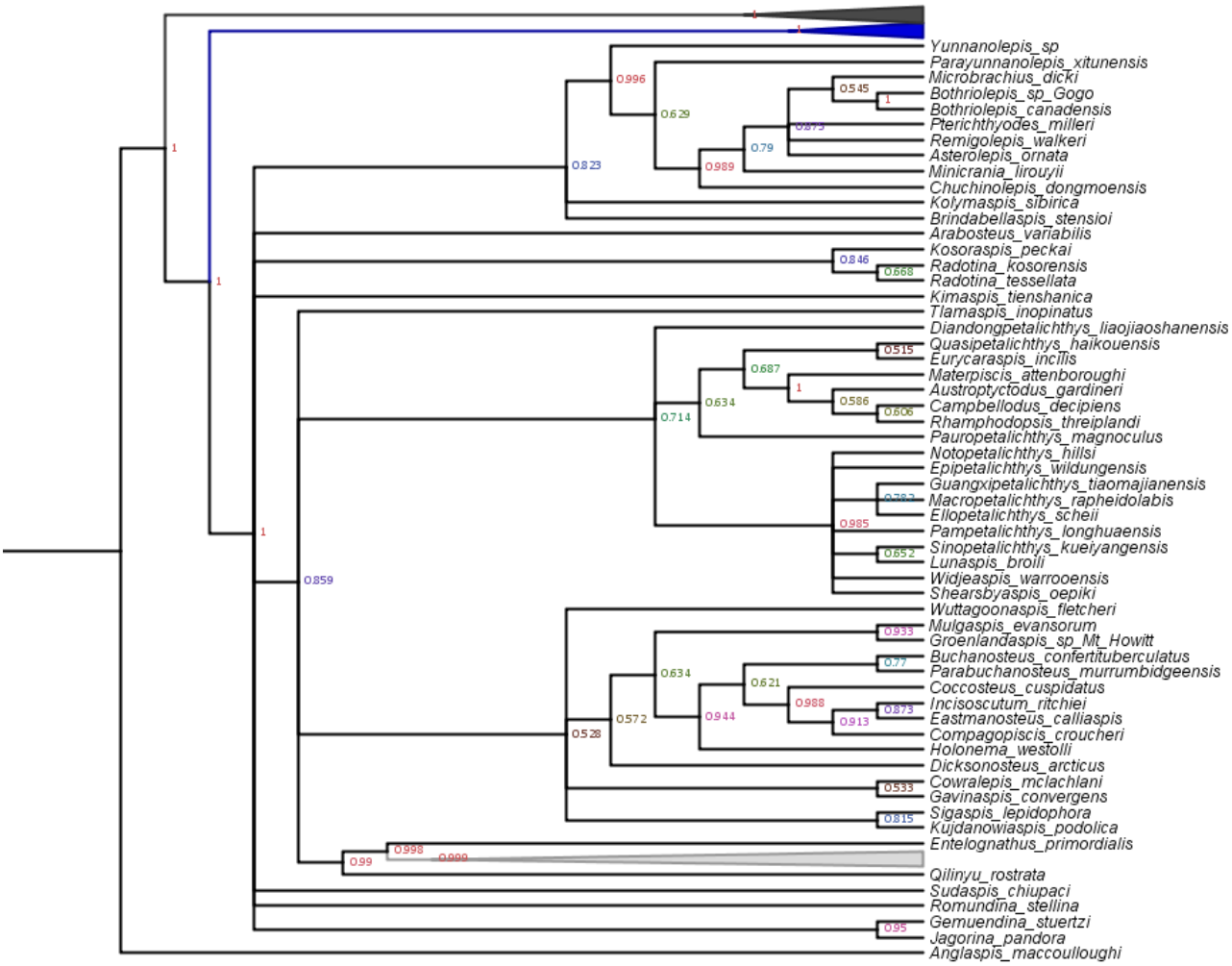

FIGURE A.2: Majority-rule consensus tree for "placoderms" resulting from Bayesian inference analysis. Frequencies of bipartitions among sampled trees (Bayesian posterior probabilities) are indicated for each node.

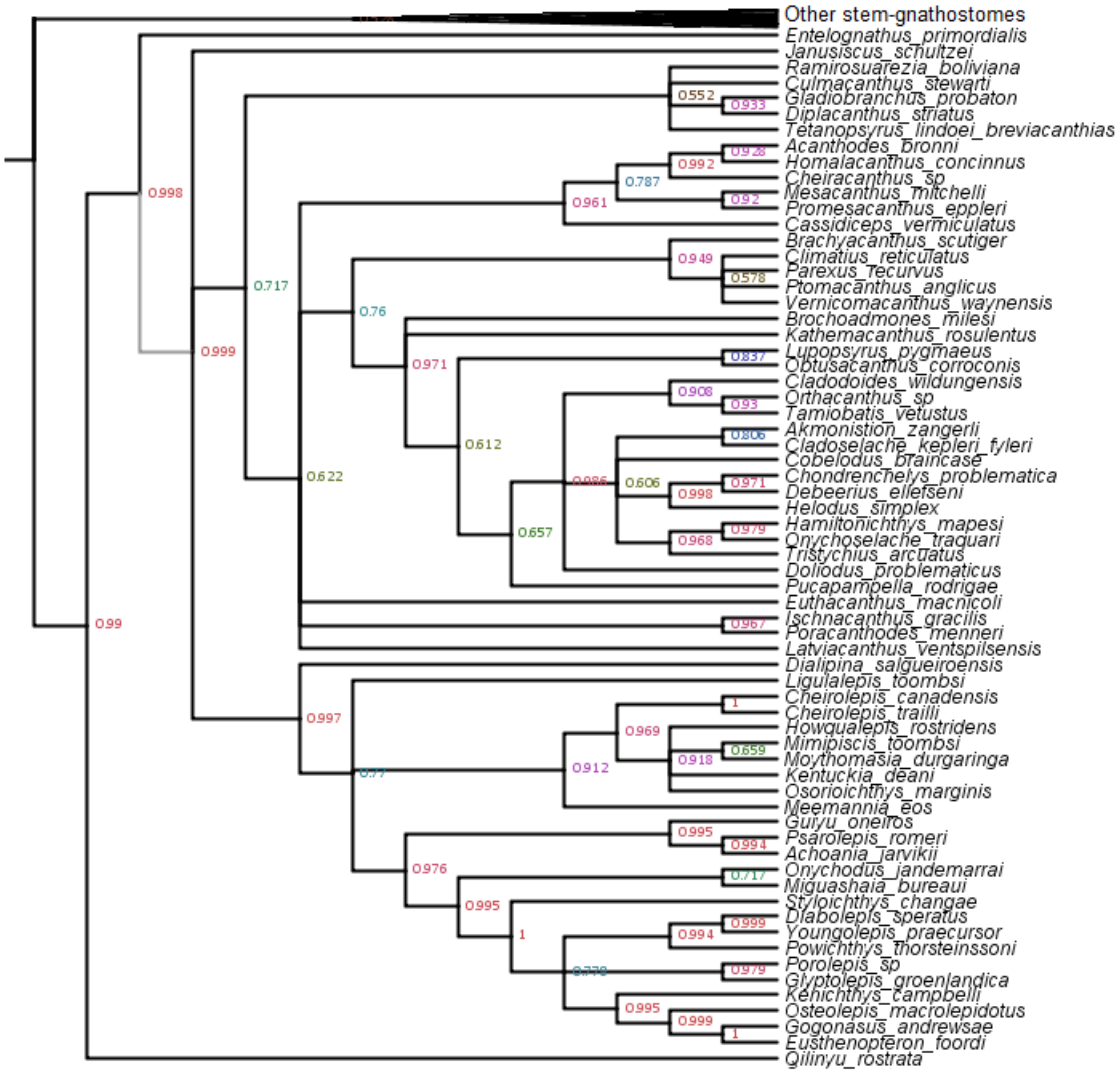

FIGURE A.3: Majority-rule consensus tree resulting from Bayesian inference analysis. Outgroups and "traditional" placoderms collapsed. Frequencies of bipartitions among sampled trees (Bayesian posterior probabilities) are indicated for each node.